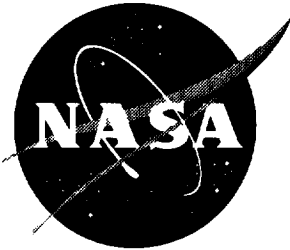


NASA/CP-1999-209690/PT1

419-101
P



First NASA/Industry High-Speed Research Configuration Aerodynamics Workshop

*Edited by
Richard M. Wood
Langley Research Center, Hampton, Virginia*

December 1999

The NASA STI Program Office . . . in Profile

Since its founding, NASA has been dedicated to the advancement of aeronautics and space science. The NASA Scientific and Technical Information (STI) Program Office plays a key part in helping NASA maintain this important role.

The NASA STI Program Office is operated by Langley Research Center, the lead center for NASA's scientific and technical information. The NASA STI Program Office provides access to the NASA STI Database, the largest collection of aeronautical and space science STI in the world. The Program Office is also NASA's institutional mechanism for disseminating the results of its research and development activities. These results are published by NASA in the NASA STI Report Series, which includes the following report types:

- **TECHNICAL PUBLICATION.** Reports of completed research or a major significant phase of research that present the results of NASA programs and include extensive data or theoretical analysis. Includes compilations of significant scientific and technical data and information deemed to be of continuing reference value. NASA counterpart of peer-reviewed formal professional papers, but having less stringent limitations on manuscript length and extent of graphic presentations.
- **TECHNICAL MEMORANDUM.** Scientific and technical findings that are preliminary or of specialized interest, e.g., quick release reports, working papers, and bibliographies that contain minimal annotation. Does not contain extensive analysis.
- **CONTRACTOR REPORT.** Scientific and technical findings by NASA-sponsored contractors and grantees.

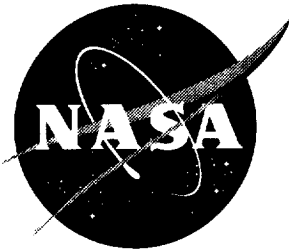
- **CONFERENCE PUBLICATION.** Collected papers from scientific and technical conferences, symposia, seminars, or other meetings sponsored or co-sponsored by NASA.
- **SPECIAL PUBLICATION.** Scientific, technical, or historical information from NASA programs, projects, and missions, often concerned with subjects having substantial public interest.
- **TECHNICAL TRANSLATION.** English-language translations of foreign scientific and technical material pertinent to NASA's mission.

Specialized services that complement the STI Program Office's diverse offerings include creating custom thesauri, building customized databases, organizing and publishing research results . . . even providing videos.

For more information about the NASA STI Program Office, see the following:

- Access the NASA STI Program Home Page at <http://www.sti.nasa.gov>
- Email your question via the Internet to help@sti.nasa.gov
- Fax your question to the NASA STI Help Desk at (301) 621-0134
- Telephone the NASA STI Help Desk at (301) 621-0390
- Write to:
NASA STI Help Desk
NASA Center for AeroSpace Information
7121 Standard Drive
Hanover, MD 21076-1320

NASA/CP-1999-209690/PT1



First NASA/Industry High-Speed Research Configuration Aerodynamics Workshop

*Edited by
Richard M. Wood
Langley Research Center, Hampton, Virginia*

Proceedings of a workshop held at
Langley Research Center,
Hampton, Virginia
February 27–29, 1996

National Aeronautics and
Space Administration

Langley Research Center
Hampton, Virginia 23681-2199

December 1999

Available from:

NASA Center for Aerospace Information (CASI)
7121 Standard Drive
Hanover, MD 21076-1320
(301) 621-0390

National Technical Information Service (NTIS)
5285 Port Royal Road
Springfield, VA 22161-2171
(703) 605-6000

PREFACE

This publication is a compilation of documents presented at the First NASA/Industry High-Speed Research Configuration Aerodynamics Workshop held on February 27-29, 1996, at NASA Langley Research Center. The purpose of the workshop was to bring together the broad spectrum of aerodynamicists, engineers, and scientists working within the Configuration Aerodynamics element of the HSR Program to collectively evaluate the technology status and to define the needs within Computational Fluid Dynamics (CFD) Analysis Methodology, Aerodynamic Shape Design, Propulsion/Airframe Integration (PAI), Aerodynamic Performance, and Stability and Control (S&C) to support the development of an economically viable High-Speed Civil Transport (HSCT) aircraft. To meet these objectives, papers were presented by representatives from NASA Langley, Ames and Lewis Research Centers, Boeing, McDonnell Douglas, Northrop-Grumman, Lockheed-Martin, Vigyan, Analytical Services, Dynacs, and RIACS.

The workshop was organized in 12 sessions as follows:

- Introduction/Overviews
- Overviews
- PAI I
- PAI II
- Analysis and Design Optimization Methods
- Experimental Methods
- Design Optimization - Applications I
- Design Optimization - Applications II
- Design Optimization - Applications III/Validation
- Reynolds Number Effects
- Stability and Control
- High Lift

Appreciation is expressed to the individuals at NASA Langley, NASA Ames, McDonnell Douglas, and Boeing who developed the structure and content of the workshop; to the session chairs and speakers who contributed to the technical quality; and to the many individuals who contributed to the administration and logistics of the workshop. A list of attendees is included in this document.

Richard M. Wood
NASA Langley Research Center

CONTENTS

Preface	iii
Attendees	xi

Part 1

Session 1

HSR Aerodynamic Performance Status and Challenges	1
Bill Gilbert, <i>NASA Langley Research Center</i> , Tony Antani, <i>McDonnell Douglas</i> , Doug Ball, <i>Boeing</i> , Rob Calloway, <i>NASA Langley Research Center</i> , Phil Snyder, <i>NASA Ames Research Center</i>	
Configuration Aerodynamics: Past – Present – Future	15
Richard Wood, <i>NASA Langley Research Center</i> ; Shreekant Agrawal, <i>MDA</i> ; Dan Bencze, <i>NASA Ames Research Center</i> ; Bob Kulfan, Doug Wilson, <i>BCA</i>	
Technology Integration Overview	41
Peter G. Coen, <i>NASA Langley Research Center</i>	

Session 2

Wind Tunnel Test Technique and Instrumentation Development at NASA Langley Research Center	65
Lawrence E. Putnam, <i>NASA Langley Research Center</i>	
4.3.4 Supersonic Laminar Flow Control, An Overview	81
Bharadvaj, Bala, <i>McDonnell Douglas</i> ; Mike Fischer, Ron Joslin, <i>NASA Langley Research Center</i> ; Lyn King, <i>NASA Ames Research Center</i> ; Pradip Parikh, <i>Boeing Commercial Airplane Group</i>	
High Lift Technology Overview	99
Z.T. Applin, <i>NASA Langley Research Center</i>	

Session 3

Experimental Results of the 2.7% Reference H Nacelle Airframe Interference High Speed Civil Transport Model	113
Gelsomina Cappuccio, <i>NASA Ames Research Center</i>	
HSCT Propulsion Airframe Integration Studies	139
Steve Chaney, <i>The Boeing Company</i>	
HSCT Nacelle Boundary Layer Diverter Study	183
Steven S. Ogg, <i>The Boeing Company</i>	

Analysis of Alternate Inlets and Nacelles for HSCT Configuration	197
P. Sundaram*, Ana Tinetti**, Alan Arslan*, Shreekant Agrawal*, Peter Hartwich*, Jay Jones*, (<i>*McDonnell Douglas Corporation; **Eagle Aeronautics, Inc.</i>)	

Session 4

High Speed Civil Transport (HSCT) Isolated Nacelle Transonic Boattail Drag Study and Results Using Computational Fluid Dynamics (CFD)	223
Anthony C. Midea,* Thomas Austin,** S. Paul Pao,*** James R. DeBonis,* Mori Mani,** (<i>*NASA Lewis Research Center, **McDonnell Douglas Aerospace, ***NASA Langley Research Center</i>)	

Transonic Drag Study for the Installed Ref. H Axisymmetric Nozzle Boattail Configurations	271
Chih Fang Shieh, Jay Jones, Shreekant Agrawal, <i>McDonnell Douglas Aerospace</i>	

Installed Transonic 2D Nozzle Nacelle Boattail Drag Study	291
M. Malone, C. Peavey, <i>Northrop Grumman Corporation</i>	

Afterbody External Aerodynamic and Performance Predictions at High Reynolds Numbers	321
John R. Carlson, <i>NASA Langley Research Center</i>	

Part 2†

Session 5

Viscous Analysis of Ref. H Based Wing/Bodies	335
Scott L. Lawrence, <i>NASA Ames Research Center</i>	

CFD Code Validation for HSCT Wing/Body and Wing/Body/Nacelle/Diverter Configurations	355
James O. Hager, Geojoe Kuruvila, Samson H. Cheung, Eric R. Unger, and Shreekant Agrawal, <i>McDonnell Douglas Aerospace</i>	

Overview of HSR Aerodynamic Optimization at Boeing	395
R.S. Conner, <i>The Boeing Company</i>	

Some Recent Enhancements to Aerodynamic Shape Optimization Methods at McDonnell Douglas Aerospace	423
Peter M. Hartwich, Eric R. Unger, Alan E. Arslan, Shreekant Agrawal, <i>McDonnell Douglas Corporation</i>	

Boeing HSR Wing Optimization Using Tranair	445
K.R. Wittenberg, <i>The Boeing Company</i>	

Advances in Design Optimization Using Adjoint Methods	493
James Reuther, <i>RIACS/AAH</i> ; David Saunders, <i>Sterling Software</i>	

†Part 2 is presented under separate cover.

Session 6

Aftbody Closure Effects on the Reference H Configuration at Subsonic and Transonic Speeds.....	529
Richard A. Wahls, Lewis R. Owens, Jr., <i>NASA Langley Research Center</i> ; W. Kelly Londenberg, <i>ViGYAN, Inc.</i>	
Model Deformation Measurement Technique – NASA Langley HSR Experiences.....	561
A.W. Burner, R.A. Wahls, L.R. Owens, W.K. Goad <i>NASA Langley Research Center</i>	
Boundary Layer Transition in the NTF: HSR Experience and Plans	579
Louis R. Owens, Jr., Richard A. Wahls, <i>NASA Langley Research Center</i> ; Marvine P. Hamner, <i>McDonnell Douglas Aerospace</i>	

Session 7

The Application of the NFW Design Philosophy to the HSR Arrow Wing Configuration	597
Steven X.S. Bauer, Steven E. Krist, <i>NASA Langley Research Center</i>	
Analysis and Inverse Design of the HSR Arrow Wing Configuration with Fuselage, Wing, and Flow Through Nacelles.....	641
Steven E. Krist, Steven X.S. Bauer, <i>NASA Langley Research Center</i>	
HSCT Multipoint Aerodynamic Performance Trades from TCA Propulsion and Planform Studies	665
Chester P. Nelson, <i>Boeing Commercial Airplane Group</i>	
CFD Planform Study of the 1400 Series.....	681
G. Kuruvila, J.O. Hager, E.R. Unger, A.E. Arslan, D.B. Bruns, P. Sundaram, G. Martin, S. Agrawal, <i>McDonnell Douglas Aerospace</i>	

Session 8

Investigation of Nonlinear Effects on Reference H Body Area-Ruling and Cambering	705
Thierry Tamigniaux, <i>The Boeing Company</i>	
Fuselage Cross-Sectional Area and Camber Optimization Using Nonlinear Aerodynamic Tools	727
James O. Hager, Shreekant Agrawal, <i>McDonnell Douglas Aerospace</i>	
Wing Design and Suction/Cooling Requirements for an HSCT With Supersonic Laminar Flow Control.....	751
Bala Bharadvaj, Dino Roman, P. Sundaram, Art Powell, K.C. Chang, <i>McDonnell Douglas Aerospace</i> ; Lian Ng, Paul Vijgen, Pradip Parikh, <i>Boeing Commercial Airplane Group</i>	

Projecting and Tracking Advanced Technology Improvements in L/D.....	781
<i>R.M. Kulfan, Boeing Commercial Airplane Group</i>	

Part 3*

Session 9

A Computational/Experimental Study of Two Optimized Supersonic Transport Designs and the Reference H Baseline.....	845
<i>Susan E. Cliff, NASA Ames Research Center; Timothy J. Baker, Princeton University; Raymond M. Hicks, MCAT; James J. Reuther, RIACS</i>	

Update to the Summary of Langley Unitary Test 1649 and Its Implications on Validity of Viscous and Inviscid Analyses.....	969
<i>S. Yaghmaee, K.M. Mejia, Boeing Commercial Airplane Group</i>	

Supersonic Aerodynamic Design Improvements of an Arrow-Wing HSCT Configuration Using Nonlinear Point Design Methods.....	1009
<i>Eric R. Unger, James O. Hager, Shreekan Agrawal, McDonnell Douglas Aerospace</i>	

Experimental Investigation of a Point Design Optimized Arrow-Wing HSCT Configuration	1041
<i>R.P. Narducci, P. Sundaram, S. Agrawal, S. Cheung, A.E. Arslan, G.L. Martin, McDonnell Douglas Aerospace</i>	

Session 10

Initial Results of Reynolds Number Testing at LaRC's NTF Using the 2.2% Reference H Model.....	1073
<i>Marvine Hamner, McDonnell Douglas Aerospace; Lewis R. Owens, Jr., Richard A. Wahls, NASA Langley Research Center</i>	

HSCT Ref-H Transonic Flap Data Base: Wind-Tunnel Test and Comparison with Theory	1109
<i>Paul M. Vijgen, Boeing Commercial Airplane Group</i>	

Assessment of Ref. H HSCT Transonic Flap and Reynolds Number Effects with the OVERFLOW Code.....	1143
<i>Max Kandula, Ross Sheckler, Dynacs Engineering Company, Inc.</i>	

Turbulence Model Comparisons and Reynolds Number Effects Over a High-Speed Aircraft at Transonic Speeds.....	1185
<i>Melissa B. Rivers, Richard A. Wahls, NASA Langley Research Center</i>	

*Part 3 is presented under separate cover.

Session 11

Critical Stability and Control Issues in High-Speed Aerodynamics for the HSCT	1215
Douglas L. Wilson, <i>Boeing Commercial Airplane Group</i> ; Norman H. Princen, <i>McDonnell Douglas Aerospace</i> ; Oran C. Harris, <i>Lockheed Martin Aeronautical Systems Company</i>	
An Experimental Database for Conventional and Alternate Control Concepts on the HSR 1.675% Reference H Model	1233
Naomi McMillin, Jerry Allen, Gary Erickson, Jim Campbell, Mike Mann, <i>NASA Langley Research Center</i> ; Paul Kubiato, David Yingling, <i>McDonnell Douglas Aerospace</i> ; Charlie Mason, <i>Lockheed Martin</i>	
High Reynolds Number Effects on HSCT Stability and Control Characteristics	1253
Michael B. Elzey, <i>The Boeing Company</i> ; Lewis R. Owens, Jr., Richard A. Wahls, <i>NASA Langley Research Center</i> ; Douglas L. Wilson, <i>The Boeing Company</i>	
Simulated Inlet Unstart and Nacelle/Diverter Effects for the Boeing Reference H Configuration	1285
Susan E. Cliff,* Timothy J. Baker,** Scott D. Thomas,** E. Aguayo** (*NASA Ames Research Center, **Princeton University)	

Session 12

Wing Leading-Edge Geometry Effects on High-Lift Performance	1327
David L. Hoyle, Marvinne Hamner, <i>McDonnell Douglas Aerospace</i>	
Impact of Alternate Concepts for Wing Planform, Leading Edge Flaps, and Trim Configuration on the High Lift Performance of the Ref H HSCT	1345
G.H. Wyatt, K.D. Visser, <i>Boeing Commercial Airplane Company</i>	
Assessment of CFD Codes for HSCT Ref. H High Lift Aerodynamics	1375
Anthony J. Saladino, Ross D. Sheckler, <i>Dynacs Engineering Co. , Inc.</i>	
Summary of HEAT 1 Aeroacoustics Installation Effects	1407
Brian E. Smith, Paul T. Soderman, Fanny A. Zuniga, <i>NASA Ames Research Center</i>	

ATTENDEES

Abdol-Hamid, Khaled S..... Analytical Services & Materials, Inc.
Adams, Bill NASA Langley Research Center
Agrawal, Shreekant McDonnell Douglas Aerospace
Allen, Jerry M. NASA Langley Research Center
Antani, Tony McDonnell Douglas Aerospace
Applin, Z. NASA Langley Research Center
Baker, Timothy J. Princeton University
Bard, William..... Northrop Grumman Corporation
Bauer, Steve NASA Langley Research Center
Beach, H. Lee NASA Langley Research Center
Bencze, Daniel P. NASA Ames Research Center
Bharadvaj, Bala McDonnell Douglas Aerospace
Bobbitt, Percy J. Eagle Aeronautics, Inc.
Burner, A. W. NASA Langley Research Center
Bushnell, D..... NASA Langley Research Center
Buttrill, C. NASA Langley Research Center
Calloway, R. L. NASA Langley Research Center
Campbell, James F. NASA Langley Research Center
Campbell, Richard L. NASA Langley Research Center
Capone, Francis J. NASA Langley Research Center
Cappuccio, Gelsomina NASA Ames Research Center
Carlson, John R. NASA Langley Research Center
Chaney, Steve..... Boeing
Chu, J. NASA Langley Research Center
Clark, Roger McDonnell Douglas Aerospace
Cliff, Susan E. NASA Ames Research Center
Coen, P. NASA Langley Research Center
Compton, W. NASA Langley Research Center
Conner, Roy S. Boeing Commercial Airplane Group
Covell, P..... NASA Langley Research Center
DeBonis, Jim..... NASA Lewis Research Center
Deere, Karen A. NASA Langley Research Center
Dollyhigh, S. NASA Langley Research Center
Domack, C. NASA Langley Research Center

Driver, Cornelius.....	Eagle Aeronautics, Inc.
Dudley, Mike	NASA Ames Research Center
Dwoyer, D.	NASA Langley Research Center
Dwyer, William P.	Northrop Grumman ATDC
Erickson, G.....	NASA Langley Research Center
Flamm, J.....	NASA Langley Research Center
Fox, Mike C.	Vigyan, Inc.
Frink, Neal	NASA Langley Research Center
Gerhardt, Heinz A.	Northrop Grumman Corporation
Ghaffari, Farhad	NASA Langley Research Center
Gibson, Berry T.....	Lockheed Martin Aeronautical Systems
Gilbert, W. P.	NASA Langley Research Center
Glaab, Lou.....	Lockheed Martin
Goldberg, Perry	McDonnell Douglas Aerospace
Goodsell, Aga.....	NASA Ames Research Center
Graber Ed	NASA Lewis Research Center
Green, L.	NASA Langley Research Center
Hager, James	McDonnell Douglas Aerospace
Hahne, David	NASA Langley Research Center
Hamner, Marvine	McDonnell Douglas Aerospace
Harris, Roy V.	NASA Langley Research Center
Hartwich, Peter.....	McDonnell Douglas Aerospace
Hefner, J.	NASA Langley Research Center
Henderson, W.....	NASA Langley Research Center
Hicks, Ray	NASA Ames Research Center/MCAT
Holloway, Paul F.....	NASA Langley Research Center
Hoyle, David	McDonnell Douglas Aerospace
Jameson, A.	Princeton University
Joslin, Ronald D.....	NASA Langley Research Center
Kandula, Max	Dynacs Engineering Co.
Kammerly, G.....	NASA Langley Research Center
Kennelly, Jr., Robert A.	NASA Ames Research Center
Keyes, Sandy.....	NASA Langley Research Center
Krist, Steve.....	NASA Langley Research Center
Kubiatko, Paul.....	McDonnell Douglas Aerospace
Kulfan, Robert M.	Boeing Commercial Airplane Group

Kuruwila, G.....	McDonnell Douglas Aerospace
LaBozzetta, Walt.....	McDonnell Douglas Aerospace
Lawrence, Scott.....	NASA Ames Research Center
Leavitt, Lawrence D.....	NASA Langley Research Center
Lessard, Wendy B.....	NASA Langley Research Center
Luckring, J.....	NASA Langley Research Center
Ludas, Kevin.....	McDonnell Douglas Aerospace
Malone, Michael B.....	Northrop Grumman
Mason, Charlie.....	Lockheed Martin
McMillin, S. Naomi.....	NASA Langley Research Center
Midea, Tony.....	NASA Lewis Research Center
Naik, Dinesh.....	Vigyan/NASA Langley Research Center
Narducci, Robert.....	McDonnell Douglas Aerospace
Nelms, Pres.....	NASA Ames Research Center
Nelson, Chester P.....	Boeing Commercial Airplane Group
Owens, L.....	NASA Langley Research Center
Ozoroski, L.....	NASA Langley Research Center
Pao, S. Paul.....	NASA Langley Research Center
Parikh, Paresh.....	TSAB/NASA Langley Research Center
Peavey, Charles C.....	Northrop Grumman
Plencner, Bob.....	NASA Ames Research Center
Pirzadeh, Shahyar.....	Vigyan
Princen, Norm.....	McDonnell Douglas Aerospace
Putman, Lawrence E.....	NASA Langley Research Center
Re, R.....	NASA Langley Research Center
Reuther, James.....	NASA Ames Research Center/RIACS
Rivers, Melissa B.....	NASA Langley Research Center
Saladino, Anthony J.....	Dynacs Engineering Co.
Sawyer, W. C.....	NASA Langley Research Center
Schuster, Ernie.....	McDonnell Douglas Aerospace
Shieh, Chih Fang.....	McDonnell Douglas Aerospace
Shields, B.....	NASA Langley Research Center
Shin, Jaiwon.....	NASA Lewis Research Center
Siclaris, Michael J.....	Northrop Grumman
Smith, Brian.....	NASA Ames Research Center
Phillip, T.....	NASA Ames Research Center

South, J.	NASA Langley Research Center
Stephens, D.	NASA Langley Research Center
Sundaram, P.	McDonnell Douglas Aerospace
Thomas, James L.	NASA Langley Research Center
Tinetti, Ana F.	Eagle Aeronautics, Inc.
Tu, Eugene	NASA Ames Research Center
Unger, Eric	McDonnell Douglas Aerospace
Vatsa, V.	NASA Langley Research Center
Veitch, Lisa C.	NASA Langley Research Center
Vijgen, Paul M.	Boeing Commercial Airplane Group
Waggoner, Edgar	NASA Langley Research Center
Wahls, Richard A.	NASA Langley Research Center
Wilhite, A. W.	NASA Langley Research Center
Wilson, Douglas L.	Boeing Commercial Airplane Group
Wing, D.	NASA Langley Research Center
Wood, Richard	NASA Langley Research Center
Wyatt, Greg	BCAG High Lift Aerodynamics
Yaghmaee, S.	Boeing Commercial Airplane Group
Yaros, Steven F.	NASA Langley Research Center
Yetter, J.	NASA Langley Research Center
Zang, T.	NASA Langley Research Center
Zuniga, Fanny A.	NASA Ames Research Center

HSR AERODYNAMIC PERFORMANCE STATUS AND CHALLENGES

HSR Aerodynamic Performance Technology Management Team

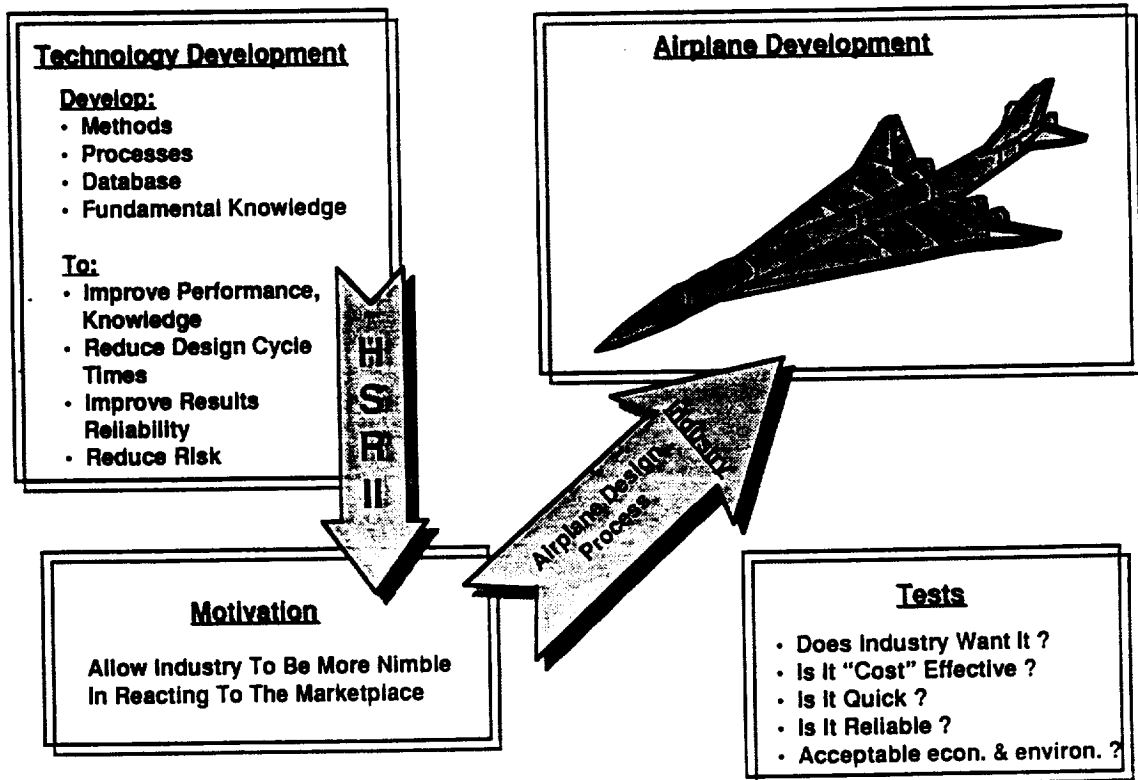
**Bill Gilbert, NASA LaRC
Tony Antani, McDonnell Douglas
Doug Ball, Boeing
Rob Calloway, NASA LaRC
Phil Snyder, NASA ARC**

**Presentation at First Configuration Aerodynamics Workshop
NASA Langley Research Center, Virginia
February 27, 1996**

Presentation Outline

- Introduction
- Aero impact on HSR
- Goals and Targets
- Progress and Status
- Remaining Challenges
- Summary

HSR Technology Development Charter



ROAD AHEAD IS STEEPER & SLIPPERY!

- **Aeroperformance has delivered on promises to date**
- **Future gains will be more difficult and will require excellent teamwork within Aero and in HSR**
- **Materials/Structures & Propulsion have encountered major problems in achieving needed gains**
 - Aero is being asked to provide more help in meeting the takeoff noise goals
- **As a result, pressure on aero to do even better will increase!**
 - We'll be squeezed to get every last drop of performance possible!
 - But we must maintain our confidence level in the performance gains we predict

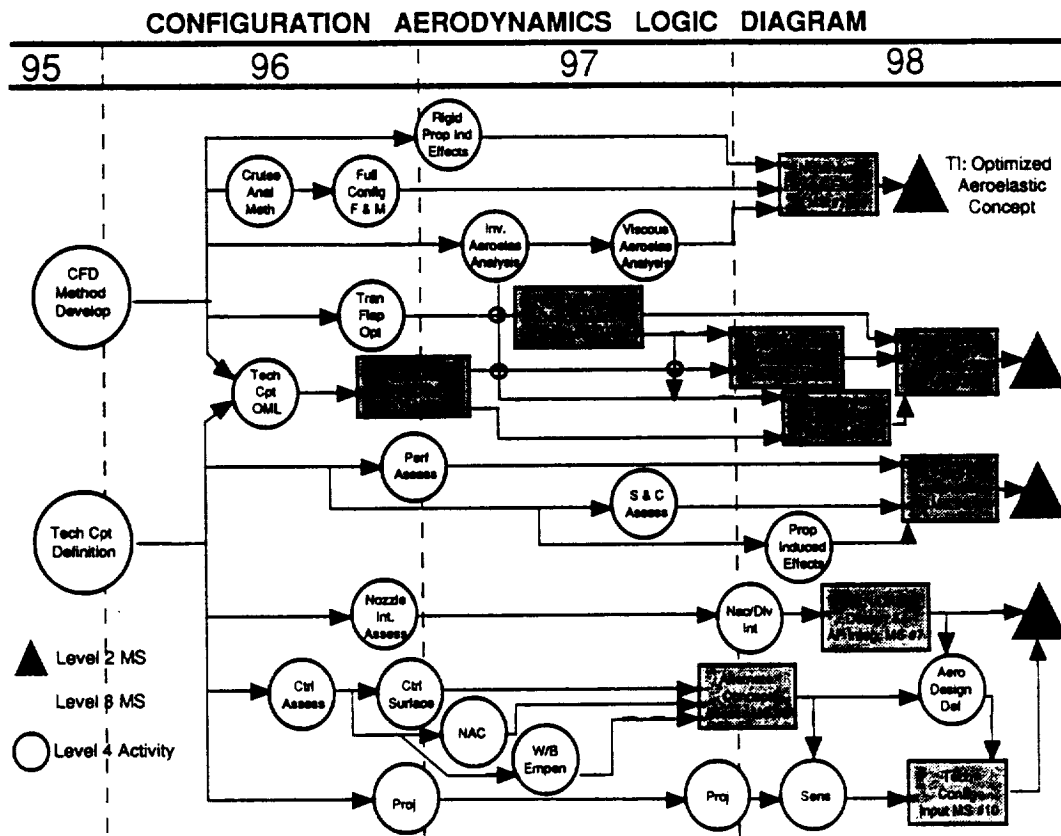
Aerodynamic Performance Objectives & Impact

Develop and validate design & analysis methods & database to:

- **Maximize low speed and cruise performance with acceptable S&C; help reduce community noise**
 - **Impacts on TOGW:**
 - **1-count drag reduction: 7K lbs @M2.4; 1K lbs @ M0.9**
 - **10% increase in highlift L/D gives about - 1.5 dB at C/B.**
 - **SLFC potential large gain(8%!), if feasible**
- **Provide good F/Q in a certifiable, safe airplane with low noise ops capability - essential to ensure viable, flyable product**
- **Soften sonic boom - goal feasible, not validated yet**

GOALS AND TARGETS

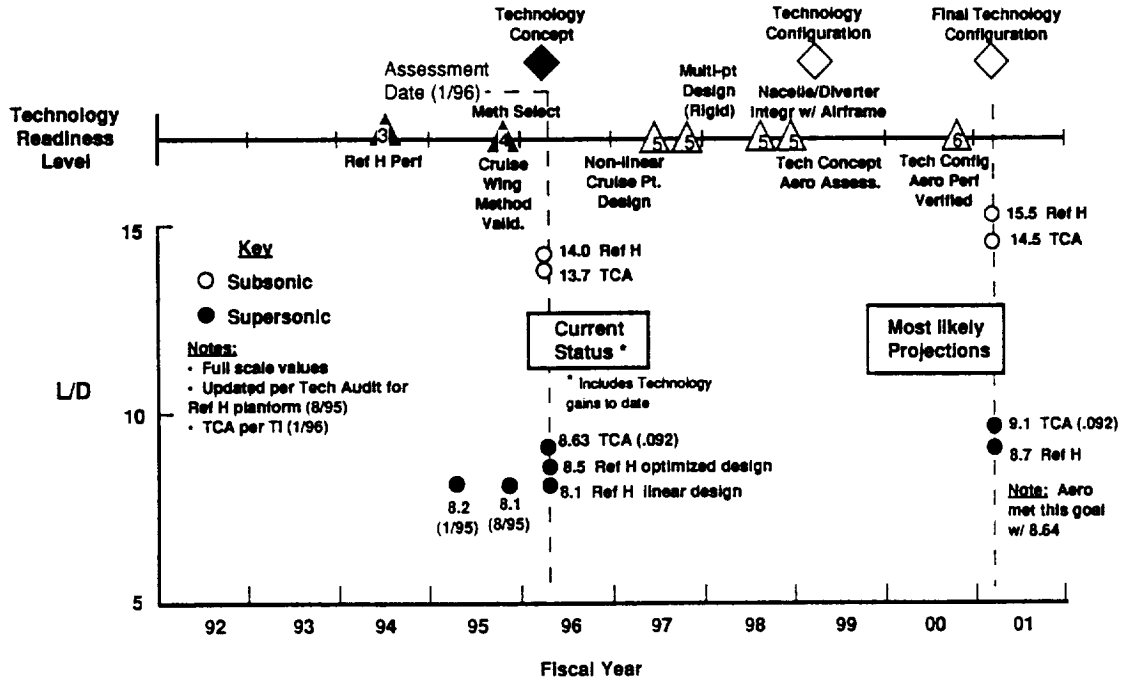
DON'T LOSE SIGHT OF THEM



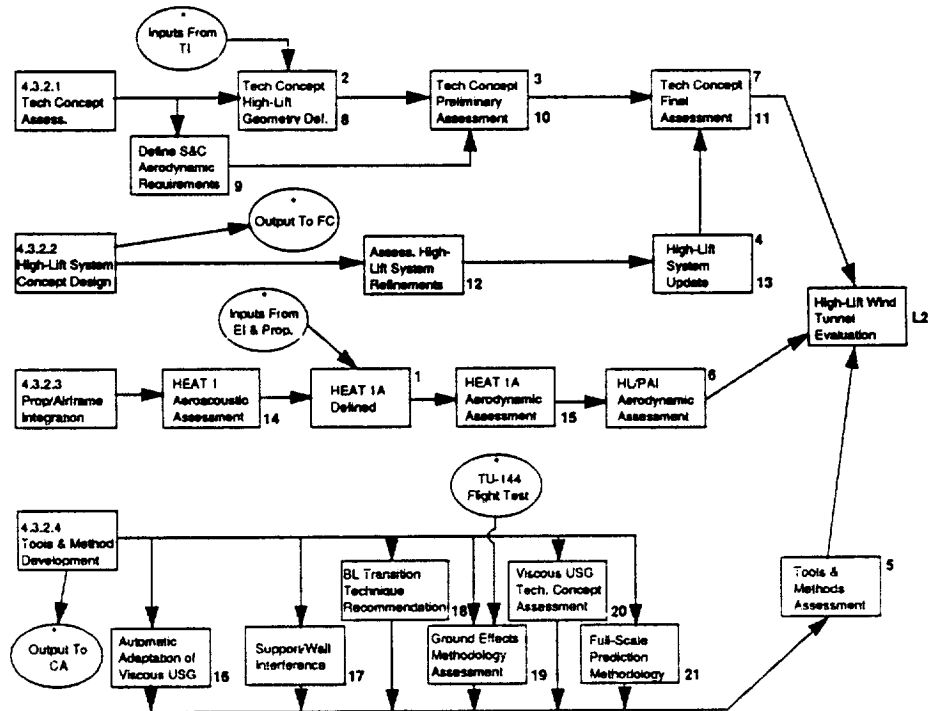


Aerodynamic Performance Configuration Aerodynamics

Technical Performance & Technology Readiness Level



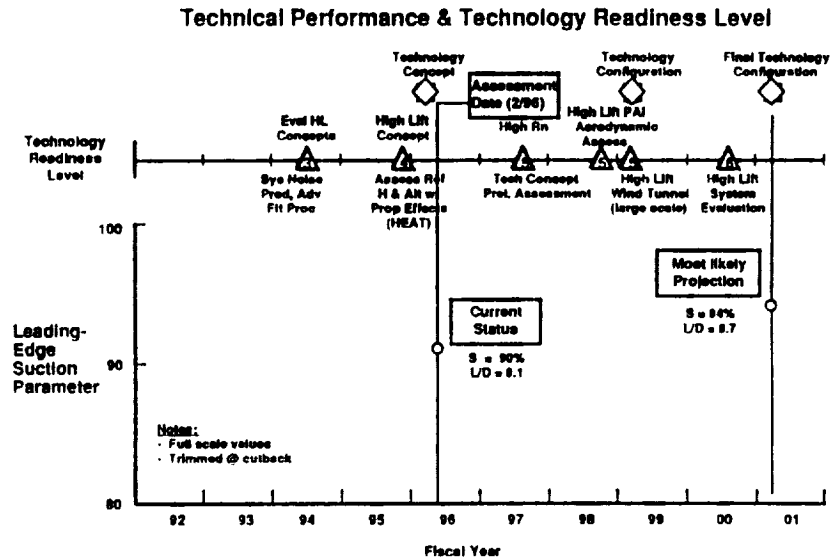
4.3.2 High Lift Technology Logic Flow Diagram



Note: Number at upper corner is Level 3 milestone number.
 Number at lower corner is Level 4 milestone number.
 * Interfaces with other program elements described in sections 3.14-15.



High Lift Technology Metrics



Progress and Status

Configuration Aerodynamics - Developed database to satisfy Level 2 milestone “Ref H Assessment”; validated nonlinear aero optimization methods and a large aerodynamic performance gain via optimization.

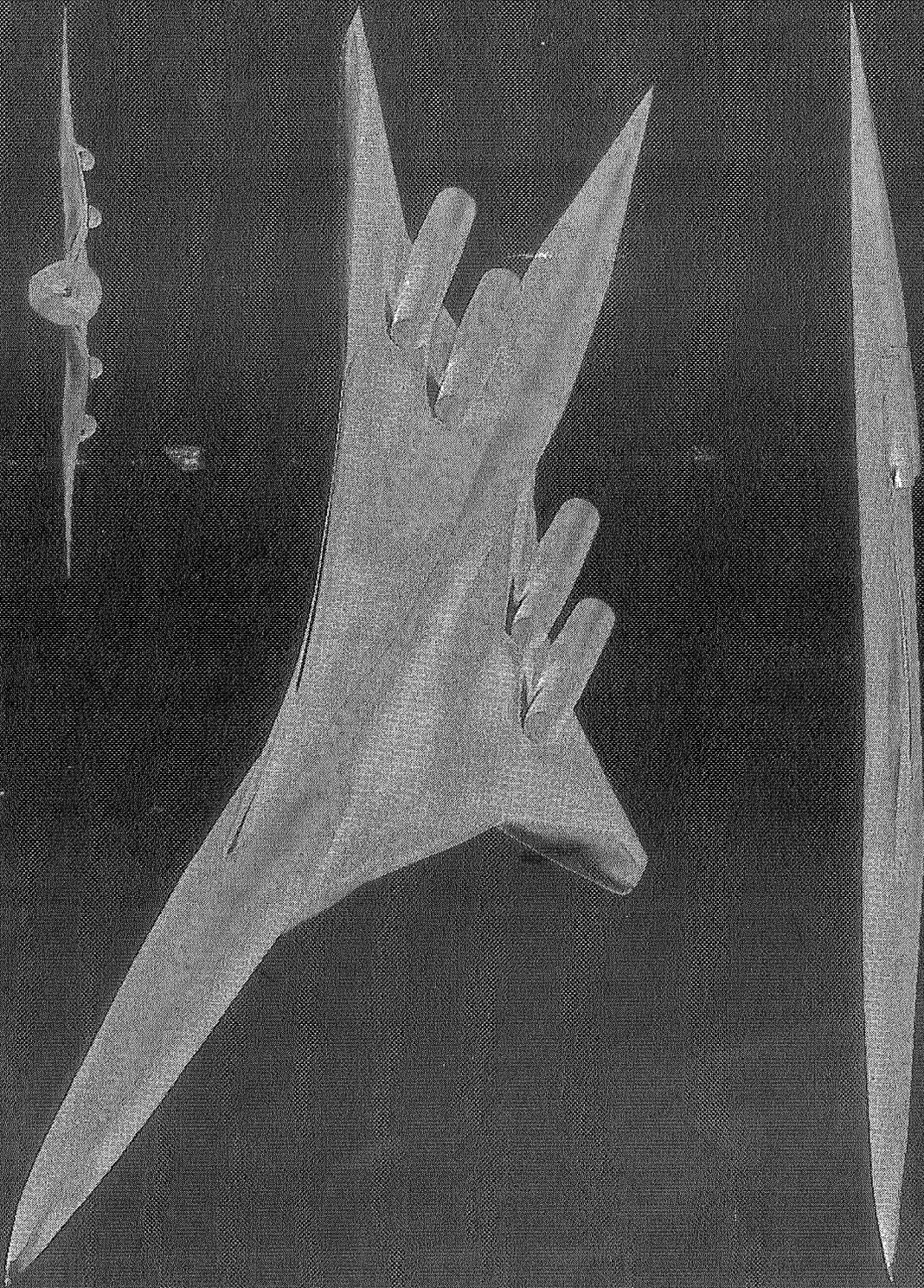
High Lift - Downselected to preferred high-lift system concept; satisfied Level 2 milestone for HEAT 1 aeroacoustic tests.

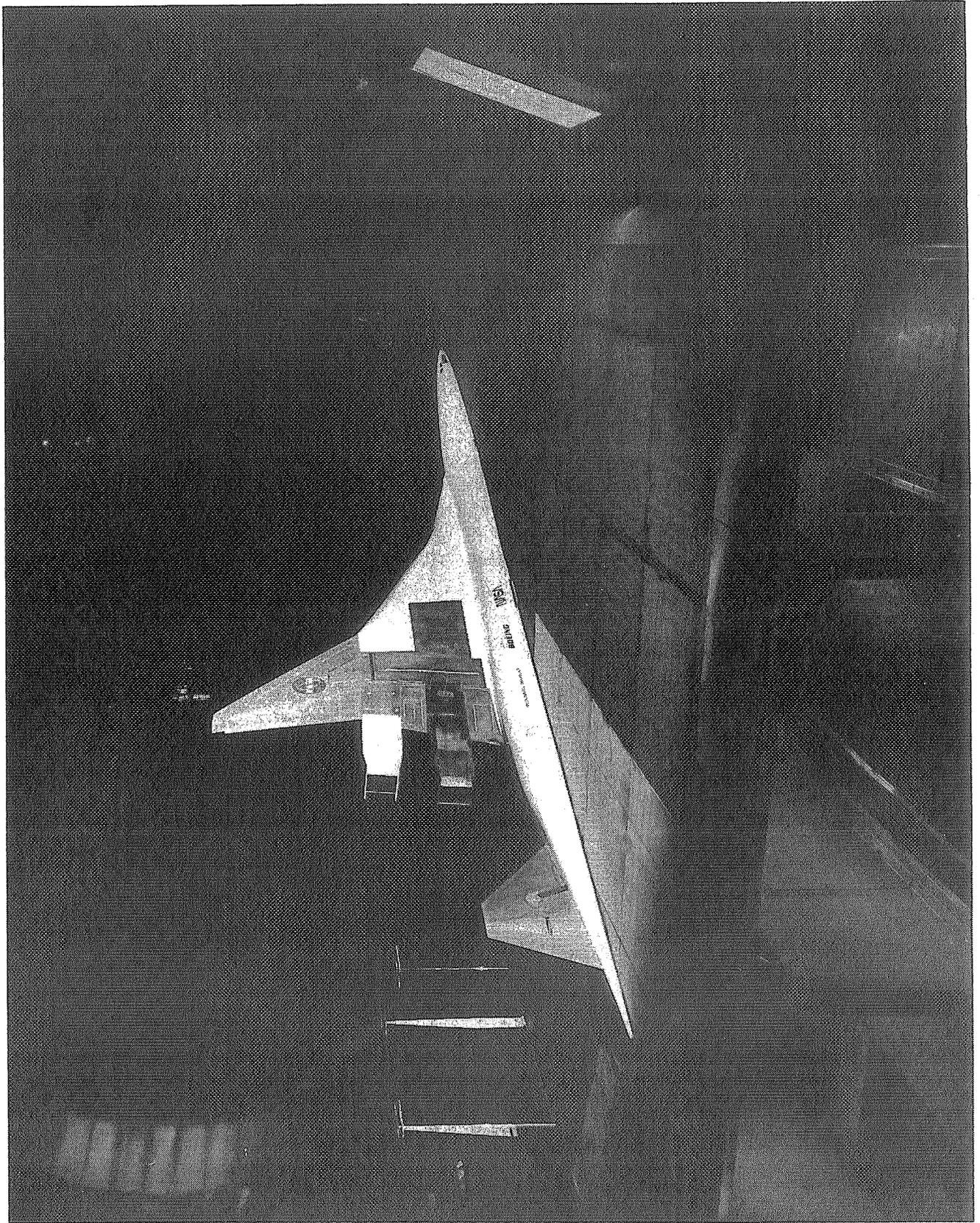
Sonic Boom - Achieved boom softening goals and acquired exceptional flight data for boom propagation methods validation.

SLFC - Transition prediction methods transferred to industry; SLFC flight experiment developed and underway.

Flight Control - Developed excellent full-envelope simulation and conducted piloted assessment of Baseline configuration

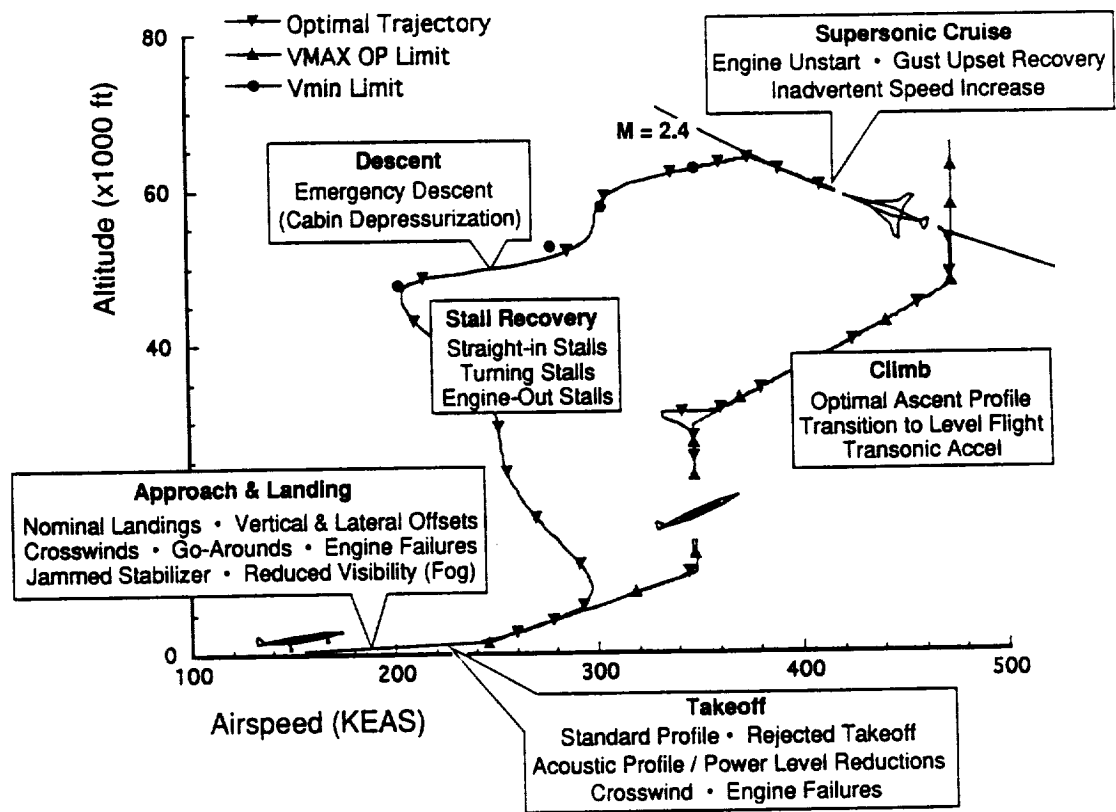
BOEING W27 CONFIGURATION: AIRPLANE $M = 2.4$ $CL = 0.12$







Ref. H Flight Regimes and Maneuver Tasks Examined



REMAINING CHALLENGES

- **Increase Performance gains**
 - within resources available
 - realizable in integrated vehicle
- **Reduce Uncertainties**
 - expected full-scale performance
 - confidence in design methods/concepts

**CONFIGURATION AERODYNAMICS DESIGN:
GEOMETRY SHAPING ALLOCATIONS BY DISCIPLINE**
Drag reductions projected for aero design at Mach 2.4

Performance:
9 to 10 counts drag reduction

Propulsion-Airframe Integration:
2 to 3 counts drag reduction

Empennage:
2 to 3 drag counts reduction

Payoff is Major:

- Performance gain gives weight savings equal to payload:
Potential 16 drag count reduction = 80-100K lbs reduction
in TOGW !
- Any additional saving expected to provide design margins for
risk reduction

...But the road to improvement has challenges:

- Must simultaneously maintain good transonic performance
- Optimization techniques must include full configuration
- Aeroelastic effects must be accounted for
- Outside trades usually make the job more difficult (i.e.
nacelle, empennage, landing gear bump size increases, etc.)
- Parasite drag penalties



CONFIGURATION AERO CHALLENGES

- Find the right complementary roles for NASA and industry to get best affordable technology into methods and airplane concepts while ensuring good, robust integration of these methods and concepts into the industry HSCT design capability.
- Begin to focus on best methods(narrow the field) to allow maturing them and improving their robustness, speed, and utility.
- Attach “belly buttons” to each key deliverable and hold them accountable for development and reporting -- within available resources -- don’t micromanage.

HIGH LIFT CHALLENGES

- **Increased Performance**
 - **Leading edge suction increase to 94% (that's a bunch!)**
 - **Accomplish gain with smaller/lighter system on TCA**
- **Reduced Uncertainty**
 - **Full scale Rn**
 - **Realistic system and aircraft geometry**
 - **Propulsion effects**

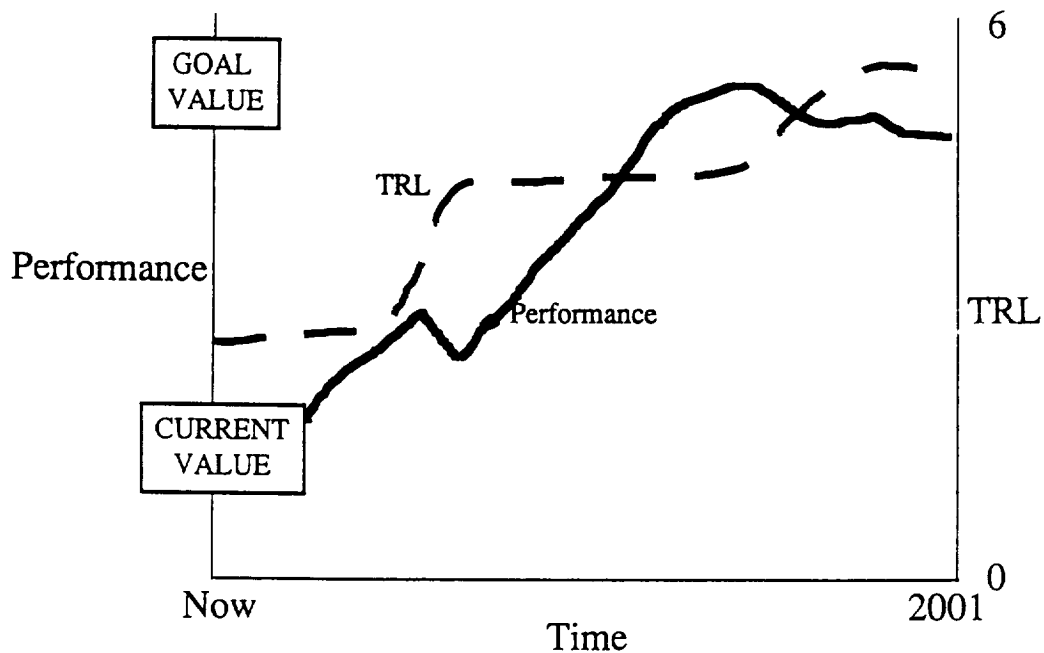
FLIGHT CONTROL CHALLENGES

- **Develop flight control laws to handle large spectrum of flight dynamics and the propulsion/flight control integration in HSCT.**
- **Help define right balance of inherent stability vs. control power for an HSCT.**
- **Continue providing high-fidelity look at the flight performance of the integrated technology baseline for HSR.**

OTHER KEY CHALLENGES

- **Limited resources -- tighter for Aero now**
- **Limited supercomputing time --**
 - **NAS oversubscribed (essential to use other supercomputing platforms where possible)**
 - **Essential for HSR AERO goals**
- **Wind tunnel facilities**
 - **availability and schedules**
 - **most effective use (quantity & quality)**

IMPORTANCE OF TECHNOLOGY READINESS AND PERFORMANCE



SUMMARY

- **Great progress to date. Thanks from the TMT.**
- **While we are developing the technology, we must learn to operate as the HSR Team versus the Ames, Langley, Douglas, or Boeing Team.**
- **Each ITD team should play to the strengths of team members as you execute your plans.**
- **We must plan our work to be achievable within the time and resources available -- and then manage the effort accordingly -- watch products versus expenditures.**
- **We must understand and address the real vehicle integration and operational constraints -- need good real-time interaction with TI and other ITD's.**
- **When we finish the HSR Program, U.S. industry should have the best HSCT design capability in the world....not NASA, but industry.**

CONFIGURATION AERODYNAMICS

Past - Present - Future

Richard Wood, NASA LaRC
Shreekant Agrawal, MDA
Dan Bencze, NASA ARC
Bob Kulfan, BCA
Doug Wilson, BCA

NASA, LaRC
February 27, 1996

The Configuration Aerodynamics (CA) element of the High Speed Research (HSR) program is managed by a joint NASA and Industry team, referred to as the Technology Integration Development (ITD) team. This team is responsible for the development of a broad range of technologies for improved aerodynamic performance and stability and control characteristics at subsonic to supersonic flight conditions. These objectives are pursued through the aggressive use of advanced experimental test techniques and state of the art computational methods. As the HSR program matures and transitions into the next phase the objectives of the Configuration Aerodynamics ITD are being refined to address the drag reduction needs and stability and control requirements of High Speed Civil Transport (HSCT) aircraft. In addition, the experimental and computational tools are being refined and improved to meet these challenges.

The presentation will review the work performed within the Configuration Aerodynamics element in 1994 and 1995 and then discuss the plans for the 1996-1998 time period. The final portion of the presentation will review several observations of the HSR program and the design activity within Configuration Aerodynamics.



MISSION

- Advance the HSCT aerodynamic performance, stability and control, and propulsion airframe integration technologies in the flight regime outside the terminal control area.
- Maintain close continuous technology integration with other High Speed research airframe and propulsion technology elements.

The mission of the Configuration Aerodynamics (CA) Integrated Technology Development (ITD) Team has two parts; first, it is to develop and improve aerodynamic performance, stability and control and propulsion airframe integration technologies for flight conditions outside the terminal control area and second, is to maintain close continuous coordination and technology integration activities with other HSR teams. Specific teams that the CA ITD coordinates with are the Propulsion Airframe Integration Working Group, Stability and control Working Group and the Technology Integration, High Lift, Flight controls, Inlet and Nozzle ITD Teams.



ORGANIZATIONAL AND TECHNICAL DIVERSITY

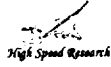
THE CONFIGURATION AERODYNAMIC TEAM:

- NASA - LaRC and ARC
- Industry - Boeing and McDonnell Douglas Aerospace
- L-M, N-G, Dynacs, Eagle, Vigyan, CSC,
AS&M, RIACS, DEI, Microcraft, Sterling...
- Academia - Princeton, Old Dominion, George Washington

TECHNICAL RESPONSIBILITIES:

- Aerodynamic Design
- Aerodynamic Performance
- Stability and Control
- Propulsion/Airframe Integration
- Computation Fluid Dynamic Tool Development
- Experimental Fluid Dynamic Tool Development
-
-
-

In support of the teams mission, the CA ITD has developed a diverse organizational technical team which is responsible for developing a broad range of technologies. The diversity of the team is critical to ensure that all possible technologies are considered within the program. As indicated above the diverse technical responsibilities requires that efficient teaming occur and that multi-use tools be employed to maximize the resources available to the team. An area of particular concern is aerodynamic design and performance improvements. This area has been and will continue to be centered around the development of drag reduction technologies and methods for design.



First NASA/Industry HSR Configuration Aerodynamics Workshop

		PCD I MILESTONES							
TASKS	FY	1994	1995	1996	1997	1998	1999	2000	2001
Industry Milestones		Prelim. Concept ▲			Prelim. Config. ▲			Firm Config. ▲	
4.3.1 Configuration Aerodynamics		Cruise Wing Meth. Valid	W/N/D Integ	Alt. Cpt. Data Base	Multi-Pt. Wing/Nac Des	Elas. Des. Meth. Avail	Data Base for Integ Config		
4.3.1.1 CFD Methodology Adaptation		Ref H Perf/Ctrls	Meth. Asses. Select	Prelim Cpt Select	Aeroprop Effects Asses	Prel. Cpt Asses	Integ Tran Perf	Aeroelas Des Meth	
4.3.1.1.1		Cruise Wing Meth Valid	Point Des. Meth. Valid	Vis. Dyn. Stab. Code	Elastic Des. Meth. Avail				
4.3.1.1.2 Configuration Evaluation		Ref H Perf/Ctrls Data Base	Altbody Closure	Pt. Des. Meth Data Base	Multi-Pt. Des. Data Base	Prel. Cpt Asses	Data Base for Integ. Config. ▲		
4.3.1.1.3 Alternate Concept Studies		W/B Des. Data Base	Transonic Flap Data Base	Ref H Dyn Stab Data Base	Aeroelastic Supersonic Sens	Elastic AC Meth. Data Base			
4.3.1.1.4 Propulsion Airframe Integration		Alt. Concept Assessment		Data Base for Ctrls/Planform					
4.3.1.1.5 Aerodynamic Integration Studies		Static Inlet Unstart	N/D Design Integ.	Static Inlet Unstart Method	Inlet Bleed/Bypass Interactions				
		Ref H Inlet Flowfield	Wing Nozzle Jet Interactions	Dynamic Inlet Unstart	Integrated Transonic Perf.				
		Ref H Perf. Asses	Prelim Cpt. Select	Alt. Cpt. Asses	Aeroelastic Wing Shapes	Prelim. Cpt. Asses	Aeroelastic Des. Meth. Valid.		
		W/B Design	Alt. Cpts. Perf. Asses	Ref H S & C Asses	Aeroprop Asses	Aeroprop Asses-II	Technology Risk assess		

The 1994-2001 CA program is outlined above in the milestone chart. The 1994-1995 period was managed according to the Planning and control Document(PCD) I. As shown above, the PCD I plan contained five sub-tasks and 14 milestones which were active for the PCD I period. A major portion of the program in this time period was the assessment of the Reference H configuration which served as the program baseline for technology developments. In addition to the Reference H focus a limited amount of research was directed at Alternate concepts within sub-tasks 3 and 5. The alternate work focused on alternate control effectors for improved stability and control and planform studies for drag reduction.

94 - 95 EXPERIMENTAL RESEARCH

• # of Facilities	5
• # of Models	10
• # of Tests	30
• # of Configurations	600
• # of Data Points	300,000
• # of Enginyears	{ 15 LaRC 8 ARC 4 MDA 4 BCA 2 LKHD

A significant portion of the effort in support of PCD I was an extensive experimental test program as outlined above. The CA ITD made use of 5 wind tunnel facilities; 2 at NASA Ames and 3 at NASA Langley. The test activities produced over a quarter million data points, 70% of those obtained were in support of stability and control and 30% in support of drag reduction. As with all aspects of the CA program, the success of the experimental activity relied on a diverse group of researchers from NASA Langley, NASA Ames, McDonnell Douglas, Boeing, and Lockheed which comprised 33 engineering work years.

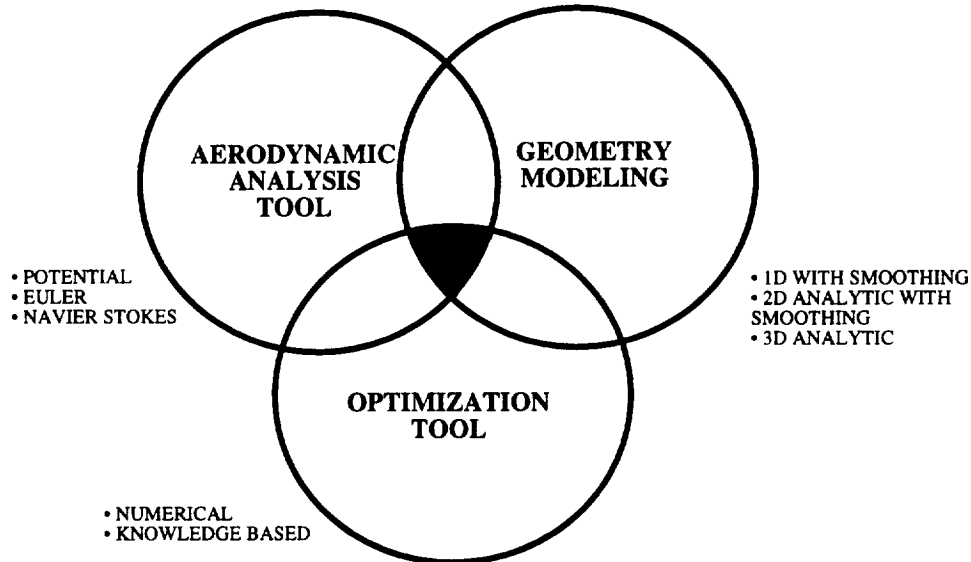
PCD I COMPUTATIONAL TOOLS

<p>INVISCID:</p> <ul style="list-style-type: none"> • AERO2S • WINGDES • TRANAIR • AIRPLANE • CFL3D • FLO57, 67, 87 • TLNS3D • USM3D 	<p>VISCOUS:</p> <ul style="list-style-type: none"> • CFL3D • GCNSfv • OVERFLOW • PAB3D • STUFF • TLNS3D
<p>CONTRIBUTING ORGANIZATIONS:</p> <ul style="list-style-type: none"> • NASA - LaRC and ARC • Industry - Boeing and McDonnell Douglas Aerospace <li style="padding-left: 100px;">- L-M, N-G, Vigyan, AS&M, RIACS • Academia - Princeton 	

Configuration Aerodynamics activity also utilized a wide range of computational tools for both aerodynamic analysis as well as design. Depicted above are the inviscid and viscous computational tools employed and the organizations which have contributed to the development of those tools. The inviscid methods range from the linear tools(AERO2S, WINGDES), to full potential (TRANAIR), to the Euler methods (AIRPLANE, CFL3D, etc..). The inviscid methods have served as the workhorses of the program to date due to the reduced grid generation time and computational resource costs. These methods have proven to be extremely robust and accurate for attached flow conditions, especially at supersonic speeds. The viscous methods employed within CA have also been fairly diverse in technology covering a wide range of solution methodology as well as gridding methodology. It is critical that an adequate assessment of the viscous tools be conducted because the importance of viscous analysis and design is expected to increase significantly during the next program period.

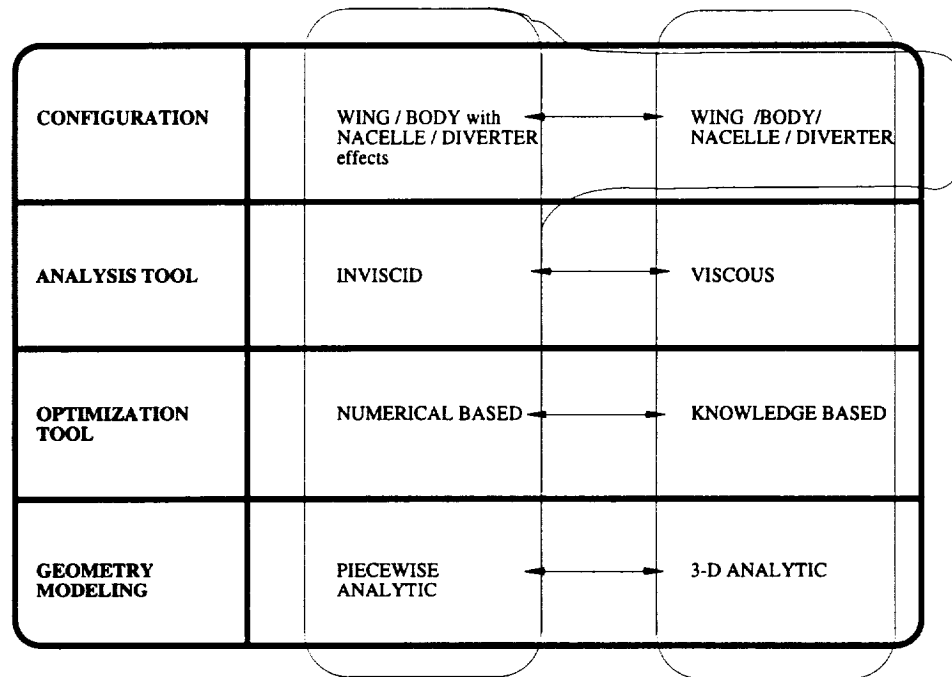
As mentioned previously, aerodynamic design is a major activity within the program. Of the methods listed above the primary aerodynamic analysis tools used in the design process are TRANAIR, FLO57-87, CFL3D(euler and Navier stokes) and OVERFLOW.

DESIGN PROCESS COMPONENTS



The aerodynamic design activities within the Configuration Aerodynamic activity have required the development of design process tools in the three areas indicated above. The areas in which design process tools are being developed are aerodynamic analysis, geometry modeling, and optimization. As previously indicated nonlinear design activities within CA have employed aerodynamic analysis tools which range from full potential to Euler to Navier-Stokes. These tools have been coupled with a variety of geometry modeling packages as indicated and have been driven by numerical optimization tools as well as knowledge driven processes. The success of the design process also requires that the above components be linked within a design concept or philosophy. The selected design philosophy will bias the selection of the aerodynamic analysis tool and the geometric model. This underlying design philosophy will be the driving force in a knowledge based design process.

PCD I AERODYNAMIC SHAPE DESIGN STUDIES



In support of the PCD I design activities the CA ITD executed three distinctly different design processes in performing four nonlinear aerodynamic cruise point shape design studies. The design processes are outlined above, as noted by the circled elements. Each design process contains four elements; the configuration under investigation, the aerodynamics analysis tool, the optimization tool, and the geometric model. As shown in the sketch the design processes used were two numerical based optimization process which utilized inviscid methods with a piecewise geometric model. The primary difference between the inviscid design processes was that one approach used the pressure field from the nacelle/diverters and the second modeled the nacelle/diverters in the design. The third process used was a viscous based design which employed a 3-D analytical geometric model and utilized a knowledge based optimization process to drive the design. As expected each of the four nonlinear aerodynamic cruise point shape design studies produced significantly different shapes yet obtained similar drag reductions from a baseline, linear-theory design.



PCD I TECHNICAL ACCOMPLISHMENTS

- Validation tests of nonlinear supersonic cruise wing/body/nacelle/diverter designs have shown up to 7cts of drag reduction.
- Experimental data show that Reynolds number and model aeroelastic effects are significant at subsonic cruise.
- Advanced experimental test techniques allow for drag measurements with 1/2 count repeatability.
- Advanced computational methods consistently compare with experimental test results within 5%. Have demonstrated cruise drag predictions within 1.5 drag counts of experimental data.

The PCD I period was successful in satisfying the objectives of the program and laying the groundwork for the PCD II period. Specific accomplishments were:

- Validation of the cruise point design processes. Test results verified a 7 count drag reduction.
- Identification of Reynolds number and aeroelastic effects at subsonic speeds.
- Development of advanced test techniques which allow drag to be measured within 1/2 count.
- Development of advanced computational methods with experimental accuracy.

PCD I MILESTONES	TECHNOLOGY CONCEPT SELECTION					
	Engine Cycle Selection	Inlet Concept Selection	Nozzle Selection	Config, Definition	Controls Selection	Aero Risk Reduction
MS-1 Design Method Adaptation		●		●		●
MS-2 Analysis Method Adaptation	●					●
MS-3 Wing/Body Design Data Base		●		●		●
MS-4 Ref H Performance and Control Data Base	●			●	●	
MS-5 Transonic Flap Data Base	●			●		●
MS-6 Afterbody Closure Assessment					●	●
MS-7 Alternate Concept Assessment				●	●	●
MS-8 Static Inlet Unstart Assessment					●	●
MS-9 Inlet Flow Field Assessment		●				
MS-10 Nacelle/Diverter Design and Integration		●	●	●		●
MS-11 Wing/Body Design		●		●		●
MS-12 Ref H Aerodynamic Performance and S&C Assessment				●	●	
MS-13 Alternate Control Concepts Assessment				●	●	●
MS-14 Preliminary Concepts Assessment Criteria	●	●	●	●	●	●

In addition to the technical accomplishments listed in the previous figure the CA activity also contributed to the definition of the Technology Concept Airplane(TCA). Shown above are the 14 active milestones during the PCD I period and their relationship to 6 critical decision gates in defining the TCA. The chart shows that CA activities and the technology developed played a significant role in the TCA development process, CA technology was especially evident in defining the configuration layout and the control effectors.

PCD II MILESTONES

FY	1996	1997	1998	1999
Program Milestones	Technology Concept		Technology Concept Aerodynamic Assessment	Technology Configuration
Level II Milestones	Reference Configuration Evaluated		Optimized Aeroelastic Concept	Technology Configuration Defined
Level III Milestones		Nonlinear Cruise Pt Design	Rigid Multi-Pt. Des. Method Nacelle/Diverter Integration Viscous Aeroelastic Analysis	Rigid Viscous Multi-Pt. Des Prop. Induced Effects Elastic Inv. Multi-Pt. Des. Aero. Design Opt. Capability
4.3.1.1 Nonlinear Rigid and Aeroelastic Analysis Method	Cruise Anal Method Select	Inv Aeroelastic Analysis	Rigid Prop Induced Effects	Viscous Aeroelastic Analysis
4.3.1.2 Aerodynamic Design Optimization Capability	Def. Of OML Wing Thickness Body Shaping	Nonlinear Cruise Pt Design	Rigid Multi-Pt. Des. Method	Rigid Viscous Multi-Pt. Des Elastic Inv. Multi-Pt. Des. Aero. Design Opt. Capability
4.3.1.3 Nacelle/Diverter Design and Airframe Integration	Assess Inlet Flow Constraints	Assess Inlet Integration	Nozzle Int. Assess	Nacelle/Diverter Integration
4.3.1.4 Technology Concept Assessment		Aerodynamic Performance	Initial Stability and Control	Prop. Induced Effects
4.3.1.99 Task Planning and Coordination	PCD 2 Inputs CA Workshop Mid Year Review	PCD 2 Updates End of Year Review	Mid Year Review PCD 2 Updates End of Year Review	Mid Year Review End of Year Review

The next phase of the HSR program will cover the time period of 1996-1998. This period will be governed by the Planning and Control Document (PCD) II and will be referred to as the PCD II period. The HSR program will redirect its focus over the next three years from the Reference H configuration to the Technology Concept Airplane. In support of this focus, the program has been rebaselined and the Configuration Aerodynamics ITD has restructured its program as indicated above. The PCD II program has been restructured into 4 technical sub-tasks and one planning sub-task. The CA program major deliverables are captured by the 8 level 3 milestones listed above. As noted in the milestones chart 6 of the 8 level 3 milestones are related to design tool development and drag reduction studies. The remaining 2 milestones support the assessment of the TCA and development of an aeroelastic analysis tool.



First NASA/Industry HSR Configuration Aerodynamics Workshop

PCD II WBS

4.3.1.1 Nonlinear Rigid and Aeroelastic Analysis Method

- 4.3.1.1.1 Rigid Full Configuration Force and Moments
- 4.3.1.1.2 Inviscid Aeroelastic Analysis
- 4.3.1.1.3 Viscous Aeroelastic Analysis
- 4.3.1.1.4 Rigid Propulsion Induced Effects

4.3.1.2 Aerodynamic Design Optimization Capability

- 4.3.1.2.1 Nonlinear Cruise Point Design
- 4.3.1.2.2 Rigid Multi-Point Design Method Formulation
- 4.3.1.2.3 Rigid Viscous Multi-Point Design
- 4.3.1.2.4 Elastic Inviscid Multi-Point Design

4.3.1.3 Nacelle/Diverter Design and Airframe Integration

- 4.3.1.3.1 Nacelle/Diverter Integration

4.3.1.4 Technology Concept Assessment

- 4.3.1.4.1 Aerodynamic Performance
- 4.3.1.4.2 Stability and Control
- 4.3.1.4.3 Propulsion Induced Effects

4.3.1.99 Task Planning and Coordination

Depicted above is the work breakdown structure(WBS) for the CA PCD II period.



PCD II GOALS

Approach:

- To acquire a comprehensive experimental and computational aerodynamic performance, stability and control data base for the HSR Technology Concept, adapt and validate point design methods and multidisciplinary design optimization methods, design and assess alternate concepts, adapt and validate methods for multi-point aeroelastic design of airframes.

Deliverables:

- Aerodynamic data base for HSR Technology Concept.
- Validated aerodynamic analysis methods for HSCT concepts.
- Validated cruise-point and multi-point aeroelastic design methods.
- Validated aerodynamic analyses and design method for propulsion airframe integration.

The CA activity has identified drag reduction as the highest leverage technology contribution towards the development of an economically viable HSCT. Based upon this fact the program is heavily biased in this direction, as indicated above. The approach to be used in the PCD II period is similar to that in PCD I, the CA activity will rely heavily on experimental activity for design validation and for TCA assessment. The design activities will include the development of technologies for point design and multi-point design including the effects of aeroelastics.

The key deliverables during the PCD II period will be the assessment of the TCA, validation of design methods, including PAI design tools, and the development of advanced aerodynamic analysis methods which account for aeroelastic effects.

DESIGN ISSUES

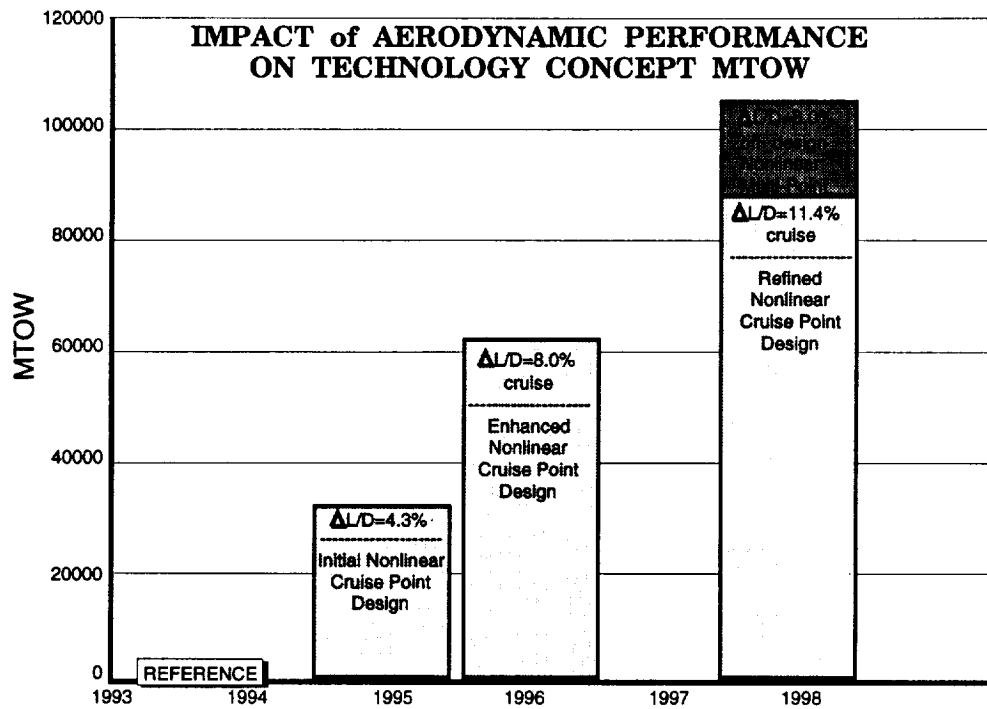
Critical Technologies

<u>Configuration</u>	<u>Test Techniques</u>	<u>Computational Methodology</u>
• Wing Shape and Volume	• Support Interference	• Efficient and Adaptive Gridding
• Fuselage Shape and Volume	• Rn Effects	• Structural Modeling
• Empennage Shape and Sizing	• Transition Fixing	• Power and Pnuematic Simulation
• Control Effector Design	• Aeroelastic Assessment	• Global/Analytic Design Variables
• Nacelle/Diverter Shape and Integration	• Foce Accounting	• Advanced Turbulence Models
• B. L. Management Techniques	• Measurement Accuracy	
	• Powered Testing	

Impact

- 15 to 18 Cts Drag Reduction from Linear Theory Design
- 87,000 to 120,000 lbs Reduction in TOGW
- Reduced Uncertainty in Transonic and Supersonic Drag Reduction
- Reduced Design Cycle Time
- Impact: Planform Selection, Payload, Vehicle Size, Engine Cycle, Inlet and Nozzle Selection

In the area of nonlinear aerodynamic shape design, there are a variety of critical configurations, experimental test techniques, and computational technologies which must be addressed if a viable design capability and thus a viable HSCT is to be developed. A listing of the most critical technologies are shown above. If the CA ITD is successful, it is expected that a 15-18 count drag reduction is achievable , from a linear theory design, which corresponds to a weight reduction up to 120,000 pounds. Another payoff to the development of these design technologies is a significant reduction in risk to Industry for product “go ahead” as well as a reduction in the design cycle time.



Shown above is a graphical display of the expected L/D improvements and resulting weight reductions associated with the point and multi-point design activities. The chart shows that a 100% improvement in the drag reduction is expected in 1996 over that achieved in 1995. And by 1998 the CA activity is expected to triple the drag reduction over the 1995 level. This level of success is critically dependent upon highly effective teamwork and a sharing of all drag reduction technologies developed within the program. The design activity is also highly dependent upon the development of advanced test techniques in the areas of aeroelastics, Reynolds number effects and transition assessment.

PCD II EXPERIMENTAL ACTIVITY

Model Number	WBS	Model	Facility	Description
1	4.3.1.2	Transonic and supersonic flow field rake	UPWT, 16'	1.7% W/B/N w pressures
2	4.3.1.2	Tech Cpt Baseline	UPWT	1.7% W/B/N w pressures
3	4.3.1.2	Tech Cpt Nonlinear Point Design	UPWT	1.7% W/B/N w pressures
4	4.3.1.2	Tech Cpt Multi Point Design	UPWT, 16'	1.7% W/B/N/Flaps w pressures
5	4.3.1.2	Tech Cpt Full Config Design	UPWT, 16'	1.7% W/B/N/Emp w pressures
6	4.3.1.2	Tech Cpt Multi-Point Design, MP 1	UPWT, 16'	1.7% W/B/N/Flaps w pressures
7	4.3.1.2	Tech Cpt Multi-Point Design, MP 3	UPWT, 16'	1.7% W/B/N w pressures
8	4.3.1.2	Tech Cpt Multi-Point Design, MP 4	UPWT, 16'	1.7% W/B/N/Flaps w pressures
9	4.3.1.2	Tech Cpt Aeroelastic, Supersonic	UPWT	1.7% W/B/N w pressures
10	4.3.1.2	Tech Cpt Aeroelastic, Transonic(shape #1)	16'	1.7% W/B/N w pressures
11	4.3.1.2	Tech Cpt Aeroelastic, Transonic(shape #1)	16'	1.7% W/B/N w pressures
12	4.3.1.3	N/D combinations (3 sets)	UPWT	Nacelle and diverters
13	4.3.1.3	Nozzle boattail drag	16'	Nozzles
14	4.3.1.3	2D Nozzles	UPWT	Nozzles
15	4.3.1.3	N/D combinations (3 sets)	UPWT	Nacelle and diverters

In support of the design activity there are a large number of wind tunnel models and test activities scheduled. These models will be used to obtain the necessary data to validate the design activities and the drag reductions obtained. Listed above are the PCD II models for support of configuration and nacelle/diverter design activities. The shaded areas correspond to models that are to be fabricated and tested in 1996. The remaining models are to be designed, fabricated, and tested in 1997 and 1998.



ANALYSIS ISSUES

Critical Technologies

<u>Experimental Aerodynamics</u>	<u>Test Techniques</u>	<u>Analysis Methods</u>
• Supersonic Cruise Drag	• Support Interference	• Viscous Modeling
• Transonic Cruise Drag	• Rn Effects	• Aeroelastic Effects
• Trim Drag	• Aeroelastic Measurements	• Accuracy, Robustness, Efficiency
• Stability and Control	• Transition Modeling	• Powered Effects
• Rn Effects	• Powered Models	• Efficient Gridding
• Power Effects		

Impact

- Reduce Program Risk Due to Uncertainty in Aircraft Performance and S&C may:
 - Size the Aircraft
 - Define Cycle and Planform
 - Limit Payload and Range
- Develop Confidence in Aircraft Performance Prediction Capability
- Understand Methods and Cost for Accurate Data
- Allow Extrapolation to Flight Conditions

The second major area of work within CA for PCD II is the aerodynamic analysis/assessment of TCA. This area of work covers performance, stability and control, and propulsion effects. As with the design area, there are a number of critical technologies in experimental aerodynamics, experimental test techniques and computational analysis methods. The assessment of the TCA will rely heavily upon both advanced experimental studies as well as advanced computational activities. Several areas that will receive close scrutiny from an experimental view will be aeroelastics, boundary-layer tripping and transition, and support interference. On the computational side the program will focus on aeroelastics, turbulence modeling, and efficient gridding. The payoff to these technologies is a reduction in program risk and the improved capability of extrapolating the results to flight.

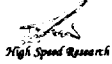


First NASA/Industry HSR Configuration Aerodynamics Workshop

PCD II EXPERIMENTAL ACTIVITY

Model Number	WBS	Model	Facility	Description
16	4.3.1.4	Grit test program	UPWT, NTF	Existing model
17	4.3.1.4	Aeroelastic test program	UPWT, NTF	Existing model
19	4.3.1.4	Tech Cpt aftbody closure	UPWT, 16', NTF	1.7% W/B/N/Emp
20	4.3.1.4	High Sn performance and S&C	NTF	2.2% W/B/N/Emp
21	4.3.1.4	Tech Cpt modular	UPWT, 16'	1.7% W/B/N/Emp
22	4.3.1.4	Tech Cpt powered semi-span	11'	W/B/N/Emp
23	4.3.1.4	Tech Cpt ref semi-span	11'	W/B/N/Emp

In support of the analysis activity there are a large number of tests scheduled for the set of wind tunnel models listed above. These models will be used to obtain the necessary data to assess the TCA and provide the ground based corrections for scaling the wind tunnel data to flight conditions. The shaded areas correspond to models that are to be fabricated and tested in 1996. The remaining models are to be designed, fabricated and tested in 1997 and 1998.

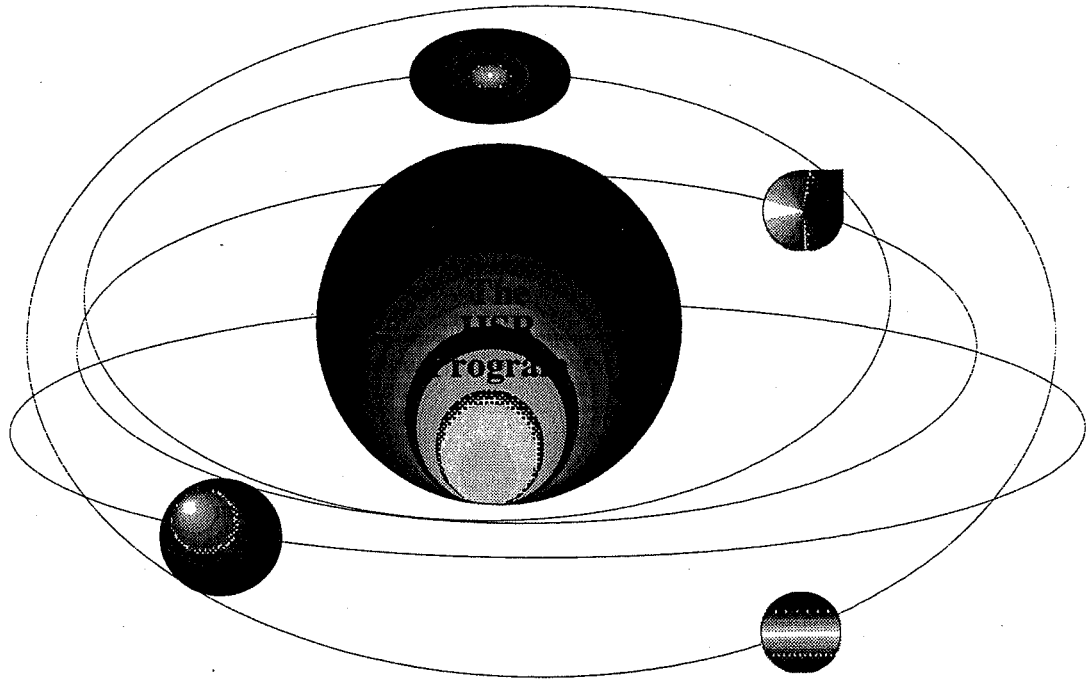


OBSERVATIONS

The previous figures and text discussed the details of the PCD I activity(past) and the PCD II activity (present). The following set of figures will highlight some personal observations from the past and will reflect on the needs of the HSR program now and in the future.



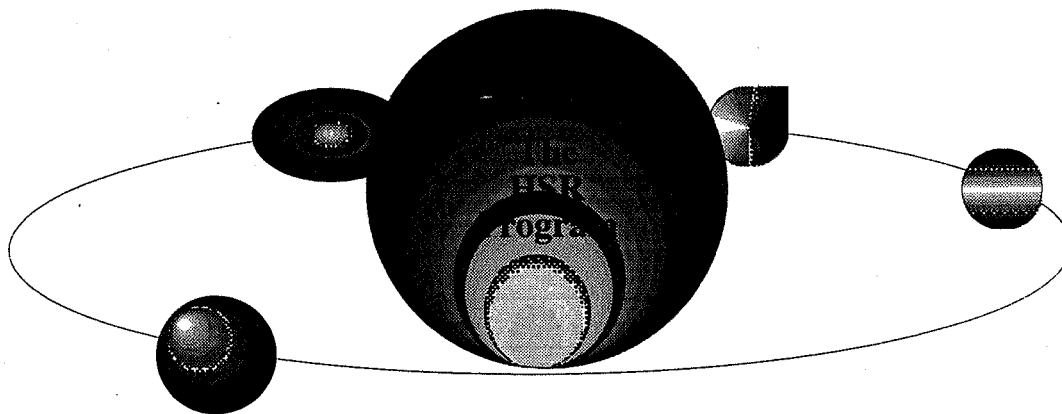
First NASA/Industry HSR Configuration Aerodynamics Workshop



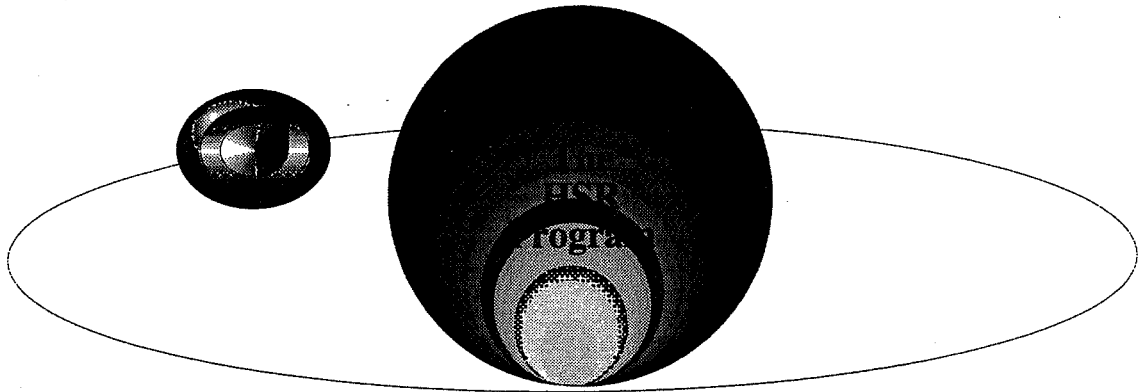
The HSR program, and especially the Configuration Aerodynamics element, has gone through significant change over the past 24 months. In 1994, the CA activity consisted of each organization operating independent of one another within the influence of the HSR program structure. As the program evolved, the CA activity had periods of alignment and misalignment from both a technical and programmatic perspective. The graphic above depicts the 1994 perspective.



First NASA/Industry HSR Configuration Aerodynamics Workshop



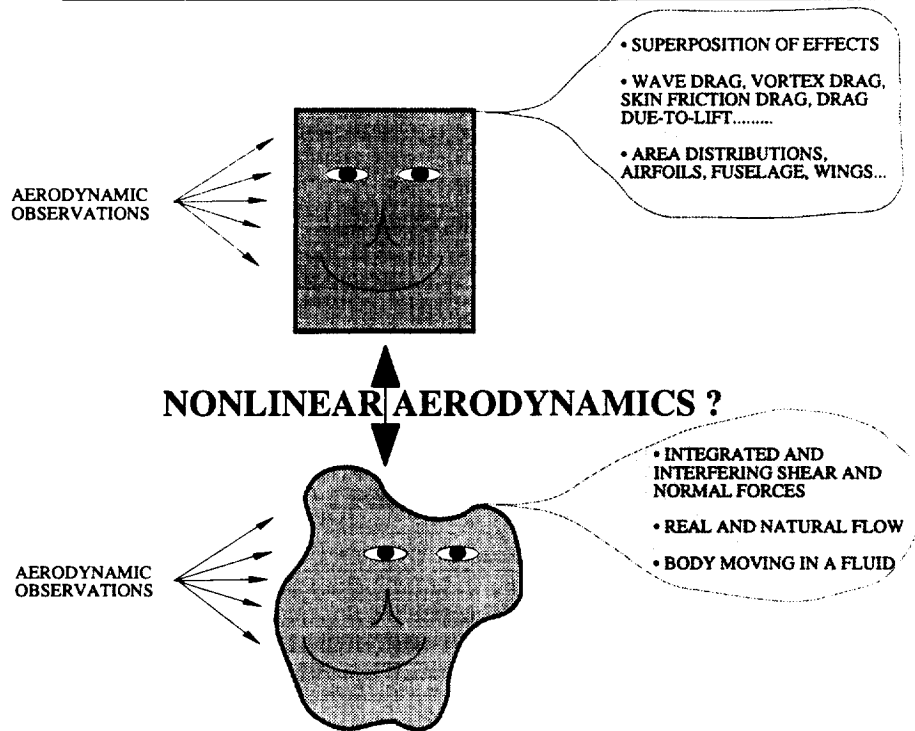
In 1995, the program adopted the PCD format, implemented team work and consensus, and began the use of schedules. These changes brought the focus of CA into alignment with the HSR program and all activities within CA centered around the HSR program. The situation had improved dramatically however it was still less than that required for program success.



The graphic shown above depicts a desirable situation for success within the program. The CA team has a single vision and operational space. This environment must maintain the characteristics of each individual organizations and must operate within the HSR program objectives and policies.

Once the programmatic aspects are achieved the CA ITD can then create a common vision for design activities. The design activity within CA is the prime focus and as such the HSR program is relying heavily on the success of CA.

However, it must be recognized that the feasible design space being investigated by CA can not be characterized by a single design approach within the HSR program but is more likely represented by a family of design approaches which are not physically connected(past). The CA ITD must assess the true character of the design space in order to find success in the drag reduction efforts.



Perhaps the most important question which must be answered is: What are nonlinear aerodynamics? And what does it mean to conduct nonlinear aerodynamic shape design. Shown above are two possible views and answers to this question. Shown on top is the traditional approach in which the explanations are provided in the standard framework and shown below is an atypical set of explanations to the same question. Each of these explanations carry with it bias errors associated with the meaning of the words and the history of the individual. However, if CA is to be successful in reducing the drag through nonlinear design then a common goal must be developed, this requires a common language. The situations of solving a linear problem with a nonlinear method or the solving a nonlinear problem with a linear method must be avoided if progress is to be made.



OBSERVATIONS

- The “REAL” nonlinear drag reduction boundaries must be identified and quantified.
 - >100% aerodynamic thrust is achievable!
 - Are Linear Theory based boundaries relative?

- Multi-Point design activity is critical to understanding the drag reduction potential of this vehicle class.
 - What design requirements are Mach number similar?
 - What performance requirements are Mach number sensitive?

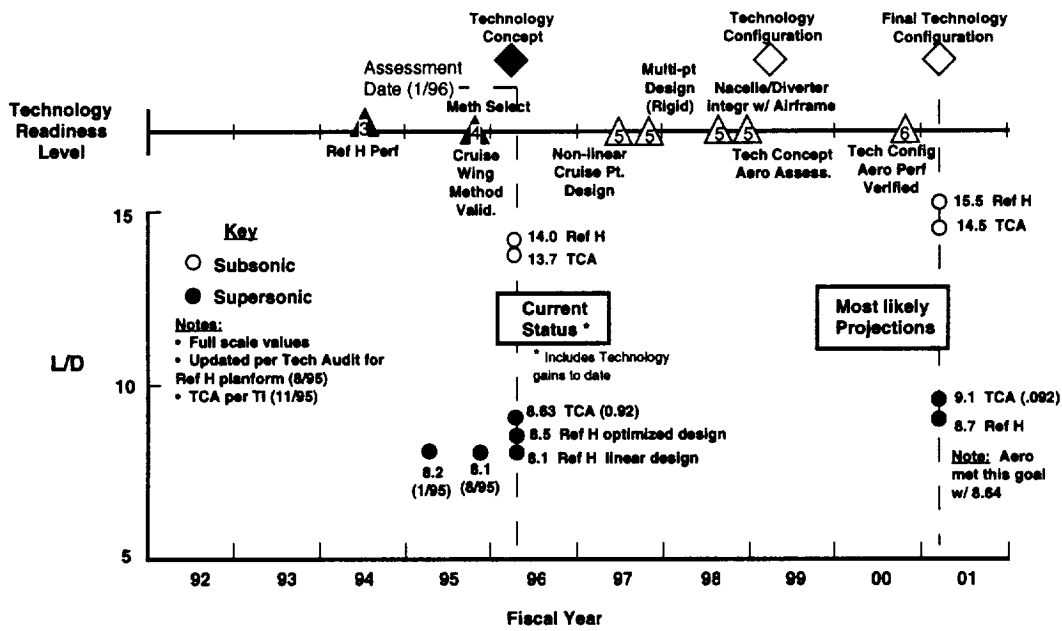
- Aerodynamic technologies for S&C improvements must be pursued.
 - Control effector design opportunities exist!
 - Stability management concepts must be explored!

- Innovation and high risk work must have a home in CA.
 - Boundary layer management for performance and S&C improvements!
 - Base drag management for performance improvements!
 - Fuselage upwash management for performance and S&C improvements!
 - Vehicle volume maximization for performance improvements!

The CA element has created for itself a number of significant technical challenges that require innovative solutions and teaming to be successful. However, before progress can be made there is a need to develop a consistent set of criteria and an understanding of the opportunities available to the CA team. Listed above are several issues which should be resolved and opportunities which must be pursued.

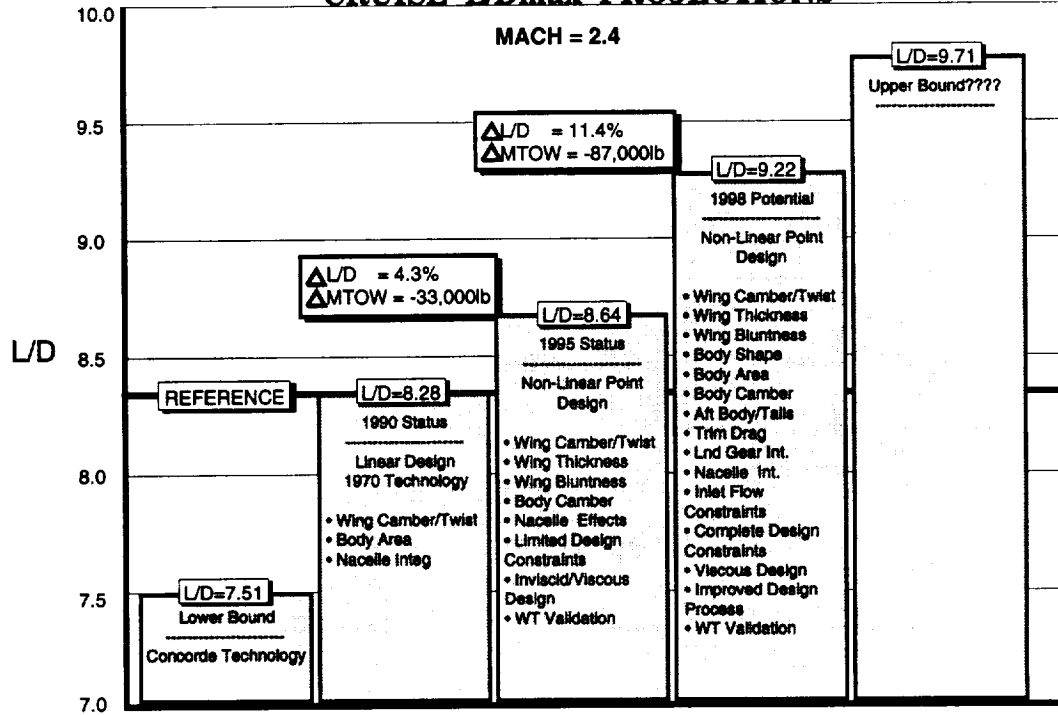


Technical Performance & Technology Readiness Level



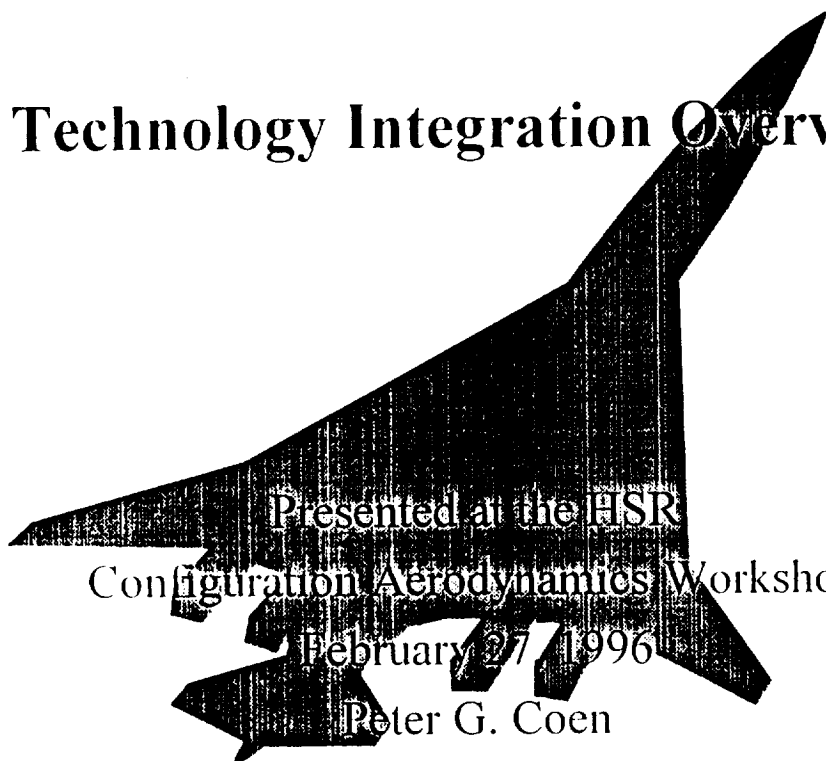


TECHNOLOGY CONCEPT CRUISE L/D_{max} PROJECTIONS





Technology Integration Overview



Presented at the HSR
Configuration Aerodynamics Workshop
February 27, 1996
Peter G. Coen



Presentation Outline

- Technology Concept Airplane Description
- LCAP Overview
- ACE Overview

Purposes of HSR Technology Concept Airplane

Trade Studies and Sensitivities:

- Common base for technology assessment, analysis and testing
- Platform for assessing technology sensitivities, for example, Off-design performance, environmental, operational
- Common base for integrated system level trade studies

Technical Consistency:

- Technology integration
- Technology cost/benefit analysis (prioritization)
- Vehicle level tracking

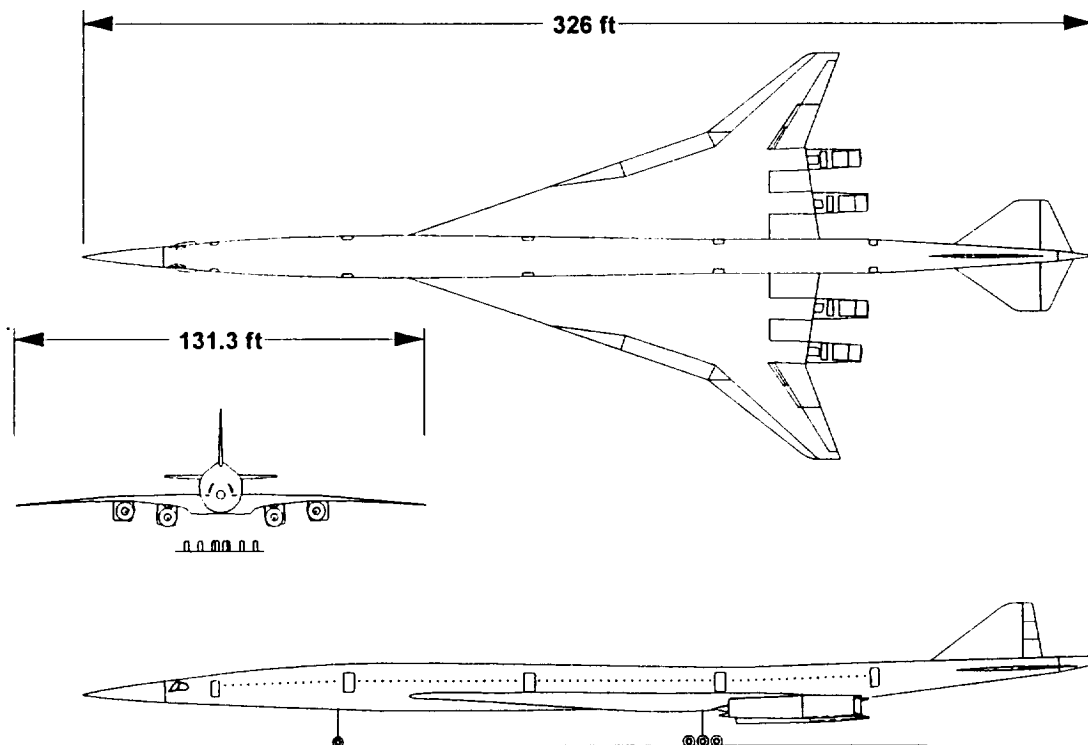
HSR Technology Baselines should be close enough to Industry baselines to ensure technology application



The HSR Technology Concept is:

- Not the latest industry baseline
- Not the vehicle for program economic assessments
- Updated only as required for technology development focus
- Not the EXCLUSIVE vehicle for technology downselects

HSR Technology Concept Airplane



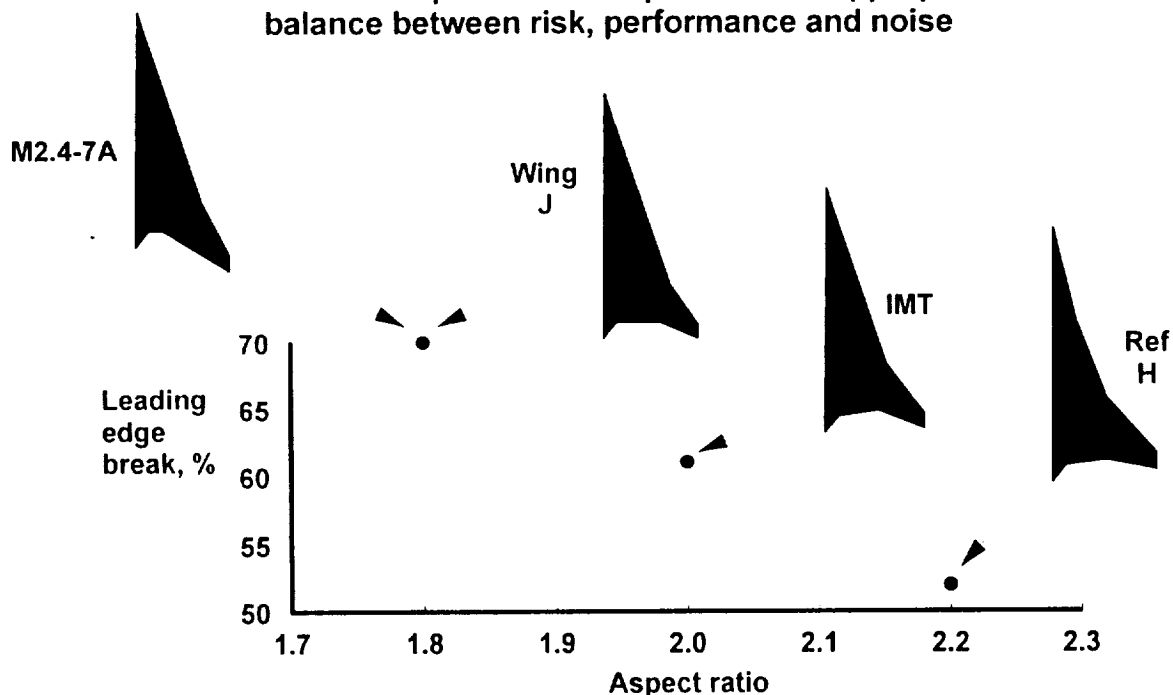


Design Assumptions

- Picked planform from planform studies conducted at Boeing and MDC
- Jointly developed a new fuselage based on MDC and Boeing best practices
- Defined a gear bay that will allow either MDC or Boeing gear concept to fit
- Switch to M3570.80 FCN MFTF
- Use "generic axi-inlet"
- Follow recommendation of Config Aero, Materials & Structures, Flight Deck, Propulsion and Environmental Impact teams

Picked Planform from Planform Studies Jointly Conducted at Boeing & MDC

- Confirmed a relatively flat design space
- Selected a planform that provides an appropriate balance between risk, performance and noise



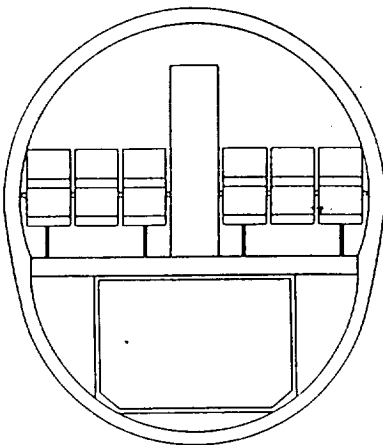


High Lift Concept

- Plain Flap
 - Leading edge flap covers 50% inboard panel and complete outer panel
 - Trailing edge flap covers entire wing span excluding engine cutouts
 - Three outboard trailing edge segments for high lift and control

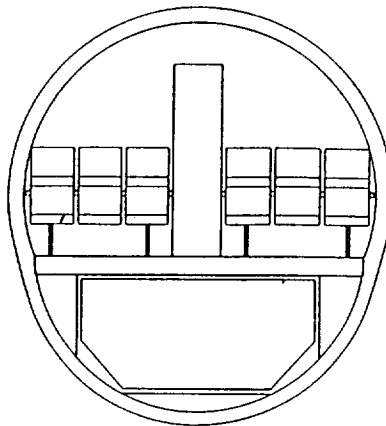
TCA Cross-Section Reflects Best Practices

MDA



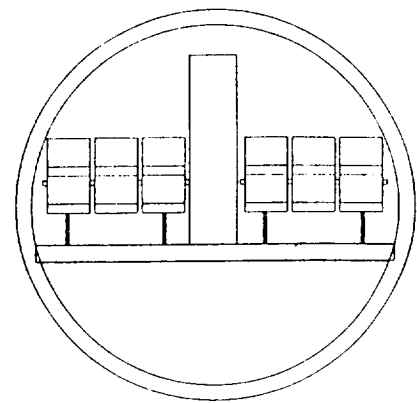
Area: 162.5 sq ft
 Baggage: 6 ft³/Pass.
 Ovalized

TCA



Area: 153.5 sq ft
 Baggage: 5 ft³/Pass.
 Ovalized

BCAG



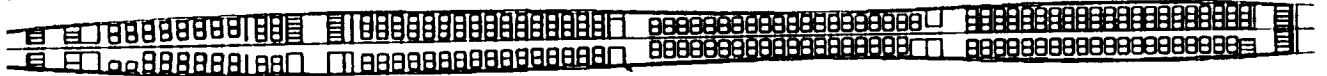
Area: 153.5 sq ft
 Baggage: 4.5 ft³/Pass.
 Circular



Interior Comparison

MDA

Body Length = 334 ft



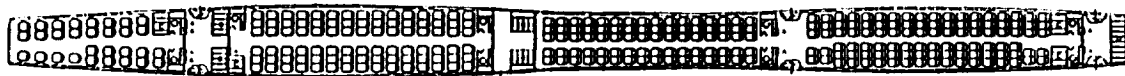
TCA

Body Length = 326 ft



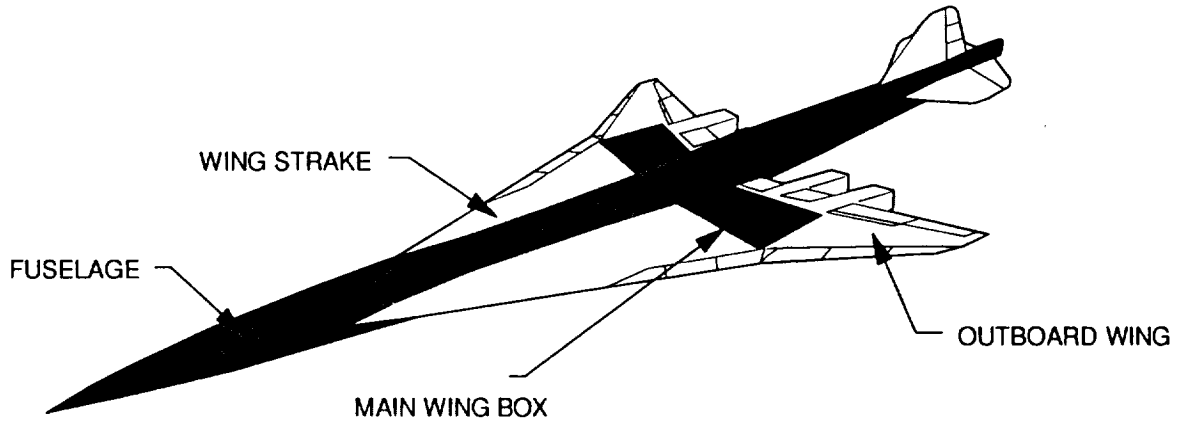
BCAG

Body Length = 314 ft





Structural Choices Made by Materials & Structures



↓ Used for TCA

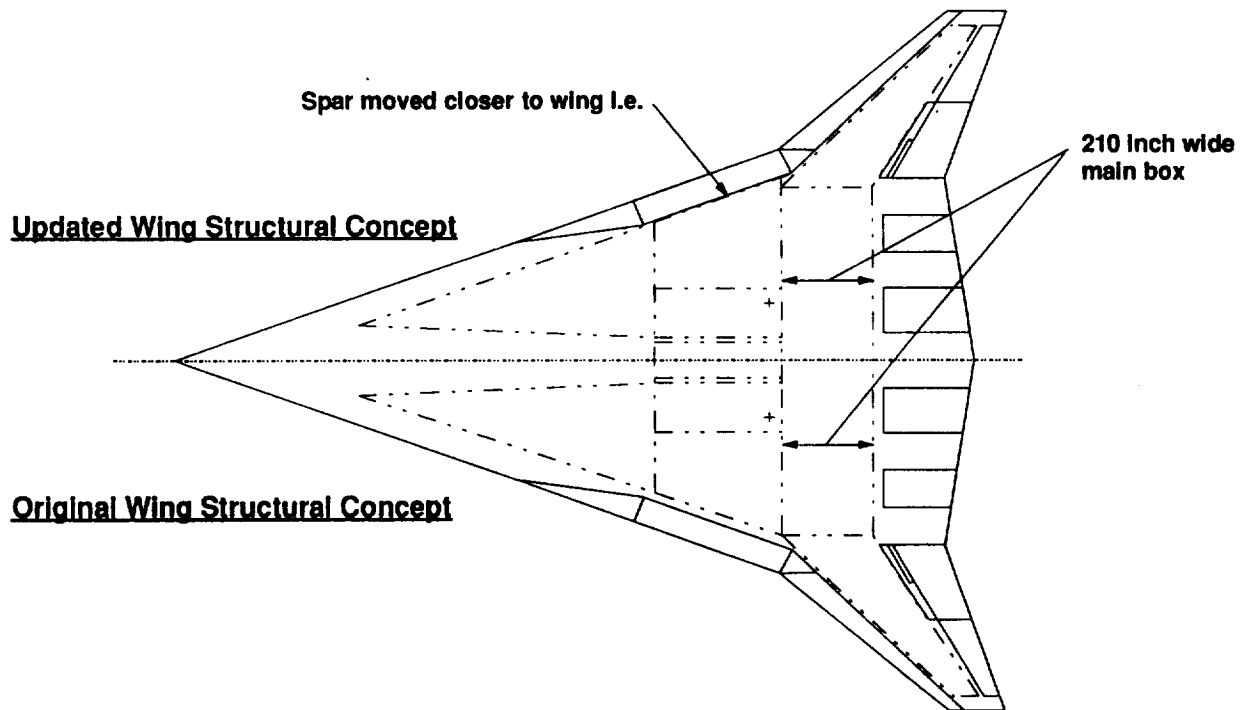
	PRIMARY	ALTERNATE
FUSELAGE	PMC S/S	PMC, TI-PMC and TI SAND
MAIN WING BOX	TI SAND	PMC and SPF/DB SAND
OUTBOARD WING	PMC SAND	
WING STRAKE	PMC and TI-PMC SAND	

Materials & Structures recommendations based on meeting the HSCT weight goal

Materials and Structures will continue research on both primary and alternate



Resolved Wing Structural Concept with Design Integration Trade Study (DITS)

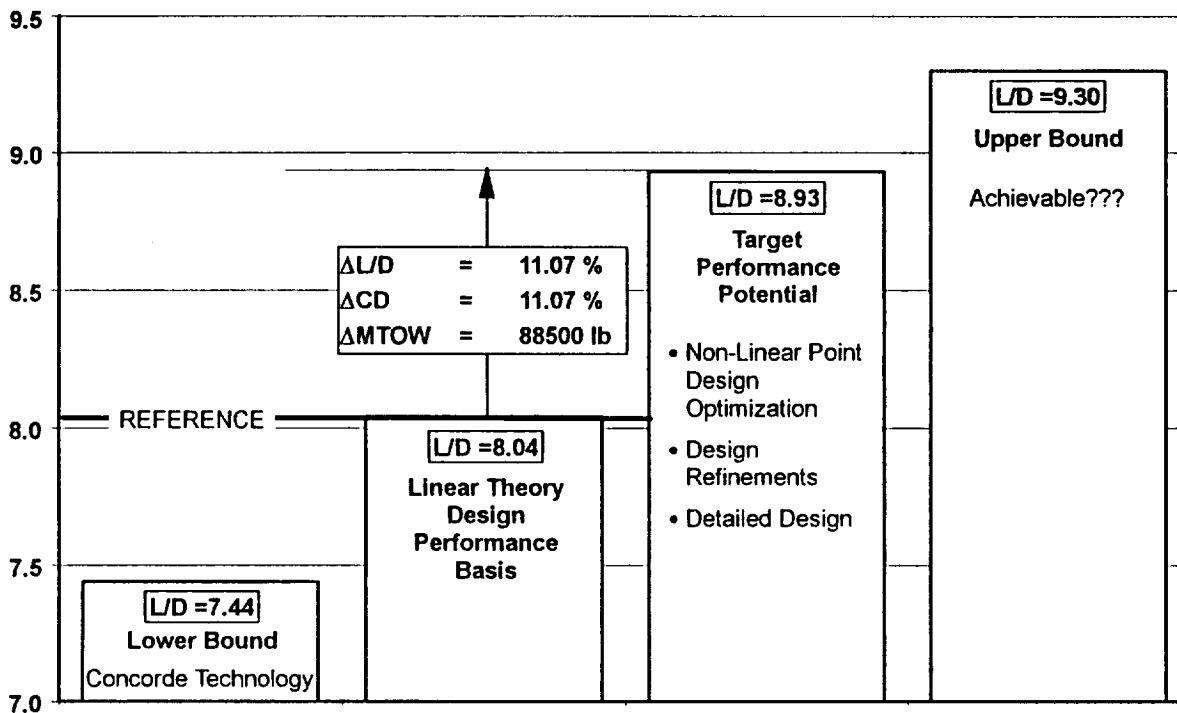




TCA Cruise L/D Projections

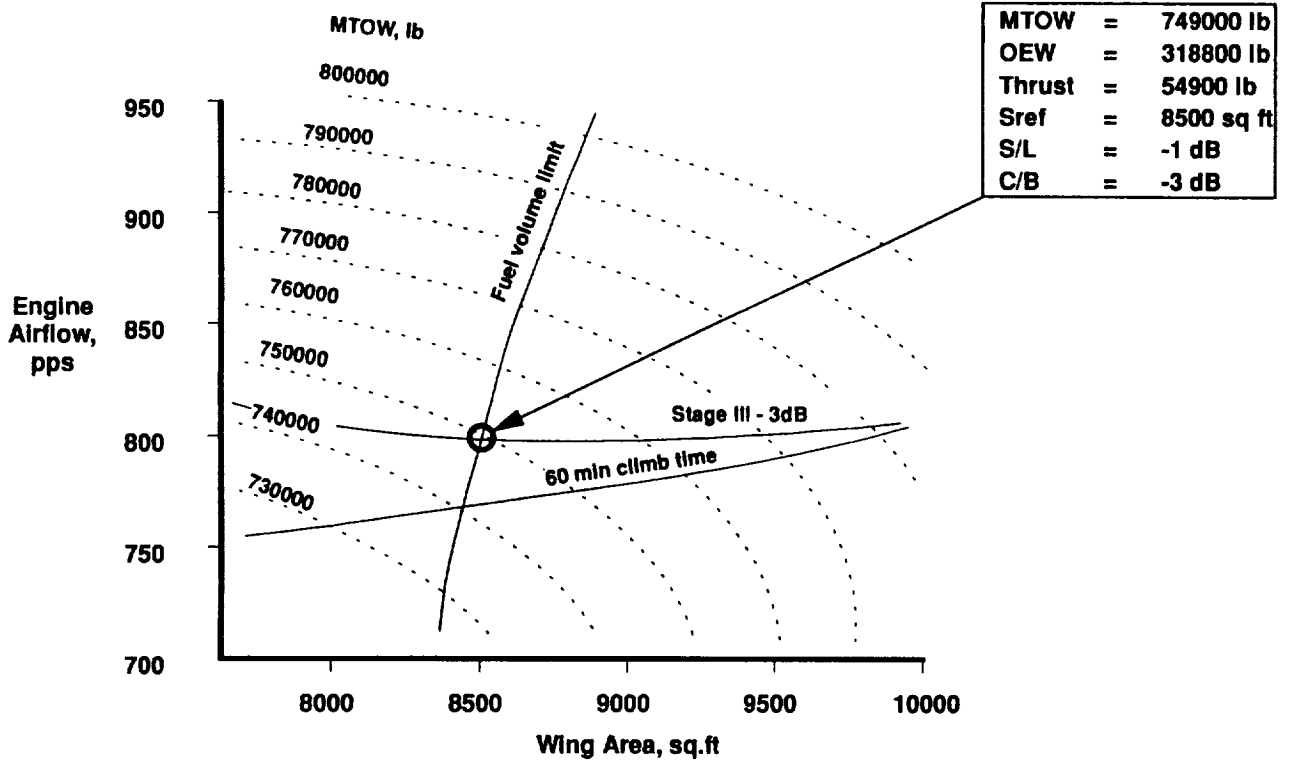
$M = 2.4$

L/D at Cruise



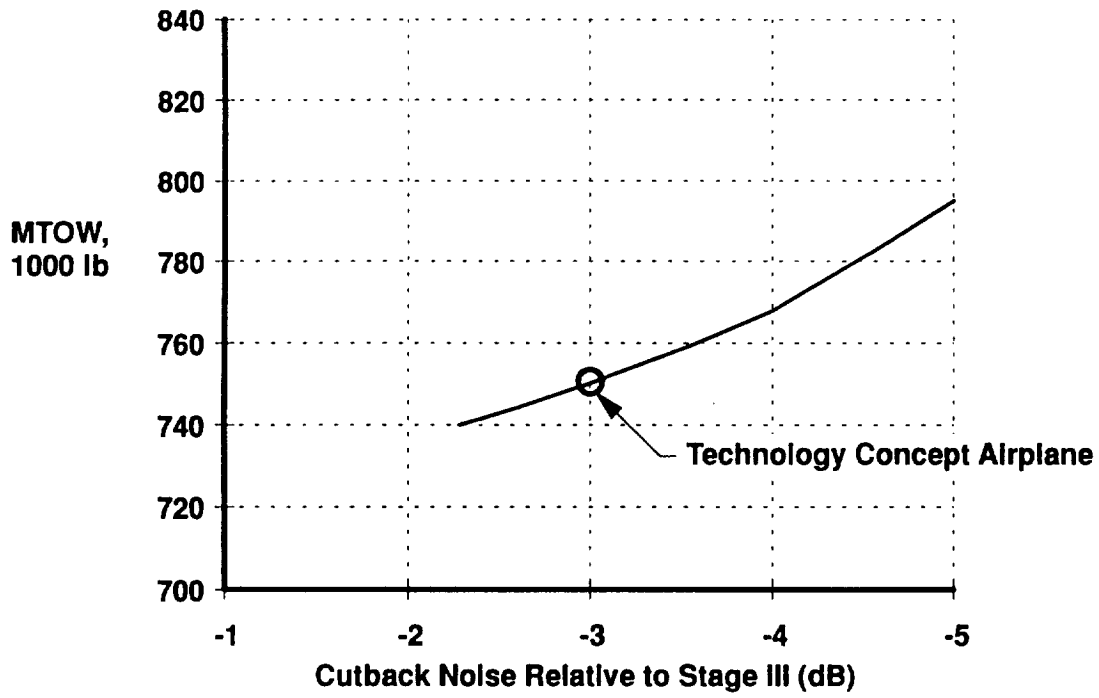


TCA Sizing Chart





Cutback Noise Sensitivity





HSR Technology Concept Airplane

OEW Changes Relative to Interim Technology Baseline

Interim Technology Baseline (sized)	302600 lb
CONFIGURATION CHANGES	+ 7500 lb
• Wing Planform and t/c distribution	
• Body length and cross-section	
TMT RECOMMENDATIONS	+ 13500 lb
• Structural material allowables and techniques	
• Engine cycle and nozzle type	
METHODS ADJUSTMENT	- 4500 lb
• Common weight accounting	
• Common weight methodology	
Technology Concept Airplane (sized)	319100 lb

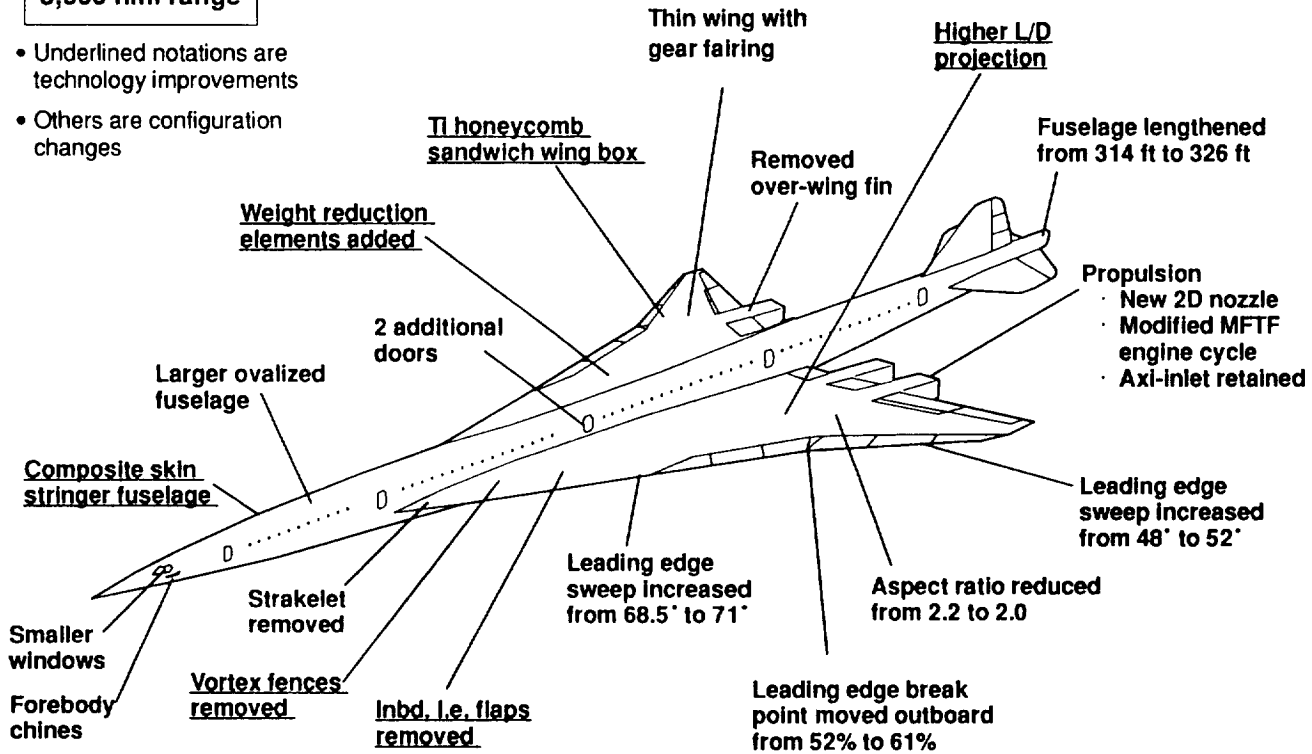


HSR Technology Concept Airplane

Changes Relative to Interim Technology Baseline

300 Passengers
5,000 nmi range

- Underlined notations are technology improvements
- Others are configuration changes





Near Term Plans

- Define OML (Outer Mold Line) by March 1, 1996
- Publish configuration document and data base by April 1, 1996

Longer Term Plans

The TCA will be used to support:

Aerodynamics

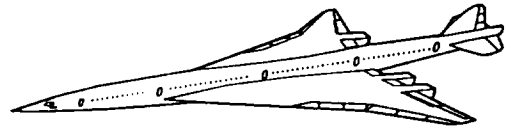
- CFD analysis/optimization
- Wind tunnel testing

Materials & Structures

- Finite element analysis
- Materials trade studies

Technology Integration

- Trade studies
- Technology tracking & assessment





LCAP Overview

- **Objective**

- Consistent evaluation of aft-tail, canard and three surface concepts to determine potential advantages for longitudinal control
- Focus on elastic behavior
 - Structural sizing with elastic loads and flutter
 - Handling and ride qualities
 - Relative MTOW
- Configuration recommendation for continued analysis

- **Approach**

- Parallel studies
 - Reference H based study by NASA with Boeing support
 - Arrow wing based study by McDonnell Douglas



Project Elements

- **Boeing configuration data**
 - External geometry based on 1080-892
 - Structural model (FEM) based on 892STR
 - Weight and mass data (updated during sizing process)
 - Pre - HSR mission ground rules
- **NASA detailed analysis**
 - Rigid and aeroelastic loads
 - linear and nonlinear data
 - Subsonic and supersonic flutter analysis
 - Optimization based structural sizing with strength and flutter constraints
 - Rigid and flexible stability and control derivatives
 - Handling and ride qualities analysis
 - Assessment of control requirements
 - Vehicle performance and sizing



Project Constraints

- **Fixed Configuration**
 - No recamber, rebalance, tail sizing or area rule
- **Longitudinal characteristics only**
- **Limited experimental data for S&C**
 - Little transonic and supersonic with tail
 - Practically no data for canard and 3 surface
- **Assess Control Requirements only**
 - No rigorous control system design
 - Simple control laws applied to facilitate analysis
- **No propulsion-aerodynamic interactions**
- **No operational considerations**
 - ground servicing, LOPA, etc.



Aerodynamic Loads

Linear aerodynamics - USSAERO

- Potential Flow method
 - Compressibility, local Mach effect
 - Wing, body and control surface analysis
- Vortex Wake shed downstream in plane of trailing edge
 - No wake rollup
- Pressures limited to stagnation and suction extremes

Nonlinear aerodynamics - USM3D

- Unstructured Euler method
 - Finite volume, cell centered tetrahedra
- Special boundary conditions for
 - Base areas created by flap, control surface porting

Good agreement with analysis and experiment



Nonlinear Loads Correction

- Euler solutions obtained at known α , δ for all load cases
- Linear solutions obtained at α , δ to match total load from Euler solutions
- Δ loads calculated on the linear solution grid
- Load redistribution applied in aeroelastic trim process

LCAP Load Cases

ID	MACH	Alt (ft)	C.G	n (g's)	L.E. Flap	T.E. Flap	C_L
LX79	2.40	60900	aft	1.0	0	0	.121
LX42	.95	29000	aft	-1.0	10	0	-.219
LX43	.95	20700	aft	2.5	10	0	.382
LX45	.95	37500	aft	2.5	10	0	.816
LX52	1.20	34500	aft	-1.0	10	3	-.177
LX55	1.20	40500	aft	2.5	10	3	.590
LX56	1.20	52000	aft	-1.0	10	3	-.409
LZ25	.50	14000	aft	2.5	26	8	1.051
LZ26	.50	27000	aft	-1.0	40	13	-.725
LZ2X	.50	14000	forward	2.5	26	4	1.051
Lz2Y	.50	27000	forward	-1.0	40	8	-.725



Current Status

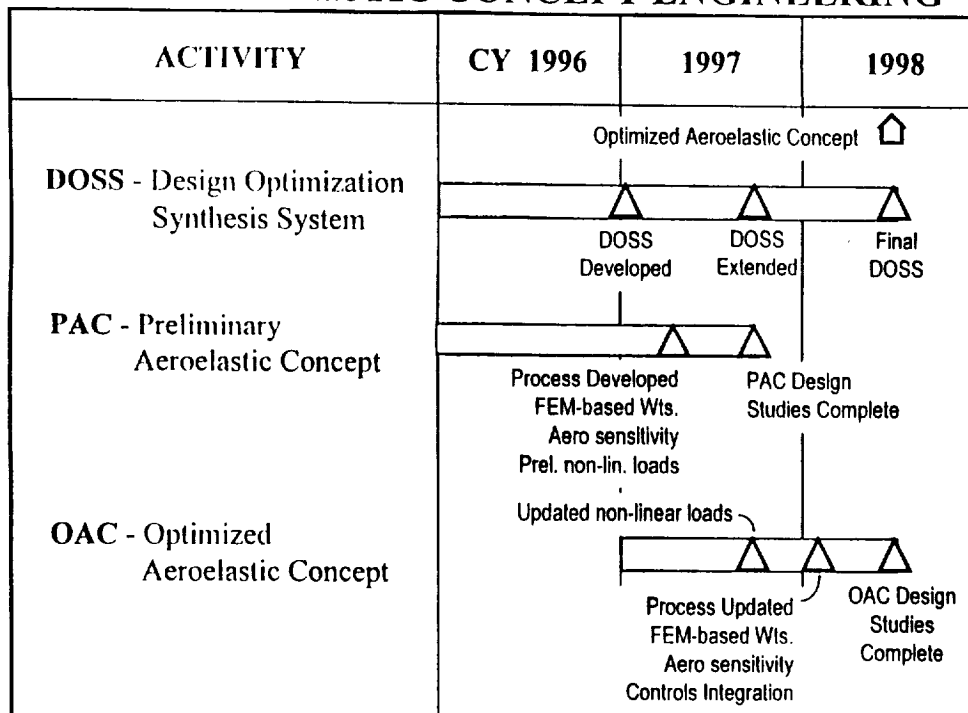
- **Activity scheduled to finish in March**
- **Aft tail configuration**
 - Completed all analysis
- **Three surface configuration**
 - Completed structural sizing with linear loads
 - Completed three cycles of sizing with nonlinear loads
 - Handling and ride qualities analysis in progress
- **Canard configuration**
 - Completed structural sizing with linear loads
 - Completed three cycles of sizing with nonlinear loads
 - Stability and control data ready

Aeroelastic Concept Engineering (ACE) Team Charter

Refine the Technology Concept Airplane (TCA) utilizing integration of aerodynamics, structures, propulsion, controls and aircraft sizing disciplines employing detailed CFD/FEM design tools and selective use of optimization techniques.

- Develop and validate processes/methods/tools to integrate the advanced technology being developed in the key individual disciplines into the aircraft design procedure
 - ensure all key interdisciplinary interactions are accounted for in the design
 - include optimization whenever/wherever feasible
 - leverage, not duplicate, work done in other elements of HSR
- Implement the new process to develop a new design - Optimized Aeroelastic Concept Airplane (6/98, Level II milestone)
- Use the new process to help guide the definition of the HSR Technology Configuration (12/98, Level I milestone)

HSR AEROELASTIC CONCEPT ENGINEERING



HSR ACE Report BKB/960223
Config. Aero. Workshop

February 27, 1996
Page 3

Features of ACE Team Optimization Strategy

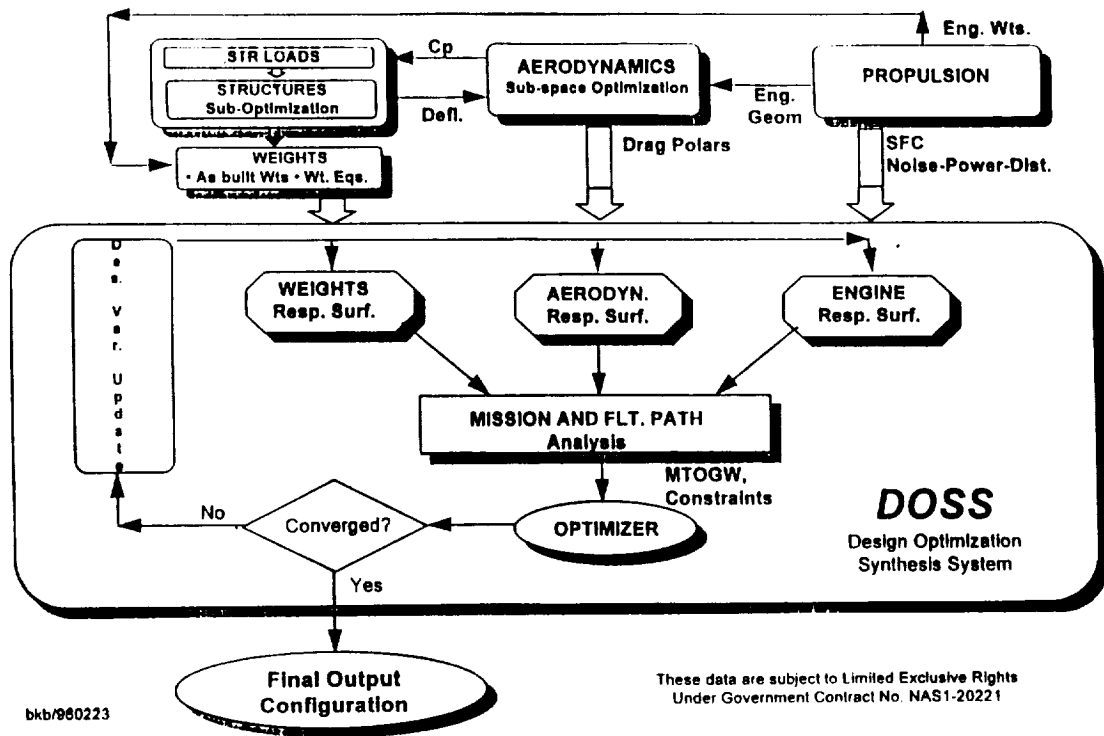
Overall Goals:

- Process accounts for all realistic airplane design constraints, and minimizes TOGW
- Process is practical and reliable
- Process is applicable at the conceptual/advanced design stage as well as at the preliminary design phase
- Process can be modified and augmented to suit specific needs of participating organizations in HSR
- It should be possible to maintain the autonomy of individual contributing disciplines

Strategy Adopted:

- The design process is split into individual contributing discipline groups
- Overall design process is based on exchanging data from the contributing discipline groups
- Individual disciplines work concurrently and maintain autonomy in prescribing procedures and processes to generate data for the design
- At the top level, the system will deal only with global variables - those design variables that have strong interdisciplinary coupling and/or significant impact on the airplane configuration
- Convergence for weakly interacting (local) design variables and the outputs achieved through multi-level iterative process
- Design system will be set up to handle realistic set of constraints

OVERALL ACE PROCESS



bkb/960223

HSR ACE Report
Config. Aero Workshop

These data are subject to Limited Exclusive Rights
Under Government Contract No. NAS1-20221

February 27, 199
Page 6

Major Deliverables from ACE Team

DOSS - Design Optimization Synthesis System

- **Basic system** that integrates data from different disciplines contributing to the airplane design (12/96) - uses "advanced design" level of data in 1996
 - configuration optimization for a fixed flight path (9/96)
 - configuration optimization with optimized flight path (12/96)
 - use system for trade studies during 1997 and 1998
- **Enhancements** to integrate additional variables and FEM & CFD data (in 97 and 98)

PAC - Preliminary Aeroelastic Concept (9/97)

- Process for FEM-based wts, non-linear CFD Aero Performance, non-linear Aero loads
- Design recommendations from optimization of wing thickness/camber/twist distributions starting from TCA FY 96

OAC - Optimized Aeroelastic Concept (6/98)

- Process to include wing-box and planform variables, and aeroservoelasticity (controls effects) using FEM-based wts, non-linear CFD Aero Performance, non-linear Aero loads
- Design recommendations from optimization of wing thickness/camber/twist, planform parameters, engine parameters, and controls parameters starting from TCA FY 96

ACE Team Activities Within HSR

(Funded by WBS 2.1.3)

ACE TO DEVELOP / PERFORM

- Develop DOSS to integrate several disciplines
- Define global design variables
- Develop process to compute sensitivity of drag polars to global variables
- Perform multidisciplinary design studies for PAC and OAC

ACE TO UTILIZE

- Lessons learned from Aerodynamics work (CA & HL) related to the following
 - CFD code accuracy, robustness, efficiency
 - corrections to analysis data from WT tests
 - efficient procedures to incorporate nacelle-diverter effects

ACE / TI TO PROVIDE

- Recommendations on optimum thickness, camber and twist distributions from PAC design studies
- Recommendations on opt. planform parameters, spar locations and engine size from OAC design studies

ACE WOULD LIKE TO COORDINATE

- With Configuration Aerodynamics on multi-point design studies

ACE's Perception of Aero Activities Within HSR

AERO TO DEVELOP / PERFORM

- Procedures to perform aerodynamic contour design optimization for given planform and constraints on spar depth and locations, etc.. Aero methods/processes will be developed for such things as - generating exact airfoil shapes for best L/D, nacelle-diverter integration for minimizing drag, leading edge shaping, high lift system definition, fuselage shaping (?)
- Develop WT database and Calibrate / improve analysis codes

AERO TO PROVIDE

- Guidance / expertise on Aerodynamics issues to support ACE funded work
 - codes to use and/or modify for computing sensitivity derivatives
 - corrections to CFD data based on WT results
 - procedure to handle nacelle-diverter effects
 - realistic low speed drag polars
- Experts to work on generating sensitivity derivatives (for ACE funded activity)

AERO TO UTILIZE / COORDINATE

- Design constraints on global variables from ACE and TI (from baseline updates)
- Coordination with ACE on multi-point design strategy and approach

RFB

Wind Tunnel Test Technique and Instrumentation Development at LaRC

By

Lawrence E. Putnam

Presented to

HSR Configuration Workshop

Feb. 28, 1996

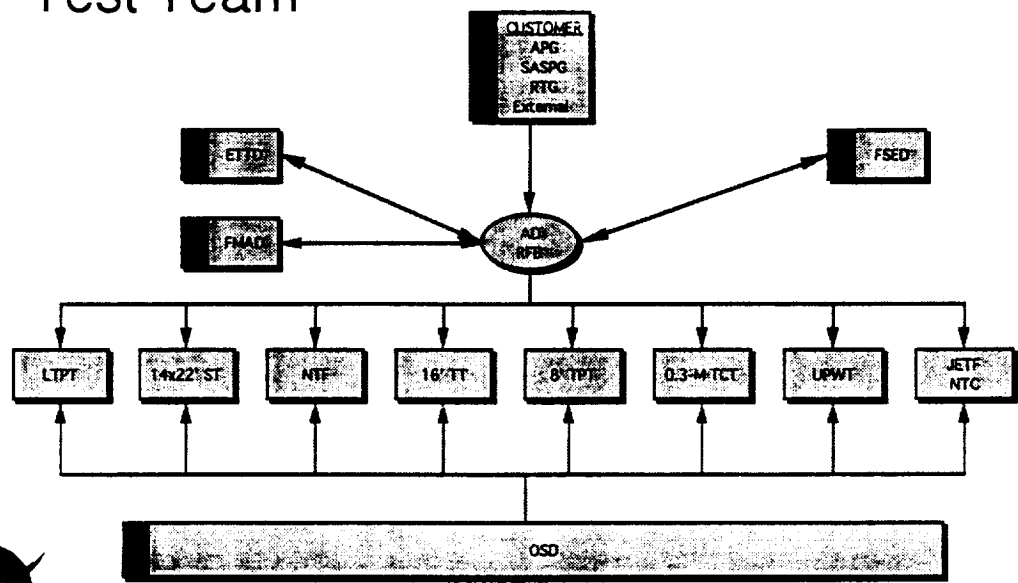


Langley Research Center

RFB



Multi-Organizational Wind Tunnel Test Team

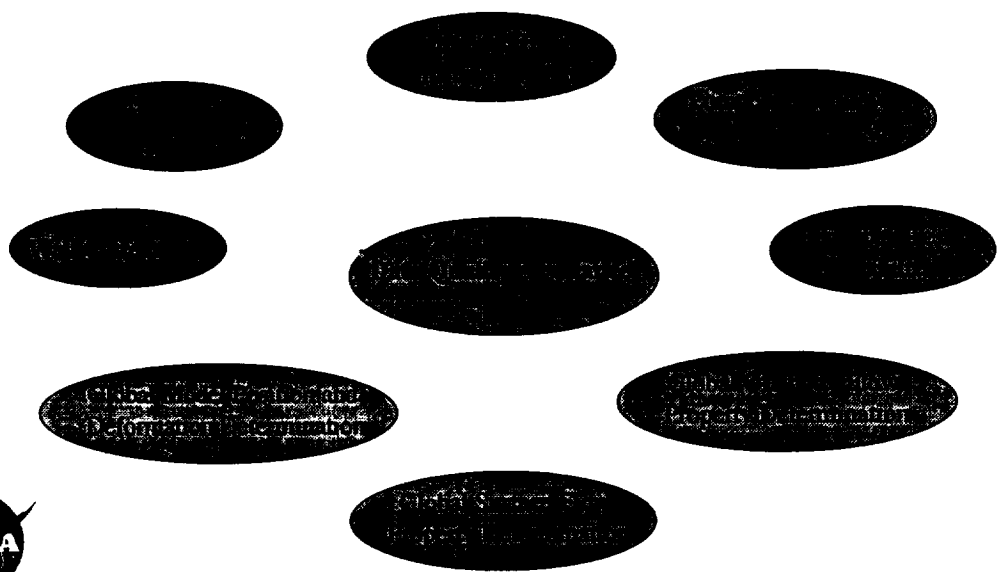


Langley Research Center

RFB



Areas of Test Technique Development



Langley Research Center

Test Technique Development Objectives

- Improved Basic Instrument Set
 - Provide capability to measure angle of attack to $\pm 0.01^\circ$ in a dynamic environment in ≤ 1 second.
 - Provide strain gage balances that are not effected by or that can be corrected for temperature gradient effects.
 - Provide balances that have significantly reduced uncertainty levels.
- Point Surface Flow Property Determination
 - Provide pressure measurement systems that minimize impact on tunnel productivity.
 - Reduce impact of electrical leads and pressure tubing that bridge the strain gage balance to zero.
 - Provide capability for measuring boundary layer characteristics.
 - Provide capability for measurement of unsteady flow characteristics.



Langley Research Center

Test Technique Development Objectives

- Global Model Position and Deformation
 - Develop optical methods for determining angle of attack with uncertainties of better than $\pm 0.01^\circ$.
 - Provide capability to measure model deformation under load in RFB wind tunnels.
 - Wing twist and deflection
 - High lift gap size
- Global Surface Flow Property Determination
 - Provide capability to determine boundary layer transition location at temperatures from 150 F to -250 F.
 - Provide user friendly pressure sensitive paint systems for RFB wind tunnels (in particular, UPWT, 16' TT, and the NTF in air).



Langley Research Center

RFB

Test Technique Development Objectives

- Global Off-Body Flow Property Determination
 - Provide non-intrusive capability to measure off body flow characteristics.
- Qualitative Flow Visualization
 - Provide non-intrusive surface flow visualization methods.
 - Provide non-intrusive off-body flow visualization methods.
- Semispan Testing Capability
 - Provide a semispan testing capability for NTF.
- Wall Corrections
 - Provide capability for routinely correcting data for wind tunnel wall effects.



Langley Research Center

RFB

Test Technique Development Objectives

- Data Uncertainty Assessment
 - Provide routine assessment of data uncertainty including bias and precision computation as part of data reduction.
 - Develop historical data base for uncertainty of all instruments.
 - Develop instrument calibration procedures that required uncertainty data.



Langley Research Center

FY 1996 Projects

- Improved Basic Instrument Set
 - Inertial Model Attitude Measurement System
 - Balance Thermal Response Improvement
 - Balance Modeling, Experimental Design and Uncertainty Improvement
- Global Model Position and Deformation
 - Assessment of OptoTrack Optical Model Attitude Measurement System
 - Development of single camera system for angle of attack and model twist determination.
 - Development of reflective plastic targets.
 - Development of laser scanning method for angle of attack determination
 - Development of laser scanning line targets.
 - Development of Moiré Interferometry method for model deformation determination.



Langley Research Center

FY 1996 Projects

- Point Surface Flow Property Determination
 - Development of a cryogenic ESP system for NTF.
 - Development of Bragg gratings for Shear Stress Measurement.
- Global Surface Flow Property Determination
 - Development of boundary layer transition location detection method for NTF.
 - Infrared method
 - Temperature Sensitive Paint
 - Hot films
- Qualitative Flow Visualization
 - Development of flow visualization systems for LaRC wind tunnels



Langley Research Center

FY 1996 Projects

- Data Uncertainty Assessment
 - Development of methodology for and assessment of data uncertainties in RFB wind tunnels.
- Wall Correction Method Development
- Semispan Test Technique



Langley Research Center

Development of Optical Angle-of-Attack Measurement Systems

- Objective
 - To develop a system of measuring angle of attack using optical techniques.
 - System shall be capable of a measurement accuracy of better than $\pm 0.01^\circ$ in a dynamic environment with no impact on tunnel productivity.
- Approach
 - Assess competing approaches through lab calibrations and prototype testing in wind tunnels.
 - Single Camera System
 - Two Camera System
 - OptoTrack
 - Laser Scanning Method
 - Select "best" system for implementation base on uncertainty of measurements and cost of implementation
- FY 1995 Accomplishments
 - Completed White Paper on state of art.
 - Completed lab calibrations and proof of concept tests in NTF and 16' TDT.
 - Completed initial comparison of OptoTrack(Boeing owned) and single camera system in the 14x22 tunnel.
 - Initiated procurement of OptoTrack.
- FY 1996 Plans
 - Develop high contrast targets.
 - Continue assessment of single camera system in the NTF.
 - Evaluate OptoTrack system..
 - Conduct risk reduction experiments for laser scanning method.
 - Document capabilities and measurement uncertainty of each approach
- Future Plans
 - Select best method and implement.



Langley Research Center

RFB

Development of Wing Twist Measurement System

- Objective
 - To develop an optical system for measuring wing twist caused by aerodynamic loads.
- Approach
 - A single camera videogrammetric system using high contrast passive optical targets on the model wing will be used to measure wing twist.
 - The target will have minimum adverse effects on the boundary layer.
 - System will be automated and user-friendly.
- FY 1995 Accomplishments
 - Completed White Paper on model deformation.
 - Demonstrated capability of system during tests in the NTF and UPWT.
 - Initiated effort to improve targets.
- FY 1996 Plans
 - Develop high contrast targets.
 - Continue assessment of single camera system in the NTF and UPWT.
 - Improve data acquisition system.
 - Refine calibration procedures to be more competitive with normal tunnel operations.
 - Document capabilities and measurement uncertainty.
- Future Plans
 - Implement production systems in NTF and UPWT.



Langley Research Center

RFB

Development of Model Deformation Measurement Systems

- Objective
 - To develop a system of measuring deformation using optical techniques.
- Approach
 - Assess competing approaches through lab calibrations and prototype testing in wind tunnels.
 - Laser Scanning Method - Uses a low-power, programmable laser beam scanning system, a galvanometer-based oscillating mirror and small infrared laser diode to paint a series of successive, parallel spanwise or chordwise lines of light on model which is recorded using CCD cameras.
 - Moiré Interferometry - makes use of optical fibers and infrared laser diodes as the basis of compact speckle interferometer systems.
- Approach Continued
 - Select "best" system for further development based on uncertainty of measurements, risk, and cost of implementation
- FY 1996 Plans
 - Acquire necessary hardware for laboratory tests of systems.
 - Perform laboratory risk reduction tests to characterize system performance and to obtain estimates of system accuracy.
 - Decide on whether to continue to development.
- Future Plans
 - If either systems shows enough promise, continue development of a prototype system and evaluate in wind tunnel tests.



Langley Research Center

RFB

Development of Bragg Gratings as Shear Stress Monitors

- Objective
 - To develop a non-intrusive method for quantitative shear stress measurements.
- Approach
 - Investigate the effects of aerodynamic shear stress on Bragg reflected spectra on germanium-doped optical fibers adhered to a metal substrate.
 - Conduct initial proof of concept lab studies to under variable aerodynamic stresses.
 - Conduct prototype testing of Bragg gratings in the ETTD subsonic wind tunnel and then the 0.3-m TCT.
 - If successful implement in the NTF.
- FY 1995 Accomplishments
 - Demonstrated that Bragg gratings exhibit measurable response to the applied shear stress.
 - Temperature effects which accompany the shear effect can accounted for by simultaneous temperature measurements.
- FY 1996 Plans
 - Conduct initial tests of concept in an appropriate wind tunnel.
- Future Plans
 - If prototype tests are successful, offer as a standard skin friction measuring technique.



Langley Research Center

RFB

Development of Cryogenic ESP Transducers

- Objective
 - To develop a ESP transducer that provides measurements at cryogenic temperatures without any type of thermal controls, that reduces number of ancillary pressure tubes crossing the balance, reduces number of calibrations required and is smaller in size.
- Approach
 - Basic ESP module design will be modified to incorporate materials that are compatible with cryogenic environment, temperature of each sensor will be measured to allow compensation for changes in bias and sensitivity, new bonding techniques will be used, and more highly doped semiconductors will be used to reduce sensitivity to temperature changes.
- FY 1995 Accomplishments
 - First 16 channel prototype system completed.
 - Thermal expansion measurements completed.
- FY 1996 Plans
 - Complete fabrication of 2nd and 3rd 16 channel prototypes.
 - Complete lab calibration and testing of 3 prototypes in 0.3-m TCT.
 - Complete analysis and selection of best fabrication method.
- Future Plans
 - Fabricate, calibrate and test 32 channel module.
 - Assess uncertainties
 - Seek commercial supplier and transfer technology.



Langley Research Center

Boundary Layer Transition Location Detection

- Objective
 - To develop user-friendly, cost-effective, minimally-intrusive method(s) for determining globally the location of boundary layer transition on models at temperatures from -250F to 130F.
 - To select by the end of FY, or sooner, initial technique(s) to be offered for routine use in the NTF.
- Approach
 - Assess competing approaches through lab calibrations and prototype testing in wind tunnels.
 - Infrared technique
 - Temperature sensitive paint
 - Hot film (not global)
 - Other
 - Select "best" system for implementation base on risk, technology readiness, cost of implementation, and uncertainty of measurements.
- Accomplishments to Date
 - Demonstrated use of IR technique down to about -150F. Will require long wave length IR cameras for lower temperatures.
 - Use of hot films down to -250F.
 - Potential of TSP in cryogenic environment by Sullivan of Purdue.
 - Team formed to develop TSP technique.
 - High risk research plan developed to provide a prototype TSP system in NTF by end of FY.
- FY 1996 Plans
 - Continue development of IR technique and define implementation requirements for NTF.
 - Conduct lab and exploratory wind tunnel studies to develop TSP.
 - Complete prototype test of TSP system in NTF.
- Future Plans
 - Select best method and implement in NTF.



Langley Research Center

Boundary Layer Transition Location Detection

- NTF Barriers and Constraints
 - Prototype system must be operational in facility by end of FY 96
 - Physical space (NTF running out of tunnel penetration space)
 - Changes/modifications should take no longer than 2 days
 - Transition data taken concurrently with other test data
 - No oil, seeding, O₂
 - Must function from -250F to 130F
 - Access holes cannot exceed 2" diameter
 - Must be able to use existing models



Langley Research Center

RFB

Boundary Layer Transition Location Detection

- Infrared Technical Barriers and Issues
 - Does not work on metal models
 - Requires an insulated coating
 - Thickness of silicon dioxide needed for insulation
 - Probably need for a composite model
 - Current technology limited to -150°F
 - Exotic imager required
 - Liquid helium cooled detector (-250°F)
 - Background thermal noise on tunnel wall
 - Special window glass
 - Test section lighting
 - Special enclosure required for camera
 - 5 minutes/per point required for data acquisition
 - Photon limited
 - Can NASA specialist recreate experiments conducted by contractor in 0.3-m TCT?



Langley Research Center

RFB

Boundary Layer Transition Location Detection

- Hot Film Technical Barriers and Constraints
 - Thickness of application
 - Not global
 - Time to calibrate
 - Availability of facility to deposit films on large models
 - Wire across balance
 - Trench required for wires in wing
 - Survivability of gauges in tunnel
 - Surface of films
 - Has problem with long cable lengths (>100ft)
 - Fabrication capability (deposited films) only available at LaRC
 - Probably could be used to validate other techniques
 - High cost - impact on other measurements



Langley Research Center

RFB

Boundary Layer Transition Location Detection

- TSP Development Underway
 - Development of cryogenic paint chemistry
 - Cooperative effort between LaRC, HSR, MDA-E, Purdue University, and University of Florida
 - Development of insulating coating
 - Paint surface finish determination and improvement
 - Assembly of data acquisition system (using existing hardware and software developed for PSP)
 - Planning for 0.3-m TCT technique development and proof of concept tests
 - Definition of system implementation requirements for NTF.



Langley Research Center

RFB

Boundary Layer Transition Location Detection

- TSP Technical Barriers and Issues
 - Thickness of applied layer
 - Quality of surface finish
 - May require an insulating layer on model
 - May require a temperature step in flow
 - Orifice protection during application
 - Lighting contrast
 - Viewing angle/model shape
 - Life of paint
 - Degradation of paint
 - Keeping paint on model
 - Safety



Langley Research Center

DATA QUALITY ASSURANCE *Toward National Standards*

Our New Environment:

We are driven by customer needs.

New Customer Needs:

*Unprecedented assessment, control and reduction of **variation** in design and testing.*



Langley Research Center

DATA QUALITY ASSURANCE *Toward National Standards*

Our Response:

1. Apply methods of **statistical process control** to all operations affecting measurement quality.
2. Establish **pre-test planning** and negotiation based on simplified, easy-to-use, uncertainty analysis.
3. Develop **standardized processes** for continuous improvement and long-term stability.
4. Develop **national standards** for evaluation of data quality and corrections in comparable national facilities.



Langley Research Center

DATA QUALITY ASSURANCE

Toward National Standards

Results So Far:

1. All RFB staff have completed Coleman and Steele short course on uncertainty analysis and test planning.
2. Simplified uncertainty analyses have been completed for core facilities plus airfoil tunnels.
3. Pre-test planning has led to significant changes in instrumentation and/or test matrix to achieve customer needs.
4. We have received strong, favorable, customer response.
5. Uncertainty analysis and statistical process control methods are now used to assess all changes in operations and facilities which might affect data quality.



Langley Research Center

DATA QUALITY ASSURANCE

Toward National Standards

Summary:

The new methodology has enabled us to look at our operations with a powerful microscope.

Consequence:

We can now see significant new opportunities to enhance customer and staff satisfaction while reducing costs and increasing productivity.



Langley Research Center

RFB

Test Techniques Available or in Development for LaRC Facilities used by HSR

- NTF
 - Micro-tuft surface flow visualization
 - Wing twist measurement
 - Boundary layer transition location (in development)
- UPWT
 - Schlieren or Shadowgraph
 - Micro-tuft surface flow visualization
 - Wing twist measurement (Prototype system demonstrated. Production system being developed.)
 - PSP
 - Vapor Screen



Langley Research Center

RFB

Test Techniques Available or in Development for LaRC Facilities used by HSR

- 16' TT
 - Micro-tuft flow visualization
 - Surface oil flow
- 14' x 22' Subsonic Tunnel
 - Micro-tuft flow visualization
 - Surface oil flows
 - Flying smoke wand
 - 3-D Laser Velocimeter
 - Global Doppler Velocimeter (development underway)
 - OptoTrack AOA (in procurement)



Langley Research Center



Concluding Remarks

- LaRC has an aggressive test technique development program underway. This program has been developed using 3rd Generation R&D management techniques and is a closely coordinated program between suppliers and wind tunnel operators.
 - Wind tunnel customers' informal input relative to their needs has been an essential ingredient in developing the research portfolio.
- An attempt has been made to balance this portfolio to meet near term and long term test technique needs.
- Major efforts are underway to develop techniques for determining model wing twist and location of boundary layer transition in the NTF.
- The foundation of all new instrumentation developments, procurements, and upgrades will be based on uncertainty analysis.



Langley Research Center

HSR S_{upersonic} L_{aminar} F_{low} C_{ontrol}_____

High-Speed Research Project

4.3 Aerodynamic Performance

4.3.4 Supersonic Laminar Flow Control An Overview

NASA Langley Research Center

HSR CA Workshop/February 27, 1996

SLFC ITD:

Bharadvaj, Bala
Fischer, Mike
Joslin, Ron
King, Lyn
Parikh, Pradip

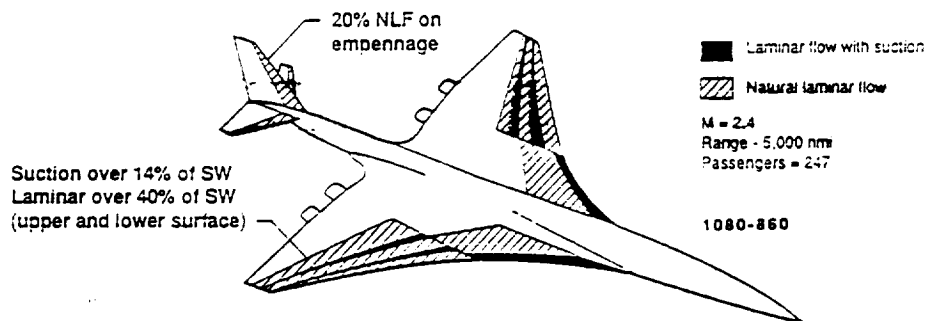
MDA
LaRC
LaRC
ARC
BCAG

SLFC Mission Statement

Develop and validate technologies for Supersonic Laminar Flow Control (SLFC) and perform the SLFC aerodynamic design for the HSCT with an assessment of the net benefit and risks.

SLFC Benefits

HLFC Application to HSCT



- Aerodynamic Benefit:** 8 to 10% Increase in Cruise L/D
- Implementation Penalties:** Systems and Structural Weight Increment, Fuel Displacement, TSFC, Suction Air Momentum Drag
- Performance Benefits:** Δ MTOW=-6 to -8%, Δ Block Fuel=-10 to -12%
 Δ Engine Airflow=-8 to -12%
- Thermal Benefits:** Reduced Skin Temperatures
- Reduced Fuel Heating rate
- Increased Materials Options

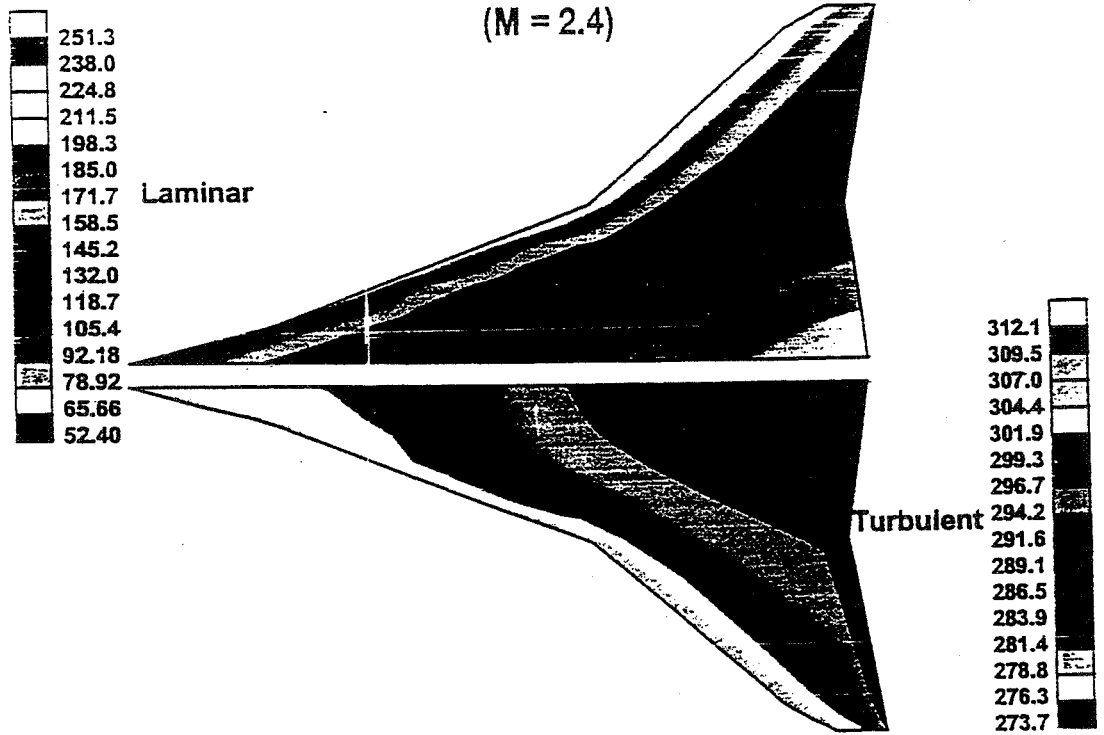
Benefits would be larger for a heavier/longer-range configuration and for HLFC scheme with wall cooling

HSR S_{upersonic} L_{aminar} F_{low} C_{ontrol}

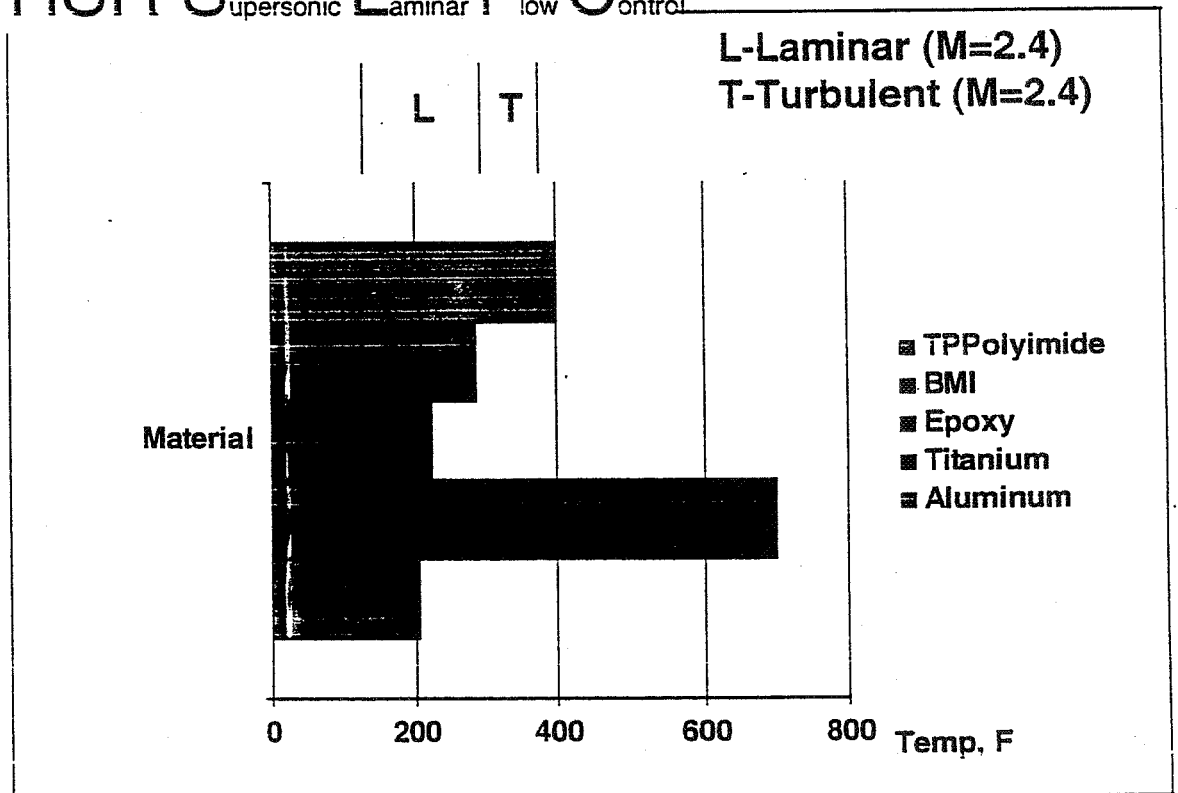
Benefits of SLFC

- 8% increase in cruise L/D (9.3=>10)
- 11% reduction in fuel burn (390,000lbs=>347,100lbs)
- 7% reduction in MTOW (740,000lbs=>688,200lbs)
- 50-100 degree(F) reduction in local skin temperatures

Laminar and Turbulent Surface Temperatures (M = 2.4)

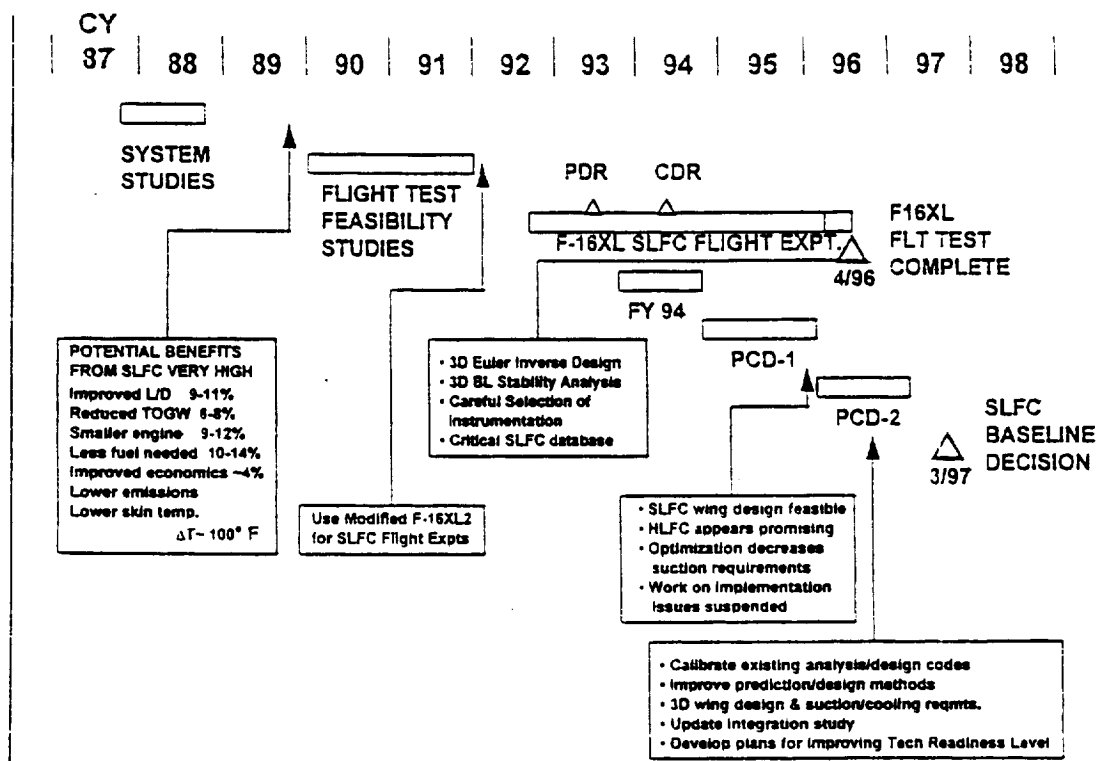


HSR S_{upersonic} L_{aminar} F_{low} C_{ontrol}



SLFC Major Issues

- BL Suction - Where? How much?
- Impact on Inviscid Drag
- Weight of Suction System
- Compatible High Lift System
- Leading Edge Protection - Insects, Ice
- Complexity & Cost of Systems and Structure
- Durability & Maintainability



4.3 AERODYNAMIC PERFORMANCE 4.3.4 Supersonic Laminar Flow Control

FY	1996	1997	1998	1999
Program Milestones:	△ Technology Concept			△ Technology Configuration
Level II Milestones:		SLFC Flight Test Complete	SLFC Baseline Decision	
Level III Milestones:	F-16XL-2 SLFC Flight Experiment Complete	TI SLFC Tools	SLFC Tools Development & Calibration Complete SLFC Aerodynamic Design	
4.3.4.1 F-16XL-2 Flight Experiment	△ Demo Phase Complete (HSR Phase I)	△ Demo Documentation Complete (HSR Phase I) △ SLFC Flight Test Database Research Phase Complete		
4.3.4.2 SLFC Tools Development & Calibration		△ Attachment-Line Transition Methodology Quiet Tunnel Data & Analysis △ N-factor Code Calibration Complete △ Calibration Against Flight Database Complete		
4.3.4.3 SLFC Aerodynamic Design		△ Improved Wing Design	△ Suction/Cooling Requirements	
4.3.4.99 Task Planning and Coordination	△ Planning & Coordination Meeting			

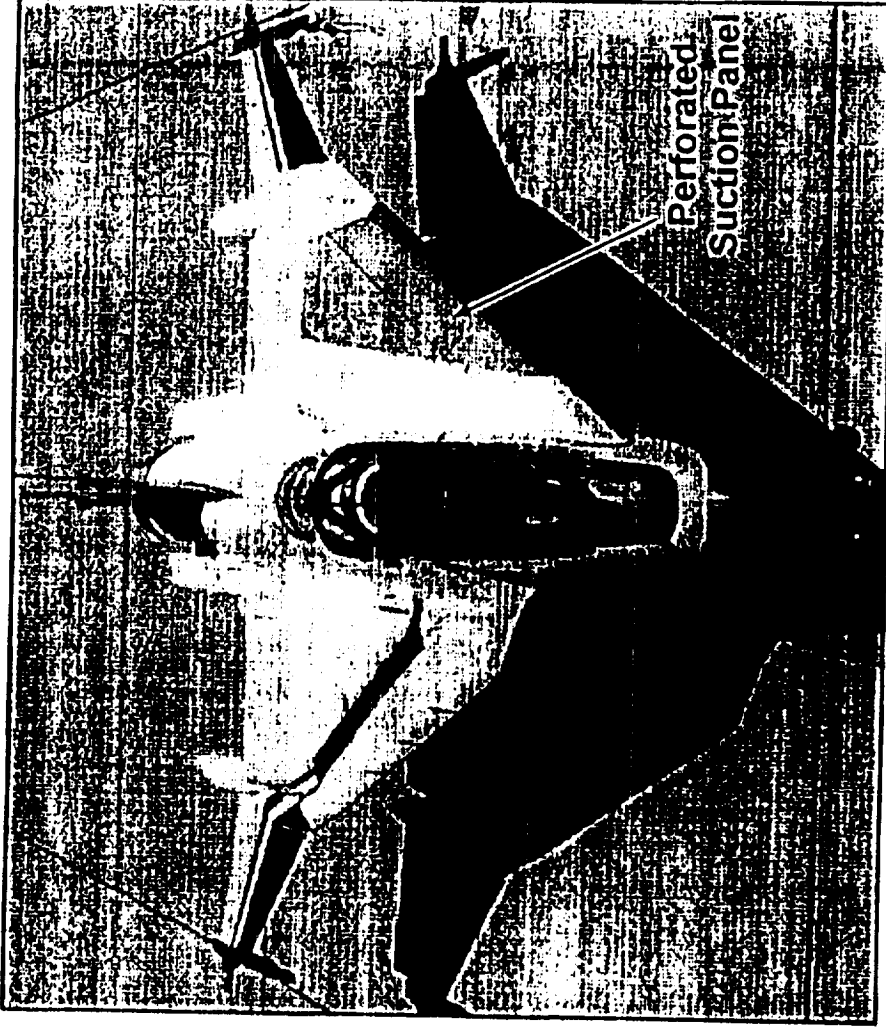
HSR S_{upersonic} L_{aminar} F_{low} C_{ontrol}

4.3.4.1 F-16XL-2 Flight Test (Hardware Demonstration)

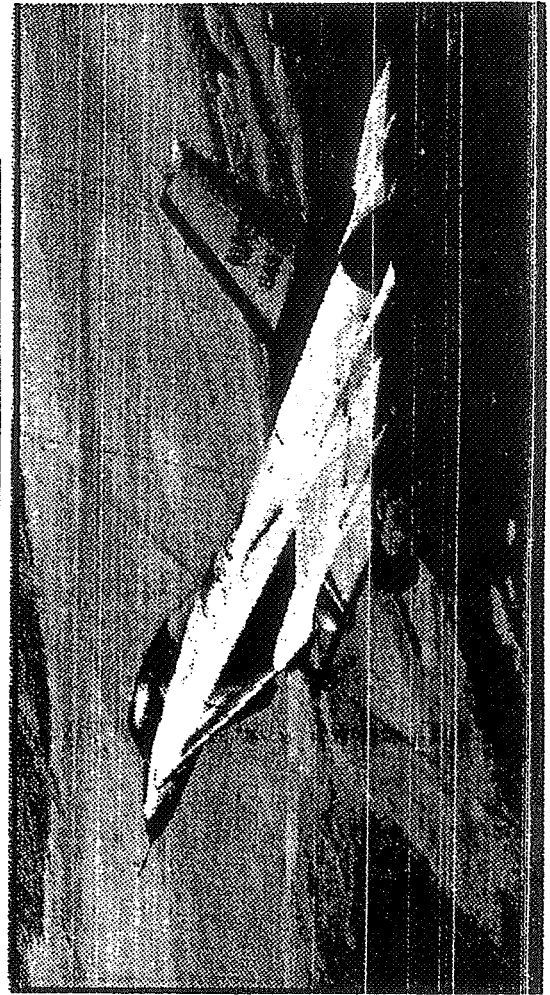
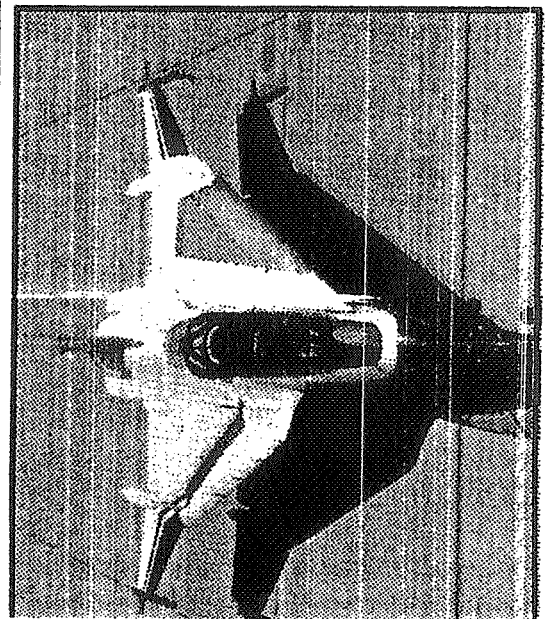
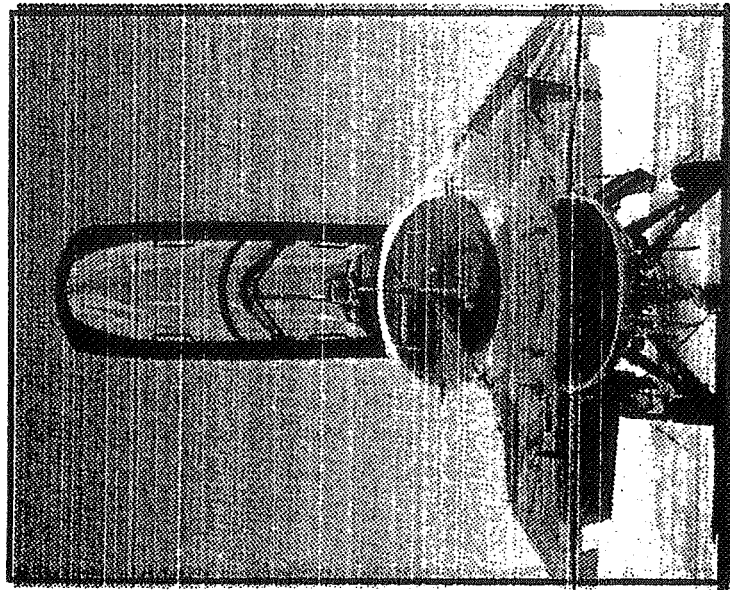
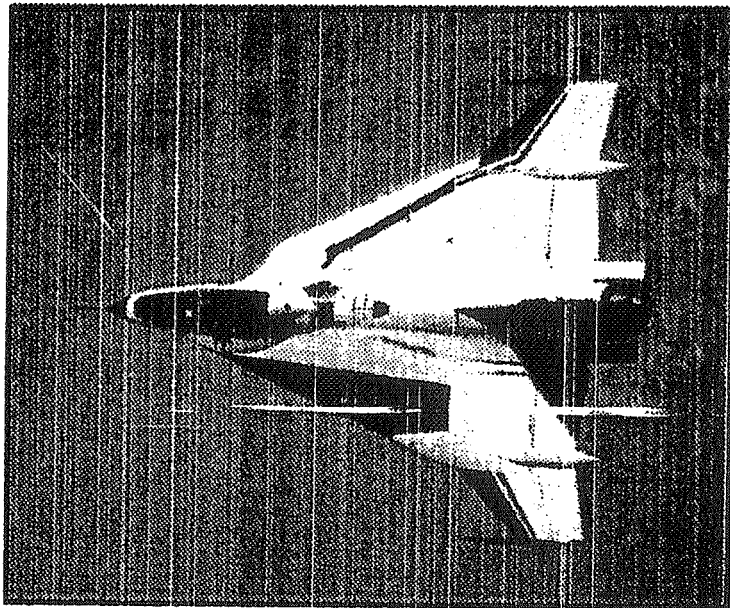
F-16XL-2 SUPERSONIC LAMINAR FLOW CONTROL EXPERIMENT

OBJECTIVES:

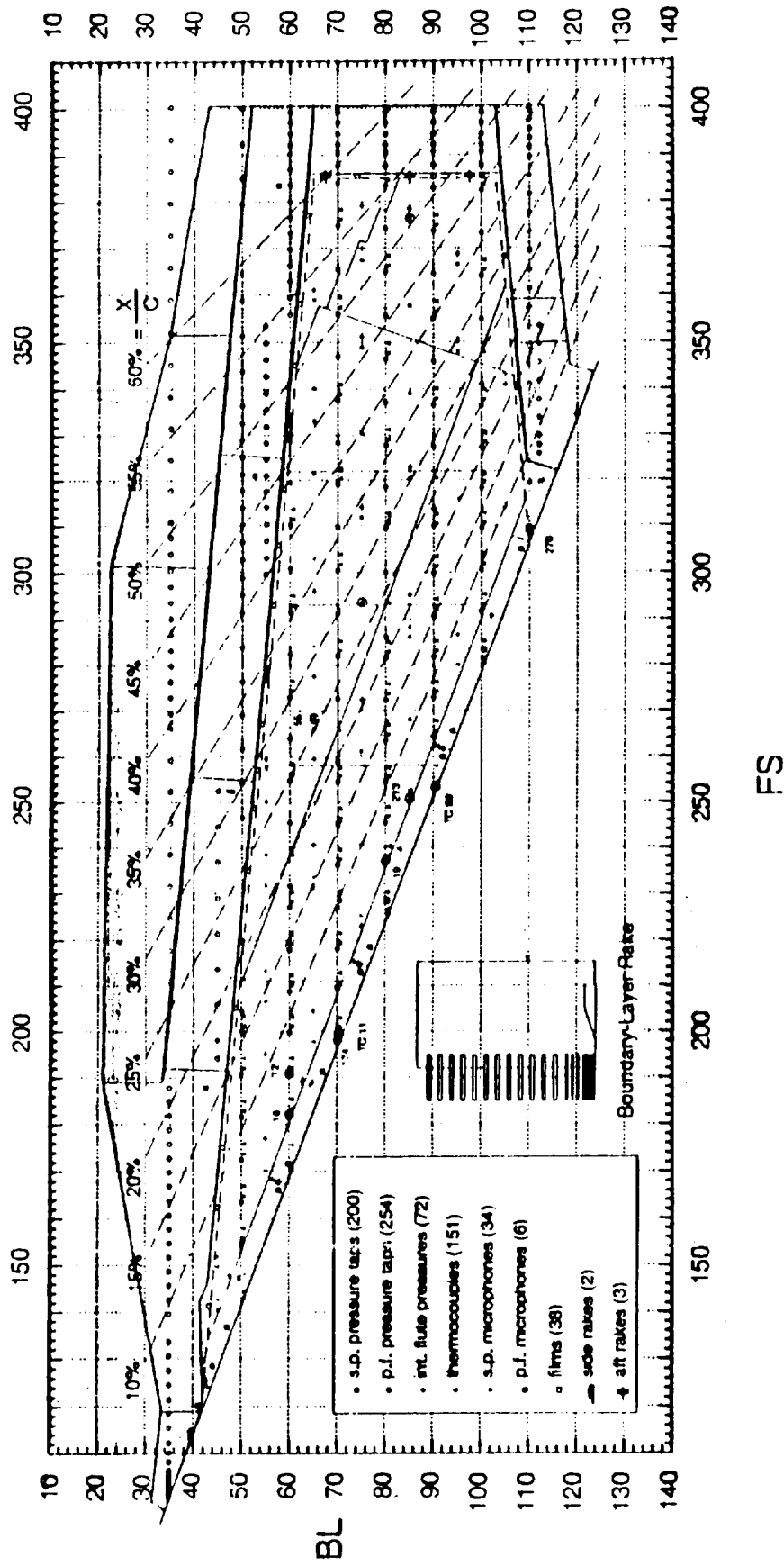
- Demonstrate achievement of laminar flow to 50-60% chord on a highly swept wing at supersonic speeds
- Obtain flight data for CFD code validation and development of design methodology
- Establish initial SLFC design criteria to provide a more realistic assessment of SLFC benefits for the HSCT



F-16XL Supersonic Laminar Flow Control Experiment



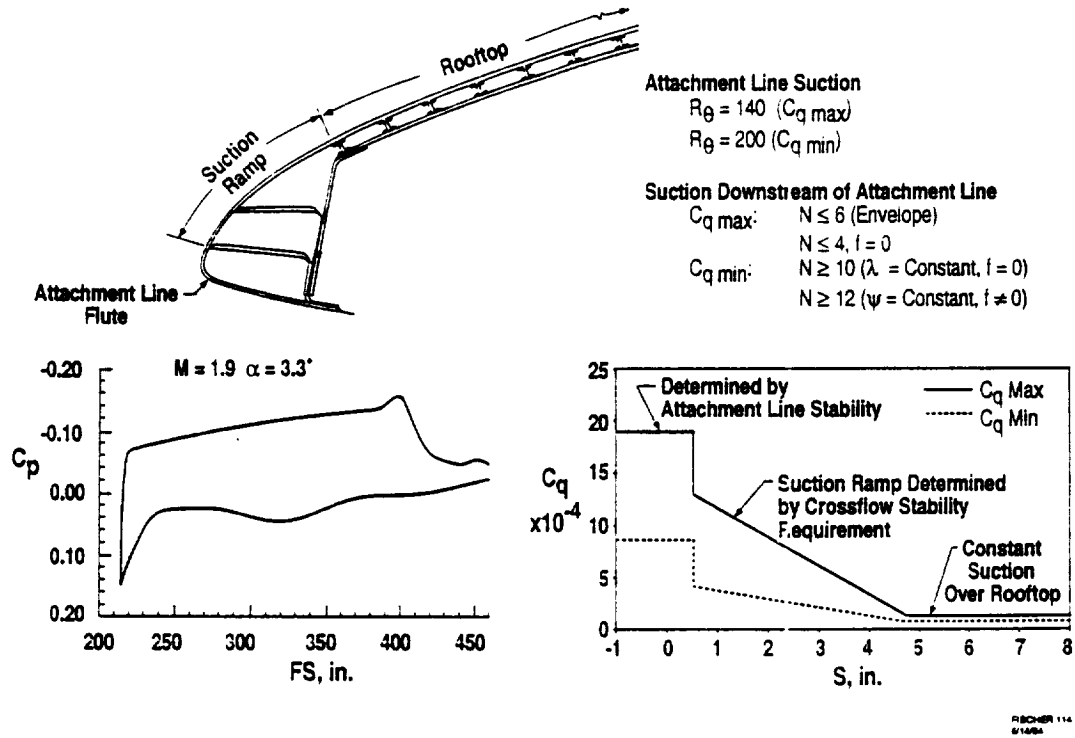
F-16XL2 SLFC WING INSTRUMENTATION



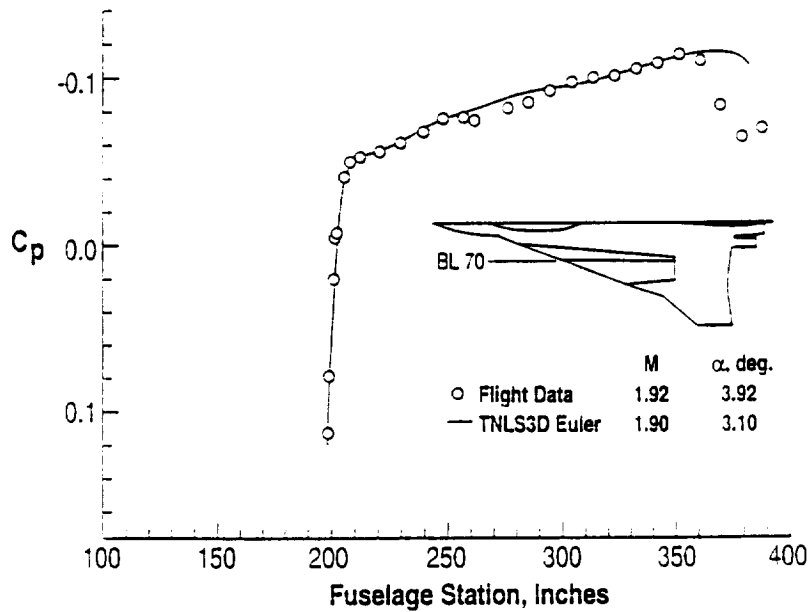
Notes: 1.) Circled instrumentation did not pass BCAG O/A.
 2.) Only the two failed Suction Panel leading edge pressure taps shown (113 total in l.e.).

NASA
 VER 11:21/95

AERODYNAMIC AND SUCTION REQUIREMENTS



F-16XL-2 SLFC Flight Experiment Comparison of Measured and Predicted Surface Pressures

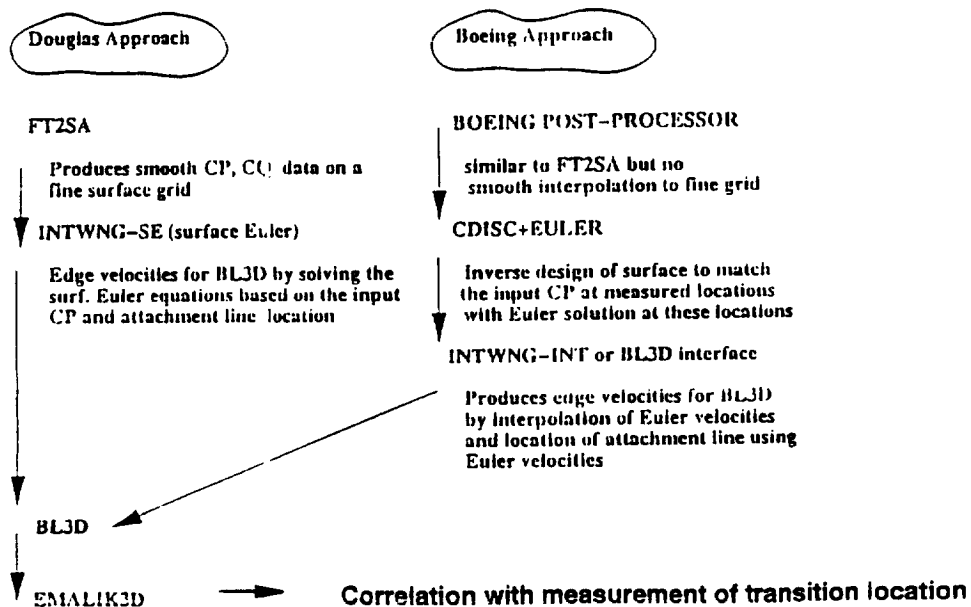


4.3.4.2 SLFC Tool Development

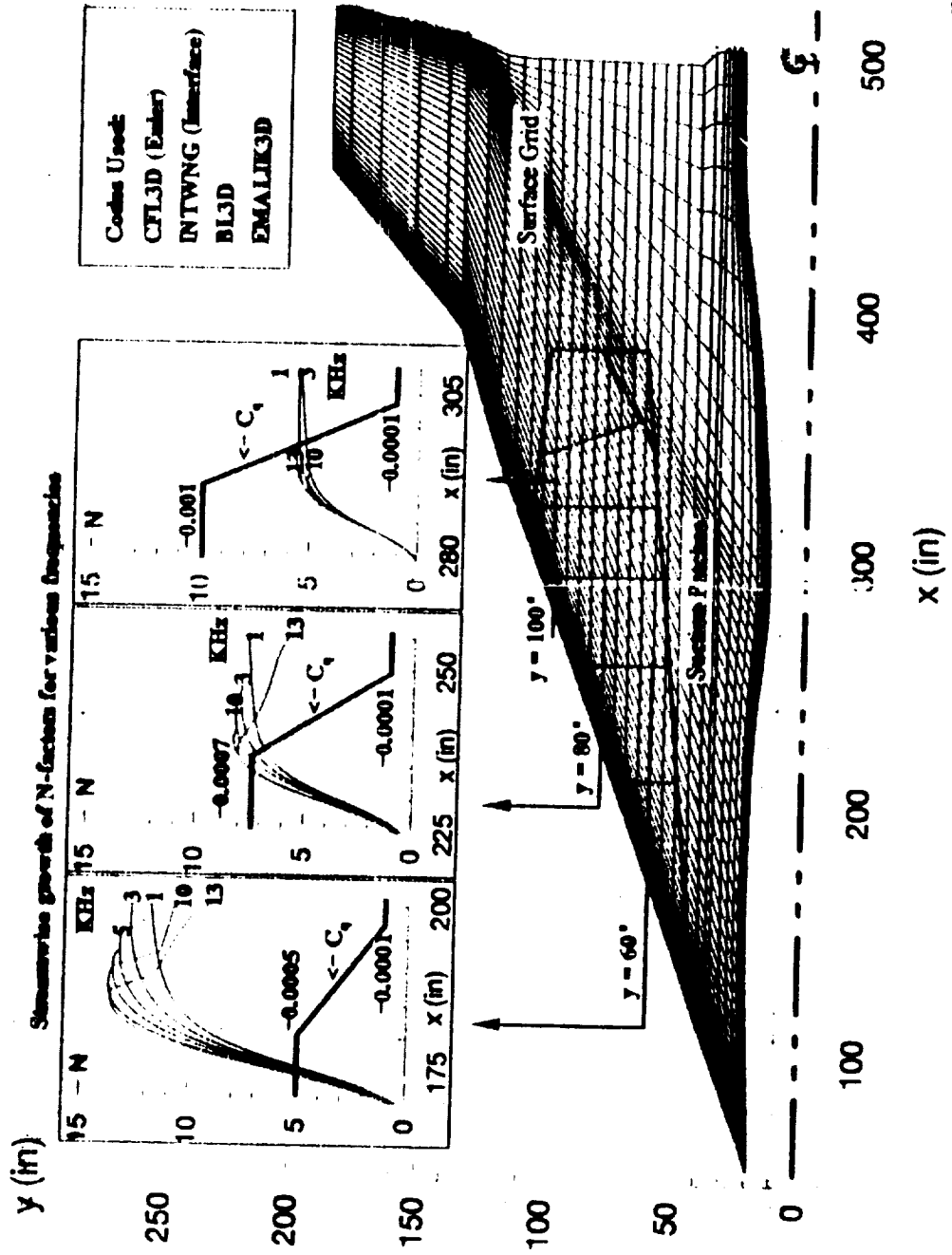
- a. Tool calibration
- b. Quiet tunnel database

Tool Calibration from F-16XL database

Flight Data: Cp, Tw, Suction flute meas.

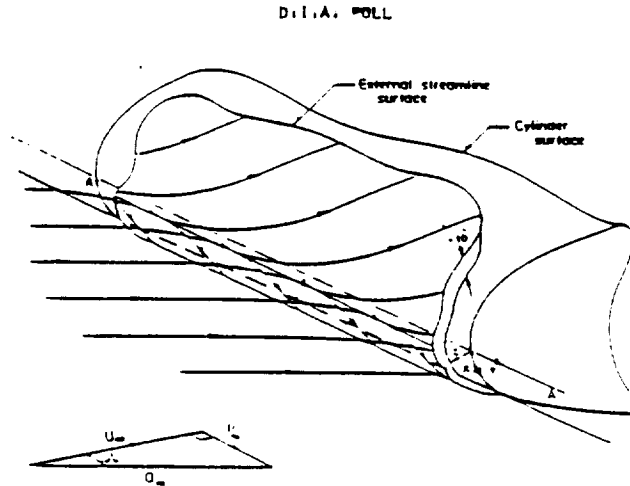


Predicted N-factors on the F16XL Suction Glove at Design Point (assuming a representative suction distribution (C_p) achieved by the suction patches)



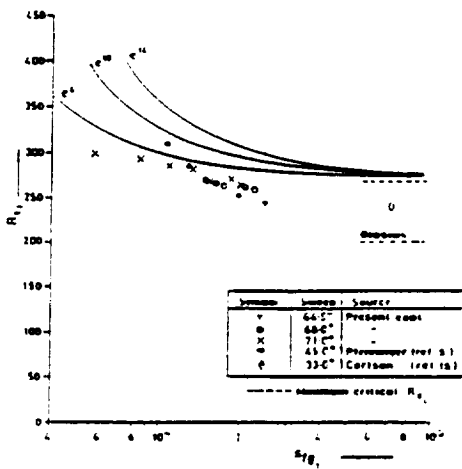
Codes Used:
 CFL3D (Euler)
 INTWNG (Interface)
 BL3D
 EMALIK3D

Sketch of Attachment-Line Region

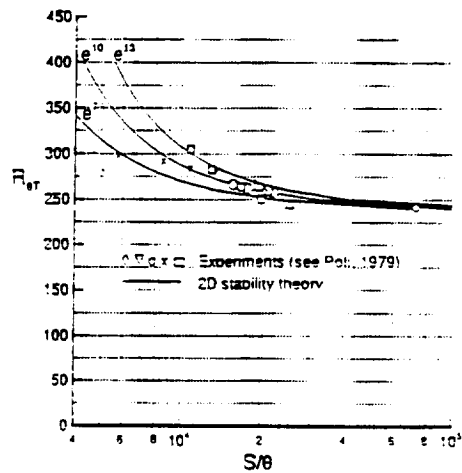


N-factor Correlation

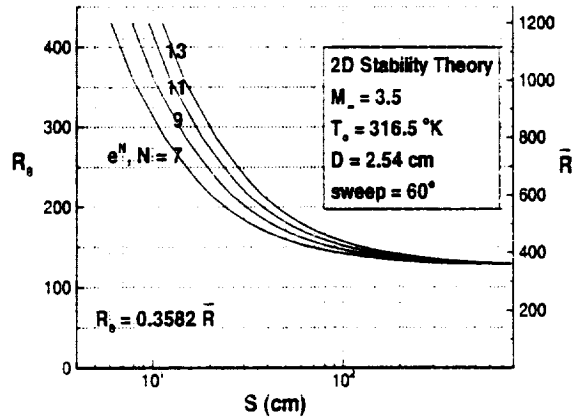
Parallel Method



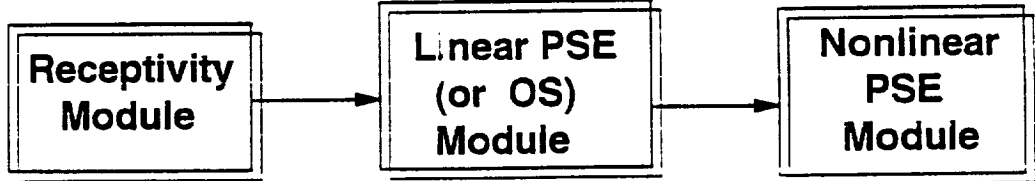
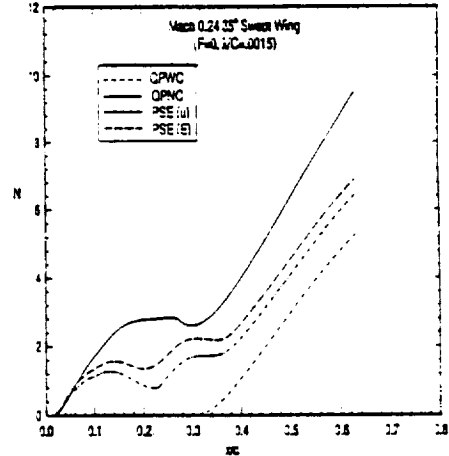
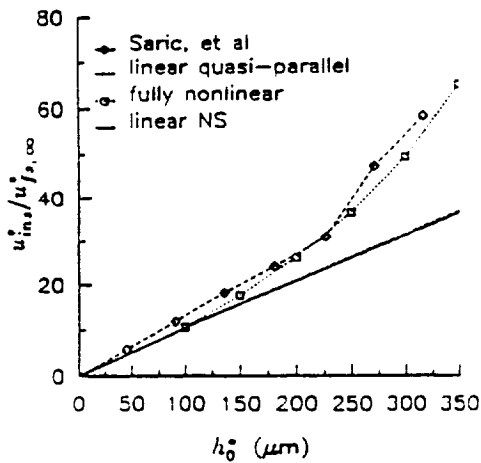
2D-Eigenvalue Approach



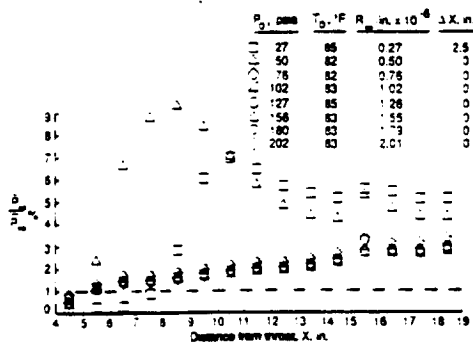
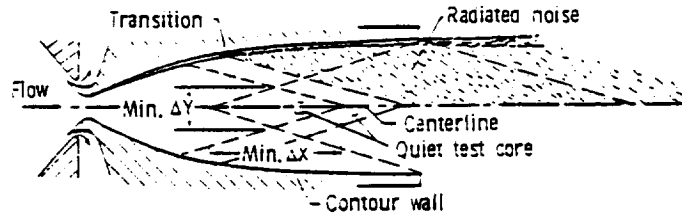
Constant N-valued Curves for Transition Correlation



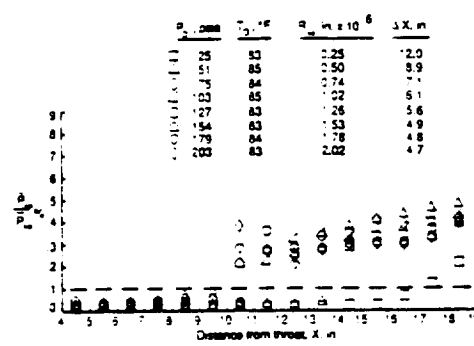
Embryonic "Next generation" tools



Significance of Quiet Tunnels



(c) Bleed valve closed, $\gamma = 0$.



(a) Bleed valve open, $\gamma = 0$.

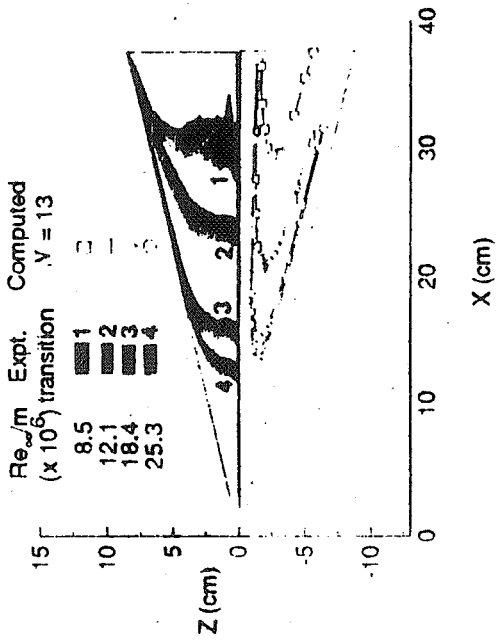


Fig. 1 Transition location correlates well with $N=13$ over a wide range of unit Reynolds numbers.

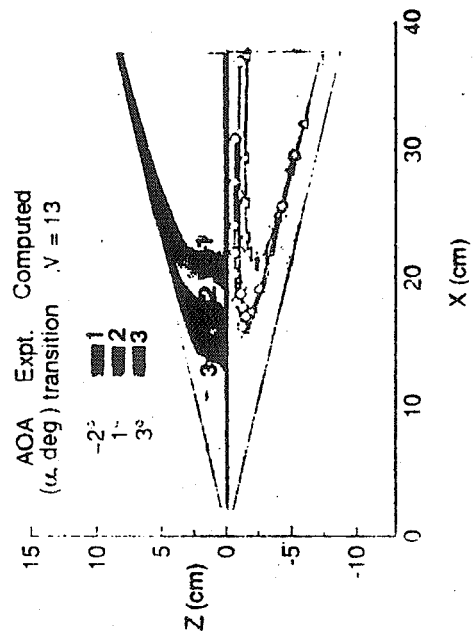


Fig. 2 Transition location also correlates well with $N=13$ over a wide range of angles of attack.

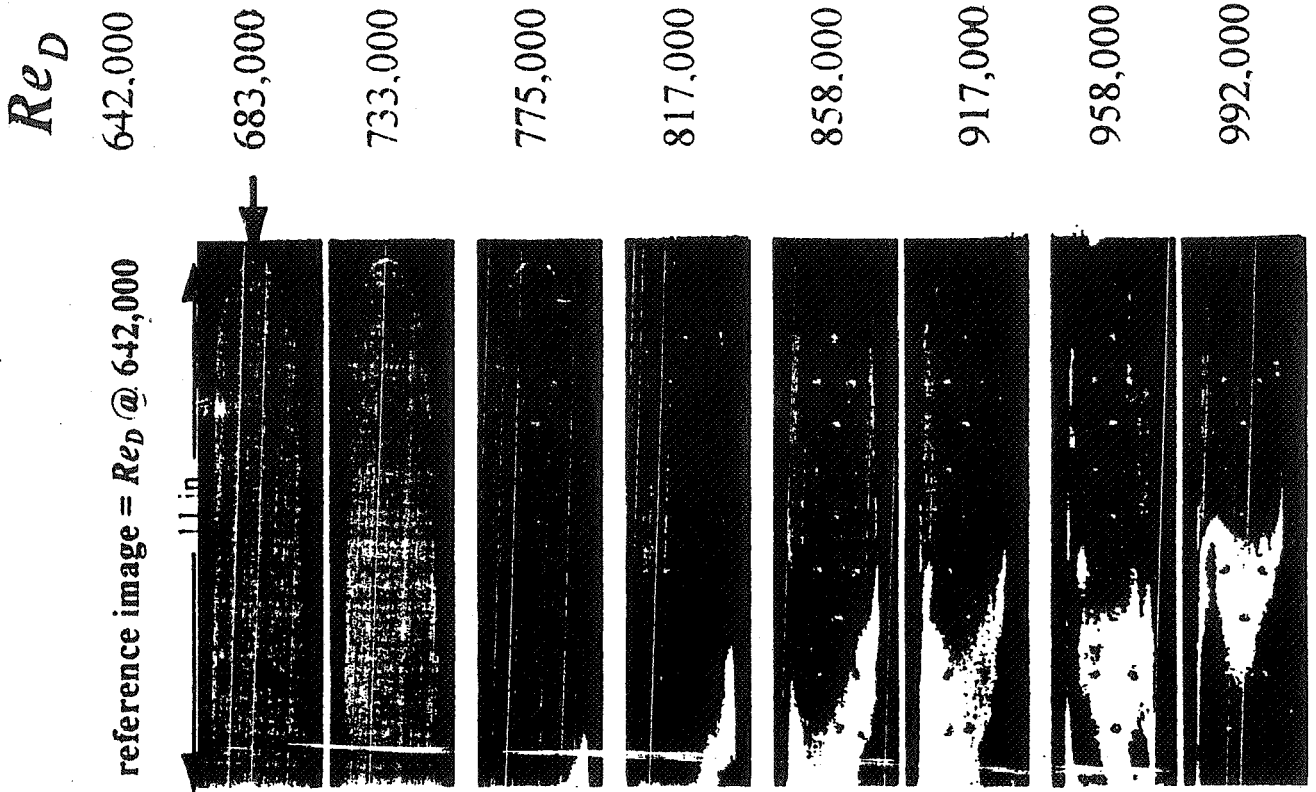
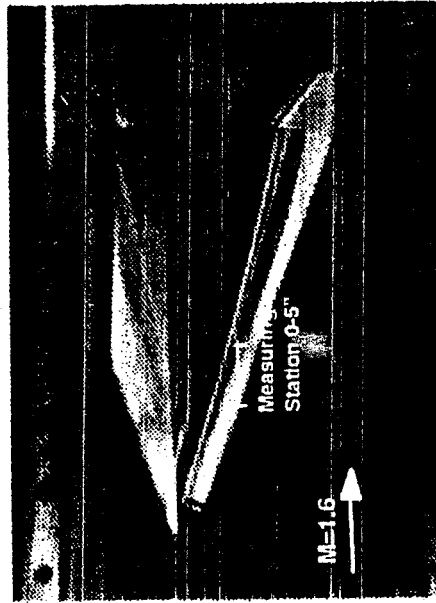


Fig. 3 Transition location on 1 in. diam. 76 deg. constant, cylindrical model via D_n using TSD

Swept Wing Model Test in FML Laminar Flow Supersonic Wind Tunnel

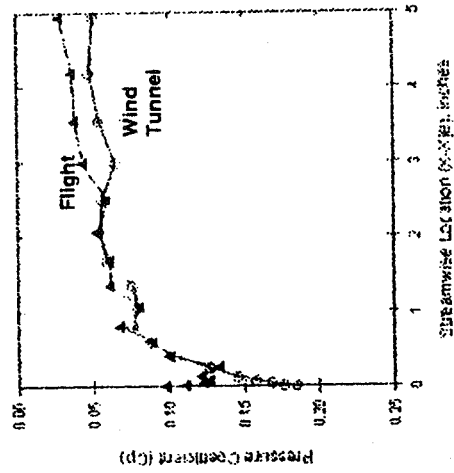


RESEARCH OBJECTIVE: Obtain pressure and transition data on a full-size segment of the F-16XL passive glove for comparison with flight data and CFD validation

APPROACH: The M1.6 Quiet Tunnel was designed to operate in the same Reynolds number range as the F-16XL laminar flow test vehicle. A pressure model was tested in FY95. The next entry will employ thermally sensitive paint to determine transition location. Transition is expected to occur due to attachment line contamination and by crossflow instability mechanisms.

APPLICATION: These tests are in support of laminar flow control for the next generation supersonic transport.

STATUS/PLANS: Pressures were measured during the first entry. A comparison with flight data is shown here (angles of attack were adjusted for best match). The next entry, expected in Feb-Mar. 1996, will investigate transition in the leading edge region.



4.3.4.3 SLFC Aerodynamic Design

- Design wing contour
- Suction & cooling requirements
- Step/gap/waviness requirements
- Compute skin friction reductions
- Calculate BLC suction requirements

Summary

SLFC Impact on HSCT:

Aerodynamic & Economic Benefits

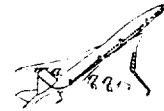
- Drag reduction, Increased L/D,
- Reduced MTOW, Lower skin temps, etc.

PCD 2:

- 4.3.4.1 F-16XL-2 SLFC Flight Experiment
- 4.3.4.2 SLFC Design Tool Methodology
- 4.3.4.3 SLFC Aerodynamic Design



HSR HIGH-LIFT TECHNOLOGY

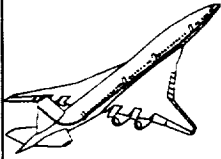


High Lift Technology Overview

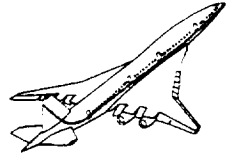
Z. T. Applin

**Presented at the
First NASA/Industry HSR Configuration Aerodynamics
Workshop**

**February 27-29, 1996
Langley Research Center
High-Lift Technology
Integrated Technology Development Team**



OUTLINE

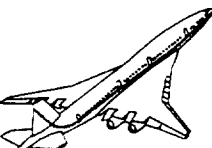


- **PCD1 Review**
 - Program content
 - Models
 - High-lift system downselect
 - Viscous USG development

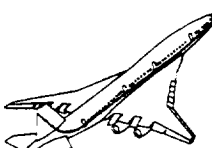
- **PCD2 Overview**
 - Planned program

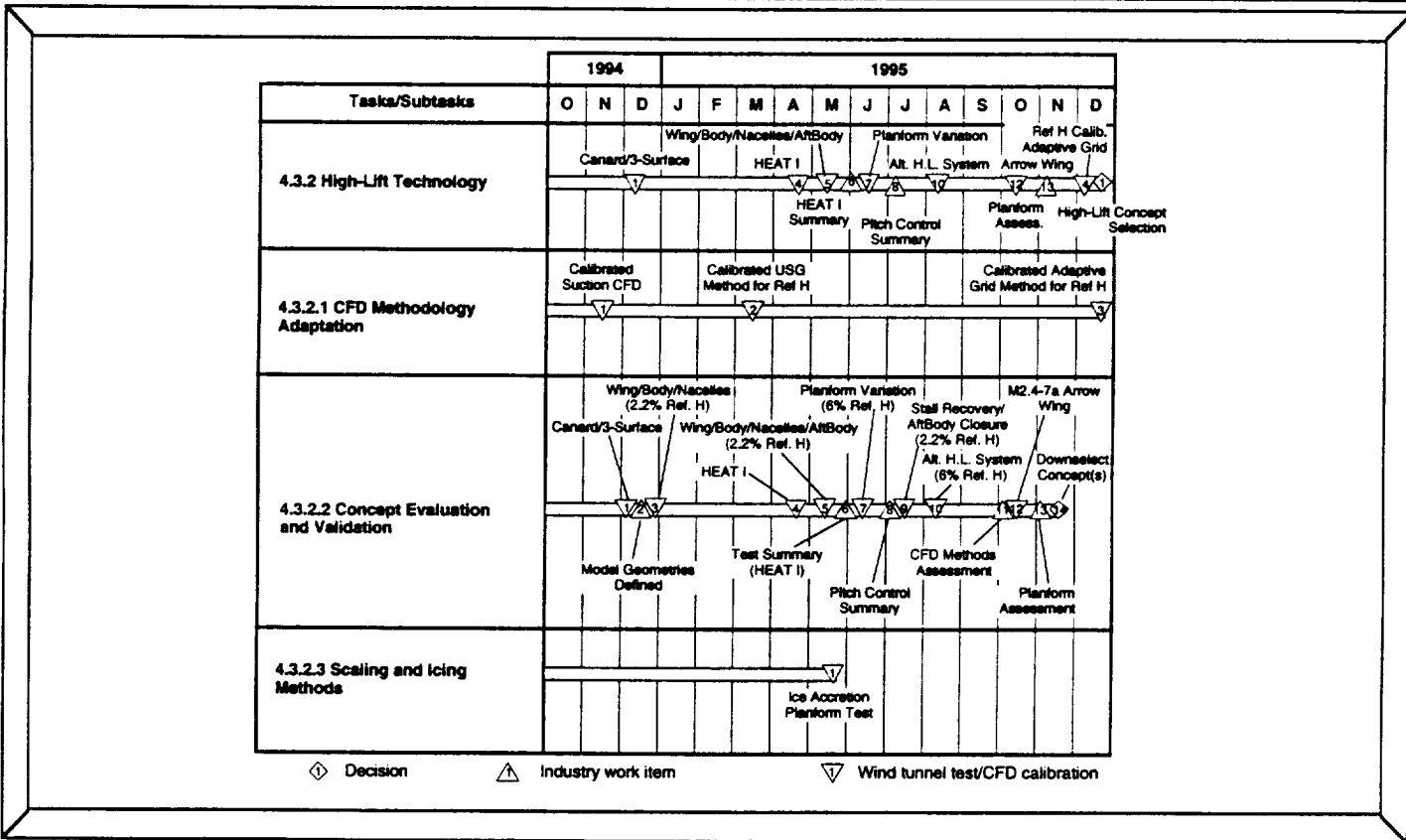
- **Summary**

PCD1 Review

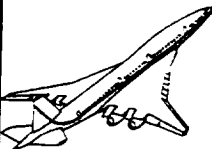


PCD1 Deliverables

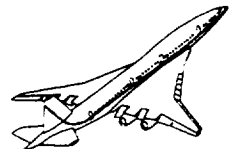




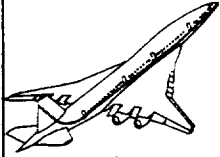
PCD2 Overview



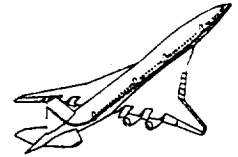
PCD2 Milestones



4.3.2 High-Lift Technology												
TASKS	FY	1996			1997			1998			1999	
Program Milestones		Technology Concept									Technology Configuration	
Level II Milestones		High-Lift Concept Selection									High-Lift Wind Tunnel Evaluation	
		HEAT 1A Defined					High-Lift System Update	Tools and Methods Assess.			Tech. Concept Final Assess.	
Level III Milestones		Tech. Concept HL Geom. Defined			Tech. Concept Prelim. Assess.			HL/PAI Aerodynamic Assess.				
4.3.2.1 Technology Concept Assessment		Tech. Concept HL Geom. Defined			Def. S&C Aero. Requirements			Tech. Concept Prelim. Assess.			Tech. Concept Final Assess.	
4.3.2.2 High-Lift System Concept Design					Assess. High-Lift System Refinements			High-Lift System Update				
4.3.2.3 Propulsion/Airframe Integration		HEAT 1 Aerodynamic Assess.						HEAT 1A Aerodynamic Assess.				
4.3.2.4 High-Lift Tools and Methods Development		Auto. Adapt. of Viscous USG			Support/Wall Interference			Ground Effects Methodology Assess.			Full-Scale Prediction Methodology	
4.3.2.99 Task Coordination and Planning					BL Trans. Technique Recom.			Viscous USG Tech. Concept Assess.				



PCD2 WBS Description



4.3.2.1 Technology Concept Assessment

Develop an efficient high-lift system for the Technology Concept HSCT aircraft configuration and provide an assessment of the low-speed aerodynamic performance and handling characteristics.

4.3.2.2 High-Lift System Concept Design

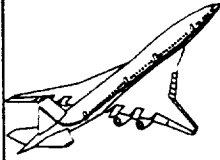
Design and evaluate refinements to the Technology Concept high-lift system in order to identify and develop areas for potential improvement which will be required in order to meet the established performance improvement goals.

4.3.2.3 Propulsion/Airframe Integration

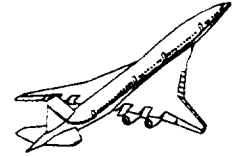
Evaluate the installation effects of the propulsion system on the low-speed aerodynamic performance and handling characteristics both in and out of the influence of the ground.

4.3.2.4 Tools and Methods Development

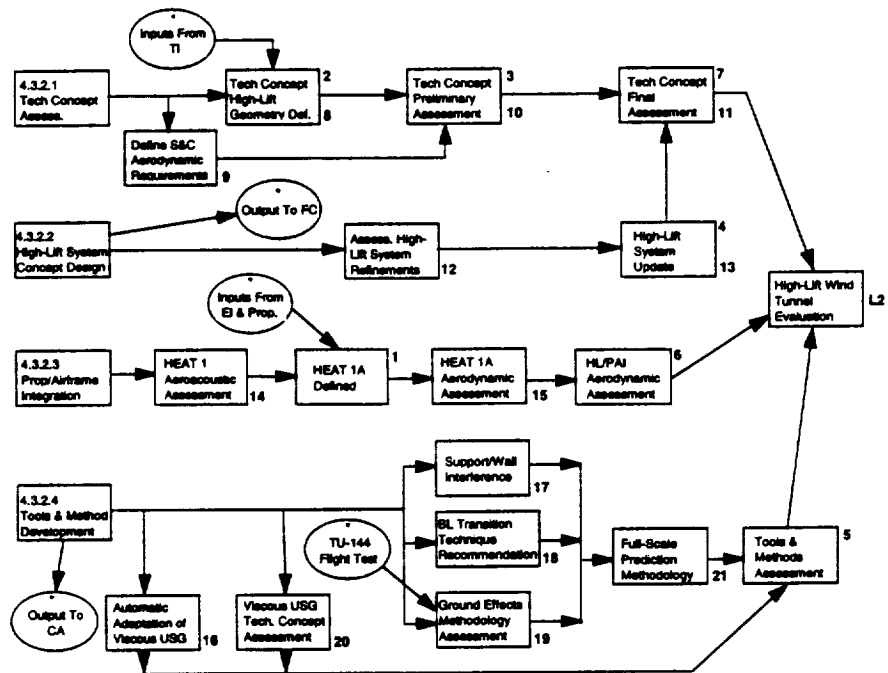
Develop the tools and methods required for the accurate assessment of the full scale aerodynamic performance of the Technology Concept HSCT configuration.



PCD2 Logic Flow



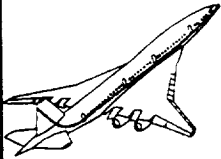
4.3.2 High Lift Technology Logic Flow Diagram



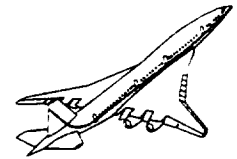
Note: Number at upper corner is Level 3 milestone number.

Number at lower corner is Level 4 milestone number.

* Interfaces with other program elements described in sections 2.14-15.



PCD2 Logic Description



4.3.2.1 Technology Concept Assessment

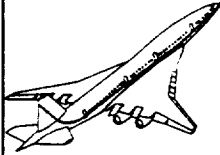
Milestone Number

Level 3

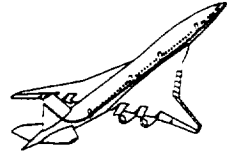
- | | |
|---|--|
| 2 | Technology Concept High-Lift Geometry Defined (May 15, 1996) <ul style="list-style-type: none">- high-lift system geometry defined in preparation for model fabrication |
| 3 | Technology Concept Preliminary Assessment (Jul 15, 1997) <ul style="list-style-type: none">- early performance and S&C assessment of Tech. Concept |
| 7 | Technology Concept Final Assessment (Sep 15, 1998) <ul style="list-style-type: none">- performance and S&C assessment of Tech. Concept leading to Tech. Config. |

Level 4

- | | |
|----|--|
| 8 | Technology Concept High-Lift Geometry Defined (May 15, 1996) <ul style="list-style-type: none">- high-lift system geometry defined in preparation for model fabrication |
| 9 | Define Stability and Control Aerodynamic Requirements (Jul 15, 1996) <ul style="list-style-type: none">- develop aerodynamic coefficient requirements based on desired handling qualities |
| 10 | Technology Concept Preliminary Assessment (Jul 15, 1997) <ul style="list-style-type: none">- early performance and S&C assessment of Tech. Concept |
| 11 | Technology Concept Final Assessment (Sep 15, 1998) <ul style="list-style-type: none">- performance and S&C assessment of Tech. Concept leading to Tech. Config. |



PCD2 Logic Description



4.3.2.2 High-Lift System Concept Design

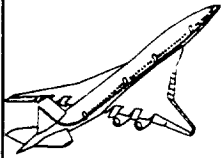
Milestone Number

Level 3

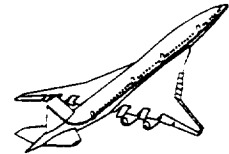
- 4 **High-Lift System Update (Sep 15, 1997)**
- interim update of high-lift system

Level 4

- 12 **Assessment of High-Lift System Refinement (Mar 17, 1997)**
- assessment of viable refinements to the high-lift system
- 13 **High-Lift System Update (Sep 15, 1997)**
- interim update to Technology Concept high-lift system



PCD2 Logic Description



4.3.2.3 Propulsion/Airframe Integration

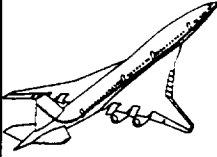
Milestone Number

Level 3

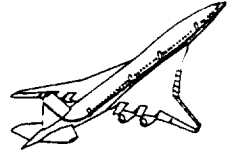
- | | |
|---|---|
| 1 | HEAT 1A Defined (Apr 30, 1996) <ul style="list-style-type: none">- definition of the technical objectives and configuration of the HEAT 1A model and subsystems |
| 6 | High-Lift/Propulsion Airframe Integration Aerodynamic Assessment (Sep 15, 1998) <ul style="list-style-type: none">- assessment of aerodynamic characteristics of current-generation HSCT |

Level 4

- | | |
|----|---|
| 14 | HEAT 1 Aeroacoustic Assessment (Apr 15, 1996) <ul style="list-style-type: none">- complete analysis of HEAT 1 aero/acoustic/propulsion test data |
| 15 | HEAT 1A Aerodynamic Assessment (Jul 15, 1998) <ul style="list-style-type: none">- complete analysis of HEAT 1A airframe/propulsion integration test data |



PCD2 Logic Description



4.3.2.4 Tools and Methods Development

Milestone Number

Level 3

5

Tools and Methods Assessment (Jun 15, 1998)

- assessment of tools and methods available for analysis and full-scale prediction of low-speed characteristics of the HSCT

Level 4

16

Automatic Adaptation of Viscous Unstructured Grid (USG) Method (Oct 15, 1996)

- development of automatic grid adaptation capability for USG method

17

Support/Wall Interference (Dec 16, 1996)

- method for correcting wind tunnel data for support and wall interference effects

18

Boundary-Layer Transition Technique Recommendation (Apr 15, 1997)

- verified technique for ensuring proper B.L. transition location

19

Ground Effects Methodology Assessment (Jul 15, 1997)

- assessment of methods for predicting ground effects from wind-tunnel data

20

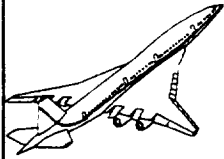
Viscous USG Technology Concept Assessment (Dec 15, 1997)

- application of viscous USG method to assess Technology Concept

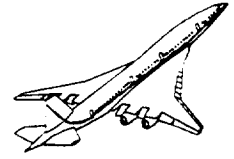
21

Full-Scale Prediction Methodology (May 15, 1998)

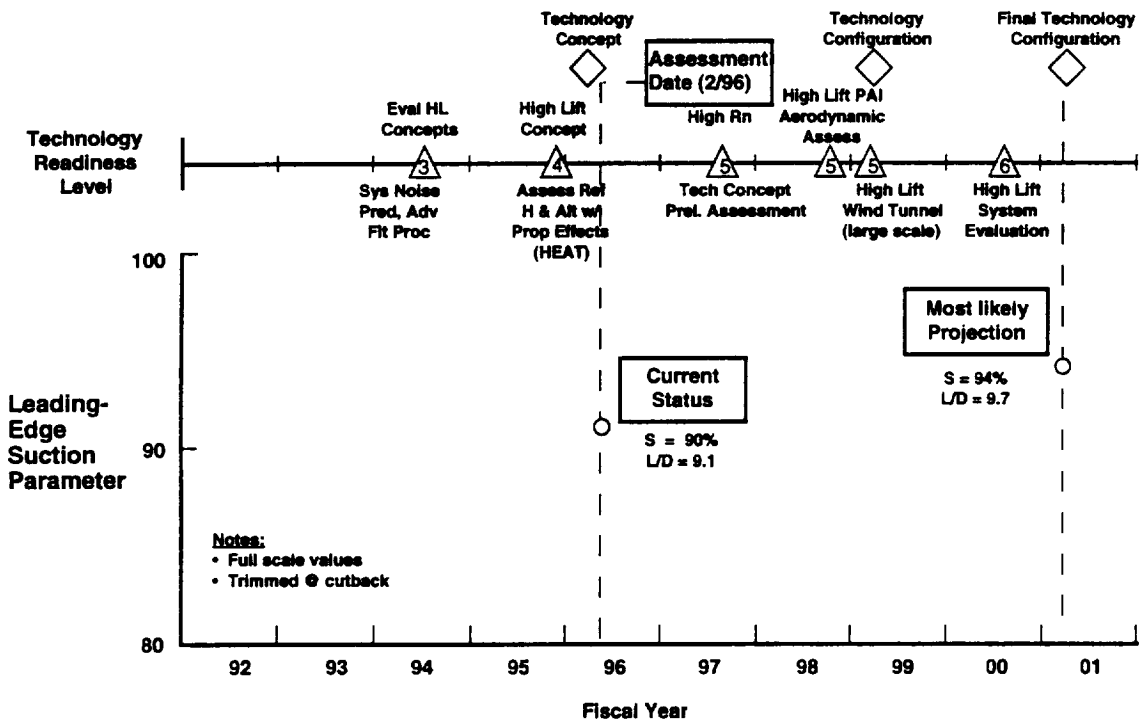
- method for extrapolation of wind tunnel results to full-scale conditions

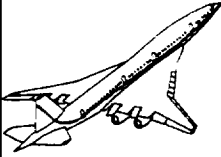


High Lift Technology Metrics

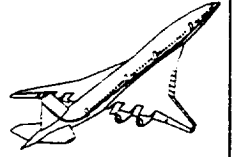


Technical Performance & Technology Readiness Level



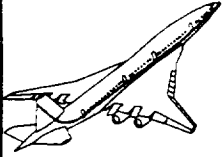


High Lift Technology Models/Facilities

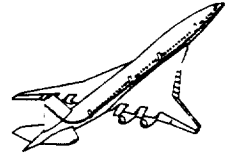


WBS 4.3.2 High-Lift Technology Model/Facility Utilization

FY	1996				1997				1998				1999
	Q1	Q2	Q3	Q4	Q1	Q2	Q3	Q4	Q1	Q2	Q3	Q4	Q1
NASA Ames													
12-Foot													
4% M2.4-7a													
4% Tech. Concept													
10/14 3wks													
40- by 80-Foot													
13.5% Sempan Ref. H													
3/13 5wks													
6/18 4wks													
NASA Langley													
16- by 22-Foot													
6% Ref. H													
4% M2.4-7a													
4% Tech. Concept													
1/8 4wks													
9/2 4wks													
12/8 2wks													
2/3 4wks													
6/2 4wks													
12/16 4wks													
NIF													
2.2% Ref. H													
12/11 6wks													
7/1 4wks													
9/18 4wks													
2/3 4wks													
NASA Lewis													
IRI													
HSCT Wing Panel													
4/1 3wks													



Summary



- **High-lift system performance will have a large impact on airplane noise and weight.**
- **Successful completion of PCD1 activities provided greater understanding of aerodynamic characteristics and configuration features important to high-lift system performance including:**
 - Reynolds number effects (Ref. H)
 - Propulsion/airframe integration effects
 - Planform effects, canard/3-surface, alternate high-lift concepts, etc.
- **PCD2 plans are aimed at achieving technology development performance goals and increasing technology readiness level for Technology Concept.**

Experimental Results of the 2.7% Reference H Nacelle Airframe Interference High Speed Civil Transport Model

Gelsomina Cappuccio
National Aeronautics and Space Administration
Ames Research Center
Moffett Field, California 94035

Experiments were conducted in the NASA Ames 9-Ft by 7-Ft Supersonic and 11-Ft by 11-Ft Transonic Wind Tunnels of a 2.7% Reference H (Ref. H) Nacelle Airframe Interference (NAI) High Speed Civil Transport (HSCT) model. NASA Ames did the experiment with the cooperation and assistance of Boeing and McDonnell Douglas. The Ref. H geometry was designed by Boeing. The model was built and tested by NASA under a license agreement with Boeing.

Detailed forces and pressures of individual components of the configuration were obtained to assess nacelle airframe interference through the transonic and supersonic flight regime. The test apparatus was capable of measuring forces and pressures of the wing body (WB) and nacelles. Axisymmetric and 2-D inlet nacelles were tested with the WB in both the in-proximity and captive mode. The in-proximity nacelles were mounted to a nacelle support system apparatus and were individually positioned. The right hand nacelles were force instrumented with flow through strain-gauged balances and the left hand nacelles were pressure instrumented. Mass flow ratio was varied to get steady state inlet unstart data. In addition, supersonic spillage data was taken by testing the 2-D inlet nacelles with ramps and the axisymmetric inlet nacelles with an inlet centerbody for the Mach condition of interest. The captive nacelles, both axisymmetric and 2-D, were attached to the WB via diverters. The captive 2-D inlet nacelle was also tested with ramps to get supersonic spillage data.

Boeing analyzed the data and showed a drag penalty of four drag counts for the 2-D compared with the axisymmetric inlet nacelle. Two of the four counts were attributable to the external bevel designed into the 2-D inlet contour. Boeing and McDonnell Douglas used these data for evaluating Computational Fluid Dynamic (CFD) codes and for evaluation of nacelle airframe integration problems and solutions.

- Objectives
 - Database for CFD Validation
 - Axisymmetric vs 2-D Inlet Nacelles
 - Nacelle Installation: Captive and In-Proximity
 - Supersonic Spillage Data
 - Steady-State Inlet Unstart Data

- Participants: NASA Ames, Boeing, and McDonnell Douglas

- Results of 2.7% Ref. H NAI Test
 - Measured 4.5 Drag Count Penalty for 2-D Inlet Nacelle
 - 2 Drag Counts Attributable to External Bevel Design
 - CFD and Wind Tunnel Tools Evaluated

An experiment was conducted from December 1993 to February 1994 in the NASA Ames 9-Ft by 7-Ft Supersonic Wind Tunnel and from March to May 1994 in the 11-Ft by 11-Ft Transonic Wind Tunnel of a 2.7% Reference H (Ref. H) Nacelle Airframe Interference (NAI) High Speed Civil Transport (HSCT) model. NASA Ames did the experiment with the cooperation and assistance of Boeing and McDonnell Douglas. The Ref. H geometry was designed by Boeing. The model was built and tested by NASA under a license agreement with Boeing.

Detailed forces and pressures of individual components of the configuration were obtained to assess nacelle airframe interference through the transonic and supersonic flight regime. The test apparatus was capable of measuring forces and pressures of the wing body (WB) and nacelles. Axisymmetric and 2-D inlet nacelles were tested with the WB in both the in-proximity and captive mode. The in-proximity nacelles were mounted to a nacelle support system apparatus and were individually positioned. The right hand nacelles were force instrumented with flow through strain-gauged balances and the left hand nacelles were pressure instrumented. Mass flow ratio was varied to get steady state inlet unstart data. In addition, supersonic spillage data was taken by testing the 2-D inlet nacelles with ramps and the axisymmetric inlet nacelles with an inlet centerbody for the Mach condition of interest. The captive nacelles, both axisymmetric and 2-D, were attached to the WB via diverters. The captive 2-D inlet nacelle was also tested with ramps to get supersonic spillage data.

Boeing analyzed the data and showed a drag penalty of four drag counts for the 2-D compared with the axisymmetric inlet nacelle. Two of the four counts were attributable to the external bevel designed into the 2-D inlet contour. Boeing and McDonnell Douglas used these data for evaluating Computational Fluid Dynamic (CFD) codes and for evaluation of nacelle airframe integration problems and solutions.

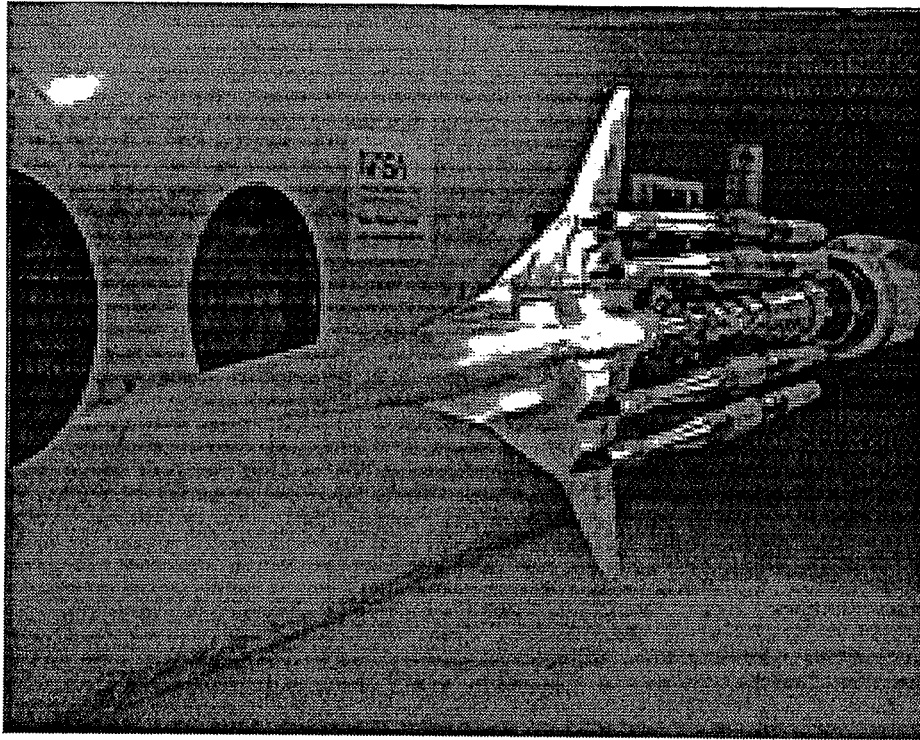


Figure 1. 2.7% Ref. H WB and MCTCB In-Proximity Nacelles in 9x7

The 2.7% Ref. H NAI model consists of a wing body (WB) and nacelles either attached using diverters or in-proximity using a Nacelle Support System (NSS). The WB represents Boeing's Ref. H geometry of an HSCT designed using linear theory. Figures 1 show the axisymmetric nacelles tested in-proximity to the WB using the NSS in the 9x7.

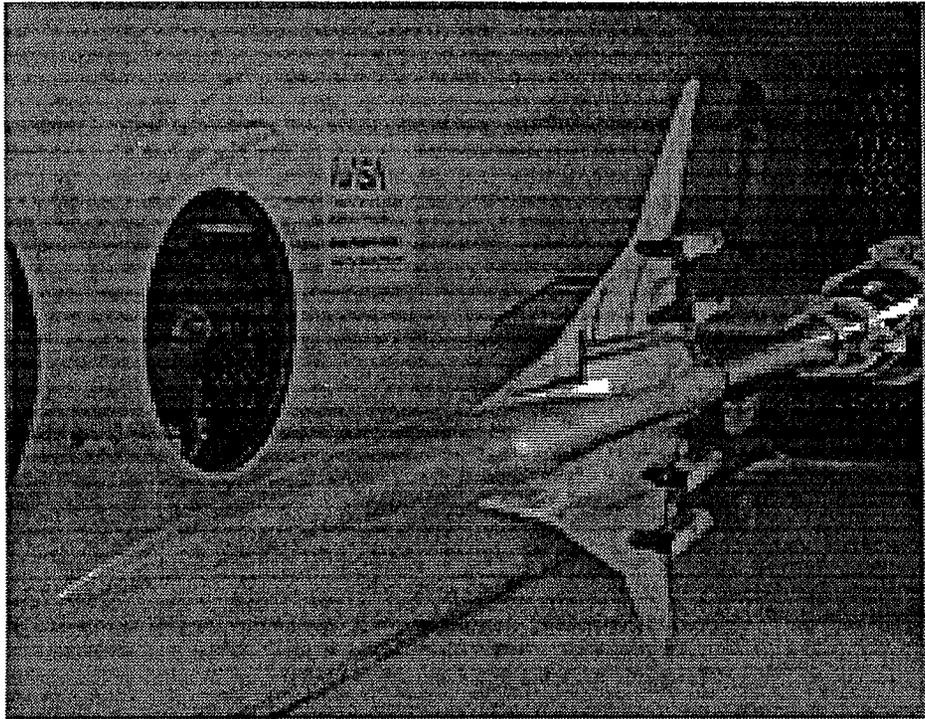


Figure 2. 2.7% Ref. H WB and BTSSI Captive Nacelles in 9x7

Figure 2 shows the BTSSI nacelles tested captively on the 2.7% Ref. H WB in the 9x7.

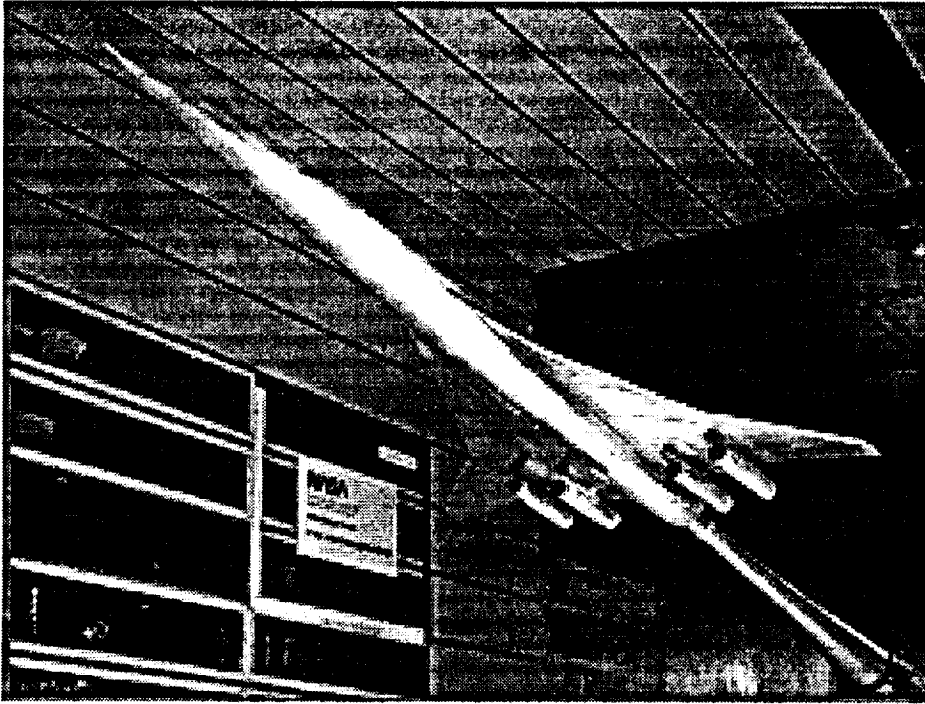


Figure 3. 2.7% Ref. H WB and MCTCB Captive Nacelles in 11x11

Figure 3 shows the axisymmetric nacelles installed on the WB and being tested in the 11x11.

- MODEL
 - Wing Body
 - Pressure Instrumentation
 - 280 on Upper and Lower Left Hand Wing Surfaces
 - 24 on Fuselage
 - Connections for 32 Pressures Taps on Right Hand Nacelles
 - 2.0 inch Diameter Task MK IA Force Balance
 - AX = ± 160 lb., N1 = N2 = ± 900 lb., S1 = S2 = ± 450 lb., and RM = ± 1000 in-lb.
 - Calibrated and Corrected for Temperature Effects on Zero Shift and Conversion Constant but not for Gradients Across Balance on AX, N1 and N2
 - 0.011 inch High Epoxy Boundary Layer Trip Discs Placed 0.64 inches Aft in Stream-wise Direction; Location Same as 1.7% Ref. H and Height based on Sizing Criteria in NASA TM 4363.

The wing is made out of 15-5 stainless steel heat treated to condition H1025. The forward and aft section of the fuselage are made out of 6061-T6 aluminum, while the mid section, that houses the balance, is made out of 17-4 stainless steel. The fuselage was cut off at station of 2904.6 inches for the model, and therefore does not include the empennage.

The upper and lower left hand wing surfaces are pressure instrumented, while the right hand wing accommodates pressure tubes from the nacelles that are mounted to the wing. Pressures were not measured on the aft fuselage base because the base collapsed to a knife edge. Tubing was installed on the sting to measure pressure just behind the balance for corrections to the data. There are 123 pressures on the upper wing surface shown in figure 4, 157 on the lower surface shown in figure 5, and 24 on the fuselage surface.

The WB forces were measured using a 2.0 inch diameter Task MK IA force balance that was housed in the balance block in the mid section of the fuselage. The capacity of the MK I balance is ± 900 lb. for N1 and N2, ± 450 lb. for S1 and S2, ± 160 lb. for AX and ± 1000 in-lb. for RM. The balance was calibrated at various temperatures so that temperature corrections could be made to get the best accuracy and repeatability out of the balance. It was very important to measure drag as accurately as possible. The balance repeated to within $\pm 0.1\%$ of full scale capacities on each gage when calibrated.

Epoxy trip discs were used to trip the boundary layer. The height chosen was 0.011 inches and they were placed 0.64 inches aft in the stream-wise direction on the upper and lower surface and 1 inch aft on the fuselage nose.

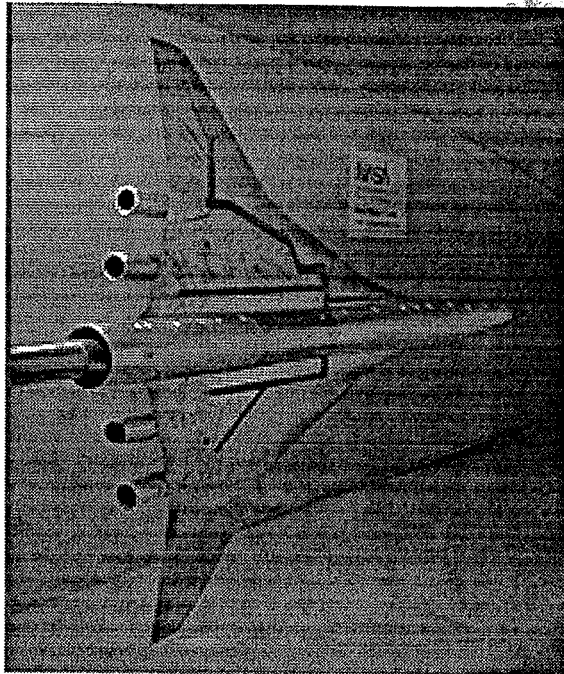


Figure 4. Upper Surface of 2.7% Ref. H WB and BTSSI Captive Nacelles in 9x7

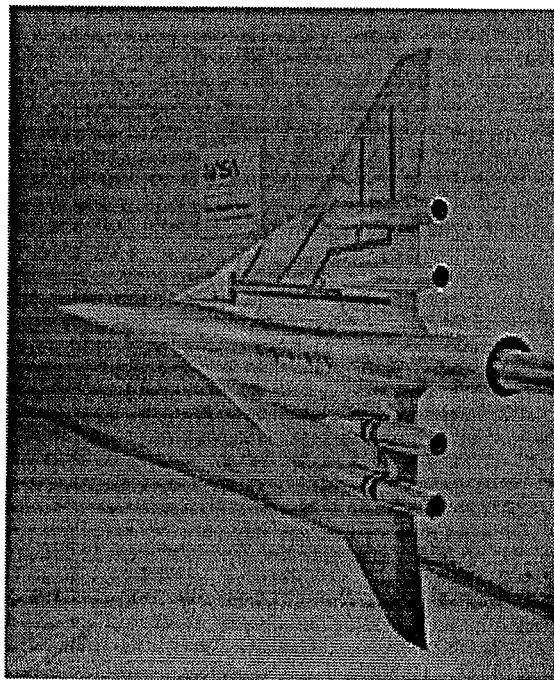


Figure 5. Lower Surface of 2.7% Ref. H WB and BTSSI Captive Nacelles in 9x7

- Captive Nacelles
 - Axisymmetric
 - Mixed Compression Translating Centerbody (MCTCB)
 - Inlet Designed for 509 lb./sec Turbine Bypass Engine (TBE)
 - Axisymmetric Nozzle
 - 2-D
 - Bifurcated Two Stage Supersonic Inlet (BTSSI)
 - Inlet Designed for 540 lb./sec TBE, but Scaled to Match MCTCB Inlet Area
 - Axisymmetric Nozzle
 - Tested with and without Ramp
- 2 Base Pressures Measured to make Force Corrections
- 3 Rows of 10 Pressure Taps: Inboard, Keel, and Outboard

The axisymmetric inlet nacelles are designated as the MCTCB, mixed compression translating centerbody, nacelles. The 2-D inlet nacelles are designated the BTSSI, bifurcated two stage supersonic inlet, nacelles.

The axisymmetric inlet nacelles represent the design for a Turbine Bypass Engine (TBE) with airflow of 509 lb./sec. The 2-D inlet nacelles represent the design for a TBE with airflow of 540 lb./sec. The 2-D inlet nacelle was scaled to match the inlet capture area of the axisymmetric inlet nacelle for this test so an evaluation of how the two types of inlets could be made.

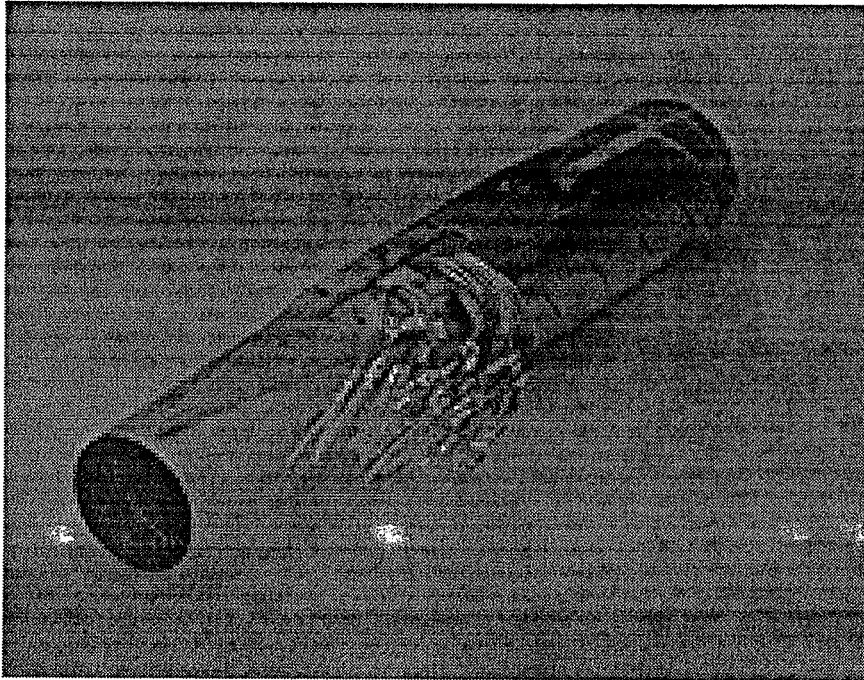


Figure 6. MCTCB Pressure Instrumented Captive Nacelle

The captive nacelles were all made out of 7075-T6 aluminum as well as the diverters. The right hand nacelles were pressure instrumented on the external and base surfaces. There are 30 external pressures on the MCTCB captive nacelles, figure 6.

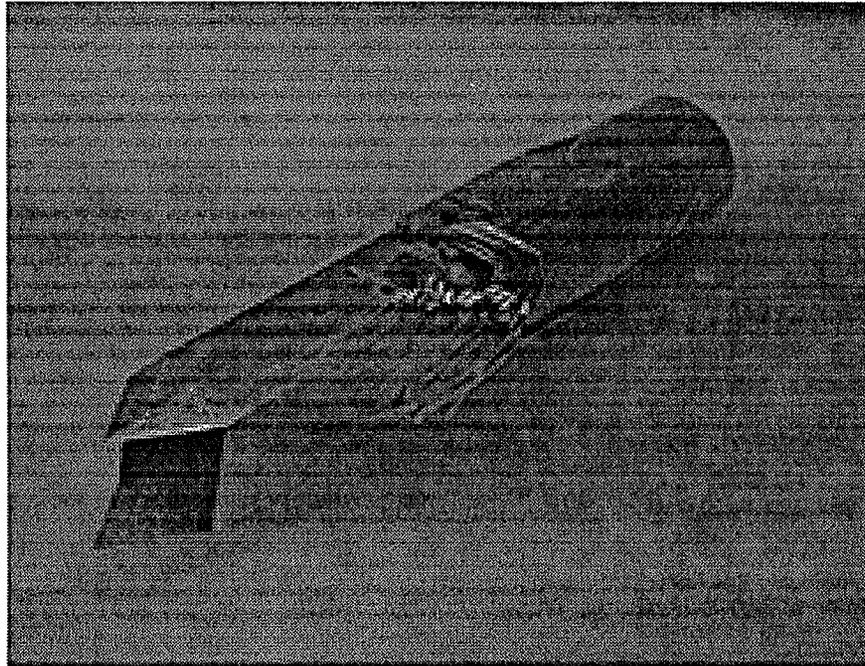


Figure 7. BTSSI Pressure Instrumented Captive Nacelle

There are 31 pressure taps on the BTSSI captive nacelles as well as one base pressure per right hand nacelle, figure 7.

- In-Proximity Nacelles
 - Nacelle Support System
 - Position in Axial, Spanwise, and Vertical
 - Mass Flow Ratio
 - Total Pressure Rakes in each Sting
 - Static Exit Pressure in each Sting
 - Based on 1972 Calibration
 - Video Camera Mounted on Sting to Monitor Nacelles
 - Remotely Controlled via Computer or Manual Drive Box
 - MCTCB Tested with and without Centerbody for
Mach = <1.2, 1.65, 1.8, and 2.4
 - BTSSI Tested with and without Ramp: First Ramp Angle
 - Left Hand Nacelles
 - 4 External Rows of 10 Pressures: Crown, Inboard, Keel, Outboard
 - 4 Internal Rows of 2 Pressures: Used to Compute RN and Mach for Skin Friction Force Correction

The in-proximity nacelles were tested using a nacelle support system (NSS). The NSS is clamped to the main sting and can remotely position four nacelles under the wing in the axial, spanwise, and vertical directions. In addition to positioning the nacelles, the mass flow can be varied through the nacelles. The two left hand nacelles are pressure instrumented and the two right hand nacelles are force instrumented with custom built flow-through balances. The MCTCB and BTSSI nacelles were tested on the NSS. The 15 motors of the NSS are controlled by a computer control system via typed commands and hot keys or by a manual driver. The primary axial drive positions all four nacelles at one time, while each nacelle can be driven individually by its own axial drive motor. There is a drive motor for spanwise positioning of the inboard nacelles and another for the outboard nacelles. Each nacelle has a vertical drive motor and the remaining four motors drive mass flow plugs for each nacelle.

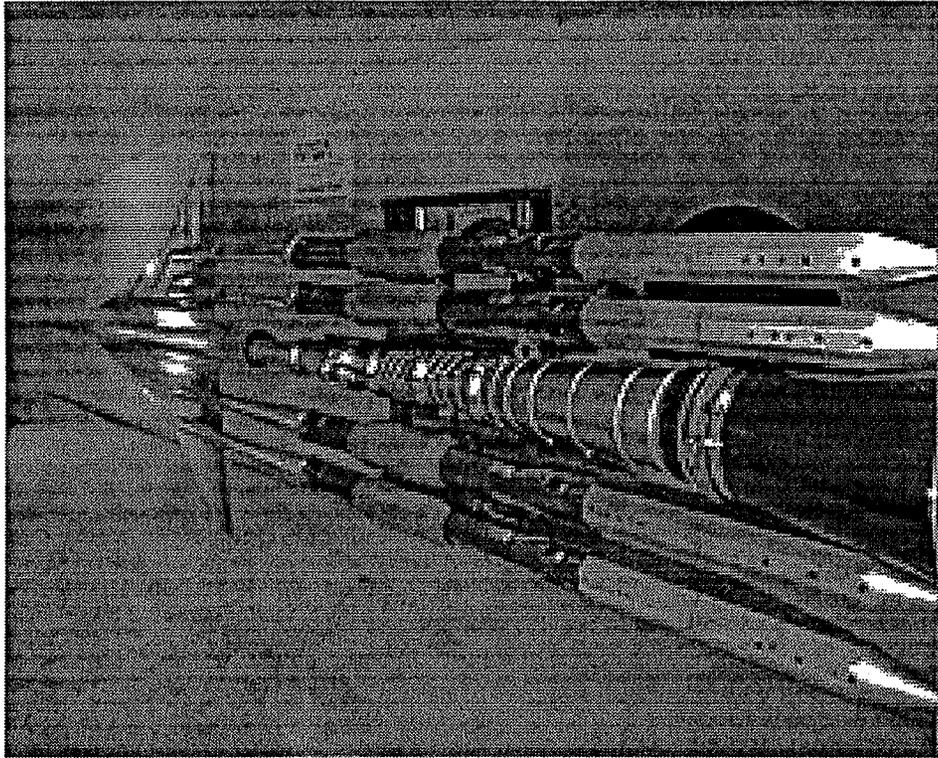


Figure 8. Lower Surface of NSS

Figure 8 shows the lower surface of the NSS. This figure illustrates the individual axial drive stings, mass flow exits, and the video camera attached to the main sting.

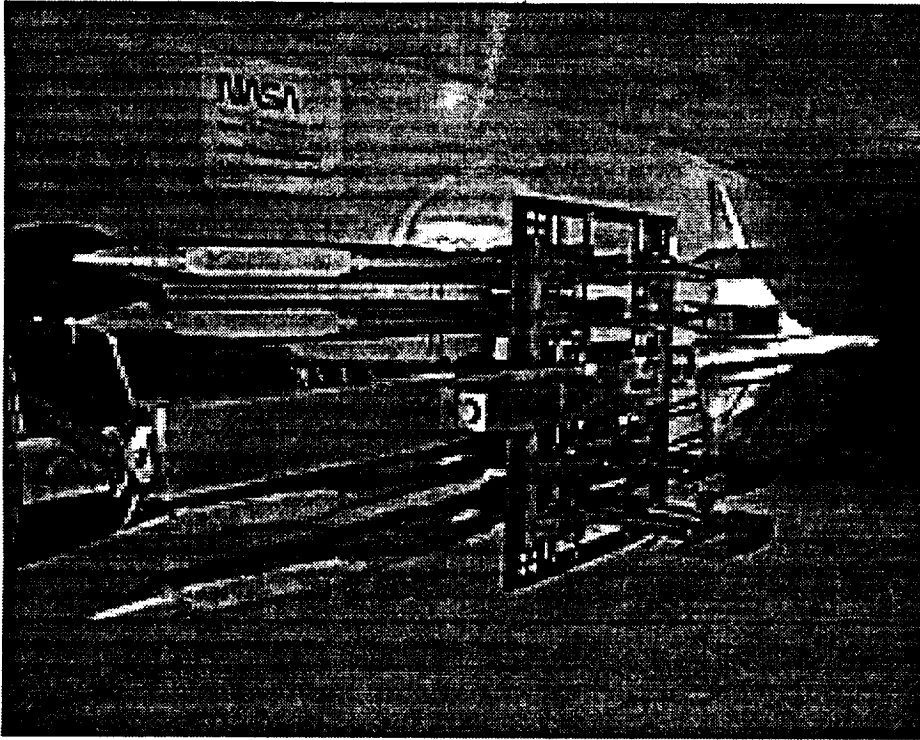


Figure 9. Upper Surface of NSS

Figure 9 shows the upper surface of the NSS. Observe the main axial drive system, spanwise, and individual vertical drives. The remotely driven vertical drive system was added to NSS for the SA1150 NAI test in 1992/93. The capability of the NSS to work more efficiently while the model is mounted in the vertical plane was also added to the NSS for this test.

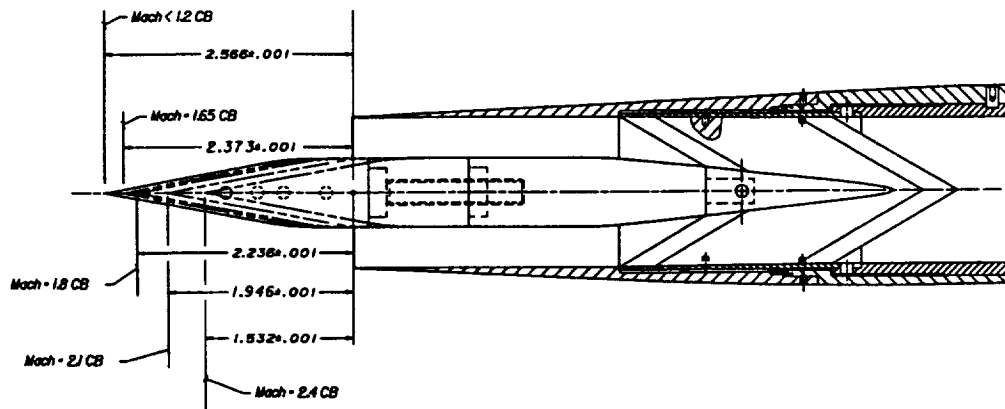


Figure 10. MCTCB Nacelle with Inlet Centerbody Assembly

During the NAI part of the test, the MCTCB nacelles were tested with and without inlet centerbodies for each of its designed Mach numbers. Supersonic spillage data was acquired at all Mach numbers for each of the inlet centerbodies installed. Figure 10 shows how the centerbody is assembled in the MCTCB nacelle. The inlet centerbody is attached to the non-metric part of the internal duct so that the nacelle balance did not measure its force. The only effects measured are how the forces of the WB and nacelles changed due to the inlet centerbody and test condition. The pressures of the WB and nacelles were also measured. The MCTCB captive nacelles were not tested with the inlet centerbody.

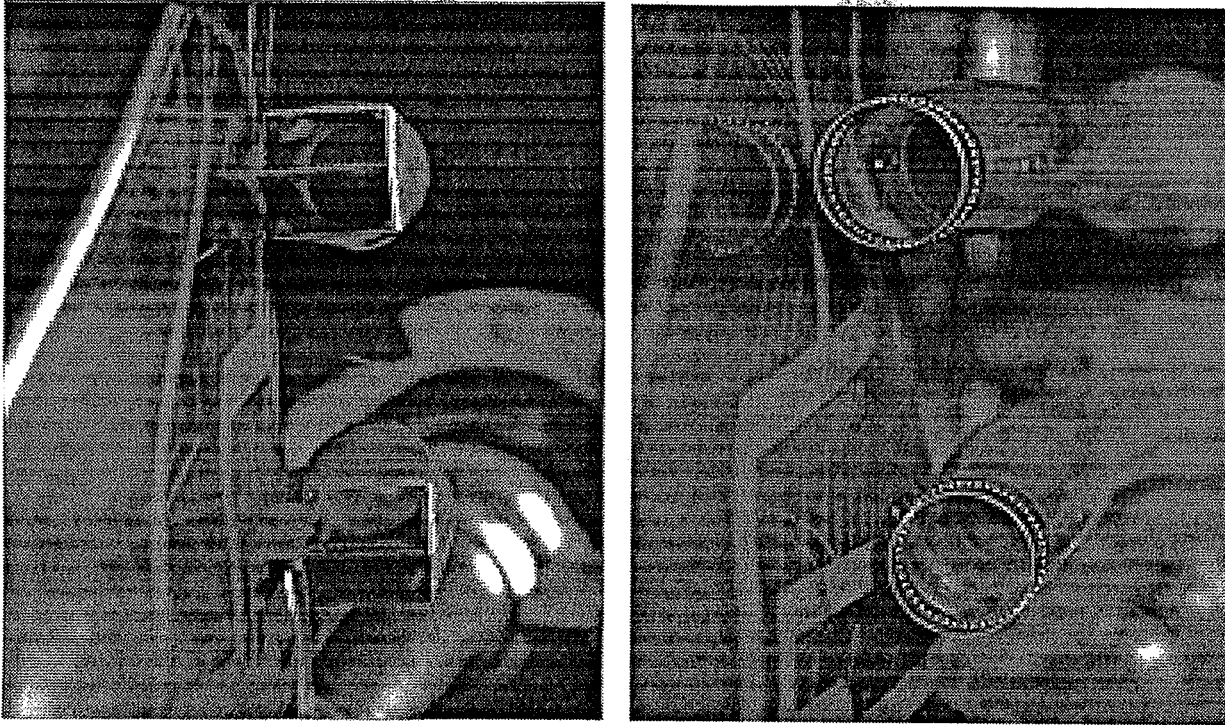


Figure 11. BTSSI and MCTCB Nacelles Installed

The BTSSI nacelles were tested with and without a ramp at all Mach numbers. Figure 11 shows the ramp installed in the BTSSI captive nacelles but was also installed in the in-proximity nacelles. The ramp only includes the first ramp angle that is part of the external flow field. The other ramp angles are internal and did not need to be modeled.

The nacelles were positioned in various locations and mass flow ratio was varied during the test. Angle of attack sweeps was the main variation in the run series, except when mass flow ratio was the varying parameter.

The left hand pressure instrumented nacelles were made out of 6061-T6 aluminum. A total of 188 pressures were measured during the test for the in-proximity nacelles. The left-hand nacelles had 40 external and 8 internal pressures for each inboard and outboard nacelle.

All of the nacelle stings had mass flow rakes. There were 16 total pressures and 4 static pressures measured per nacelle. Figure 11 illustrates the MCTCB pressure instrumented in-proximity nacelles.

- In-Proximity Nacelles (Continued)
 - Right Hand Nacelles Instrumented with a Force Flow Through Balance
 - Primary and Backup AX = ± 10 lb., N1 = N2 = ± 40 lb., and RM = ± 10 in-lb.
 - Calibrated and Corrected for Temperature Effects on Zero Shift and Conversion Constant on AX, N1 and N2
 - Corrections to Axial Force
 - Pressure within the Fwd- and Aft- Balance Cavities
 - Pressure on the Fwd Lip Cavity
 - Across the Balance Seal
 - Calibration
 - f (Fwd Lip Cavity Pressure, Balance Force)
 - Skin Friction on the Nacelle Metric Internal Lip: Average Turbulent SF based on RN and Mach
 - BTSSI Metric Internal Duct Transition
 - BTSSI Ramp

The right hand force instrumented nacelles were made out of 17-4 stainless steel. The force instrumented nacelles housed flow through type balances that were designed and built by MicroCraft. The capacity of each balance is ± 40 lb. for N1 and ± 40 lb. for N2, ± 10 lb. for AX1 and AX2, and ± 10 - in-lb. for RM. The nacelle balances repeated to within ± 0.1 % full scale capacities of each gage when calibrated.

Corrections were made to the axial force measurements. Force corrections were made due to pressures measured within the forward and aft balance cavities. A force correction was made due to the pressures on the forward lip cavity. A force correction was made due to a force across the balance seal. A force correction was made due to the skin friction on the metric part of the internal duct ahead of the balance and past the inlet lip. A force correction was made due to the transition occurring in the BTSSI internal duct in the same region. Finally, a force correction was made due to the ramp installed in the BTSSI. Each of these forces was computed during the test except for the internal duct transition and ramp for the BTSSI. These two particular forces were estimated at all conditions subsequent to the test and then applied during the test. The other forces were computed based on the pressures and forces measured during the test. There were a total of 12 pressures, 6 for the inboard and 6 for the outboard, measured.

The MCTCB inlet centerbodies were attached to the non-metric portion of the internal duct and therefore no corrections were needed. The BTSSI ramp was attached to the metric portion of the internal duct. This in turn is measured by the nacelle balance. This force was estimated by Boeing at each condition subsequent to the test. The wind tunnel data was corrected for the force generated by the ramp during the test.

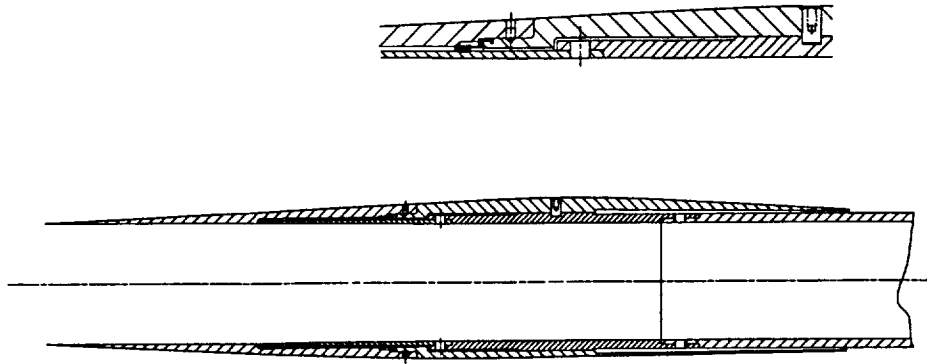


Figure 12. MCTCB Force Nacelle Assembly

Figure 12 shows the how the balance is installed in the MCTCB nacelle. Notice the location of the seal and the break between metric and non-metric parts of the internal duct. The balance measures the forces generated by the metric portion of the nacelle.. The metric portion includes the entire external nacelle surface and the forward 2.746 inches of the internal duct. Pressure taps were located on the front of the non-metric internal duct sleeve ahead of the balance. Pressure taps were also located on the forward part of the balance to measure a forward cavity pressure and on the aft part of the balance to measure aft cavity pressure. The same pressures were measured for the balance installed in the BTSSI nacelle. The installation of the balance in the BTSSI nacelle is exactly the same as for the MCTCB nacelle. The metric portion of the BTSSI internal duct is 4.628 inches. The BTSSI nacelle internal duct transitions from a 2-D cross-section to a circular one. The balance measures the force generated by this transition. The wind tunnel data is corrected for this force that were estimated by Boeing subsequent to the test at each condition.

- TEST PROGRAM
 - 9x7 from Dec. '93 to Feb. '94
 - Mach = 1.65, 1.8, 2.1, and 2.4
 - RN = 3 Million/Ft
 - Angle-of-Attack = -2° to 10°
 - Mass Flow Ratio = 1 to 0
 - Sublimation
 - UV Oil Flow Visualization
 - Schlieren
 - UV Crystal Flow Visualization
 - 11x11 from Mar. '94 to May '94
 - Mach = 0.8, 0.9, 0.95, 1.2, and 1.3
 - RN = 3 Million/Ft
 - Angle-of-Attack = -2° to 10°
 - Mass Flow Ratio = 1 to 0
 - Sublimation

Running was done at Mach numbers of 1.65, 1.8, 2.1, and 2.4 at a constant Reynolds number (RN) of 3x10⁶/ft for the 9x7 test. Running was done at Mach numbers of 0.9, 0.95, 1.2 and 1.3 at a constant RN of 3x10⁶/ft for the 11x11 test. The runs consisted of alpha and mass flow sweeps. The alpha sweeps were done from -2° to 5° by 0.25° and 5.5° to 10° by 0.5° increments. The mass flow sweeps were established by controlling the mass flow plugs from fully opened to closed. Seven plug positions between fully opened and closed were part of the mass flow sweep. The actual mass flow numbers depended on the configuration and the test conditions. Repeat runs were done throughout the test to establish drag data accuracy and repeatability.

When the nacelles were run isolated, the 9x7 test was run at Mach = 1.627, 1.771, 2.061, and 2.35 and the 11x11 test was run at Mach = 0.8, 0.9, 0.95, 1.193, and 1.29. These were the estimated local Mach numbers the inlet would see if the WB was present. The mass flow sweeps were done at 4°, 4.5°, and 5° to bracket the cruise point. When the nacelles were tested without the WB, the settings were 2.9°, 3.4°, and 3.9°. These numbers represent the same angle but without the incidence angle of the nacelles. Data was taken at 9 plug positions for each angle-of-attack to capture when the inlet would unstart. In addition to the runs described above, data was taken for the nacelles positioned differently from the location when the nacelles are mounted captively. Axial, span-wise, and vertical position studies were done. Effect of NSS on the WB forces was run also. On several occasions, data was taken for angle-of-attack sweeps at a constant mass flow ratio. The data taken at the constant mass flow ratio represents an engine throttle setting.

Wing Body	NSS	BTSSI	Ramp	MCTCB	Centerbody
X					
X		X			
X		X	X		
X				X	
X	X	X			
X	X	X	X		
X	X			X	
X	X			X	Mach 1.65
X	X			X	Mach 1.8
X	X			X	Mach 2.4
	X			X	Mach 2.4
	X			X	Mach 1.65
	X			X	Mach 1.8
	X			X	
	X	X	X		
	X	X			
X	X	X			

Table 1. Model Configurations Tested in 9x7

Table 1 lists the order of the model configurations tested in the 9x7. At the onset of the test, many studies were performed to optimize the data acquisition and tunnel condition settings. A sampling rate, humidity, balance temperature soak, cavity pressure settling time, and **bridge effect studies** were performed. During each configuration a number of repeat runs were done for the alpha sweeps to establish the repeatability and accuracy of the data. During the mass flow ratio sweeps, the mass flow was varied on one nacelle side at a time to get the effect of unstart on the wing body and nacelle forces. Pressures on both the wing and nacelles were also measured during the mass flow sweep runs. A mass flow sweep was done only on the right hand outboard (RO) nacelle at 3 constant angle-of-attacks to get the forces of the RO nacelle and WB. After these runs, mass flow sweep was done on the left hand outboard (LO) nacelle at the same 3 constant angle-of-attacks to get the nacelle and wing pressures. There were times when mass flow ratio was varied in both RO and RI nacelles to get mutual unstart effect on WB and nacelles.

Wing Body	NSS	BTSSI	Ramp	MCTCB	Centerbody
X					
X		X	X		
X		X			
X				X	
X					
X	X	X	X		
X	X	X			
X	X	X	X		
X	X			X	
X	X			X	Mach 1.2
	X			all	Mach 1.2
	X			all	
	X	outboard	X	inboard	
	X	outboard		inboard	
X	X			X	
X	X			X	Mach 1.2
X					
X				X	

Table 2. Model Configurations Tested in 11x11

Table 2 lists the order of the model configurations tested in the 11 x 11. This test was much shorter and more difficult to run because of inherent interference problems due to testing at transonic speeds. Similar studies up front were done in the 11x11 as the 9x7. The same type and quality of data were striven for here.

- DATA
 - Repeatability: $\Delta C_D < 0.5$ CTS
 - Accuracy: Data Compared with 1.7% Ref. H in BSWT $\Delta C_D < 2$ CTS
 - Nacelle Installation Drag Increments at Cruise
 - MCTCB: $\Delta C_D = 4.8$ CTS
 - BTSSI: $\Delta C_D = 9.3$ CTS
 - Flow Visualization

The data taken during these tests were extensive and this report does not give it justice. A lot of the data was and is still be analyzed by NASA, Boeing, McDonnell Douglas, and Lockheed. The emphasis of this report is on the data quality and overall difference between the MCTCB and BTSSI nacelles.

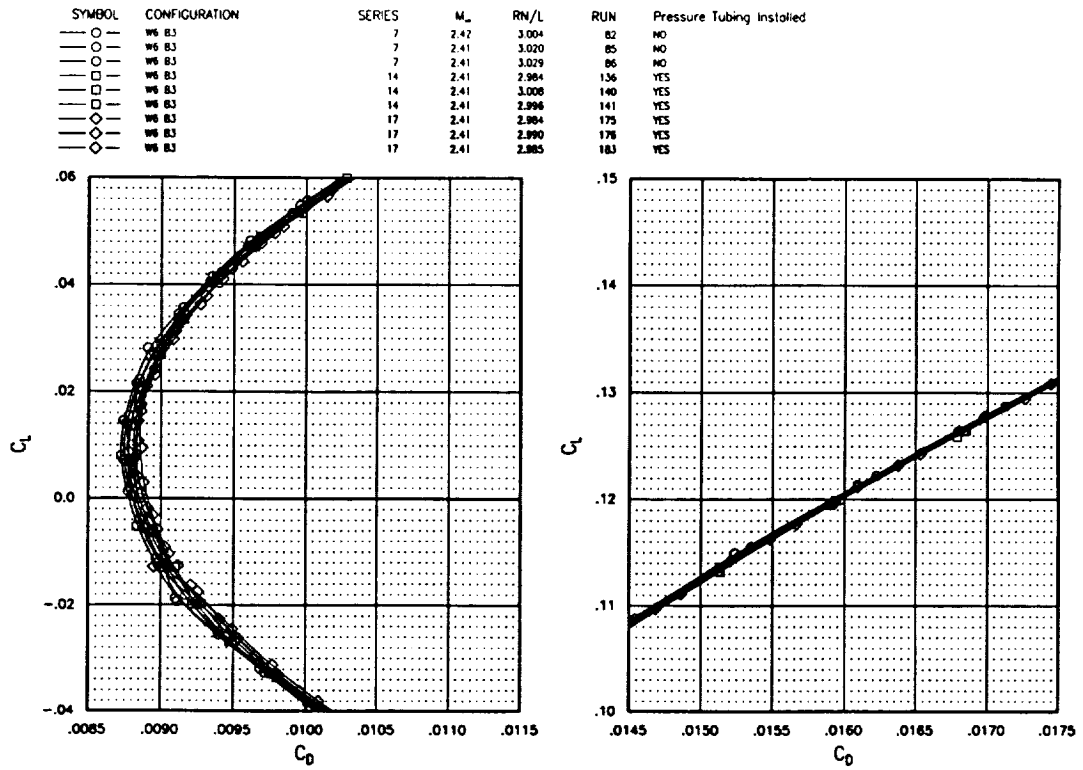


Figure 13. Drag Polar of WB Repeat Runs

It was very important to make sure the data quality was good to be able to distinguish differences between many configurations. Drag repeatability had to be less than 0.0001 or 1 drag count. The data generated during the test turned out to be better. It was less than a 0.5 drag count most of the times. Items that contributed to this result were detail procedures, calibrations, and measurements of the WB and nacelle balances, and angle-of-attack. Figure 13 shows a representative drag polar of repeat runs.

SYMBOL	CONFIGURATION	M _∞	RN/L	RUN	SCALE
○	ARC 198197: W6 B3	2.41	2.984	136	0.027
○	ARC 198197: W6 B3	2.41	3.008	140	0.027
○	ARC 198197: W6 B3	2.41	2.996	141	0.027
□	BSWT 628: W6 B3	2.39	7.586	215	0.01675
□	BSWT 628: W6 B3	2.39	7.567	225	0.01675
□	BSWT 628: W6 B3	2.39	7.573	238	0.01675

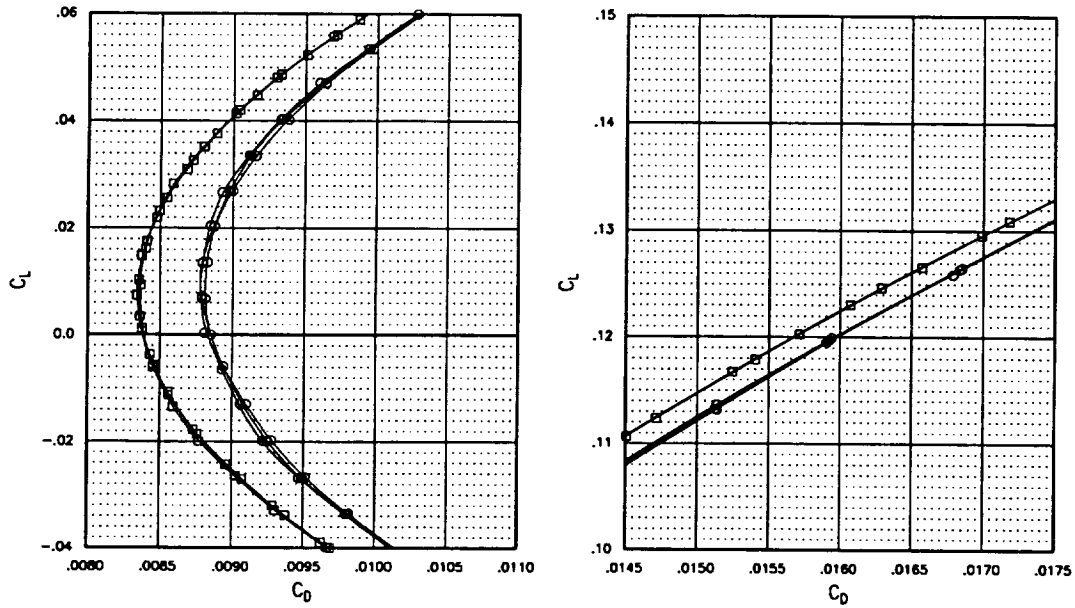


Figure 14. Drag Polar of 2.7% vs 1.7% Ref. H WB: Skin Friction $\Delta C_D = 0.0006$

The test began with many studies. There were sampling rate, humidity, balance temperature, and pressure bridging effect studies. Each of these studies established the best conditions for taking data. The first evaluation of the data came when comparisons were done with data collected on the 1.7% Ref. H model in the Boeing Supersonic Wind Tunnel (BSWT). This comparison established the magnitude level of the data. On average the data from the 2.7% Ref. H WB was 2 counts higher than the 1.7% Ref. H model over the angle-of-attack range. The 2 counts is attributable to trip drag. Figure 14 shows the drag polar for this comparison. The plot shows 6 counts more which is due to the skin friction of the model at different scales and RN.

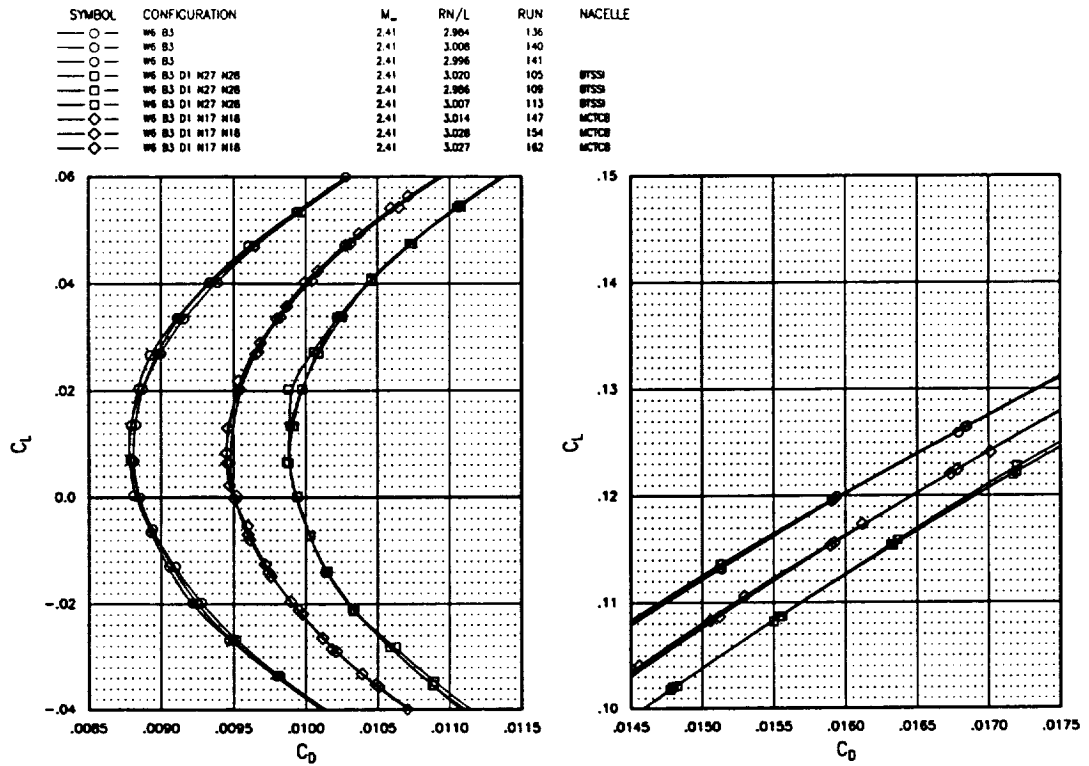


Figure 15. Drag Polar of MCTCB vs BTSSI Captive Nacelles Installed

The BTSSI nacelle measured 4.5 drag counts higher than the MCTCB. This increment was the same between the captive and the in-proximity testing. Figure 15 shows the drag polar of this comparison. The in-proximity testing measurements were 1.6 drag counts lower than in captive mode. This in turn says that the 1.6 counts are due to the diverter.

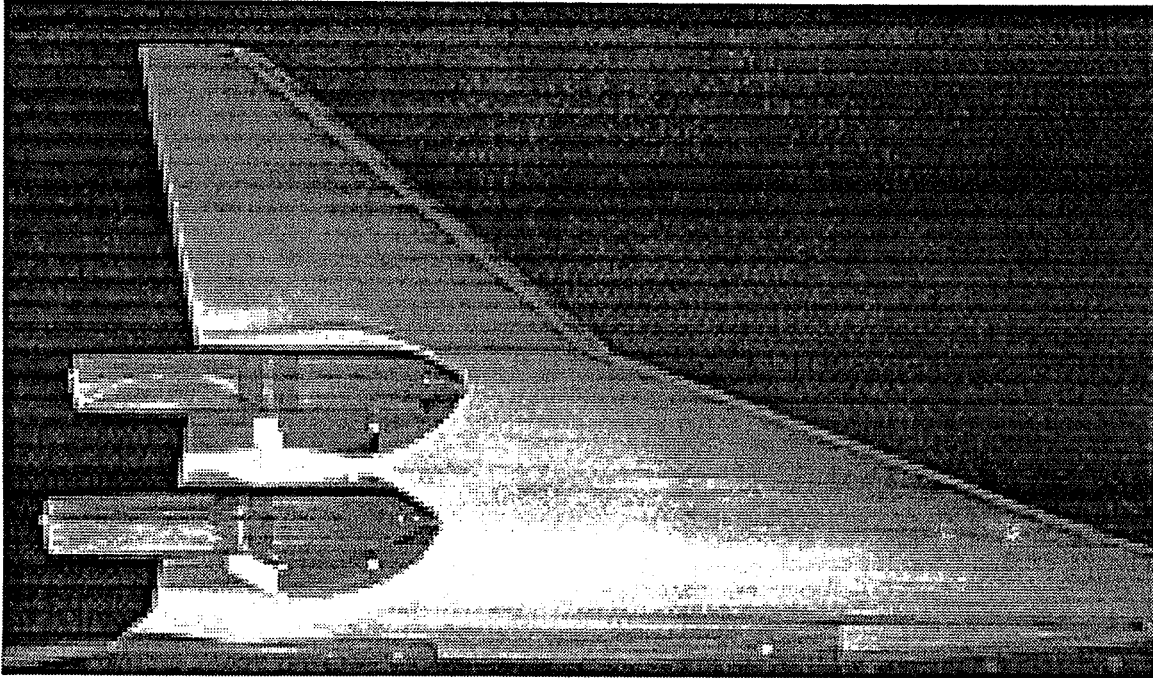


Figure 16. UV Oil Flow Visualization on WB and BTSSI In-Proximity Nacelles at Mach = 2.4

Data was also taken for supersonic spillage and steady-state inlet unstart effects. Flow visualization was performed to verify the boundary layer tripped using sublimation. Ultra-Violet (UV) Oil flow visualization was performed to evaluate the flow at all supersonic conditions with nacelles installed. Schlieren photos and video were taken when the nacelles were tested isolated to document the mass flow effect on the flow field around the nacelle and on inlet unstart. Figure 16 is a representative photo of flow visualization done in the 9x7.

- CONCLUSION
 - BTSSI
 - 4.5 Drag Counts Higher than MCTCB
 - 2 Drag Counts Attributable to the External Bevel Designed into the 2-D Inlet Contour
 - CFD Verified What Wind Tunnel Measured After the Test
 - Emphasis on Data Quality
 - Pre-Test Calibrations of Model Support System for Angle-of-Attack Measurements
 - Procedure for Measuring Reference Angle-of-Attack in Horizontal Plane
 - Balance Temperature Calibrations and Operating Procedures
 - Humidity and Data Sampling Studies
 - Drag Repeatability < 0.5 CTS in 9x7
 - Analysis and Reporting of Data will be in a NASA CTM
 - Data is Available from ARC or LaRC Data Base

Overall the test was a high quality data taking test. The test showed that the BTSSI nacelle has a drag penalty over the MCTCB. During the test a lot of the data was analyzed for its completeness. After the tests were over, Boeing and McDonnell Douglas had tasks to analyze the data and compare results to their CFD analysis. Data is still being analyzed by Boeing and Lockheed. NASA will report on the test in more detail. The NASA report will be a NASA CTM. The data is available through the author or through NASA Langley. Included with the data is the run schedule and descriptions of the forces and configurations.



HSCT Propulsion Airframe Integration Studies

Steve Chaney

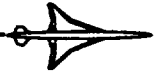
The Boeing Company

- **Inlet Spillage Interference Analysis and Modelling**
 - *** **Lockheed Martin (Charlie Novak) *****

- **Supersonic Cruise PAI Drag Issues (Boeing)**
 - **CFD Validation, CFD/Test Comparisons**
 - **Bifurcated / Axisymmetric Inlet Drag Differences**

The Lockheed Martin spillage study was a substantial effort and is worthy of a separate paper. However, since a paper was not submitted a few of the most pertinent results have been pulled out and included in this paper. The reader is urged to obtain a copy of the complete Boeing Configuration Aerodynamics final 1995 contract report for the complete Lockheed documentation of the spillage work.

The supersonic cruise studies presented here focus on the bifurcated - axisymmetric inlet drag delta. In the process of analyzing this delta several test/CFD data correlation problems arose that lead to a correction of the measured drag delta from 4.6 counts to 3.1 counts. This study also lead to much better understanding of the OVERFLOW gridding and solution process, and to increased accuracy of the force and moment data. Detailed observations of the CFD results lead to the conclusion that the 3.1 count difference between the two inlet types could be reduced to approximately 2 counts, with an absolute lower bound of 1.2 counts due to friction drag and the bifurcated lip bevel.



Inlet Spillage Interference Analysis and Modelling

- **Data Analysis: NASA Ames Ref H 9x7 & 11 ft tests**
- **CFD Modelling: OVERFLOW**
 - **Isolated**
 - **Nacelle-in-Proximity**

HSCT High Speed Aerodynamics

1.0 INTRODUCTION

The technical objective of this study was to conduct analyses to determine effects of inlet oblique shock (nominal) spillage interference. This was done for nacelles in proximity to wing using force and pressure data obtained in NASA wind tunnel testing of a 2.7% scale model of the Boeing Reference H HSCT Configuration. Selected wind tunnel data were compared to computational fluid dynamics (CFD) analysis methods to determine if nominal spillage effects can be reliably predicted by CFD methods.

The technical approach taken during this study consisted of three parts. First the NASA-ARC Data Management System Utilities (CDDMS) were used to reduce the 2.7% Reference H Nacelle-Airframe Interference (NAI) wind tunnel data from tests conducted in both the 9'x7' and 11'x11' test facilities for:

- isolated Mixed-Compression Translating Centerbody (MCTCB) nacelles,
- isolated Bifurcated Two-Stage Supersonic Inlet (BTSSI) nacelles,
- nacelle-to-nacelle interference with the MCTCB and BTSSI geometries,
- nacelle-in-proximity to wing/body with the MCTCB, BTSSI and Ref. H geometries.

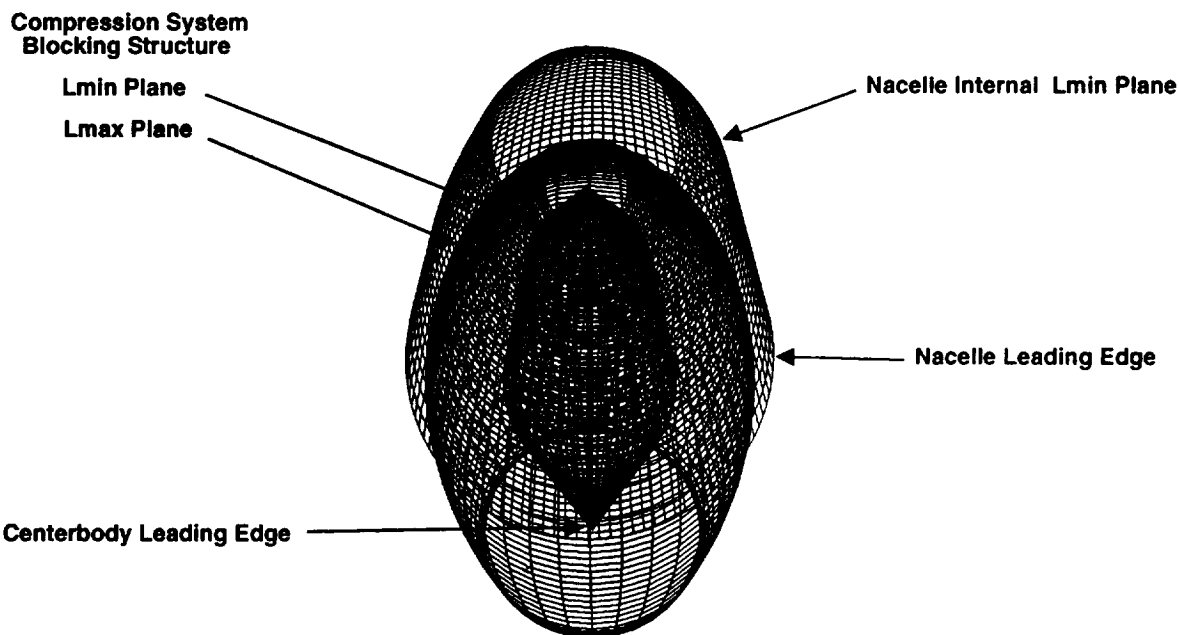
Second, and of equal importance to the data analysis, is the implementation of NASA-developed OVERFLOW CFD methodologies in analytical modeling. This was used to ensure prime/sub methodology compatibility and coordination. Emphasis was placed on the modeling of the nominal spillage conditions for:

- Mach numbers of 1.80 and 1.30,
- MCTCB and BTSSI nacelle geometries,
- isolated, nacelle-to-nacelle, and nacelle-in-proximity conditions.

As the final step in the approach, comparisons were made using CDDMS, FAST, PLOT3D and AcePlot to investigate CFD utility with respect of the accuracy and reliability in determining forces and surface static pressures.

MCTCB Compression System CFD Grid Topology

HSCT High Speed Aerodynamics



HSCT High Speed Aerodynamics

CFD Model(s) Development , MCTCB Compression System Gridding

Activities were also focused on developing compression system topologies, block overlapping strategies and viscous-spaced faces which would capture the spillage effects associated with the nacelles operating at nominal conditions using the OVERFLOW CFD methods. *Phantom* and *collar* grids were used to eliminate all *orphan points* with the PEGSUS code. Near-wall point spacing on the isolated MCTCB and BTSSI grids were held to 1.0E-03 and 1.0E-04 inches respectively in an effort to correctly describe the boundary layer growth on the ramp and the resultant shock displacement.

The MCTCB compression system geometry modeling was initiated first. An H-O topology was selected for the creation of a single block for each of the nacelles using the "K" direction as periodic. Overlapping at the leading and trailing edges of the centerbody were used to assure that the nominal spillage flowfield was captured. The singular axis typical to this type of topology was replaced by singular points at the leading and trailing edges of the centerbodies. When completed the grids were run through PEGSUS to develop the "*chimera*" or overlapping interpolants for subsequent OVERFLOW analysis. The MCTCB nacelle and Mach 1.8 centerbody surface grids shown in figure above resulted in PEGSUS-developed blocks with zero *orphan points*. The MCTCB centerbody grids were sized at 80 x 40 x 20.

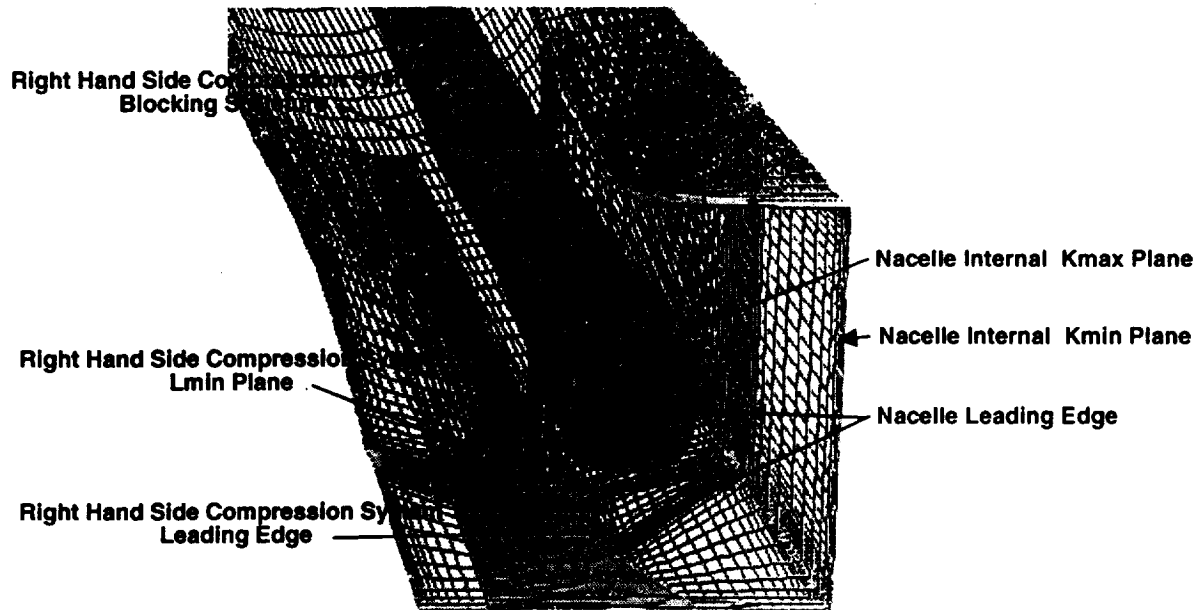
Rapid translation of the MCTCB compression system position within the nacelle was made possible using the block translation/rotation/scaling feature within PEGSUS. That enabled the centerbody to be moved from design to off-design conditions with minimal grid/blocking modifications.

The following combined grids were developed with zero *orphan points* using PEGSUS:

- isolated MCTCB without compression system,
- isolated MCTCB with Mach 1.8 centerbody and outflow planes
- integrated Ref H/MCTCB with unstated (Mach 1.2 setting) centerbodies and outflow planes,
- integrated Ref H/MCTCB with Mach 1.8 centerbodies and outflow planes.

BTSSI Compression System CFD Grid Topology

HSCT High Speed Aerodynamics



HSCT High Speed Aerodynamics

CFD Model(s) Development , BTSSI Compression System Gridding

The BTSSI compression system geometry modeling process adopted a preferred topology and blocking strategy. The fall-back approach to the grid topology selected was selected when difficulties arose while PEGSUS was being exercised in defining the overlap interpolators. In order to capture the viscous interaction between the ramps and inlet sidewalls, a block H-H grid topology was selected. Each nacelle has two additional blocks that share the geometry of the internal nacelle and ramps. The blocks overlap for approximately 50% of their length on both the leading and trailing edges of the ramp(s). Each block's dimensions were 109 x 75 x 45.

The BTSSI nacelles/compression system grids required several modifications that enabled PEGSUS to formulate high quality (orphan-free) interpolators. Our efforts entailed preservation of the existing grid topologies from the flow-through cases (examined in earlier studies) and adapting collar grids which were used to tie the ramp-to-wall regions together. For illustration purposes the H-H ramp blocks, H-O nacelle internal block and O-H ramp collar grid are shown in figure. Complete geometry representations which required the internal collar grids were:

- isolated BTSSI without compression system,
- isolated BTSSI with 1st ramp and Mach 1.3 outflow plane,
- isolated BTSSI with 1st ramp,
- integrated Ref. H/BTSSI with 1st ramps and Mach 1.3 outflow planes,
- integrated Ref. H/BTSSI with 1st ramps.

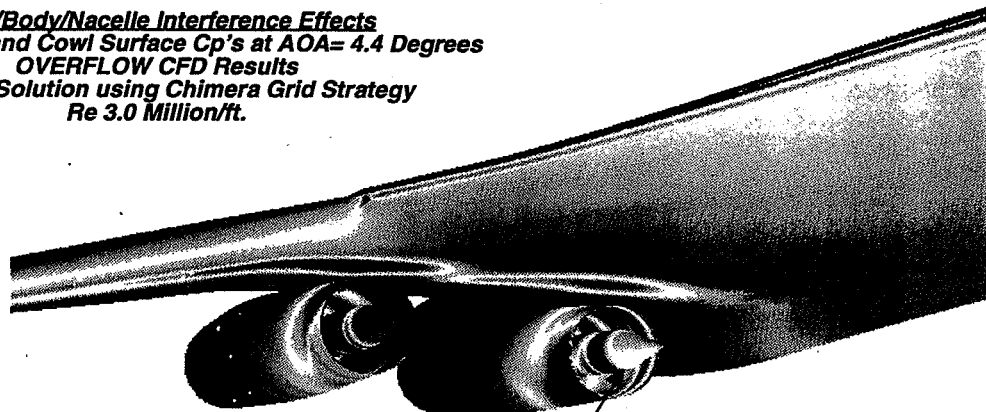
The completed grids were used for subsequent OVERFLOW analysis and comparison with experimental data.

REF H WITH MCTCB NACELLES / CENTERBODIES IN PROXIMITY AT MACH 1.80

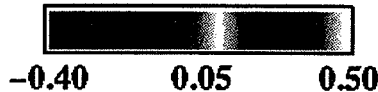
HSCT High Speed Aerodynamics

Aerodynamic/Propulsion Reference Conditions
Extrapolated Outflow Boundary Conditions Prescribed for Inlet
Freestream Inflow Boundary Conditions Prescribed for Nozzle

Wing/Body/Nacelle Interference Effects
Centerbodies and Cowl Surface Cp's at AOA= 4.4 Degrees
OVERFLOW CFD Results
Viscous Solution using Chimera Grid Strategy
Re 3.0 Million/ft.



PRESSURE COEFFICIENT



Centerbody Cp's Indicate Inboard to Outboard
Mach Number Variation

HSCT High Speed Aerodynamics

OVERFLOW Surface Pressure Results for Reference H / MCTCB

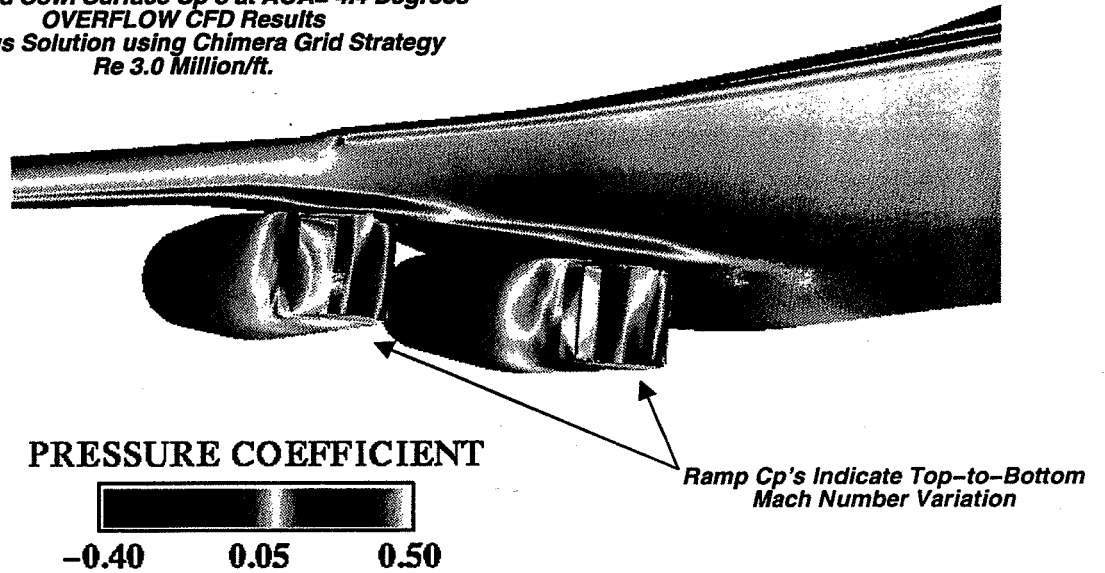
The behavior of the inboard and outboard MCTCB nacelles and centerbodies is shown in figure with respect to the static pressure coefficient values at a freestream Mach of 1.80. The regions internal to each of the nacelles show somewhat differing in magnitude. To insure that the internal shock losses did not affect the nacelle external flow and nozzle performance and in-turn deviate from the flow-through aerodynamics reference condition, the CFD boundary conditions were selected and set for both the inlet and the nozzle of each nacelle. The inlet outflow was extrapolated at the mid-nacelle location, while freestream inflow conditions were set internal to the nacelle midpoint. Points stranded between the inflow-outflow bounds were simply removed from the computations using the IBLANK option.

REF H WITH BTSSI NACELLES / RAMPS IN PROXIMITY AT MACH 1.80

HSCT High Speed Aerodynamics

Aerodynamic/Propulsion Reference Conditions
Extrapolated Outflow Boundary Conditions Prescribed for Inlet
Freestream Inflow Boundary Conditions Prescribed for Nozzle

Wing/Body/Nacelle Interference Effects
Ramp and Cowl Surface Cp's at AOA= 4.4 Degrees
OVERFLOW CFD Results
Viscous Solution using Chimera Grid Strategy
Re 3.0 Million/ft.



HSCT High Speed Aerodynamics

OVERFLOW Surface Pressure Results for Reference H / BTSSI

Static pressures on the nacelles and inlet ramps are shown in figure above. Ramp and cowl pressure again indicate a small amount of Mach number variation in the capture flow for each nacelle. The boundary conditions were set to insure that the aerodynamic reference conditions replicated the test as much as possible.



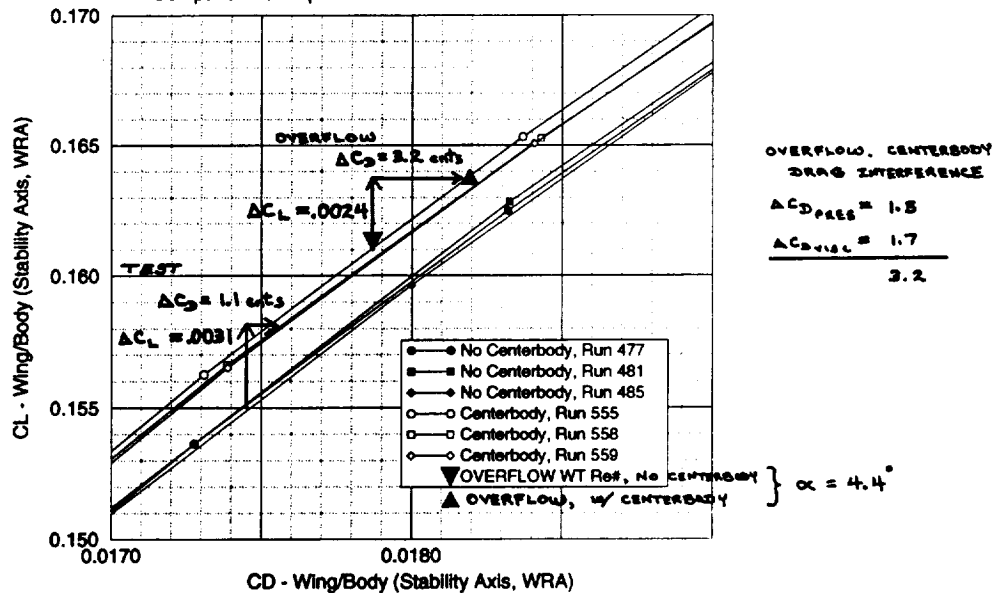
HSR Configuration Aerodynamics Workshop

HSCT High Speed Aerodynamics

OVERFLOW Computations at Mach 1.80

REF H/MCTCB in Proximity, Mach 1.80

Comparison of Experimental and OVERFLOW CFD Results



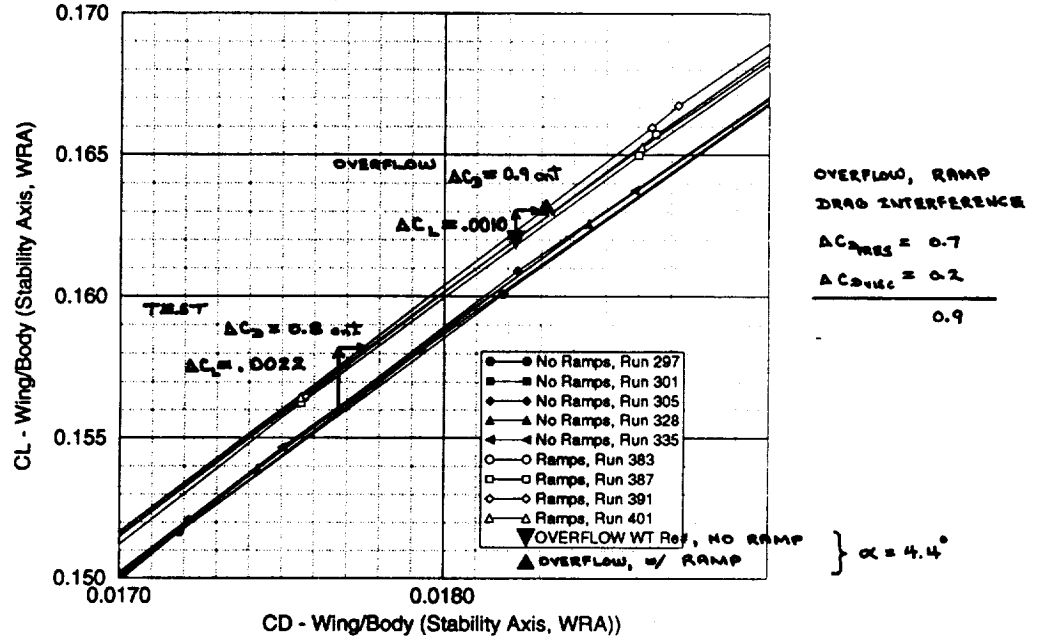
The test data indicates a favorable wing/body interference due to centerbody at Mach 1.8 of -2.2 counts at constant lift. The OVERFLOW result for the no centerbody case with axisymmetric flow through nacelles-in-proximity is very similar to the OVERFLOW results at Mach 2.4, about 2 to 3 counts less than the test data. The OVERFLOW prediction of the centerbody supersonic spillage effect obtained the correct trends but the absolute magnitude is off. The test data indicated a lift increment of 0.0031 at constant angle of attack, OVERFLOW predicted 0.0024. The OVERFLOW drag increment was substantially higher than test increment at constant angle of attack. Half of the OVERFLOW drag increment was due to changed friction drag on wing.



OVERFLOW Computations at Mach 1.80

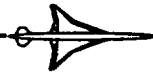
REF H/BTSSI in Proximity, Mach 1.80

Comparison of Experimental and OVERFLOW CFD Results



The test data indicates a favorable wing/body interference due to ramp at Mach 1.8 of -1.5 counts at constant lift. The OVERFLOW result for the no centerbody case with axisymmetric flow through nacelles-in-proximity is very similar to the OVERFLOW results at Mach 2.4, about 2 counts less than the test data. The OVERFLOW prediction of the centerbody supersonic spillage effect obtained the correct trends but the absolute magnitude is off. The test data indicated a lift increment of 0.0022 at constant angle of attack, OVERFLOW predicted 0.0010. The OVERFLOW drag increment was nearly equal to the test increment at constant angle of attack.

The spillage interference due to the bifurcated inlet compression ramp is measurably less than the axisymmetric centerbody interference. This is not surprising as the bifurcated pushes most of the spillage flow to the sides of the inlet, while the axisymmetric has large component of spillage redirected up into the wing lower surface.



Conclusions and Recommendations

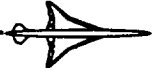
- **Much more to learn from Ames spillage data.**
- **Wing/body spillage interference is small and favorable:**
 - **Axi / Centerbody interference = -2.2 cnts (M=1.8),**
 - **Bif / Ramp interference = -1.5 cnts.**
- **CFD captures trends and magnitudes.**
 - **More analysis required to improve absolute accuracy.**

HSCT High Speed Aerodynamics

Conclusions and Recommendations

Data acquired in the NASA-Ames Reference H / NAI Tests are of high quality and represents the state-of-the-art in nacelle-airframe interference databases. Future use of the database should include a detailed tare bookkeeping reassessment with respect to the nacelle flow-through balances. Small differences in projected areas within the balance may result in additional corrections and potentially decrease the differences between experiment and analytical models

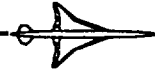
Nominal spillage effects are small and to be determined accurately using CFD requires that the pressure gradient effects on the wing/body's lower surface be modelled accurately in the analysis. Future work should include grid convergence sensitivity studies for the nacelles in proximity using spacings which are compatible with the nacelle's near wall spacing.



SUPERSONIC CRUISE PAI STUDIES

Team Members: Steve Chaney - Aerodynamics
Steve McMahon - Propulsion
Steve Ogg - Aerodynamics

This section contains all the supercruise studies performed by Boeing. Steve Chaney and Steve Ogg are members of the Boeing HSCT High Speed Aerodynamics staff. Steve McMahon is a member of the Boeing HSCT Propulsion Design staff.



CONFIGURATION DEFINITION

- Reference H Configuration
 - Baseline Nacelles: Axi Inlet, Axi Nozzle, 509 pps
 - Bifurcated : Bifurcated Inlet, Axi Nozzle, 509 pps
 - * Nozzle has slight variation from baseline.
- Nacelle Installations Configured this year:
 - DSM Nozzle: Axi Inlet, 2-D nozzle, 673 pps (Supersonic & Transonic Nozzle settings)
 - Axisymmetric Equivalent of DSM: Axi Inlet, Axi Nozzle, 673 pps (Supersonic & Transonic Nozzle settings)
 - Bifurcated/DSM: Bifurcated Inlet, 2-D Nozzle, 673 pps
 - * Straight inlet dropped to provide outboard channel clearance,
 - * Reflexed inlet to provide clearance.
 - Axi Inlet, DSM Nozzle, 509 pps
 - Bifurcated Inlet, DSM Nozzle, 509 pps

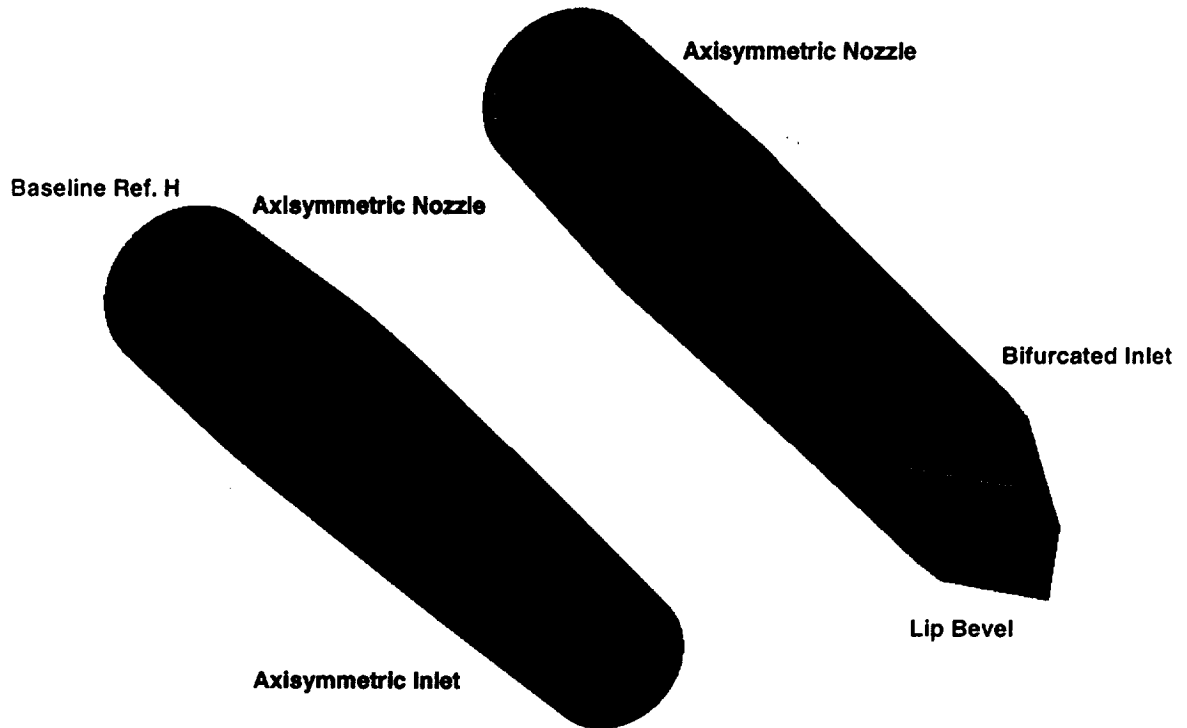
The wing/body used for these studies was the Ref. H. The baseline nacelles designed for this configuration had axisymmetric inlets / axisymmetric nozzles, and flowed 509 pps. A bifurcated inlet / axisymmetric inlet nozzle nacelle was designed for the ARC testing of the 2.7%-scale Reference H. Since the Reference H configuration was developed the engine size required for a given wing size has grown. A nacelle was configured that represented the current 'best' design for the Ref. H wing. The result was a nacelle that flowed 673 pps, had an axisymmetric inlet, and a 2-D nozzle. Nozzle settings were configured for this nacelle for both the supersonic cruise condition and transonic conditions. In order to assess the 2-D nozzle versus axisymmetric nozzle effects on airplane aerodynamic performance an axisymmetric equivalent of the 2-D nozzle was designed and attached to the same inlet. An installation of a bifurcated inlet nacelle with the 2-D DSM nozzle on the Ref. H was also performed. The axi - 2D and bifurcated - 2D nacelles were also scaled down to 509 pps and installed on Ref. H to enable comparisons to the original Ref. H baseline nacelles.

The installation guidelines were: (1) diverter LE height equal to boundary height at nacelle inlet, (2) nacelles not buried in wing, (3) nacelle maximum diameter (break between forecowl and nozzle boattail) located as close as possible to wing TE. In addition, the diverter was constrained by a structural box width that the inlet attached to; resulting diverter width was 32 inches. Diverter LE was located 6 inches back from inlet lip.

It was possible to locate the 673 pps axisymmetric inlet - DSM nozzle nacelles using these guidelines, however, as one of the following figures discusses, this installation had a wing/diverter/nacelle channel at the wing TE that was considered too small. The nacelle maximum diameter was moved down (while holding diverter LE height constant) to alleviate this channeling. Both the 509 and the 673 bifurcated inlet nacelles were too long to install and adhere to all of the above the rules. The 509 bifurcated nacelles were installed with the same TE diverter height but the diverter LE height was nearly twice as big as required. The 673 bifurcated required dropping both the inlet and the nacelle maximum diameter down to prevent burying nacelle in wing and choking the diverter channel completely. A 673 bifurcated installation was also completed with a reflexed (curved) inlet shape to nearly meet meet all the guidelines above.

**Baseline Nacelle Configurations**

509 pps

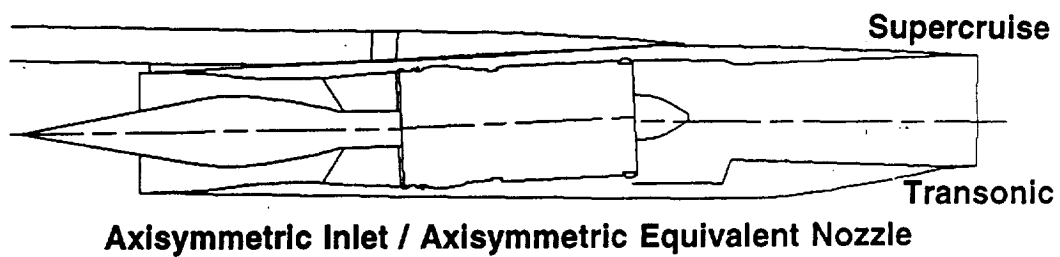
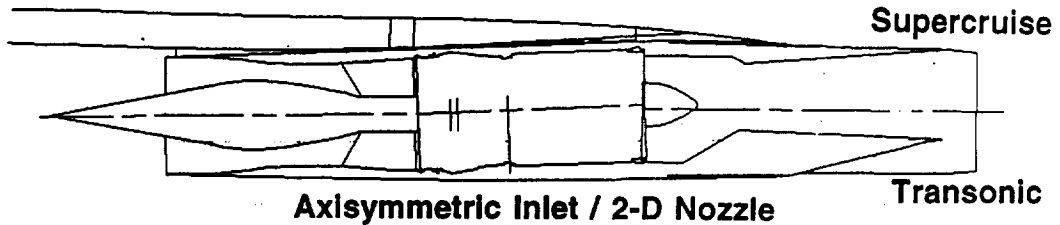


The two baseline Ref. H nozzles as tested in the ARC 2.7%-scale model tests are shown. The key difference between the two was the square cross section of the bifurcated inlet and the bifurcated lip bevel necessary for structural rigidity. The nozzles were only slightly dissimilar and were assumed to be the same aerodynamically. However, detailed analysis of PAI aerodynamics in this study showed that the 'slight difference' was definitely measurable and had a significant effect on results. The axi-axi nacelle had a slightly longer and canted downward nozzle that carried more lift than the bifurcated nacelle nozzle. This will be discussed in more detail in later charts.



DSM INSTALLATION ON REFERENCE H

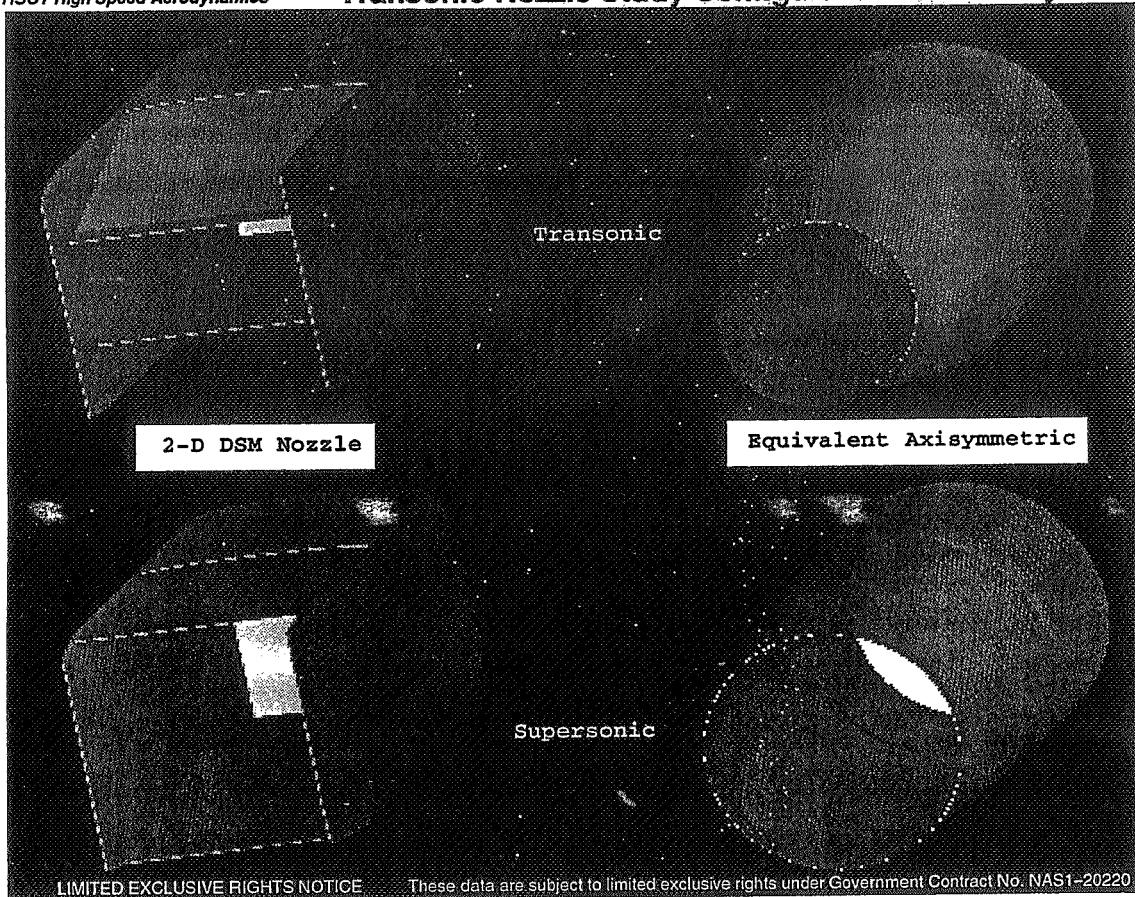
673 pps / 7100 sq.ft.



Cross-Section @ Wing TE

The installation of the DownStream Mixer (DSM) nozzle on the Ref. H wing is shown for both the baseline 2-D nozzle and the axisymmetric equivalent. The current design guideline for axisymmetric nacelles of locating the maximum diameter at the wing TE had to be modified for the 2-D nozzle if the same diverter is kept. As shown, the nacelle was dropped down to alleviate any choking that might have occurred in the channel between the wing, nacelle, and diverter. The diverters for the two configurations were kept the same in order to provide as consistent a comparison between the them as possible.

Alternative diverter designs were investigated that extend to the full width of the nacelle to completely remove possibility of choking in channel and could allow moving 2-D nozzle back up to wing.



Details of the 2-D and axisymmetric nozzles at the supersonic and transonic operating conditions are shown. The key feature of the 2-D nozzle at the transonic condition was the side walls or 'ears' on either side of the nozzle. Another important feature was the large nozzle angles at the transonic conditions for both the axisymmetric and 2-D that lead to separation of the external flow.



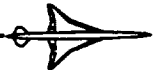
ANALYSIS / DESIGN TOOLS

- Linear Theory - Current PD tool.
 - Linear B.C. means axisymmetric nacelles, no diverters.
- TRANAIR (Full Potential) - W/B optimization, PAI analysis
 - * Solution adaptive.
 - Most versatile higher order method.
- OVERFLOW (N-S) - W/B, W/B/N detailed analysis.
 - * Central difference, ARC3D.
 - * Baldwin-Barth.
 - Most accurate method.

The current PD tool for HSCT PAI design and analysis is the linear theory design code. The studies in this task were all performed with TRANAIR and OVERFLOW due to the complex geometry modeling required and the requirement to assess viscous effects.

TRANAIR is a Boeing developed code for analyzing compressible flow over arbitrary complex configurations at subsonic, transonic, or supersonic freestream Mach numbers. It solves the non-linear, full potential equation subject to a variety of boundary conditions, modeling wakes, inlets, exhausts, porous walls, and impermeable surfaces. The flow field is divided into a locally refined rectangular grid which is generated internally by the code. This grid may be adapted to the solution through a sequence of several grids. The surface boundary is divided into networks of panels where separate boundary conditions can be specified. TRANAIR is usually executed on a CRAY for typical wing/body/nacelle configurations.

OVERFLOW, a thin layer Navier-Stokes code using overset grid methodology, was developed at NASA Ames. In this multi-block method the individual grids are not required to match exactly at boundaries, but instead must overlap in order for information to be passed from one grid to another. The Baldwin-Barth turbulence model was used for nearly all viscous runs made for this study. All the OVERFLOW runs were done on the NAS C-90.



ANALYSIS TOOL FLOW AND SOLUTION TIMES

Code	PreProcessing, Gridding,etc	NAS Solution C90 hrs	NAS Solution Clock hrs
Wing / Body			
Linear Theory	< 1/2 day	-	-
TRANAIR 500k boxes	1/2 - 2 days	2.5 hrs	6 - 16 hrs
OVERFLOW 2.9 million pts	1 - 5 days	7 hrs	6 - 16 hrs
Wing / Body / Nac / Diverter			
Linear Theory	< 1/2 day	-	-
TRANAIR 750k boxes	1 - 10 days	3 hrs	6 - 16 hrs
OVERFLOW 7-8 million pts	2 - 30 days	15 - 20 hrs	overnight

As a result of continuing pressures on NAS computer resources, and discussions that occurred at the HSR CFD workshop in February of this year, an effort was made to reduce the size of the OVERFLOW grid as all of the different PAI configurations to be analyzed were to be built on this grid. In addition, some refinements were made to improve the force prediction accuracy (see following chart).

The OVERFLOW grid sizes and solution times (as charged on NAS C-90) are shown below, along with similar data for TRANAIR, and typical pre-processing flow times. Both the TRANAIR and OVERFLOW gridding flow times are highly dependent on the similarity of the new loft with the previous loft gridded, the format of the loft's surfaces, and whether a new grid topology is required.



OVERFLOW GRIDDING / DRAG STUDIES

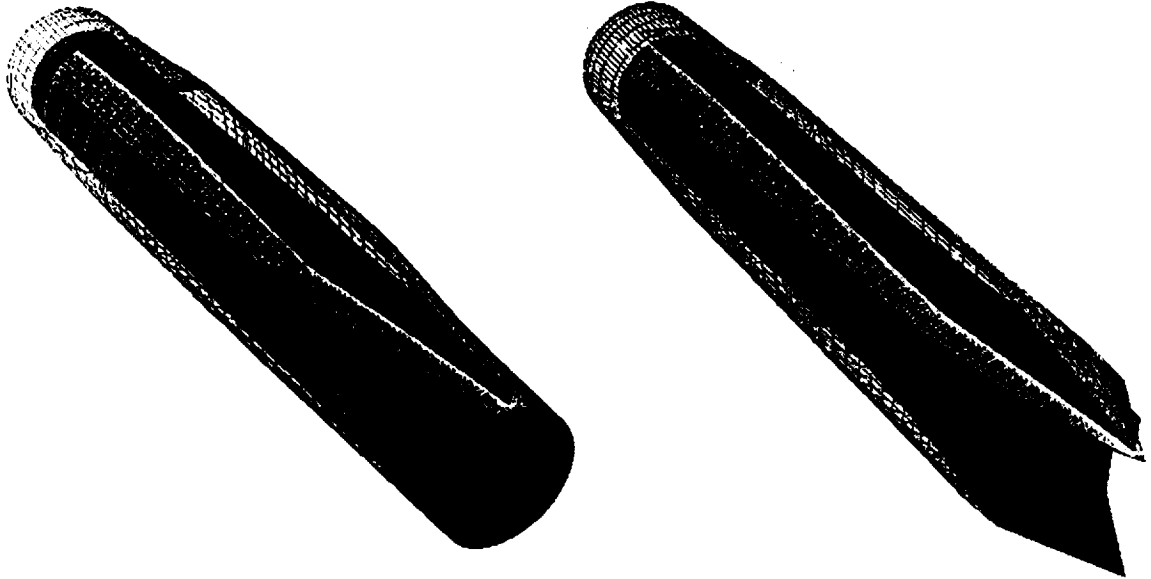
- **OVERFLOW Grid Size Reduced Considerably**
 - * No Loss in Accuracy (Wing/Body: 4.5 million to 2.9 million).
- **Detailed Absolute Drag Analysis Lead to Process Changes:**
 - * **OVERFLOW Force Integrator (FOMOCO) With Specified Temp.**
 - * **Three cells of constant size at wall before stretching radially.**
- **Detailed comparison of OVERFLOW and test results highlighted uncertainties in test data that need to be resolved:**
 - * **Trip Drag**
 - * **Aeroelastic Effects**
 - * **Internal Nacelle Duct Forces**

The OVERFLOW gridding process was improved throughout the year to both improve efficiency and improve accuracy. The surface grid density was changed only slightly. The fuselage grid was refined somewhat at the tip and tail, and grid stations were added to match wind tunnel aft body cut-off stations exactly for force integrations. This was a very dense surface grid, especially around the nacelles. The distance to the first point off the surface in the volume grid to $y_{plus}=1$ for the ARC 9x7 test condition. The length of the wing C-grid aft of the TE was decreased from 2000 inches to 400 inches. The amount of overlap between several of the grids was more than required; it was decreased. The box grid around the wing/body had extended to the outer boundary. The box grid was reduced in size to just enclose the wing/body, and an ellipsoidal grid was then extended to the outer boundary. The wing C-grid was spread vertically aft of the TE to improve communication with adjacent grids. The grid was changed to have three equally spaced cells at the surface.

Detailed comparison of the OVERFLOW results with test data indicated that the CFD results were very accurate, but there were some unresolved uncertainties that cloud the final conclusions to some degree. These uncertainties are the drag of the boundary layer trip disks used in the AMES 9x7 tunnel, the change in the wind tunnel measured forces due to the aeroelastic deflection of the wing, and the internal nacelle duct lift pressure force which turned out to be not insignificant as has been assumed; each is discussed in following charts.



**Ref. H Wing/Body/Nacelle/Diverter OVERFLOW Surface Grid
Inboard Axisymmetric and Bifurcated Inlet Installations**



Grid points have been removed for clarity.

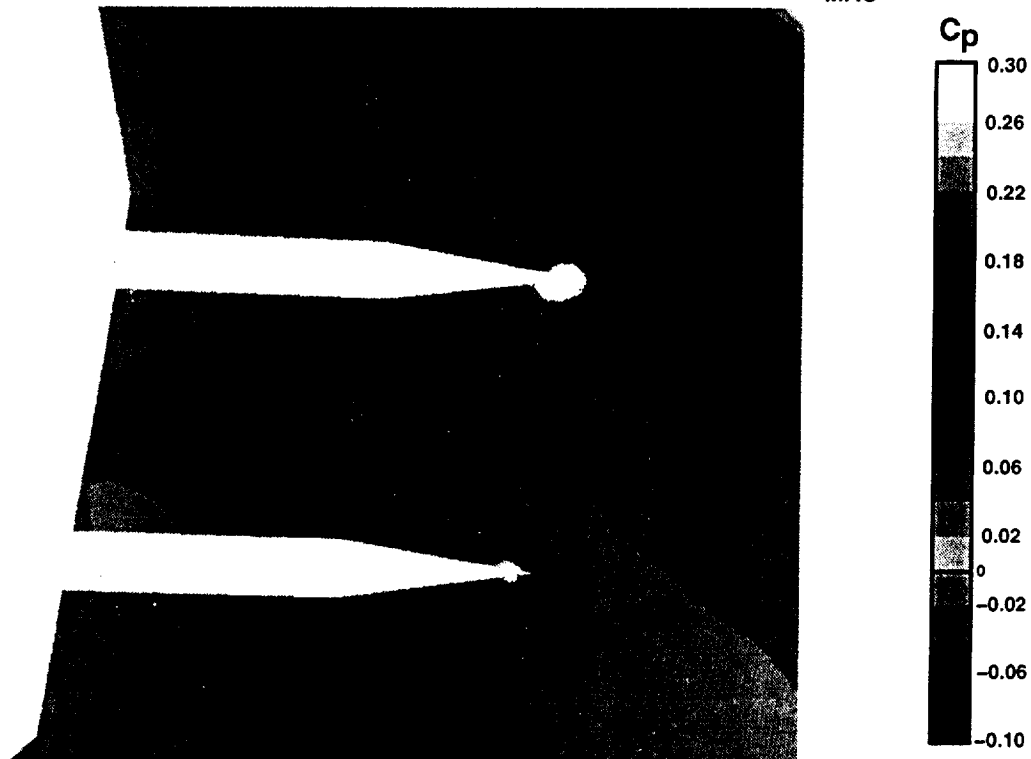
The OVERFLOW grid for the wing/body/nacelle/diverter configurations used 17 blocks; 5 for the wing/body, and 3 each for the nacelles, and 2 for each diverter. The bifurcated inlet nacelle has 8.3 million grid points, the axisymmetric had 7 million. This grid has a very dense surface distribution around the nacelle installation. The volume distribution has been built for the NASA Ames 9x7 test condition with the 2.2%-scale Ref. H model.

The nacelle and diverter surface grids are shown in the figure (for the inboard nacelles). The diverter sides were modelled with a single grid that wraps around the LE of the diverter. The diverter aft fairing was a separate grid that overlaps onto the wing upper surface and the nozzle. The nacelle was made up of 3 grids: forecowl, nozzle, internal.

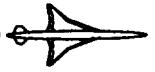
A polar was run for both inlet types to allow a complete comparison of aerodynamic characteristics. Each angle of attack was typically run 1600 to 2000 steps from scratch (no restarts) and cost 15 to 20 hours on vonneumann. After 1600 steps the residuals were converged 3 orders of magnitude or more for every block.



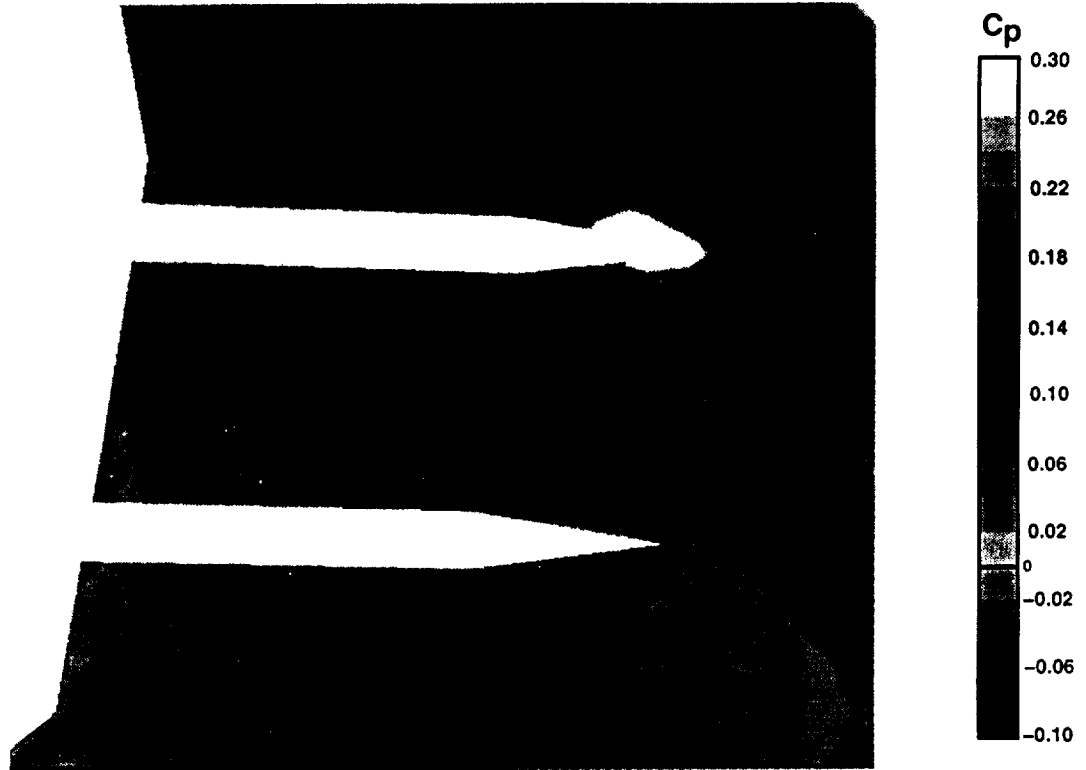
Ref. H Wing/Body/Nacelle/Diverter Lower Surface Pressure Contours
Axisymmetric Inlet – Axisymmetric Nozzle, Mach 2.4, $\alpha = 4.4$, $Re_{MAC} = 7$ million



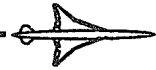
The wing lower surface pressure contours from OVERFLOW are shown in the figure for the captive axisymmetric configuration (wing/body/axisymmetric/diverter). The diverter planform can be clearly seen. The pattern was a typical one seen previously in TRANAIR simulations of nacelle installations: diverter shock merging with nacelle shock, expansion at diverter shoulder, recompression along diverter sides (and some influence from adjacent nacelle). The primary difference from TRANAIR surface pressure contours for the same case was the shock angle from the diverter being more swept forward for the OVERFLOW solution due to diverter buried in boundary layer (TRANAIR pressure contours for this same case are shown later in the diverter study section).



Ref. H Wing/Body/Nacelle/Diverter Lower Surface Pressure Contours
 Bifurcated Inlet – Axisymmetric Nozzle, Mach 2.4, $\alpha = 4.4$, $Re_{MAC} = 7$ million



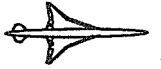
This figure shows the lower surface pressure contours for the bifurcated installation. Comparing with the previous figure some appreciable differences were noted. The additional length of the inlet/diverter pushed the highest pressure region forward on the wing; the low pressure off the diverter shoulder expansion covered a larger area of the wing. The high pressure region near the front of the inlet/diverter was much larger for the bifurcated than for the axisymmetric. This was due to the relatively high angle of the lip bevel on the bifurcated creating a shock and resulting high pressure that raised the pressure on all the surrounding components. Pressure integration on the wing lower surface indicated that the bifurcated configuration had higher total lift on the wing than the axisymmetric ($CL = 0.04719$ versus 0.04666). Note that these pressures also acted on the nacelle upper surface to create a negative lift force that was amplified in the case of the bifurcated by the flat top of the inlet.



Ref. H Wing/Body/Nacelle/Diverter Lower Surface Oil Flow
 Axisymmetric Inlet – Axisymmetric Nozzle, Mach 2.4, $\alpha = 4.4$, $Re_{MAC} = 7$ million

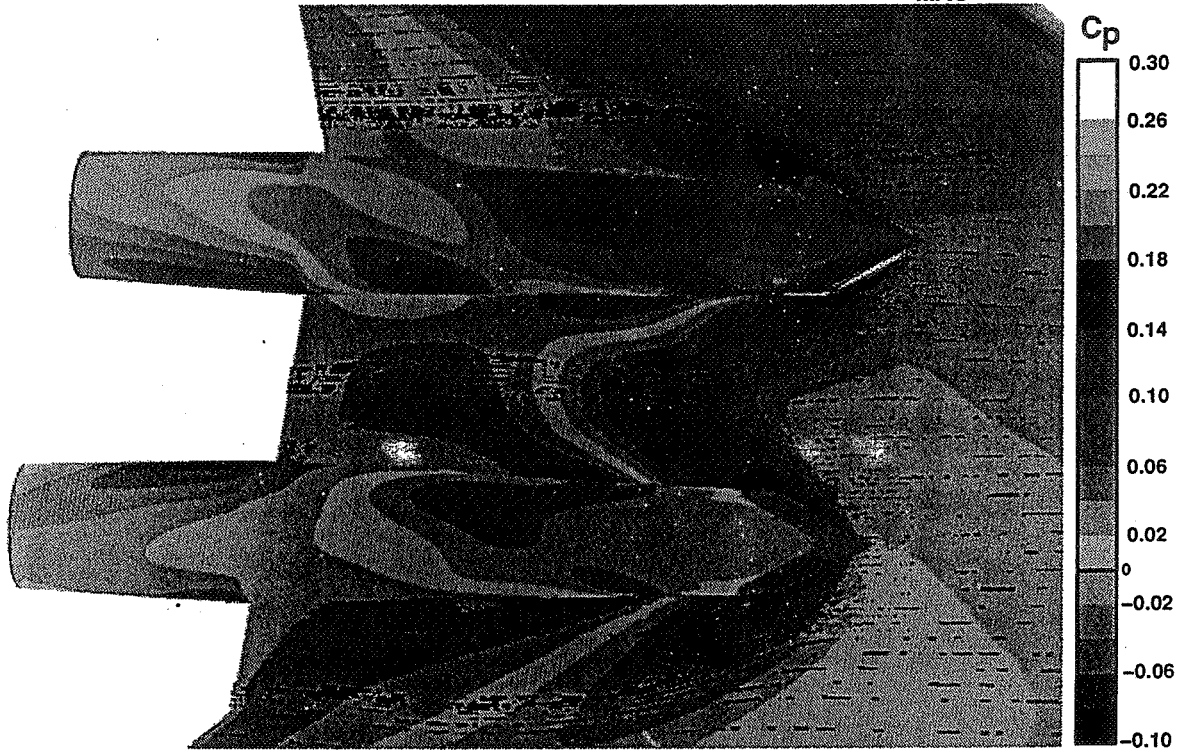


The next two figures are identical to the previous two except that the nacelles have been added and surface streamlines (simulated oil flow) have been plotted. The figure below is the axisymmetric installation. The following figure is the bifurcated installation. The streamline patterns are very similar for the two nacelles. The nozzles on the axisymmetric installation were observed to carry slightly more positive pressure on the lower surface than the bifurcated installation. This has been attributed to the small geometry difference between the two that was discussed earlier in the configuration description section. The effect will be confirmed later in report by more negative pressures on top of nozzle of axisymmetric installation and differences in integrated lift.



HSCT High Speed Aerodynamics

**Ref. H Wing/Body/Nacelle/Diverter Lower Surface Oil Flow
Bifurcated Inlet – Axisymmetric Nozzle, Mach 2.4, $\alpha = 4.4$, $Re_{MAC} = 7$ million**

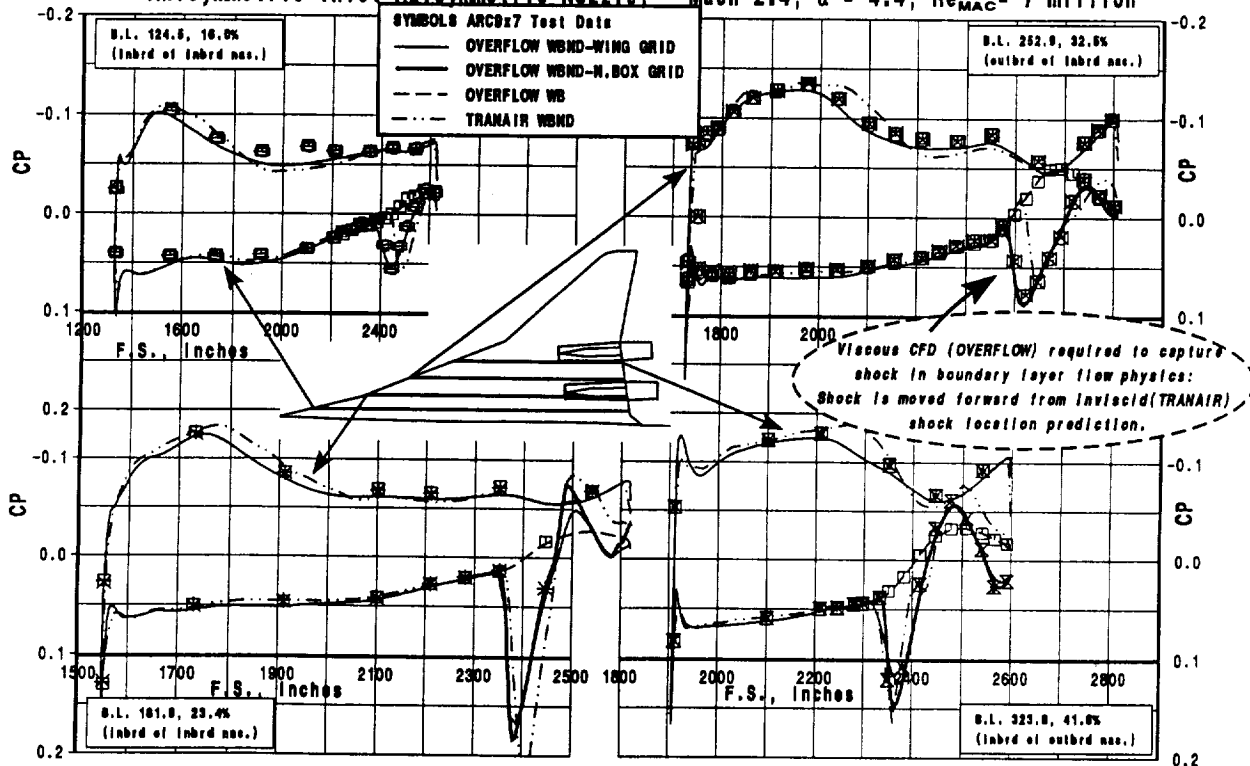


See text for previous figure.



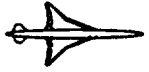
Ref. H Wing/Body/Nacelle/Diverter Chordwise Pressure Distribution

Axisymmetric Inlet-Axisymmetric Nozzle, Mach 2.4, $\alpha = 4.4$, $Re_{MAC} = 7$ million



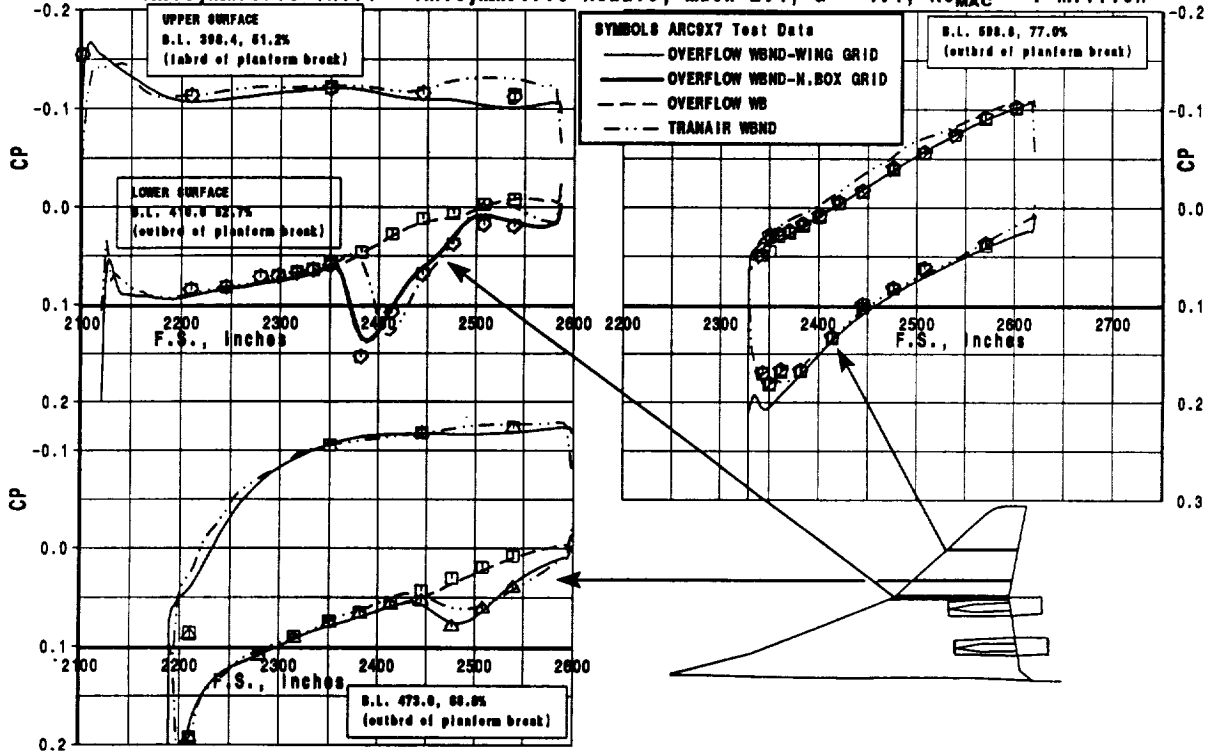
The pressure distribution calculated by OVERFLOW for the captive axisymmetric case is compared with test and TRANAIR in these figures. Chordwise pressure distributions on the inboard wing panel are shown in the figure below. Chordwise pressure distributions on the outboard wing panel are shown following figure. The basic comparison of the theoretical results with the test data for the wing/body upper and lower surface have been discussed extensively previously and will be ignored here; the focus of this discussion will be on the nacelle effects. The results were as expected with the viscous modelling of OVERFLOW providing a consistently better match of the diverter/nacelle shock location on the wing lower surface than the inviscid modelling of TRANAIR. This discrepancy became more pronounced the farther the pressure row was from the diverter. OVERFLOW was able to capture both the location and magnitude of the nacelle/diverter shock very accurately.

One OVERFLOW line was labelled WING GRID; this was pressure data interpolated from the wing grid. The line labelled N.BOX GRID was from the box grid that surrounds each nacelle and also conforms to the wing lower surface. It was slightly more dense than the wing grid as was evident in several of the plots where it captures the steepness of the nacelle/diverter shock slightly better than the wing grid.

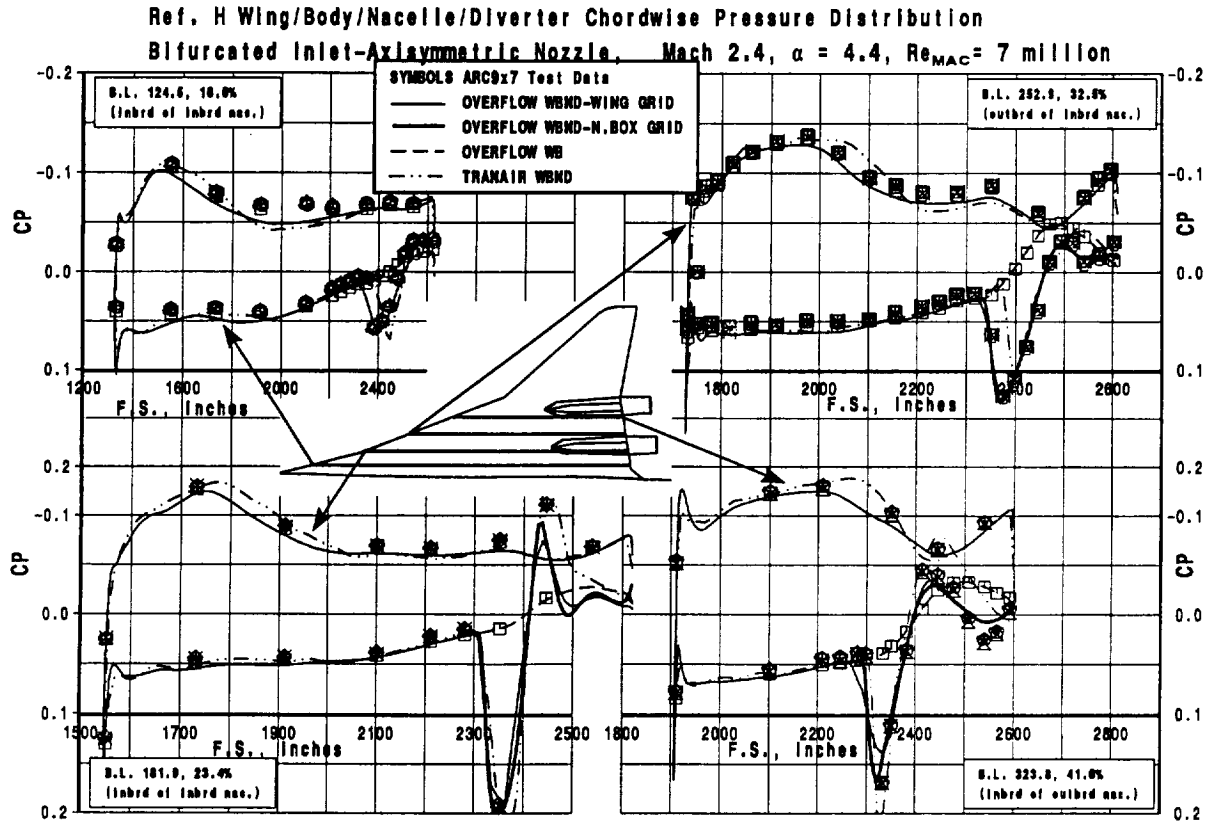


Ref. H Wing/Body/Nacelle/Diverter Chordwise Pressure Distribution

Axisymmetric Inlet - Axisymmetric Nozzle, Mach 2.4, $\alpha = 4.4$, $Re_{MAC} = 7$ million

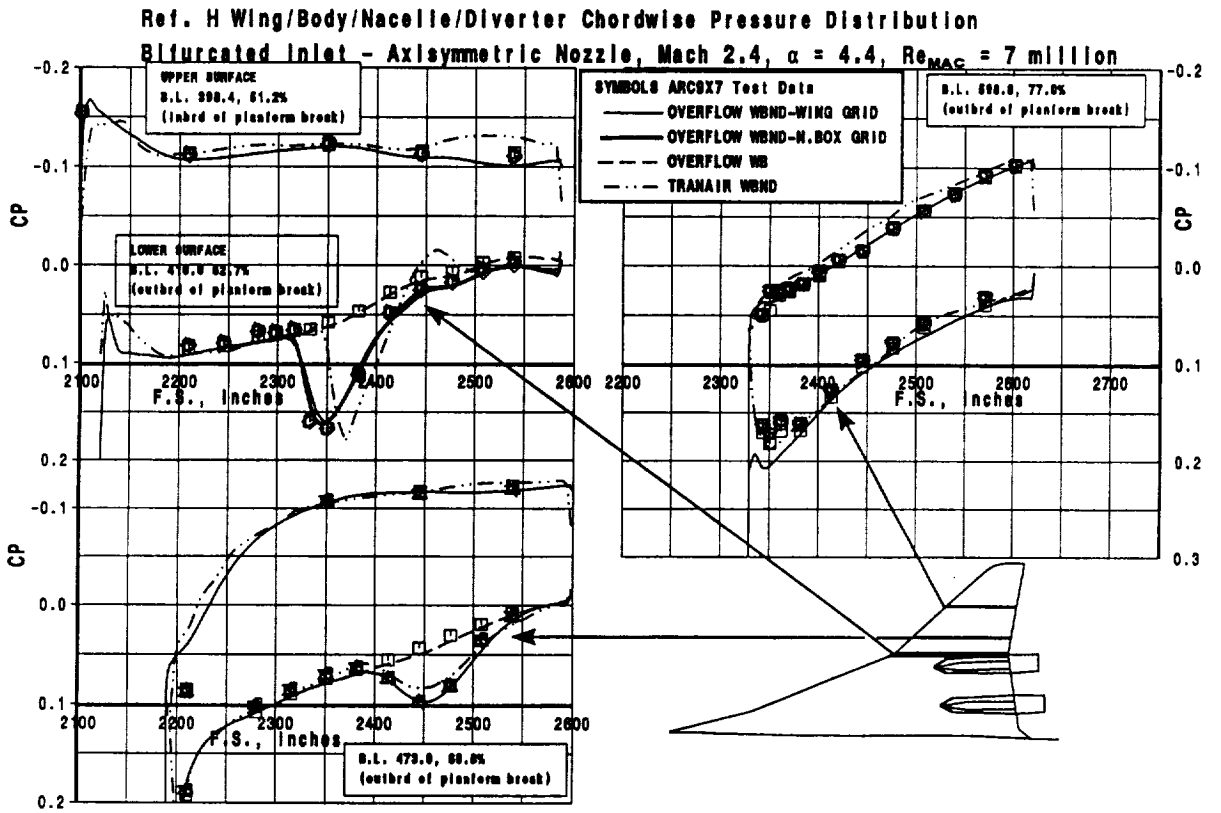
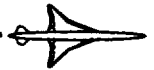


See text for previous figure.

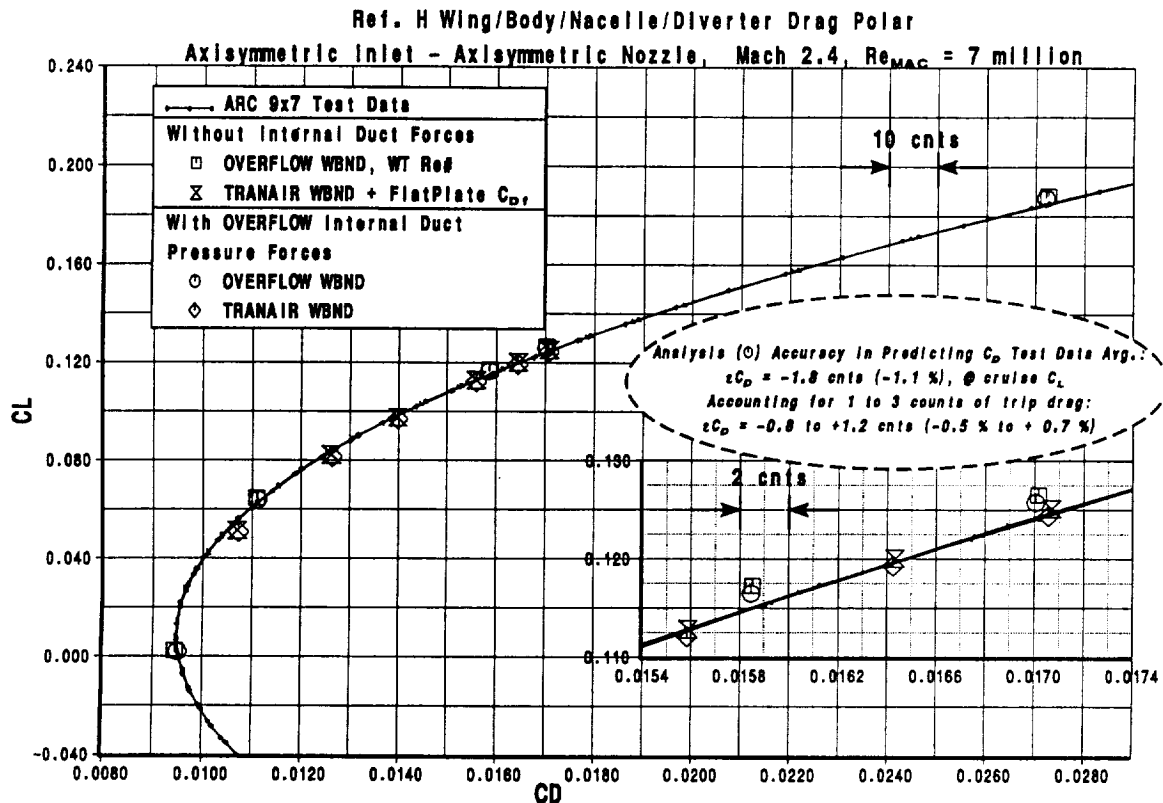
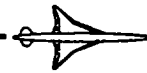


The next two figures are also chordwise pressure distribution comparisons, but for the bifurcated nacelle installation. The shape and magnitude of the nacelle/diverter pressure field was again modelled very accurately by OVERFLOW.

These successful comparisons of OVERFLOW pressure data to the test data lead to the following figures where the pressures have been integrated to produce forces and moments for comparison to test data.

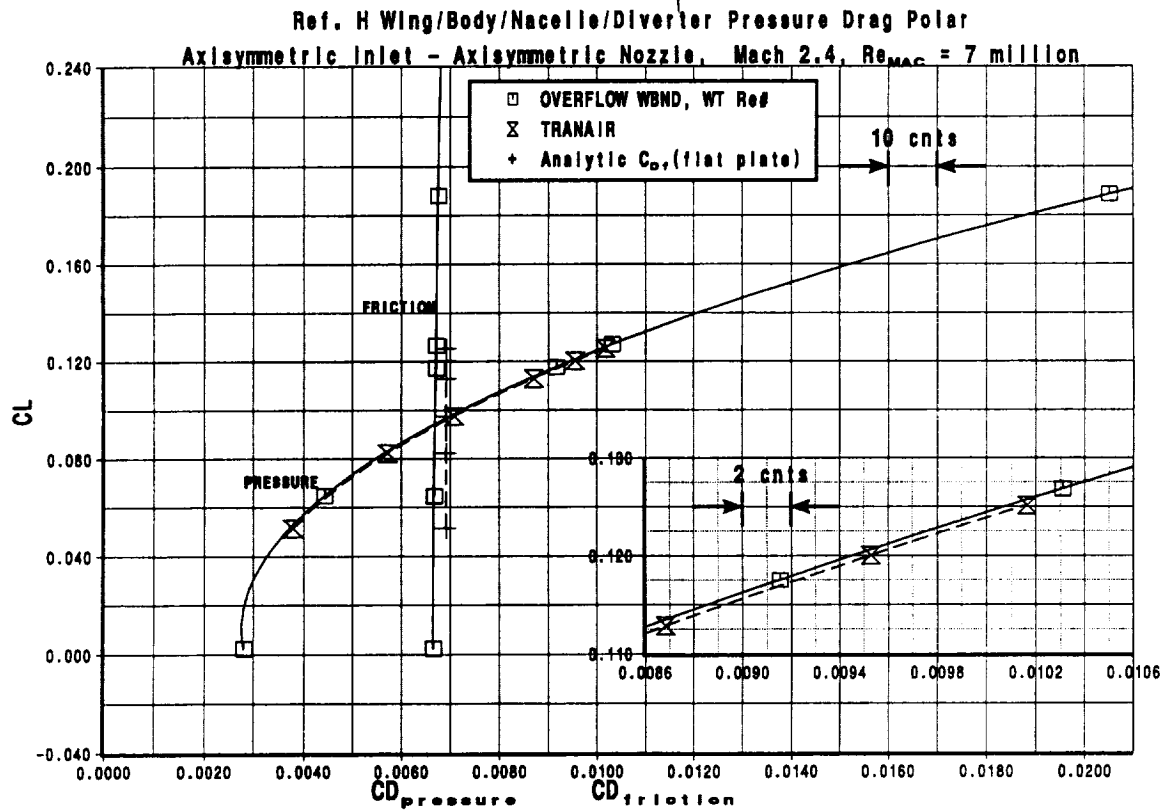


See text for previous figure.



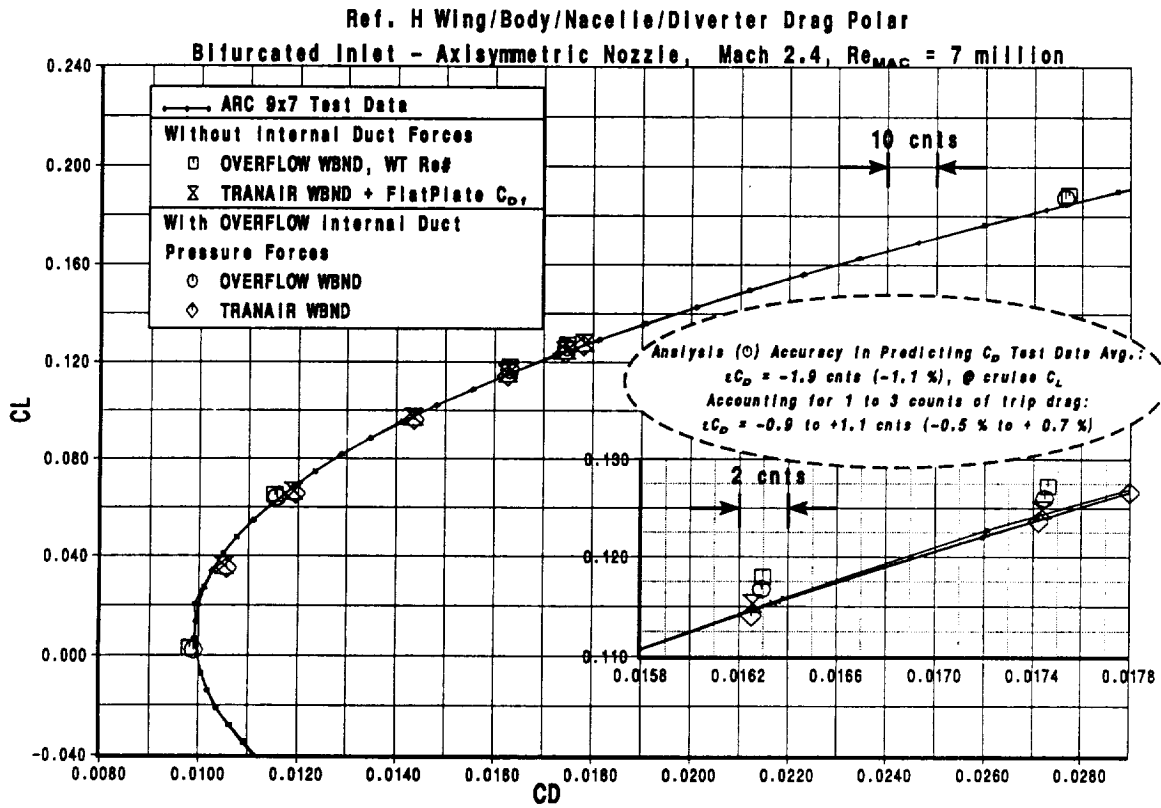
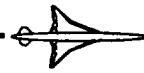
A drag polar for the captive axisymmetric configuration is shown in the figure. The OVERFLOW drag value labelled 'Without Internal Duct Forces' was about 3 counts lower than test. This discrepancy is in-line with previous OVERFLOW solution results for the wing/body and wing/body/nacelle-in-proximity configurations. The discrepancy has been at least partially attributed to the drag of the trip discs which has been found to be 1 to 3 counts. In addition to the trip drag that was in the test data (not corrected out), another discrepancy or correction between test and theory has been discovered. Two corrections were applied to the test data to adjust for unwanted nacelle forces; the base drag was removed and an estimate of the internal skin friction was removed. However, the OVERFLOW results indicated that the nacelle internal ducts were also carrying a large amount of lift (lift coefficient about -0.0013 at cruise, 1% of cruise lift). This value was large enough that it effected the drag polar comparison on the blown-up scales. There are two ways it could be applied, either the OVERFLOW value could be reduced by this amount (the OVERFLOW force integration does not currently include this lift), or the test data could be increased by this value. It was decided to include the internal pressure lift in the CFD data just for the purpose of comparison to the test data. This corrected point was shown as the circle symbol in the figure; it was about 1.8 counts less than the test data drag level at cruise (the OVERFLOW internal duct pressure lift was also applied to the TRANAIR data).

The note surrounded by the dashed oval was added to this plot for the milestone 10 input which required an assessment of CFD accuracy in calculating test data. In this plot, and all other plots that follow that have similar notes the CFD data have been compared to an average of the test data. For the OVERFLOW data shown here, given a trip drag range of 1 to 3 counts, the error was -0.5% to +0.7% of cruise drag.

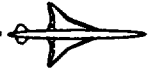


In order to remove friction drag differences between flat plate and OVERFLOW from the OVERFLOW to TRANAIR comparison a pressure drag polar was also constructed. The pressure drag and the friction drag are both shown on the large scale axes. The blown-up axes plot shows that the pressure drag difference between TRANAIR and OVERFLOW was about 0.8 counts at constant lift. Note that although the flat plate and OVERFLOW skin friction values differ by about 2 counts, the assumption of small variation with angle of attack was validated by the OVERFLOW results. The drag difference between OVERFLOW and flat plate skin friction was consistent for all the configurations analyzed and presents an area for possible investigation.

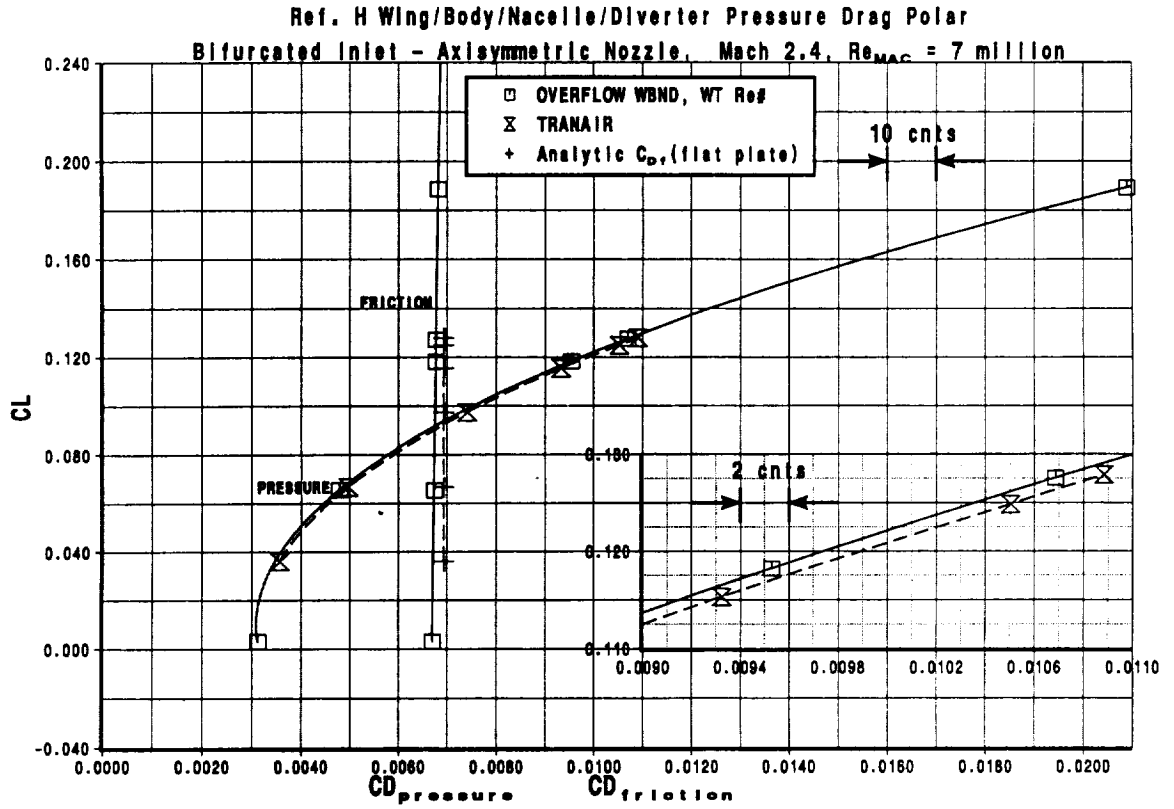
As stated earlier all of the OVERFLOW cases were run with the one-equation Baldwin-Barth turbulence model. Recently a new version of OVERFLOW was released with the one-equation Spalart-Allmaras model. This version was run on the current OVERFLOW wing/body grid and the different turbulence model was found to give nearly identical skin friction values (.06 count different). All calculations have used all turbulent no-slip surfaces (no laminar run).



A drag polar for the captive bifurcated installation is shown. After the internal duct correction the bifurcated nacelle OVERFLOW prediction was 2 counts less than test data.



HSCT High Speed Aerodynamic:

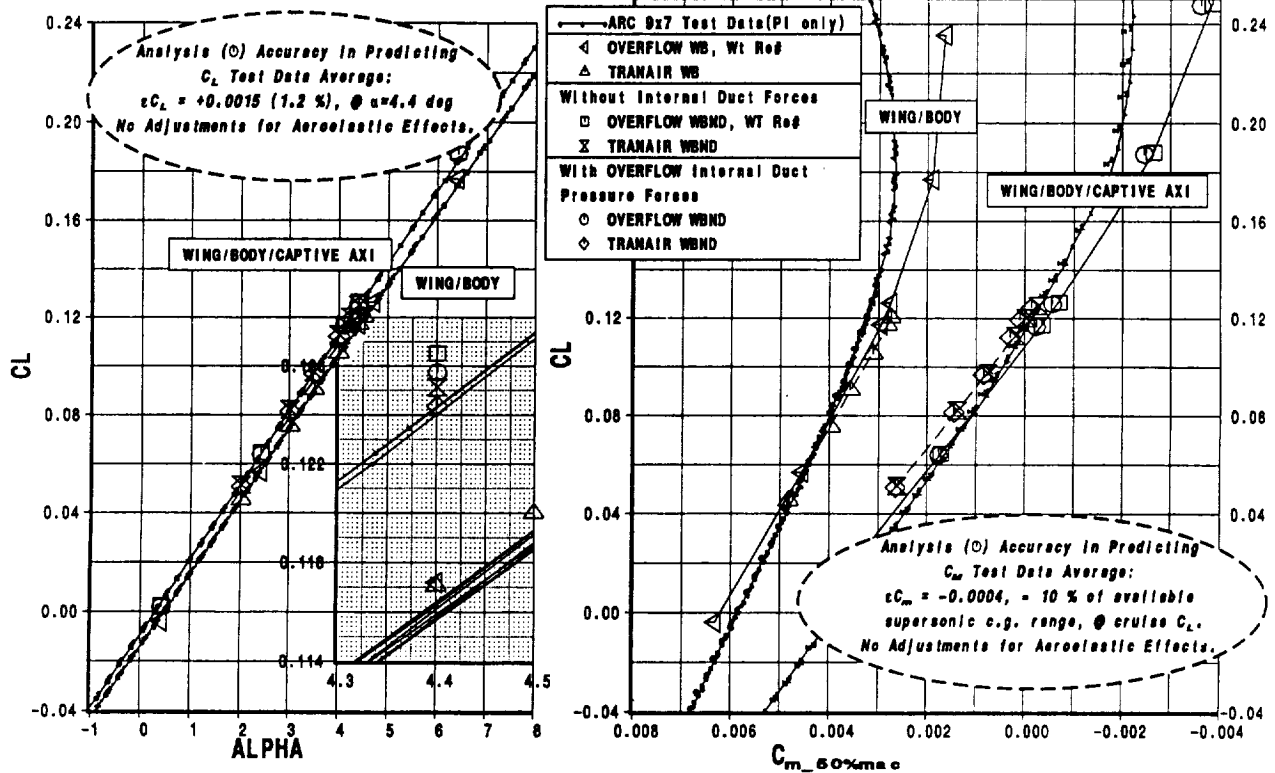


The pressure drag polar plot shown here indicates the same trends as seen for the axisymmetric configuration pressure drag polar shown previously. TRANAIR results were about 1.5 counts higher than OVERFLOW at constant lift.



HSCT High Speed Aerodynamics

Ref. H Wing/Body/Nacelle/Diverter Lift & Pitching Moment
 Axisymmetric Inlet - Axisymmetric Nozzle, Mach 2.4, $Re_{MAC} = 7$ million



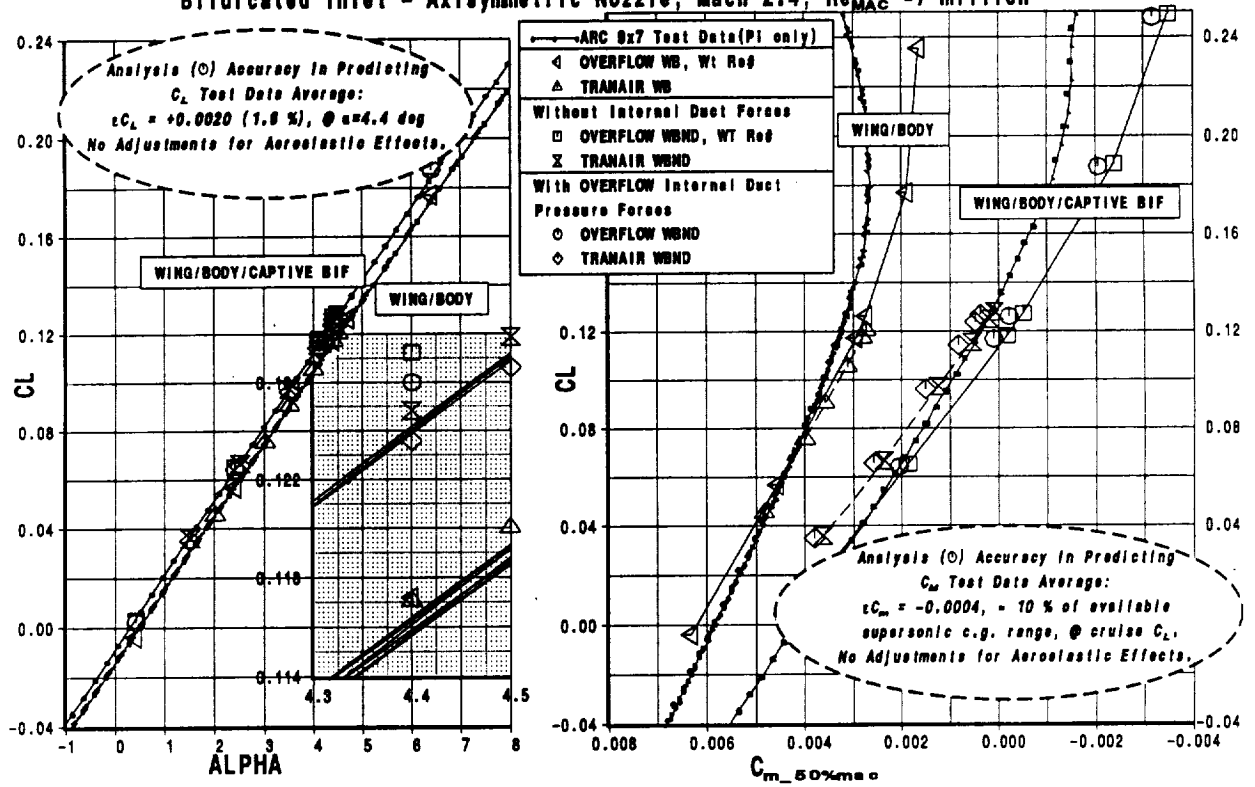
The lift force and pitching moment predicted by TRANAIR and OVERFLOW are shown in this figure for the captive axisymmetric installation. After the nacelle internal duct correction was made the OVERFLOW prediction was found to be about the same amount higher than test than the wing/body alone data (1.2% of cruise lift). This delta was attributed to aeroelastic effects in the wind tunnel data. The CFD results had what appears to be a moment center shift compared to test data for both wing/body and wing/body/nacelle. A portion of this was due to the aeroelastic effect discussed for the lift force comparison (the wing tips in the test are unloading, behind the moment center, resulting in less nose down moment). At the cruise point the OVERFLOW analysis was 0.0004 less than the test data. For a supersonic available c.g. range of 3% of MAC, this error was equivalent to about 10% of available c.g. range. The accuracy requirement of 1% of available c.g. range would be a pitching moment error of 0.00004. This may be an unobtainable level of accuracy. This requirement should probably be loosened in its absolute pitching moment accuracy to 10% of available c.g. range, and a pitching moment slope accuracy specified. The latter will require resolution of the pitching moment rotation seen in all the CFD to test comparisons.



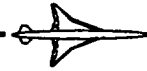
HSCT High Speed Aerodynamics

Ref. H Wing/Body/Nacelle/Diverter Lift & Pitching Moment

Bifurcated Inlet - Axisymmetric Nozzle, Mach 2.4, $Re_{MAC} = 7$ million



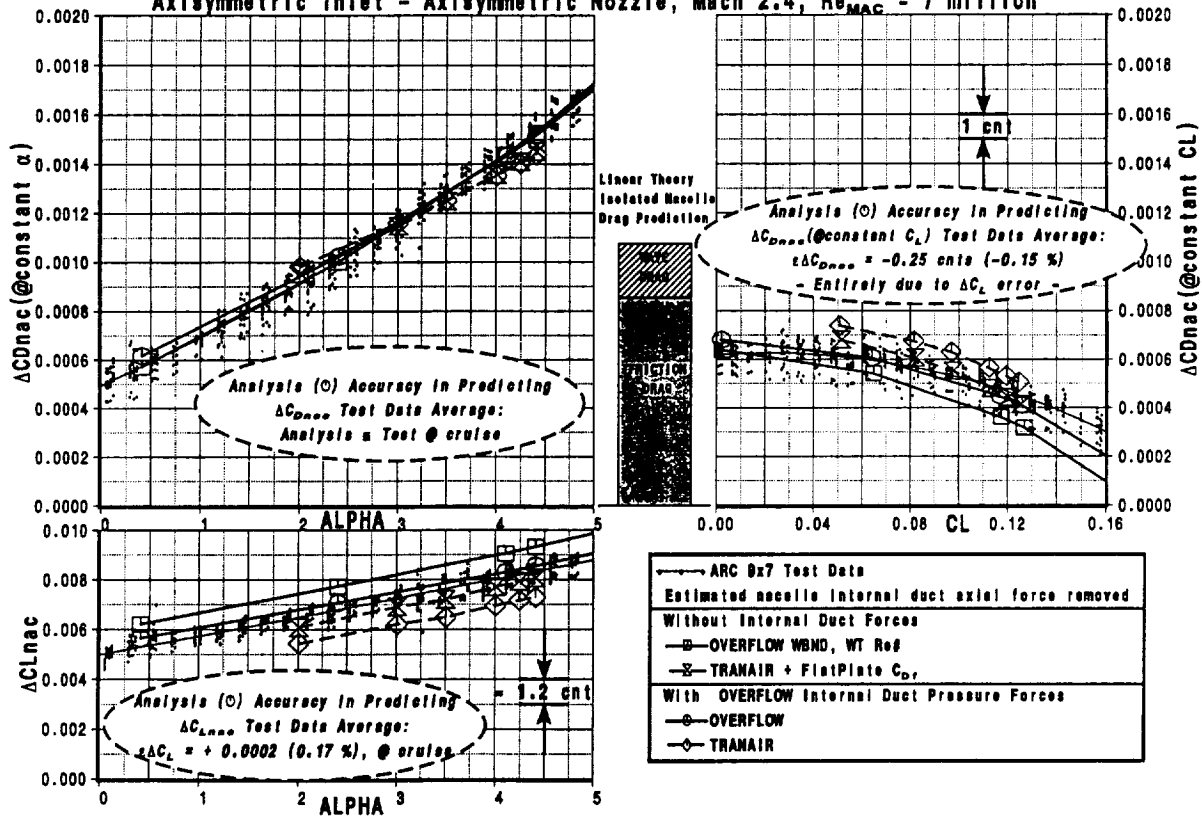
The captive bifurcated lift and pitching moment results are shown. The bifurcated nacelle OVERFLOW prediction was 1.6% higher than than the test data and indicated the same pitching moment trends as seen for the axisymmetric.



HSCT High Speed Aerodynamics

Ref. H Wing/Body/Nacelle/Diverter PAI Force Increments

Axisymmetric Inlet - Axisymmetric Nozzle, Mach 2.4, $Re_{MAC} = 7$ million



Nacelle force increments are shown for the axisymmetric inlet nacelle. In the upper plot on the left the wing/body drag was subtracted from the wing/body/nacelle/diverter drag at the same angle of attack; the lower figure was obtained through a similar calculation for lift. The figure on the right was obtained by subtracting the wing/body drag from the wing/body/nacelle/diverter drag at the same lift value. This last increment yields the installed nacelle drag at a given lift coefficient and represents essentially the value obtained from the upper left plot minus the lift interference drag from the lower left plot, i.e. the lift gained through installing the nacelles allows the airplane angle of attack to be lowered while still obtaining the same lift as for wing/body. Lift and drag traded this way are essentially proportional to the lift over drag ratio for small movements on the drag polar around the cruise point. The installed axisymmetric nacelle drag increment measured in the wind tunnel test was 4.7 counts (@ $CL=1.17$). Note that this is approximately equal to the drag value from the upper left (15.2 counts @ 4.4 deg) minus the lift benefit from the lower left ($0.0084/8 = 10.5$ counts). It is also interesting to note that the nacelles can be installed for a drag increment less than isolated skin friction of the nacelles.

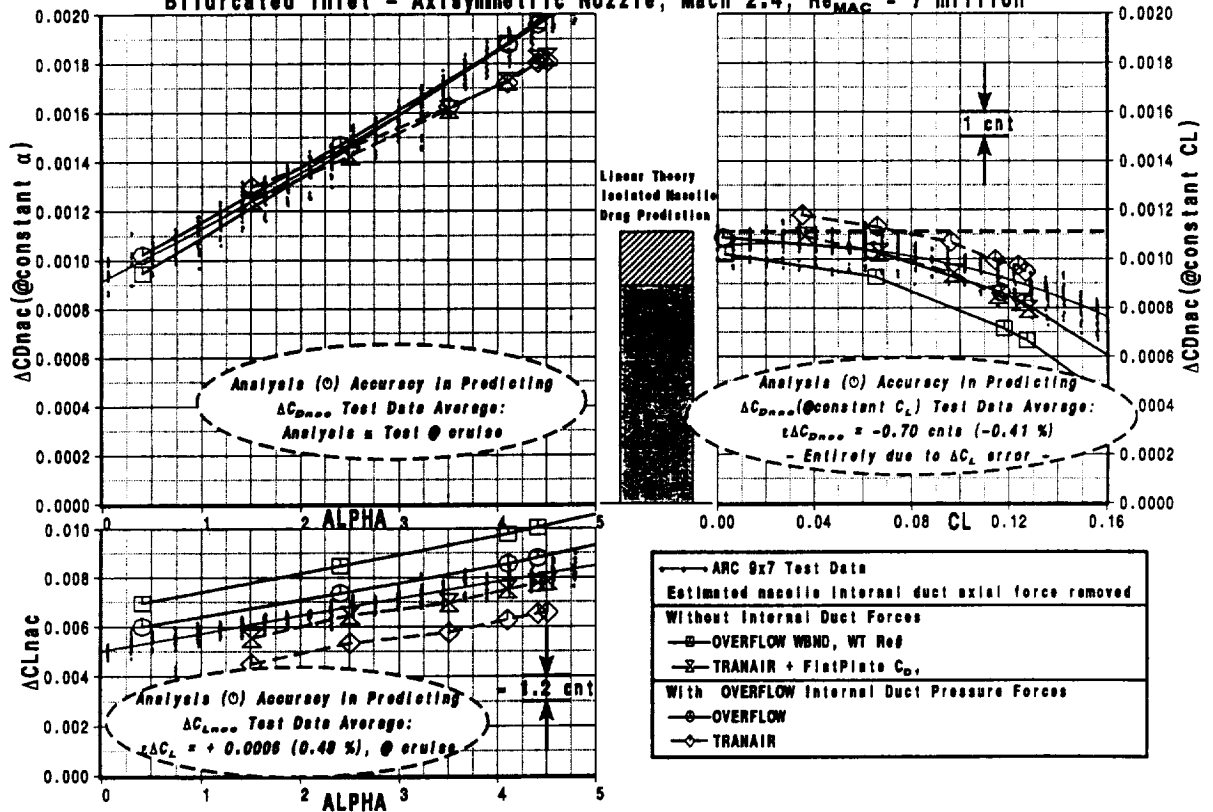
The OVERFLOW analysis predicted a nacelle drag increment (at constant angle of attack) that was essentially equal to a curve fit of the test data. The predicted lift increment was higher than test by 0.17 % of cruise lift. The drag increment at constant lift (4.4 counts) was lower than test by 0.15 % of cruise drag and came entirely from the lift error. The OVERFLOW increments discussed here are with the internal duct pressures included in order to simulate the wind tunnel data.



HSCT High Speed Aerodynamics

Ref. H Wing/Body/Nacelle/Divertor PAI Force Increments

Bifurcated Inlet - Axisymmetric Nozzle, Mach 2.4, $Re_{MAC} = 7$ million

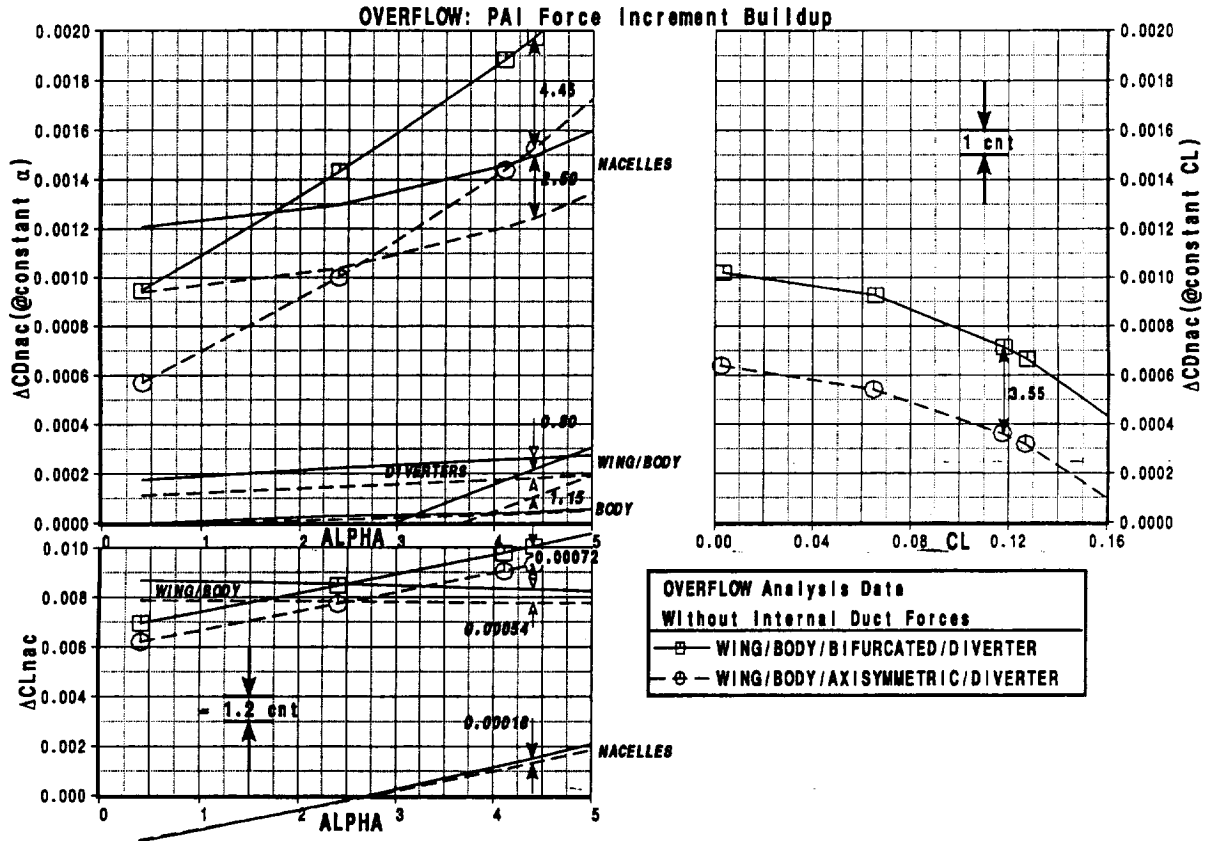


Both TRANAIR and OVERFLOW were not as accurate predicting the bifurcated nacelle force increments. TRANAIR in particular was low in predicting both drag and lift at constant angle of attack; but the effects are cancelling and the installed drag force increment was not as far off. OVERFLOW again predicted the drag increment at constant angle of attack almost exactly. The lift prediction was higher than test (as for the axisymmetric) by 0.48 % of cruise lift. The measured installed nacelle drag increment was 9.3 counts (@ CL=.117). The OVERFLOW value was 8.7 counts which was lower than test by 0.41 % of cruise drag.



HSCT High Speed Aerodynamics

Ref. H Wing/Body/Nacelle/Diverter, Inlet Comparison, Mach 2.4, $Re_{MAC} = 7$ million

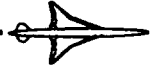


In this next section the difference between the bifurcated and axisymmetric inlet nacelles as measured in the wind tunnel ($9.3 - 4.7 = 4.6$ counts) and predicted by OVERFLOW ($8.7 - 4.4 = 4.3$ counts) are discussed. As seen in the preceding section it appeared that OVERFLOW was capturing the flow features important to the nacelle installation and predicting the forces and moments accurately as well. The advantage of the CFD solution over the test data was that individual components and flow features could be examined in some detail. This capability was utilized in this section to investigate the bifurcated / axisymmetric drag difference.

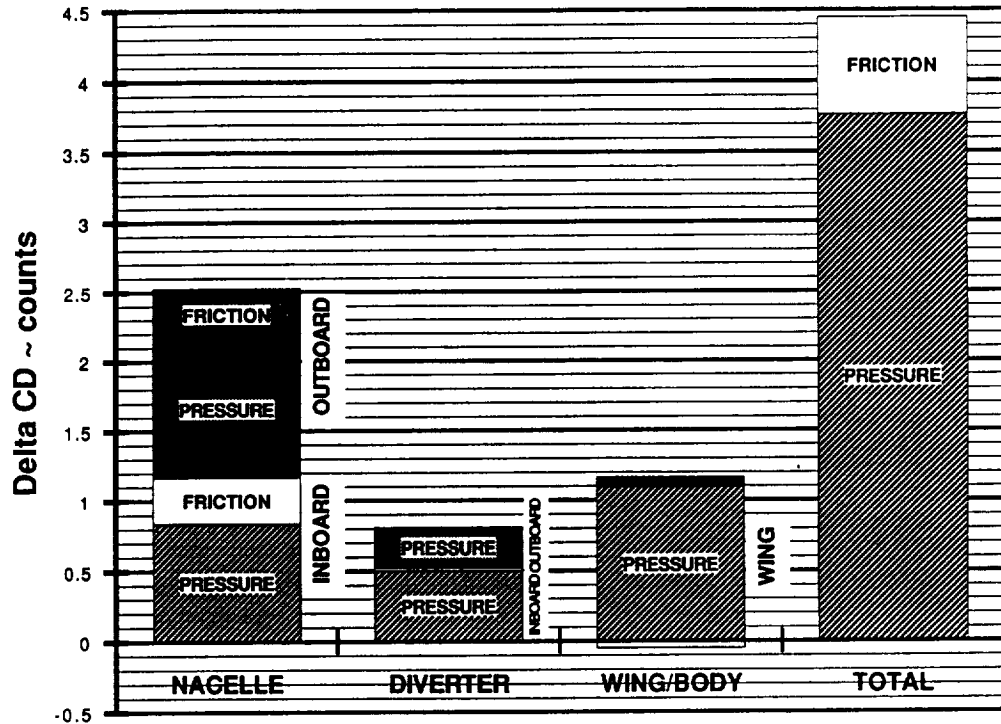
The figure shows the nacelle force increments for the two types of nacelles as predicted by OVERFLOW. These data do not have the internal lift forces included as these tend to confuse the comparisons and in realistic installation the inlet would be aligned with the underwing flowfield such that a flow through nacelle would not have internal lift forces. The result was that the installed drag difference between the nacelles dropped from 4.3 to 3.55 counts. The difference was due to the different locations and cross sections of the inlets in the underwing flowfield causing different amounts of lift to be carried by the internal ducts of the two nacelle types.

The drag difference between the two nacelles at constant angle of attack was shown to be made up primarily of the drag on the nacelles themselves (2.5 counts) in addition to approximately a count each for the diverters and the wing.

The lift difference between the two nacelles is due to higher lifting pressures on the wing lower surface for the bifurcated installation and a slightly higher nacelle lift for the bifurcated.



Ref. H Wing / Body / Nacelle / Diverter, Inlet Comparison, Mach 2.4, ReMAC = 7 million
 OVERFLOW: Bifurcated - Axisymmetric Component Drag Increments @ Alpha=4.4 deg



In the figure below the drag difference between the two nacelles at angle of attack of 4.4 degrees was broken down into pressure and friction components. The nacelle delta was found to be composed of 0.7 counts of friction drag (due to the increased length of the bifurcated) and 1.8 counts of pressure drag (primarily from the bifurcated inlet lip bevel).

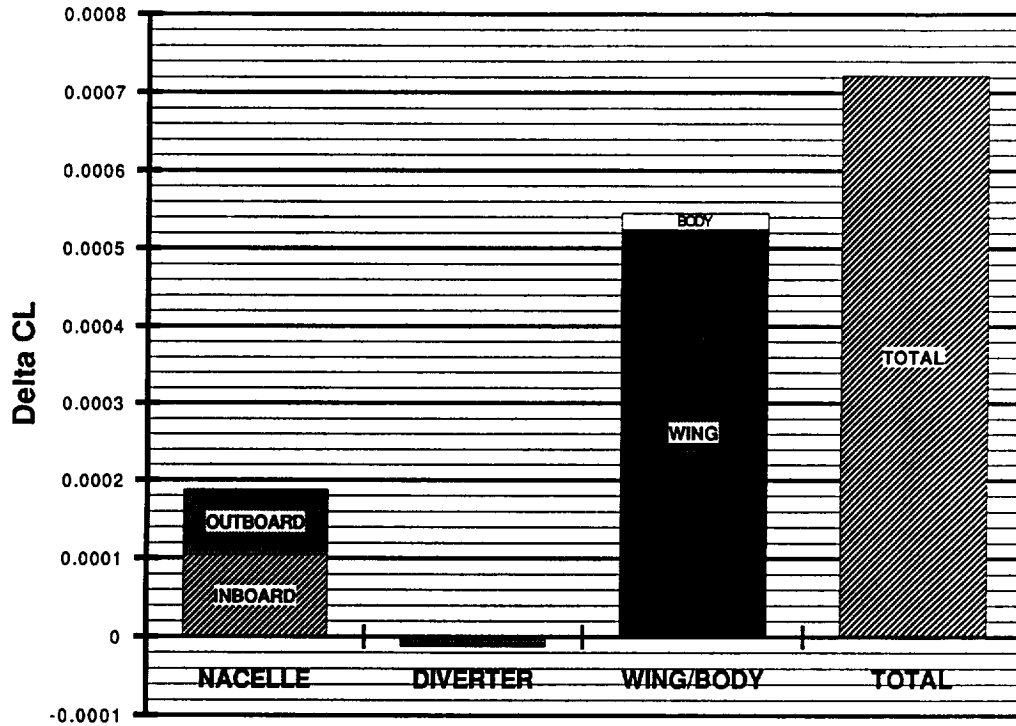
Both inboard and outboard bifurcated nacelle diverters had increased pressure drag and a very small difference in friction drag over the axisymmetric. This was partially due to the taller diverter for the bifurcated (difficulties with bifurcated installation resulted in diverter height about twice what required; discussed in configuration definition section above). However, as subsequent figures will show the bifurcated diverter also had a substantially larger high pressure region on the forward facing ramp, probably due to lip bevel pressures.

The wing/body drag difference was nearly all due to increased drag on the wing lower surface with the bifurcated installation. There was a small negative friction delta due to larger diverter area cut out of wing lower surface for the bifurcated, and a small pressure drag increment on the body. The wing increment was probably primarily due to the larger extent of the diverter shoulder expansion pressures sucking back on the wing reflex (in the bifurcated installation the diverter shoulder was located farther forward).



HSCT High Speed Aerodynamics

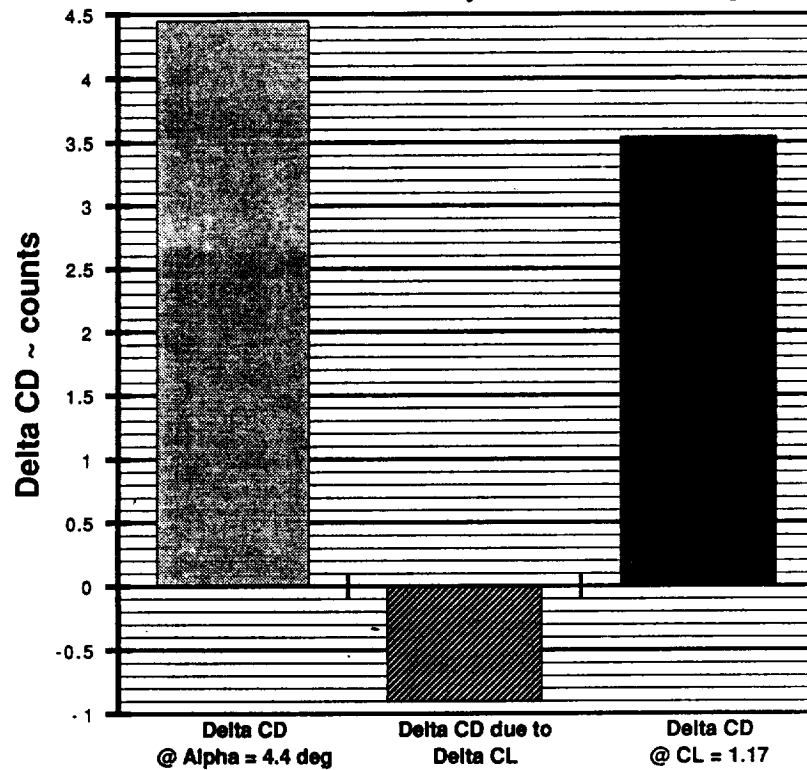
Ref. H Wing / Body / Nacelle / Diverter, Inlet Comparison, Mach 2.4, ReMAC = 7 million
 OVERFLOW: Bifurcated - Axisymmetric Component Lift Increments @ Alpha=4.4 deg



The breakdown of the lift differences between the bifurcated and axisymmetric nacelles is shown. As discussed earlier, the additional lift for the bifurcated installation was due primarily to the wing, with an additional amount split equally between the two nacelles.



Ref. H Wing / Body / Nacelle / Diverter, Inlet Comparison, Mach 2.4, ReMAC = 7 million
OVERFLOW: Bifurcated - Axisymmetric Installed Drag Buildup

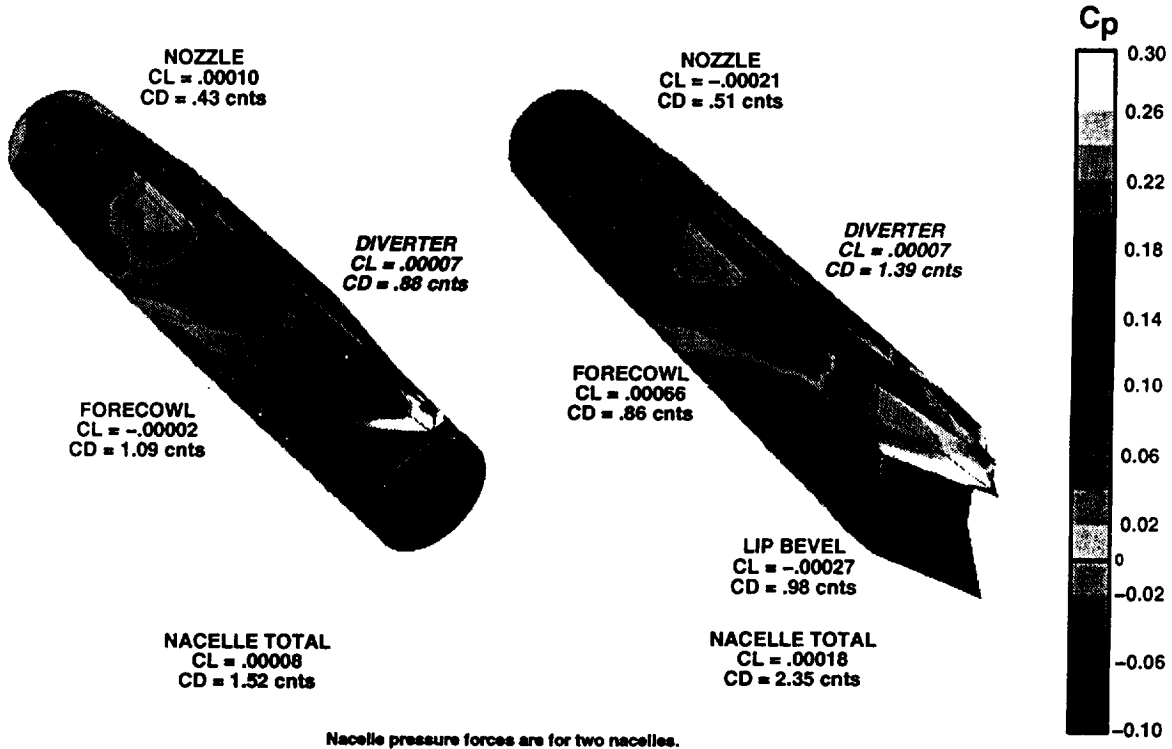


In this figure the delta lift from the previous figure has been converted into a drag increment and summed with the drag delta at constant angle of attack to show how the installed drag delta between the bifurcated and axisymmetric nacelles can be obtained.

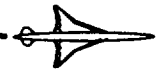


HSCT High Speed Aerodynamics

**Ref. H Wing/Body/Nacelle/Diverter Inlet Comparison, Mach 2.4, $Re_{MAC} = 7$ million
OVERFLOW: Inboard Nacelle Pressure Contours @ $\alpha = 4.4$ deg**

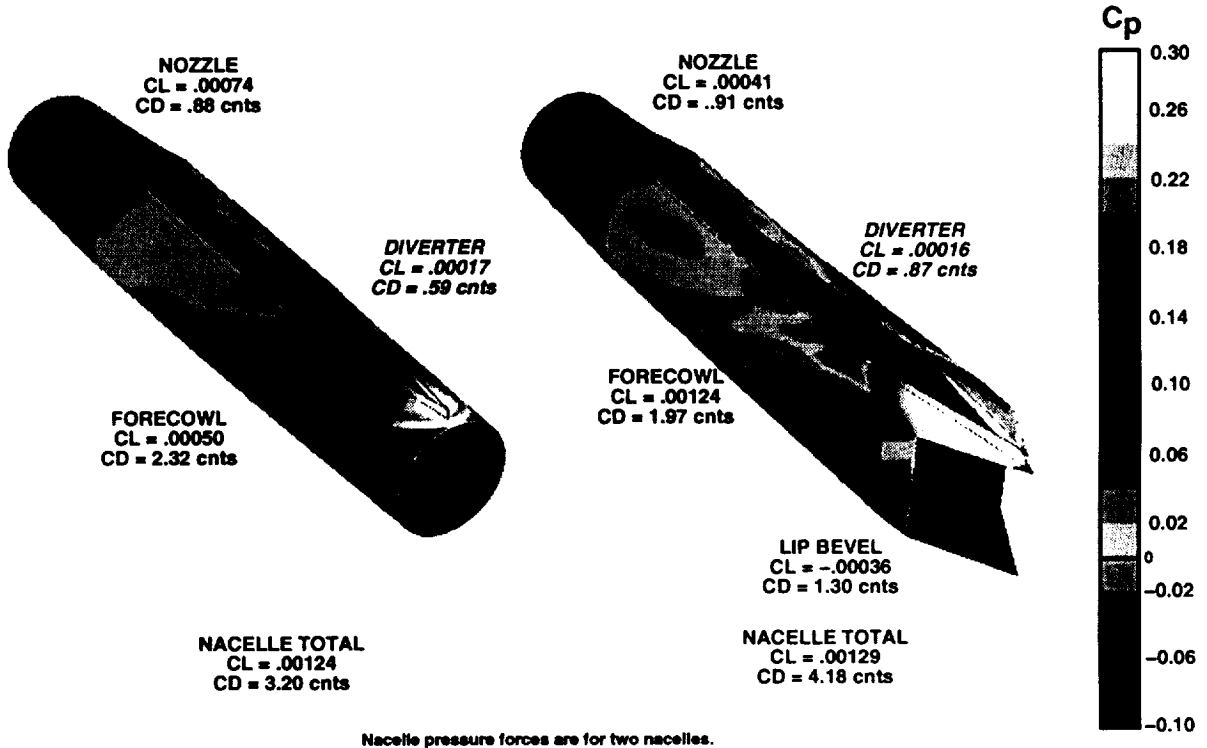


This figure shows the inboard nacelle surface pressures for the two nacelle types along with the integrated pressure forces for individual nacelles components. An observation of the bifurcated lifting forces shows how the nacelle had large force swings moving aft from the lip bevel: the lip bevel carried negative lift, the forecowl carried positive lift, the nozzle carried negative lift. In addition, the bifurcated nacelle nozzle carried substantially less lift than the axisymmetric nacelle nozzle; this was evident in the pressures on the top of the nozzle (as well as, on the nozzle lower surface as discussed previously). The lift difference between the two nozzles ($CL = -0.00031$) has been attributed to the small geometry differences discussed earlier and is equivalent to 0.4 counts of drag. The increased diverter drag is clearly seen to be primarily the result of a much larger extent of high pressure on the forward facing ramp; this is due to interference with the lip bevel pressure field.

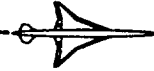


HSTC High Speed Aerodynamics

**Ref. H Wing/Body/Nacelle/Diverter Inlet Comparison, Mach 2.4, $Re_{MAC} = 7$ million
OVERFLOW: Outboard Nacelle Pressure Contours @ $\alpha = 4.4$ deg**



The outboard nacelle pressure distribution and force components are compared in the figure. The nozzle lift difference ($CL = -0.00033$) was equal to the inboard value which was equivalent to an additional 0.4 counts of drag difference on the bifurcated nacelle. The implication of these lift differences was that if the nacelles had been built with identical nozzles the drag difference between the two nacelle types would have been reduced by 0.8 counts.



Bifurcated - Axisymmetric Inlet Drag Delta

- Mach 2.4, Supersonic Cruise $C_L = 0.12$
- Reference H Wing/Body, Bifurcated and Axisymmetric Inlets, Axisymmetric Nozzle

DESCRIPTION	C_D , counts	SOURCE
BIFURCATED - AXISYMMETRIC DRAG DELTA	4.6	Test: 2.7% Ref H @ARC 9x7
• Internal Duct Lift Differences	- 0.7	Overflow: N-S simulation (test Re#)
• Nozzle Geometry Difference	- 0.8	Overflow
CORRECTED BIF - AXI DRAG DELTA	3.1	
• Bifurcated Inlet Lip Bevel	0.5 ⇒	0.5 Tranair($\Delta C_D=2\text{cnts}, \Delta C_{D_L}=-1.5\text{cnts}$)
• Diverter Height & Location	0.5 ⇒	0.0 Estimate (Overflow)
• Wing Reflex + Misc Interference	1.4 ⇒	1.0 Estimate (Overflow)
• Friction Drag	0.7 ⇒	0.7 Overflow
REDUCTION IN BIF - AXI DRAG DELTA	3.1 ⇒	2.2, Range ≈ 1.5 to 2.5 cnts

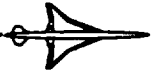
In summary, the original bifurcated-axisymmetric inlet drag delta of 4.6 counts can be modified with the results from the OVERFLOW analysis:

Measured delta 4.60 counts
 Internal lift correction - 0.70
 Dissimilar nozzles - 0.80

New delta 3.10 counts

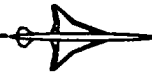
This delta is composed of increased diverter pressure drag, increased wing pressure drag, lip bevel drag, and a nacelle skin friction drag increment (0.7 counts). The current lip bevel has about 2 counts of pressure drag, but internal Boeing IR&D studies have shown that it also increases the lift on the wing to such a degree that the drag reduction of going to a bevel-less geometry only reduces the drag by 0.5 counts. However, this reduction is probably not available as the propulsion design team reports that the current lip bevel angle of 4 deg may be a minimum. Moving the bifurcated diverter LE aft will have multiple effects: it appears that the diverter could be moved out of the high pressure region near the lip bevel, the expansion from the diverter shoulder would cover a smaller region on the wing lower surface (good for drag and lift), and the disturbance from the diverter LE would no longer be ingested by the inlet. If, in addition, the wing was reflexed to match the nacelle installation (less reflex than Ref. H) the diverter height could be reduced.

It has been estimated that the minimum level that the bifurcated-axisymmetric increment could be driven down to from the 3 count level above is 1.5 to 2.5 counts (equal to the 0.7 friction delta plus 0.8 to 1.8 counts of nacelle & installation effects).



CONCLUSIONS & RECOMMENDATIONS

- **CFD to test comparisons indicate that OVERFLOW provides accurate absolute and incremental aerodynamic data for PAI investigations.**
 - **Recommend resolving CFD - flat plate skin friction drag discrepancies.**
 - **Recommend resolving experimental data uncertainties: trip drag level, accounting process for internal duct lift forces, and aeroelastic effects.**
- **Current Bifurcated-Axisymmetric Inlet drag difference adjusted from 4.6 to 3.1 cnts as result of OVERFLOW to test data comparisons:**
 - * **-0.7 cnts due to internal lift correction,**
 - * **-0.8 cnts due to dissimilar nozzles.**
- **Recommend that all future configurations align inlet with underwing flow field and/or do pretest estimates of internal duct lift.**



CONCLUSIONS & RECOMMENDATIONS

- **Estimated bifurcated inlet drag penalty 1.5 - 2.5 cnts.**
 - **Axisymmetric Nozzle.**
 - **Several additional analyses required to confirm this delta on Reference H.**
 - * **Diverter moved aft on bifurcated installation.**
 - * **Wing lower surface modified for bifurcated.**
- **No bifurcated inlet work in CA on TCA in 1996.**
 - **Inlet downselect Nov 1 will use 2 cnts unless additional work done to properly install bifurcated on TCA wing and develop 2D nozzle effects.**

HSCT Nacelle Boundary Layer Diverter Study

Steven S. Ogg
The Boeing Company

The objectives of this study were to understand how lift and drag are affected by diverter geometry, to develop a potential diverter geometry for the Technology Concept Airplane (TCA) that increased lift at constant angle of attack and lift to drag ratio, and to provide insight into how the wing camber in the vicinity of the diverters and nacelles should be shaped.

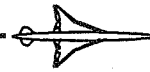
The Reference H wing-body configuration was used to study the impact of boundary layer diverter planform shape on aerodynamic characteristics. In order to make the results more applicable to the TCA a systematic variation of nacelle and diverter geometry was performed. The nacelles were first scaled to 673 pps to more accurately match the TCA engine airframe matching. The impact of changing from a purely axisymmetric nacelle to one that has an axisymmetric inlet which transitions to a 2D nozzle was then explored. The diverter planform was then varied with consideration for the wing alone pressure distribution and the geometrical relationship of the 2D nozzle to the wing.

Boundary layer diverters, such as the wedge-slab variant of the Reference H configuration tend to dominate the pressure field in the region of the nacelles due to the strong compression field from the wedge and the strong expansion field from the diverter shoulder. An examination using the TRANAIR full potential code of candidate diverters highlights potential areas of improvement in diverter geometry and in wing camber design in the region of the nacelles.

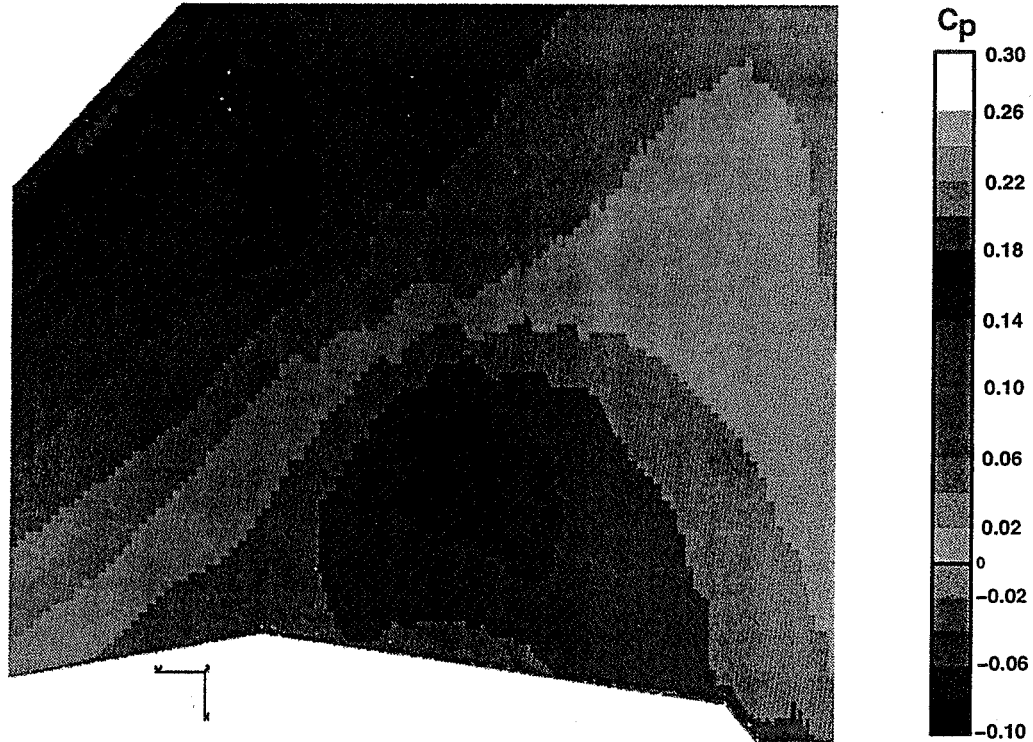


ALTERNATE NACELLE AND DIVERTER CONFIGURATIONS

- **Baseline Reference H**
- **Engine Size / Diverter Placement**
- **Axi-2d versus Axi-Axi Nacelles**
- **Alternate Diverter**

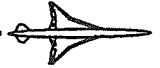


Ref. H Wing/Body Lower Surface Pressure Contours
Tranair, Mach 2.4, $\alpha = 4.4$

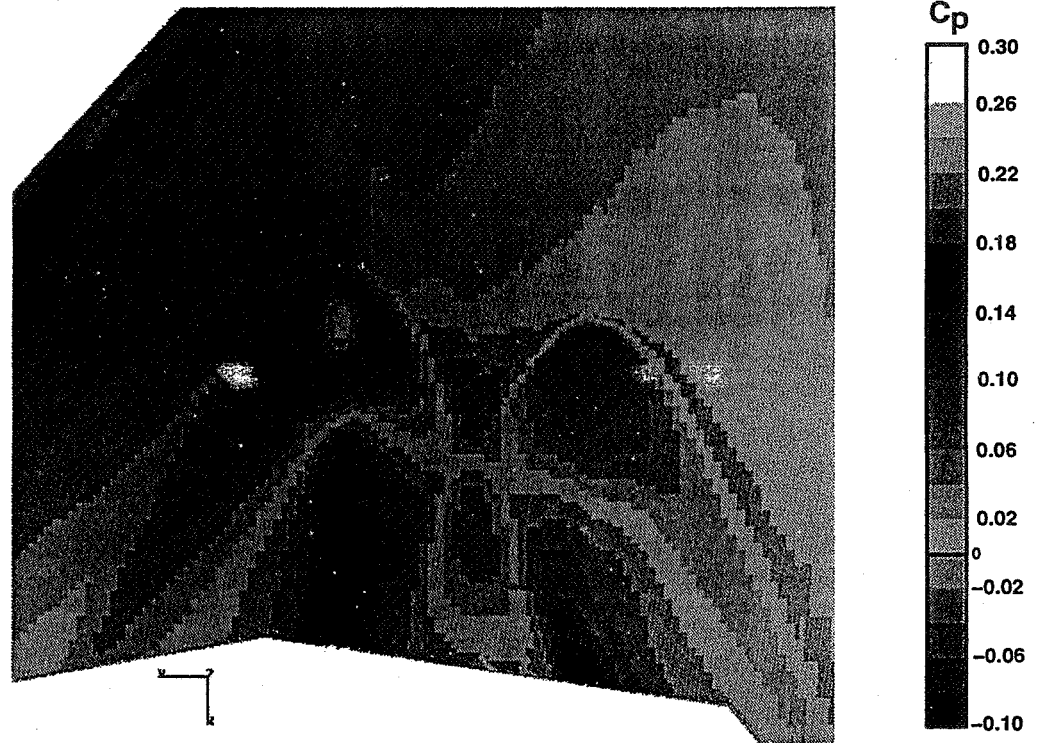


Reference H wing/body

Pressure coefficient contours on the wing lower surface of the Reference H wing/body configuration are shown in the region of the nacelles. Note the low pressure region due to the wing camber reflex which is designed to create a thrust component from the positive nacelle pressure field. Observe also that the region of lowest pressure is significantly forward of the trailing edge of the wing which becomes important when designing diverter geometry.



Ref. H Wing/Body 509pps Axisymmetric Nacelles in Proximity
Wing Lower Surface Pressure Contours, Tranair, Mach 2.4, $\alpha = 4.4$

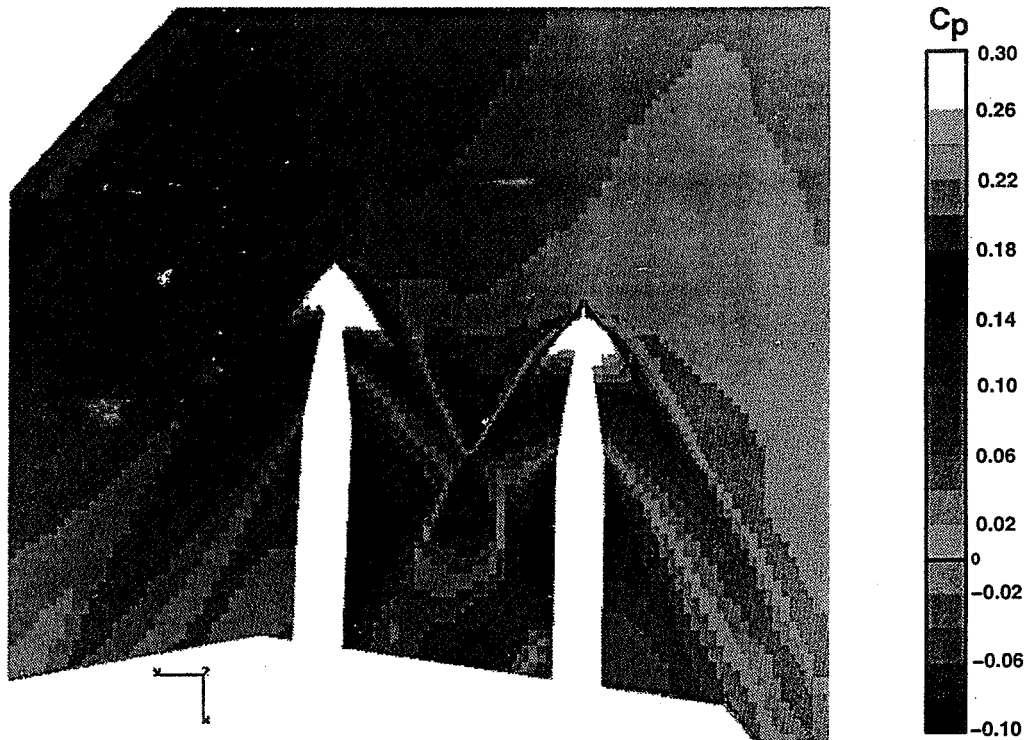


Reference H. 509 pps axisymmetric nacelles in proximity. wing lower surface pressures

Pressure coefficient contours on the wing lower surface for the Reference H wing/body configuration with 509 pps axisymmetric nacelles in proximity are shown. The nacelles produce positive to neutral pressures over most of the wing camber reflex region where negative pressures existed for the wing-body alone case. The positive pressures in this region increase lift and reduce drag. Note the two concentrated regions of lower pressure that still exist. It would be very desirable to design a combination of wing camber and diverter shape that minimized this low pressure region which reduces lift and increases drag.



Ref. H Wing/Body Captive 509pps Axi., Lower Surface Pressure Contours
Tranair, Mach 2.4, $\alpha = 4.4$

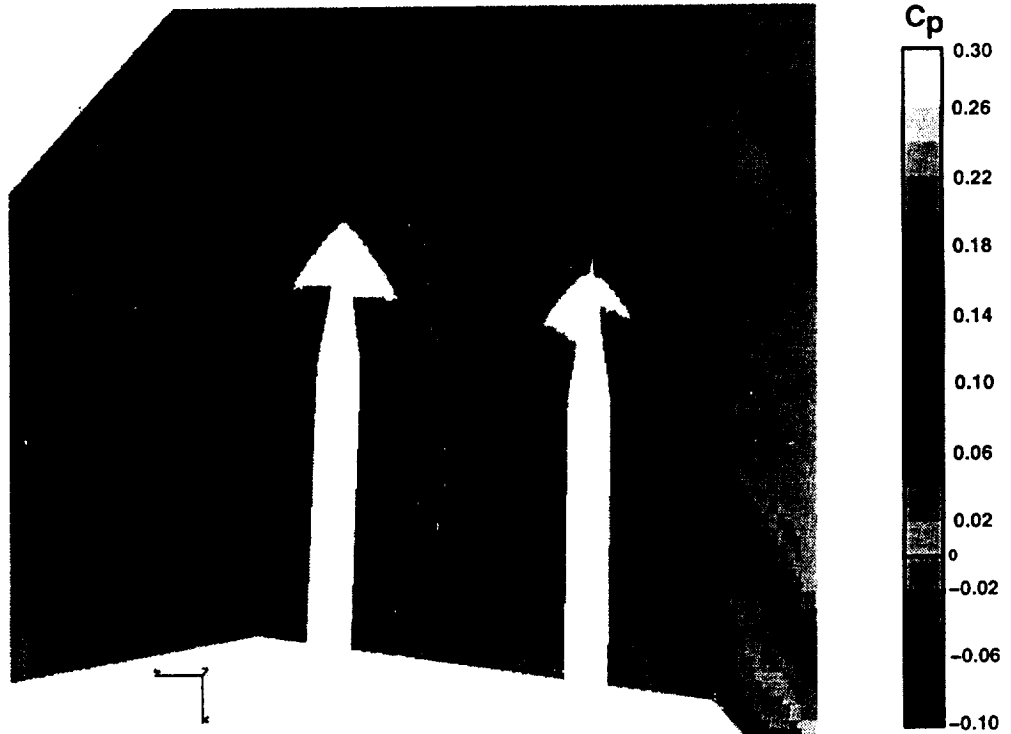


Reference H. captive 509 pps axisymmetric nacelles. wing lower surface pressures

Pressure coefficient contours on the wing lower surface for the Reference H wing/body configuration with wedge/slab boundary layer diverters and 509 pps axisymmetric nacelles are shown. The most notable features of this configuration in comparison to the in-proximity case shown previously are the increased shock strength and positive pressure due to the boundary layer diverters and the strong expansions and resulting lower pressure regions just aft of the diverter shoulders (transition from the wedge to slab geometry). Relative to the wing/body case this configuration has the following TRANAIR predicted pressure force coefficient increments; delta CL=0.0100 and delta CD=.00099. These number indicate that the diverters and nacelles are being installed for less than skin friction with the added bonus of increased lift at a constant alpha.



Ref. H Wing/Body Captive 673pps Axi. (Equivalent Area to Axi-2D)
Lower Surface Pressure Contours, Tranair, Mach 2.4, $\alpha = 4.4$

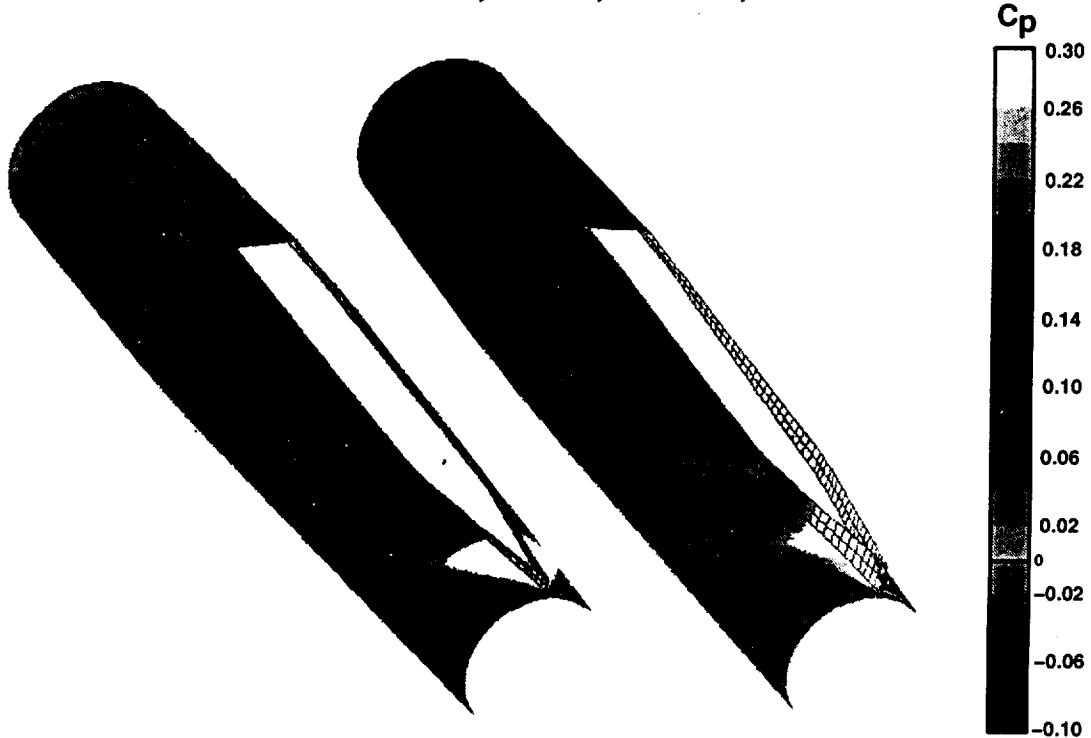


Reference H. captive 673 pps axisymmetric nacelles. wing lower surface pressures

Pressure coefficient contours on the wing lower surface for the Reference H wing/body configuration with wedge-slab boundary layer diverters and 673 pps axisymmetric nacelles are shown. This nacelle size more closely represents the engine airframe matching anticipated for the Technology Concept Airplane. The axial area distribution of this nacelle closely matches that of the axisymmetric inlet/2d nozzle nacelle to be found later in this section. The pressure forces impact of the engine size increase and shape change are, as follows: $\Delta CL = .0006$ and $\Delta CD = .00021$. This shows a significant increase in drag with little increase in lift. This is due in part to the forward movement of the diverter shoulder with its expansion acting in the area of maximum reflex of the wing camber and over a greater area such that the impact of the increased area over which the positive diverter wedge/nacelle pressure field is felt is negated. The drag on the increased size nacelle accounts for over half of the total drag increment although the movement of the diverter wedge/nacelle shocks forward also increases the body drag by 0.5 counts.

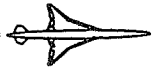


**Ref. H Wing/Body Captive 673pps Axisymmetric Nacelles
Nacelle Pressure Contours, Tranair, Mach 2.4, $\alpha = 4.4$**

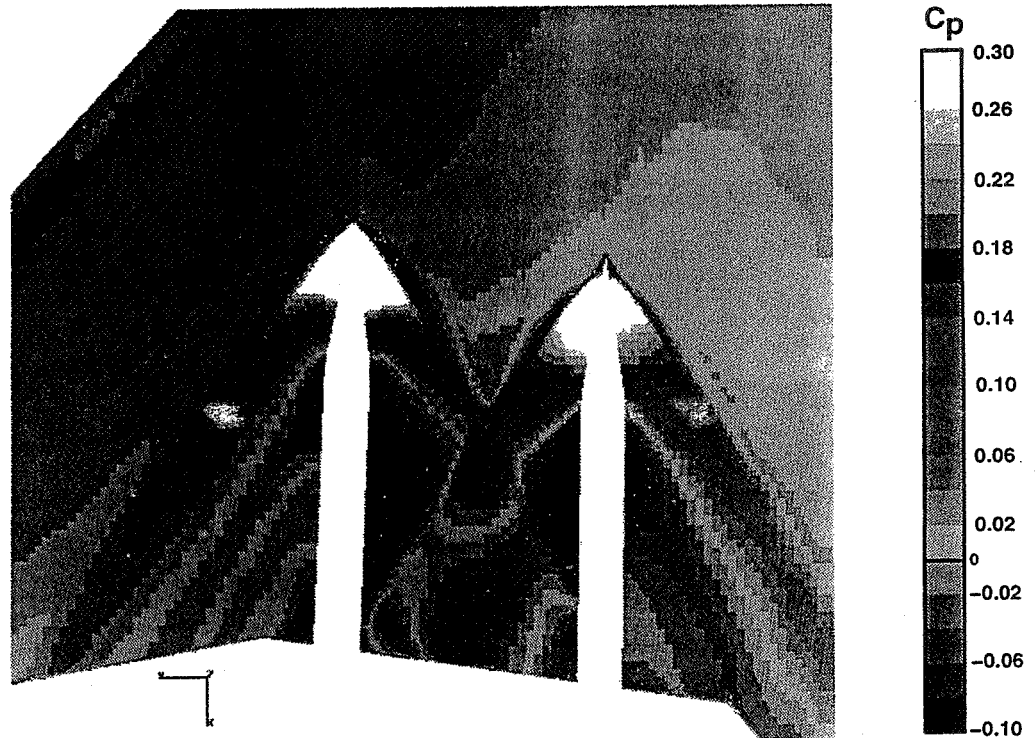


Reference H. captive 673 pps axisymmetric nacelles. nacelle pressures

Pressure coefficient contours on the nacelles for the Reference H wing/body configuration with wedge-slab boundary layer diverters and 673 pps axisymmetric nacelles are shown. This nacelle size more closely represents the engine airframe matching anticipated for the Technology Concept Airplane. The axial area distribution of this nacelle closely matches that of the axisymmetric inlet/2d nozzle nacelle to be found later in this section. The pressure distribution over the nacelles is very similar to that for the baseline 509pps nacelles. The axisymmetric nacelles with 2d nozzles will be compared to this case.

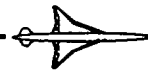


Ref. H Wing/Body Captive 673pps Axi-2d,
Lower Surface Pressure Contours, Tranair, Mach 2.4, $\alpha = 4.4$

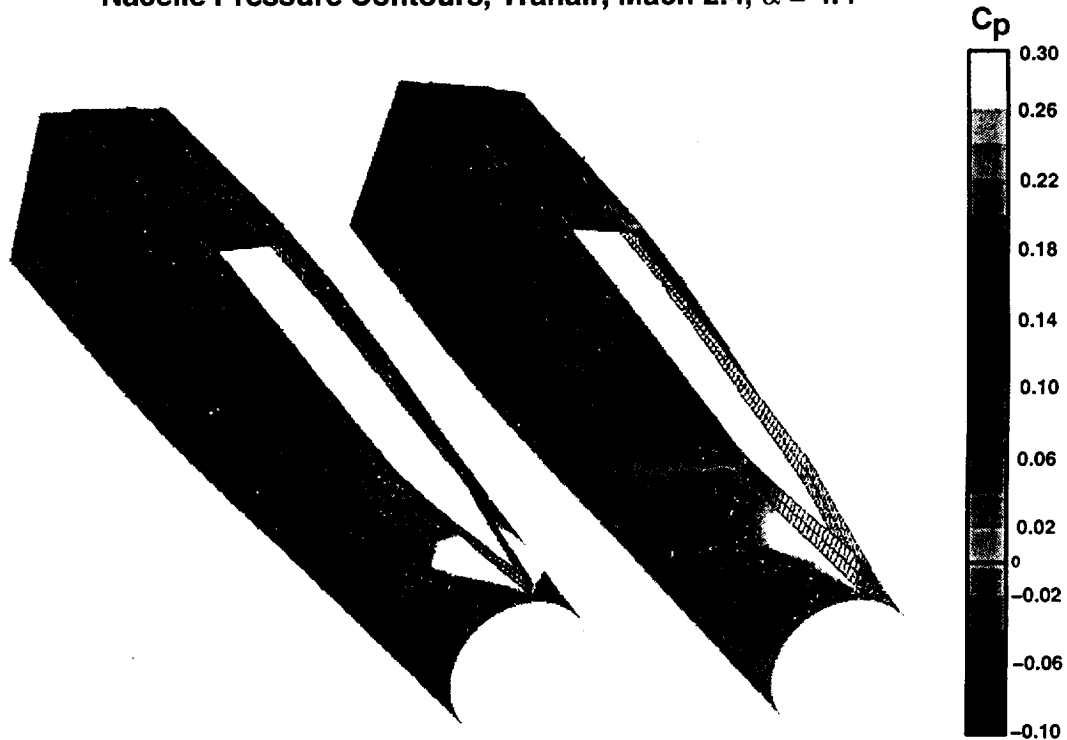


Reference H. captive 673 pps axi-2d nacelles. wing lower surface pressures

Pressure coefficient contours on the wing lower surface for the Reference H wing/body configuration with wedge-slab boundary layer diverters and 673 pps axi-2d nacelles are shown. The axi-2d nacelle has an axisymmetric inlet that transitions to a 2d nozzle. This nacelle concept is similar to that chosen for study on the Technology Concept Airplane. The axisymmetric nacelle in the previous figure has nearly the same longitudinal area distribution as this axi-2d nacelle although the nozzle for the axi-2d case has been lowered relative to the wing trailing edge to provide relief to the channel formed by the wing/diverter/2d nozzle geometry. Only subtle changes are seen in the pressure distributions between the axi-2d and axi-axi cases. The axi-2d case tends to increase the intensity of the expansion at the diverter shoulder, but reduce the region of influence of this expansion. This is apparent on the inboard side of the inboard diverter and the outboard side of the outboard diverter. The transition of the forebody from circular to rectangular is believed to cause this variation. The region in between the nacelles and near the trailing edge of the wing also shows a general increase in pressure level relative to the axi-axi case. The pressure force increments (axi-2d minus axi-axi) are as follows: delta $CL = .0010$ and delta $CD = .00013$. Most of the increase in lift is on the lower surface of the wing. The drag difference is spread out across nacelles (0.4 cts), diverters (0.4 cts), wing (0.2 cts), and body (0.3 cts). At a constant lift coefficient the axi-2d nacelle can be installed for no drag penalty on the Ref. H wing/body. A plus is the increase in lift at constant angle of attack which allows improved wing body integration within the constant cabin floor angle constraint.



**Ref. H Wing/Body Captive 673pps Axi-2d
Nacelle Pressure Contours, Tranair, Mach 2.4, $\alpha = 4.4$**

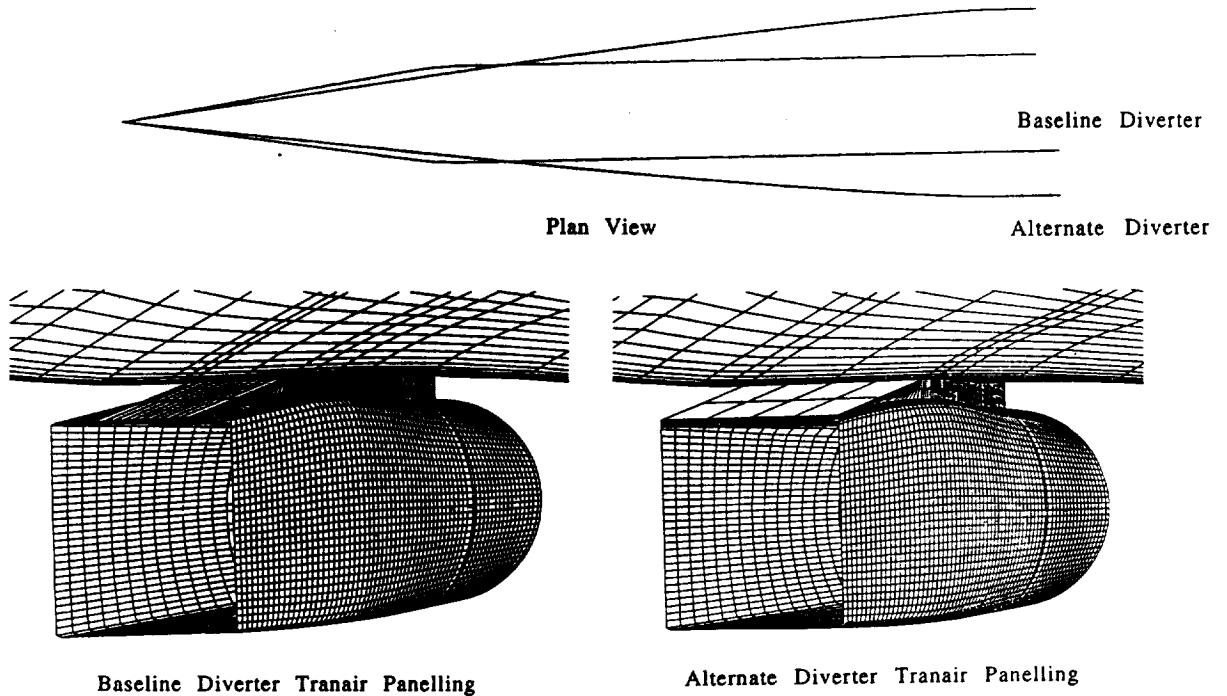


Reference H. captive 673 pps axi-2d nacelles. nacelle surface pressures

Pressure coefficient contours on the nacelle surfaces for the Reference H wing/body configuration with wedge-slab boundary layer diverters and 673 pps axi-2d nacelles are shown. The axi-2d nacelle has an axisymmetric inlet that transitions to a 2d nozzle. This nacelle concept is similar to that chosen for study on the Technology Concept Airplane. The axisymmetric nacelle in the previous figure has nearly the same longitudinal area distribution as this axi-2d nacelle although the nozzle for the axi-2d case has been lowered relative to the wing trailing edge to provide relief to the channel formed by the wing/diverter/2d nozzle geometry. See the previous facing page text for comments on pressures and forces.



Alternate Diverter Geometry

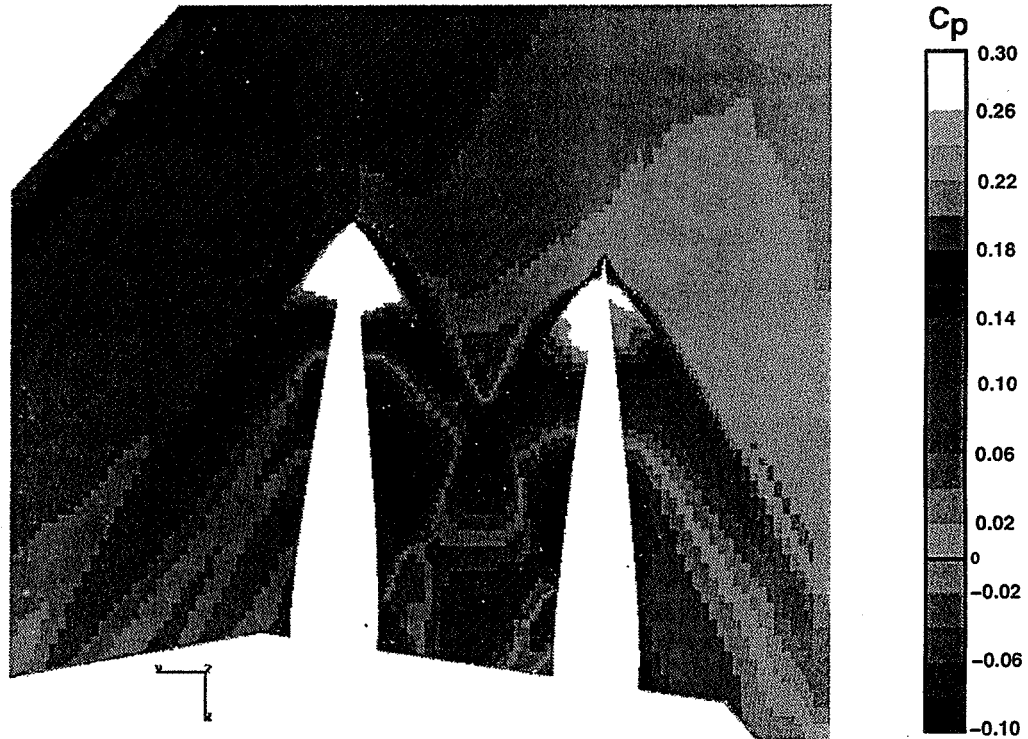


Reference H. captive 673 pps axi-2d nacelles. alternate diverter geometry

Planform shape of the alternate diverter is compared to that of the baseline diverter. These two diverter shapes meet consistent structural width requirements near the shoulder of the baseline diverter. The installed 673pps axi-2d nacelles are shown for both the diverters as well. The objective of the alternate diverter is to increase the lift interference of the diverter/nacelle combination by reducing the strength and extent of the flow expansion at the baseline diverter shoulder. A secondary objective is to provide flexibility in the vertical positioning of the nozzle relative to the trailing edge of the wing. The alternate diverter accomplishes this by removing the channel between wing, diverter, and nacelle.



Ref. H Wing/Body Captive 673pps Axi-2d, Alternate Diverter
Lower Surface Pressure Contours, Tranair, Mach 2.4, $\alpha = 4.4$

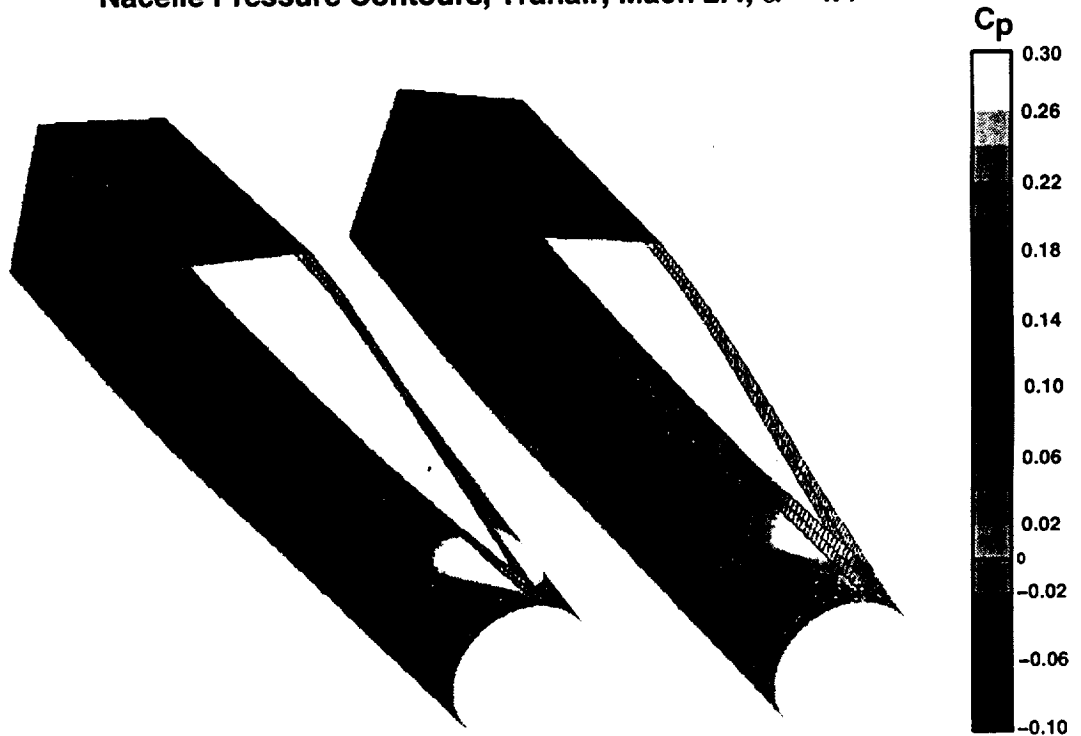


Reference H. captive 673 pps axi-2d nacelles. alternate diverters. wing lower surface pressures

Pressure coefficient contours on the wing lower surface for the Reference H wing/body configuration with alternate boundary layer diverters and 673 pps axi-2d nacelles are shown. Relative to the baseline diverter case a significant reduction in the intensity and region of influence of the expansion at the location of the baseline diverter shoulders is evident. The pressure force increments relative to the baseline wedge/slab diverter are as follows: $\Delta CL=0.0010$ and $\Delta CD=0.00001$. The lift increment is carried on the lower surface of the wing. There is a reduction in wetted area for the configuration with the alternate diverter equal to approximately a quarter of a count of drag. The alternate diverter has several potential benefits: reduced drag at the cruise lift coefficient, increased lift at a constant angle of attack (which as mentioned previously improves the integration of the wing and body), and an increase in diverter volume for structure or systems. This diverter variation was fairly simplistic in concept (being constant in plan view from inboard to outboard and also symmetric) and a more exhaustive study of diverter geometry perturbation is definitely warranted however, a wing with less reflex in the vicinity of the nacelles (and monotonic in the x direction) would provide a much better platform for study.



**Ref. H Wing/Body Captive 673pps Axi-2d, Alternate Diverters
Nacelle Pressure Contours, Tranair, Mach 2.4, $\alpha = 4.4$**



Reference H, captive 673 pps axi-2d nacelles, alternate diverters, nacelle surface pressures

Pressure coefficient contours on the nacelle surfaces for the Reference H wing/body configuration with alternate boundary layer diverters and 673 pps axi-2d nacelles are shown. As with the wing lower surface pressure contours, a reduction in strength of the expansion at the location of the maximum wing reflex (also the location of the baseline diverter shoulders) relative to the baseline diverter is observed.



CONCLUSIONS AND RECOMMENDATIONS

ALTERNATE NACELLE AND DIVERTER CONFIGURATIONS

- Installation of the 673pps axi-axi nacelle increased pressure drag at constant lift by 1.3 counts relative to the baseline Ref. H axi-axi nacelle at 509pps.
- An axi-2d nacelle can be installed with no drag penalty relative to an axi-axi nacelle on the Reference H planform.
- An alternate diverter provided a reduction in drag of 1.2 counts by reducing the region of negative lift caused the the wedge/slab diverter shoulder (on the baseline diverter).
 - Recommend reducing the wing camber reflex.
 - Recommend validation of the alternate diverter concept with a Navier-Stokes code.
 - Recommend that the alternate diverter shape be used as starting point for diverter designs for future configurations having 2d nozzles.



Analysis of Alternate Inlets and Nacelles for HSCT Configuration

P. Sundaram *, Ana Tinetti **, Alan Arslan *, Shreekant Agrawal *,
Peter Hartwich *, and Jay Jones *

This paper presents the computational investigation of the PAI related study to evaluate various installation parameters in an attempt to minimize the cruise drag of the HSCT configuration with nacelles installed. In particular, an assessment is made of the supersonic cruise point aerodynamic performance of axisymmetric and 2-D inlets installed on the MDC M2.4-7A Opt5 wing/body/nacelle/diverter (W/B/N/D) geometry. Earlier analysis and experimental study on Ref. H configurations have shown that the installed axisymmetric nacelles have better drag characteristics compared to the 2-D nacelles. However, in that study, the optimum wing/body geometry for each nacelle installation was not determined. The present investigation evaluates the aerodynamic performance of the optimized wing/body geometry accounting for the effects of two inlet concepts, namely the axisymmetric and 2-D inlets.

The wing/body configuration chosen for the present investigation is the Opt5 geometry. The nacelles are sized to fit the realistic MFTF A12 engine and are installed with either axisymmetric or 2-D bifurcated inlets. Results of the analysis including nacelle position, nacelle cambering, diverter width, and diverter leading-edge sweep modifications of the baseline Opt5 nacelle configuration are presented. CFL3D Euler analysis showed that the 2-D inlet nacelles have nearly 4.5 counts of higher pressure drag compared to the axisymmetric nacelles before optimization. After wing/body optimization with the nacelle effects, the drag difference increased to 5.2 counts. Examination of the results indicates that adverse nacelle/diverter/wing geometry for the 2-D inlet nacelles may account for a significant part of the drag penalty.

* McDonnell Douglas Corporation, Long Beach, CA.

** Eagle Aeronautics, Inc., Newport News, VA.

Acknowledgments

HSR Team

Budd Bobbitt (Eagle Aeronautics, Inc.)

Grant Martin (MDC)

Brent Bates (ViGYAN, Inc.)

This study was supported by the HSR team. Thanks to the BCAG HSR Inlet team for providing the 2-D inlet model inside geometry for the analysis. Special thanks to Percey (Bud) Bobbitt of Eagle Aeronautics, Inc. for his valuable suggestions during the course of the investigation. Also, thanks to Brent Bates of ViGYAN, Inc. for generating the original grid for the 2-D inlet geometry as well as CFL3D solution with ramps. Thanks to Grant Martin for his help during the preparation of this report.

Objectives

- Assess the cruise point performance of axisymmetric and 2-D inlet nacelles to help the inlet downselect
- Evaluate the various installation parameters to obtain the optimum nacelle installation

The primary objective of the present study is to assess the cruise point aerodynamic performance of axisymmetric and 2-D inlets. In the process of this study, additional installation parameters such as the nacelle position and camber as well as diverter thickness and leading-edge sweep have been investigated. The results of this study are needed for the inlet downselect process.

Overview

- Background
- Nacelles in the forward and aft locations
- Alternate inlet assessment
 - axisymmetric and 2-D inlets
- Geometry optimization
 - wing/body optimization for both axisymmetric and 2-D inlets
- Nacelle/diverter integration analysis
 - diverter leading-edge sweep and outboard diverter width
 - nacelle camber
- Summary

First, a background on the Opt5 wing/body/nacelle/diverter geometry is given. Following this, the paper describes the nacelle repositioning study that was considered for the present alternate nacelle investigation and presents the comparison of forces and moments between the forward and aft nacelle positions. Once the proper nacelle locations have been determined, the axisymmetric inlet considered so far is replaced by a 2-D inlet shape. At this stage, the axisymmetric and 2-D inlet installation benefits are compared. After this, the wing/body optimization in the presence of the two inlet concepts is performed and the results are compared. Next, the diverter width and sweep modifications for the axisymmetric nacelles in the aft location are investigated. Lastly, the axisymmetric nacelle cambers are altered in order to evaluate the effectiveness of the camber modifications on the overall installation aerodynamics. Throughout the paper, numerical flow visualizations that provide understanding of the flow field changes due to the installation modifications are included. Finally, the results are summarized and important areas of future work is highlighted.

Opt5 W/B/N/D Axisymmetric Nacelles with Axisymmetric Inlets

- Geometry based on the MDA Arrow Wing linear design, M2.4-7A
- Opt5 geometry design based on camber and twist and fuselage camber optimization of M2.4-7A
- FLO67/QNMDIFF nonlinear design optimization code
- Nacelle size lofted from scaling the MFTF A12 engine geometry
- CFL3D Euler results obtained for the W/B/N/D geometry
- Cruise point design validated in the LaRC UPWT tunnel TS #2.

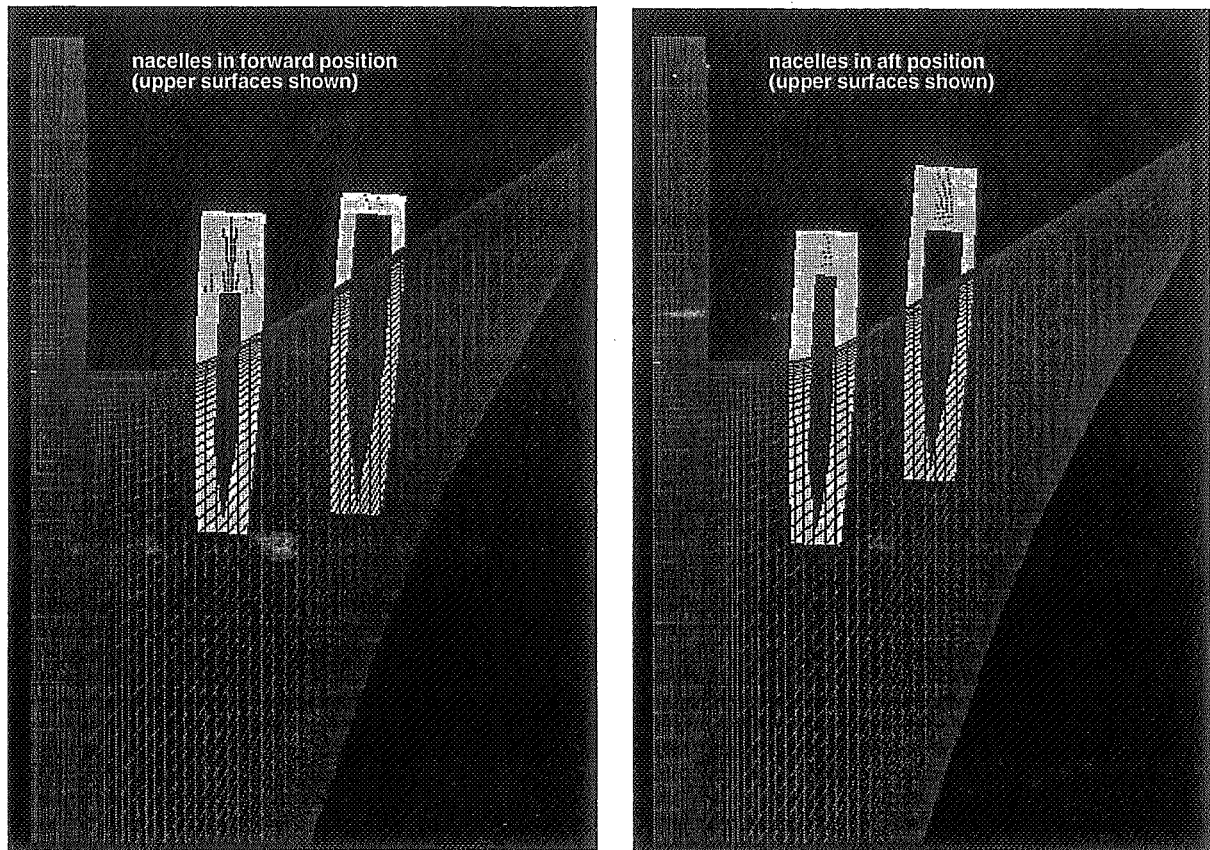
The McDonnell Douglas HSCT Configuration Aerodynamics team designed and developed a cruise point ($M_\infty = 2.4$) optimized wing/body geometry using the FLO67/QNMDIFF nonlinear optimization code. The Opt5 geometry was obtained through a wing camber and twist, and fuselage camber nonlinear optimization of the M2.4-7A Arrow Wing linear design of MDC. The Opt5 nacelles with axisymmetric inlets were sized to fit the MFTF A12 engine. The nacelles were located at their original M2.4-7A nacelle position (forward) under the wing. CFL3D Euler results of the wing/body/nacelle/diverter (W/B/N/D) geometry were obtained and the computed results showed good comparison with the LaRC UPWT wind tunnel TS #2 test data, thus validating the nonlinear cruise point design methodology.

Nacelle Installation Guidelines

- Nacelle location (in planform) based on vehicle technology perspectives
- Nacelle vertical location based on the wing/body (computed) 3D boundary layer height
- Inlet face aligned with the local wing/body flow field
- Diverter height sufficient to ensure a smooth channel flow between the wing lower surface and the nacelle
- Diverter top long enough to limit the backward facing ramp angle to be around 10°

The actual integration of the nacelles under the wing is based on some ground rules. First, the nacelles location in planform is determined by the vehicle technology perspectives such as structural requirements and the overall aerodynamic constraints. The vertical location of the nacelles is to prevent the ingestion of the boundary layer flow into the nacelle at flight Reynolds number. To determine this, the boundary layer thickness obtained from the wing/body 3DBL program was used. Another important factor for the vertical location of the nacelles is to provide a uniform flow in the channel region between the nacelles and wing lower surface, called the channel criterion. Past MDA studies have shown that the ratio of minimum diverter height to the diverter leading edge height should be at least 0.6. Also, the inlet face is aligned with the local flow obtained from the CFL3D wing/body Euler analysis. Finally, when lofting the diverter top surface, it was ensured that its length to height ratio was adequate to provide a backward facing ramp angle of around 10° .

Nacelle Repositioning – M2.4–7A Opt5 W/B/N/D

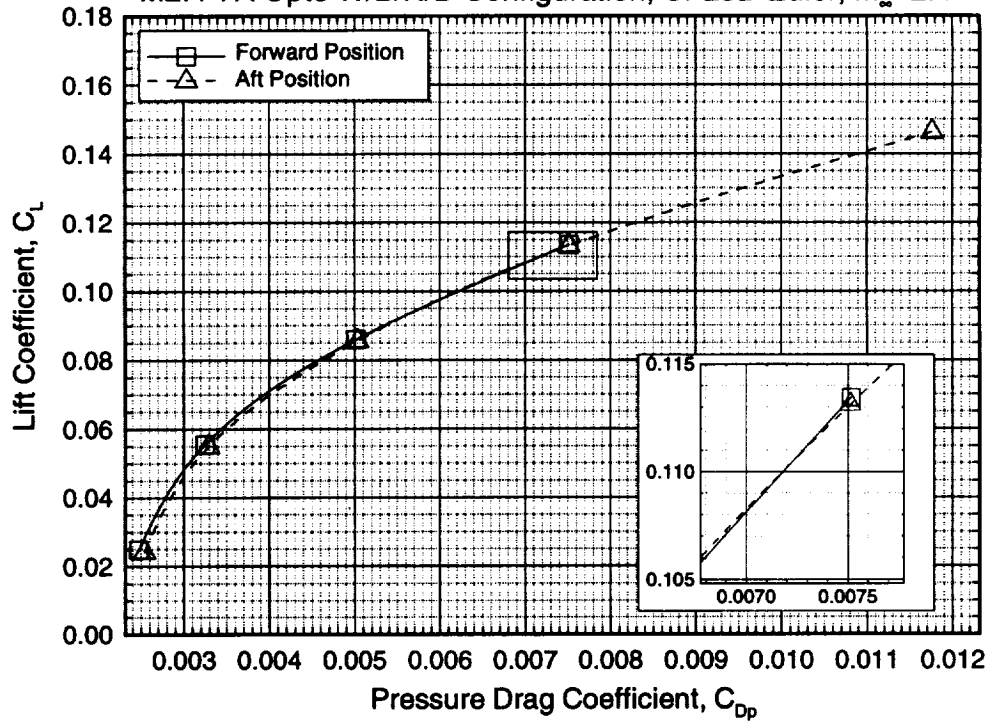


The first configuration modification examined was that of changing the position of the two nacelles both longitudinally and laterally. One of the objectives of the present study was to compare the performance of axisymmetric and 2-D inlets. The Technology Integration (TI) team determined that moving the nacelles aft from their original forward position of the M2.4–7A Opt5 nacelle position was better overall from the vehicle technology perspective. Further, due to the fact that the 2-D inlet was about 8 feet longer than the axisymmetric, an aft location of the nacelles that was suitable for both the axisymmetric and 2-D inlet nacelles was chosen. The nacelles were moved longitudinally to locate the maximum nacelle diameter or cross-sectional area at the wing trailing edge.

The figure above shows the comparison of the aft nacelle location with the original Opt5 (forward) nacelle location. In the forward location, the inboard and outboard nacelle inlet face centerline is located at (2566.18", 18267.84") and (2592.46", 454.297"), respectively. In the nacelle aft location, the inboard nacelle moved nearly 35" forward and 37" inboard while the outboard nacelle moved nearly 32" aft and 60" inboard compared to the forward nacelle location of Opt5.

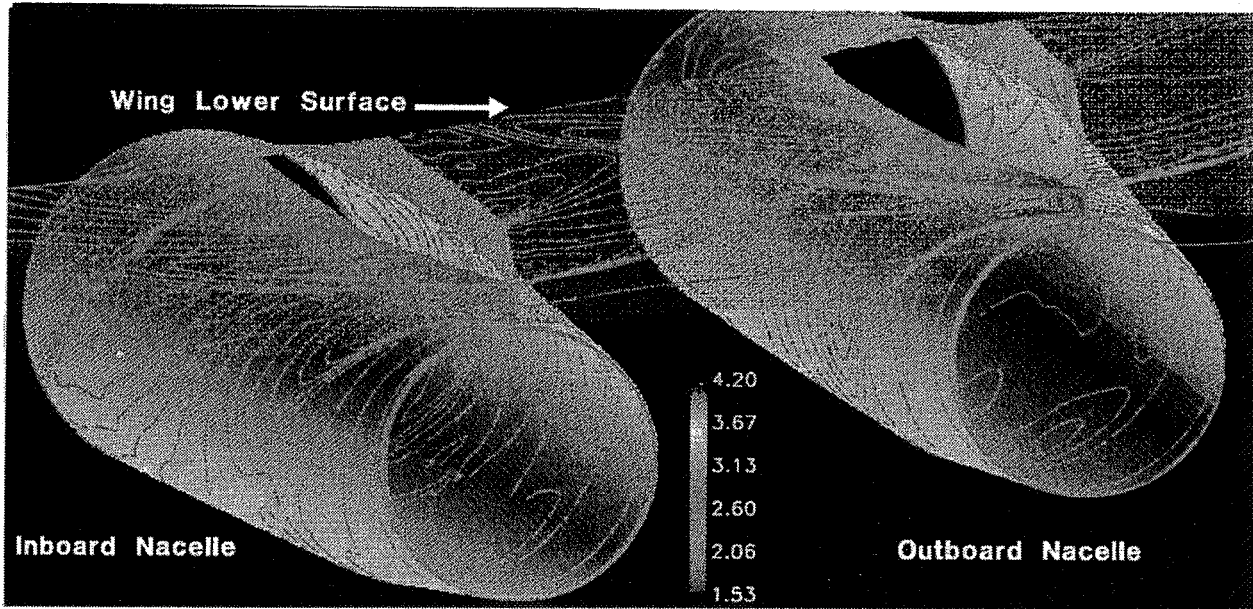
Pressure Drag Polars for Axisymmetric Nacelles with Thick OB Div.

M2.4-7A Opt5 W/B/N/D Configuration, CFL3D Euler, $M_\infty=2.4$



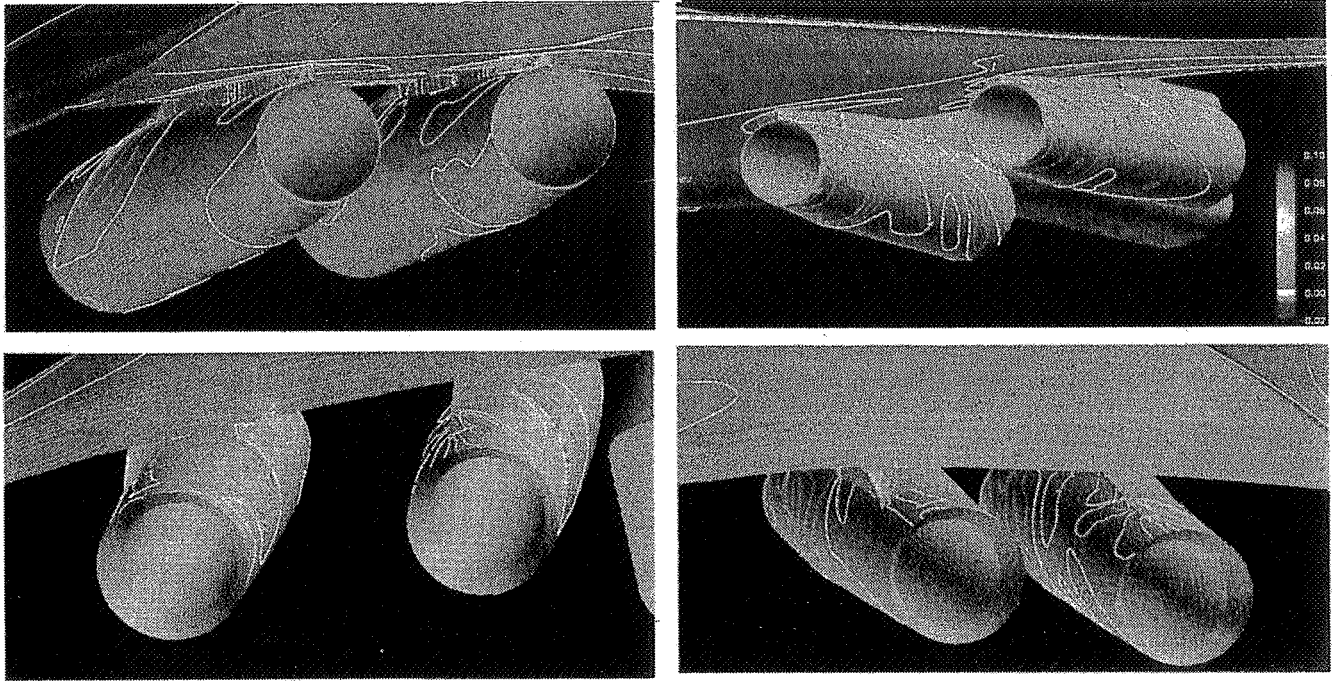
Next, a comparison of the computed results of the forward and aft nacelle location is made. The lift curve results indicate that there is practically no difference between the two nacelle locations and hence is not shown. Also, the repositioning of the nacelles has a negligible effect on the drag, as seen in the figure above.

Mach Number Contours for the M2.4-7A Opt5 Wing/Body/Nacelle/Diverter Configuration, Nacelles in Aft Position with Original Diverters
CFL3D Euler, $M_\infty = 2.4$, $\alpha = 1.9^\circ$



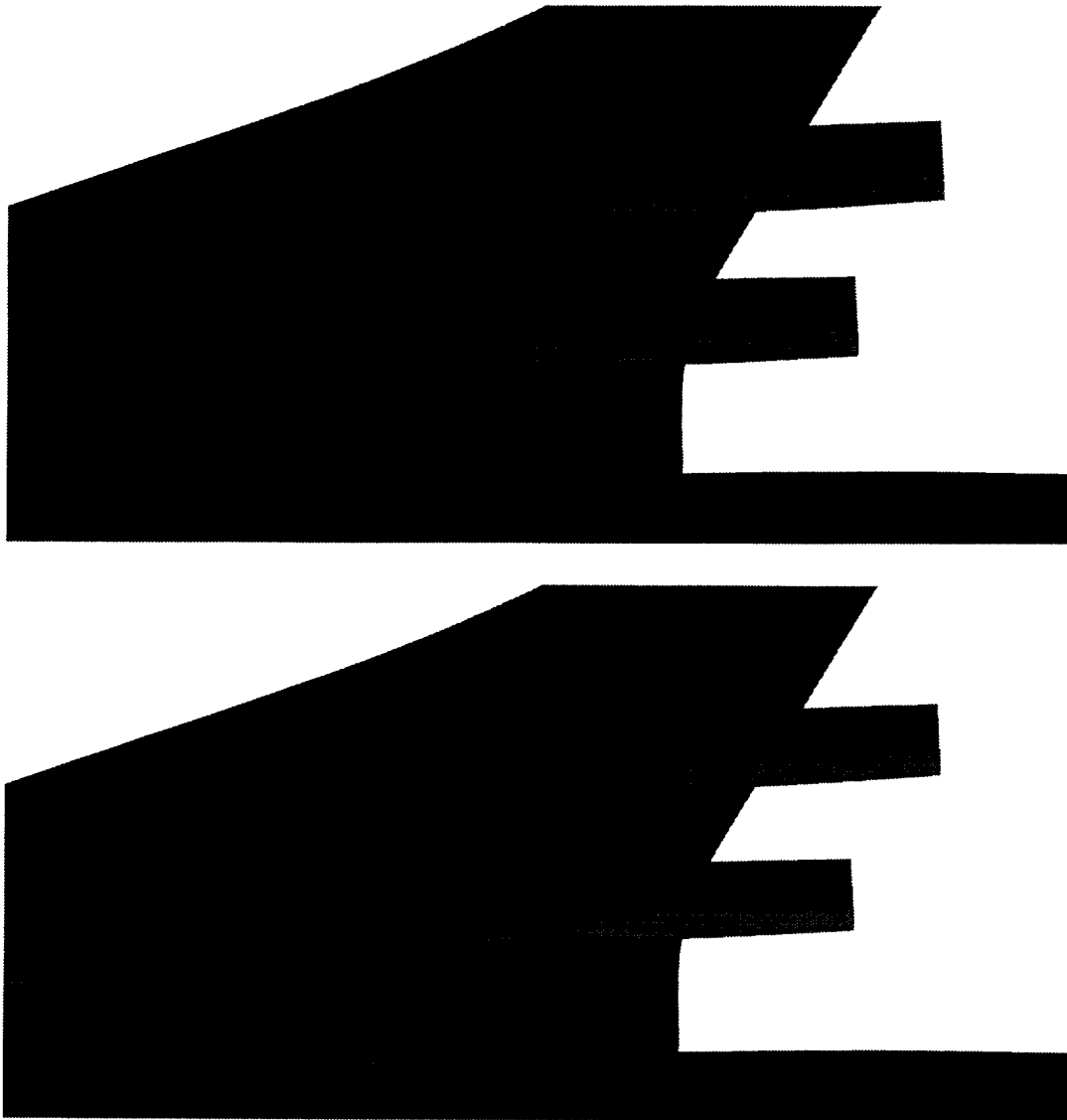
The Mach number contours shown above indicate a diverter shock, as indicated by the concentration of contours near the diverter leading edge that gets relieved along the nacelles. As seen from the transparent wing lower surface contours, the inboard diverter shock hits the expansion region of the outboard region and a shock-expansion interaction pattern is observed in the channel region between the two diverters and on the lower surface of the wing.

Pressure Drag Contours for the M2.4-7A Opt5 Wing/Body/Nacelle/Diverter
Nacelles in Aft Position with Original Diverters, CFL3D Euler, $M_\infty = 2.4$, $\alpha = 1.9^\circ$



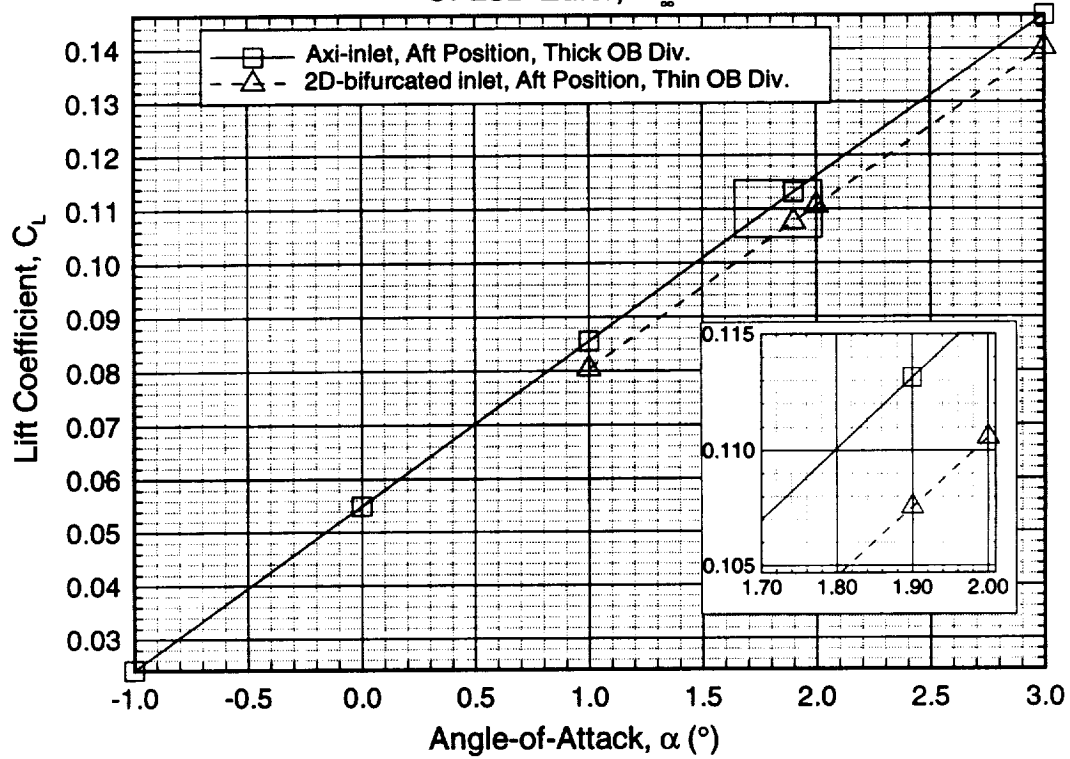
This picture shows the pressure drag contours obtained from the CFL3D Euler solution for the Opt5 wing/body/nacelle/diverter configuration with axisymmetric inlet nacelles in the aft location. The four views shown in the picture need some explanation. The top left picture is the pilot's left side view and the top right is the wingman's view while the bottom two figures show the views from the rear of the aircraft looking towards and away from the fuselage to observe the outboard and inboard sides of the nacelles, respectively. Similar views will be shown later for other configurations to compare the drag contours of different inlet and nacelle modifications. As expected, the results show that the diverter leading-edge region experiences significant amount of drag due to the high pressure acting on a forward facing surface. Also, the outboard side of the outboard diverter top experiences similar levels of drag. This is due to very high expansion in that neighborhood. Additional points will be discussed when these drag contours are compared with those for the 2-D inlet nacelle geometry.

Installed Axisymmetric and 2-D Inlet Nacelles



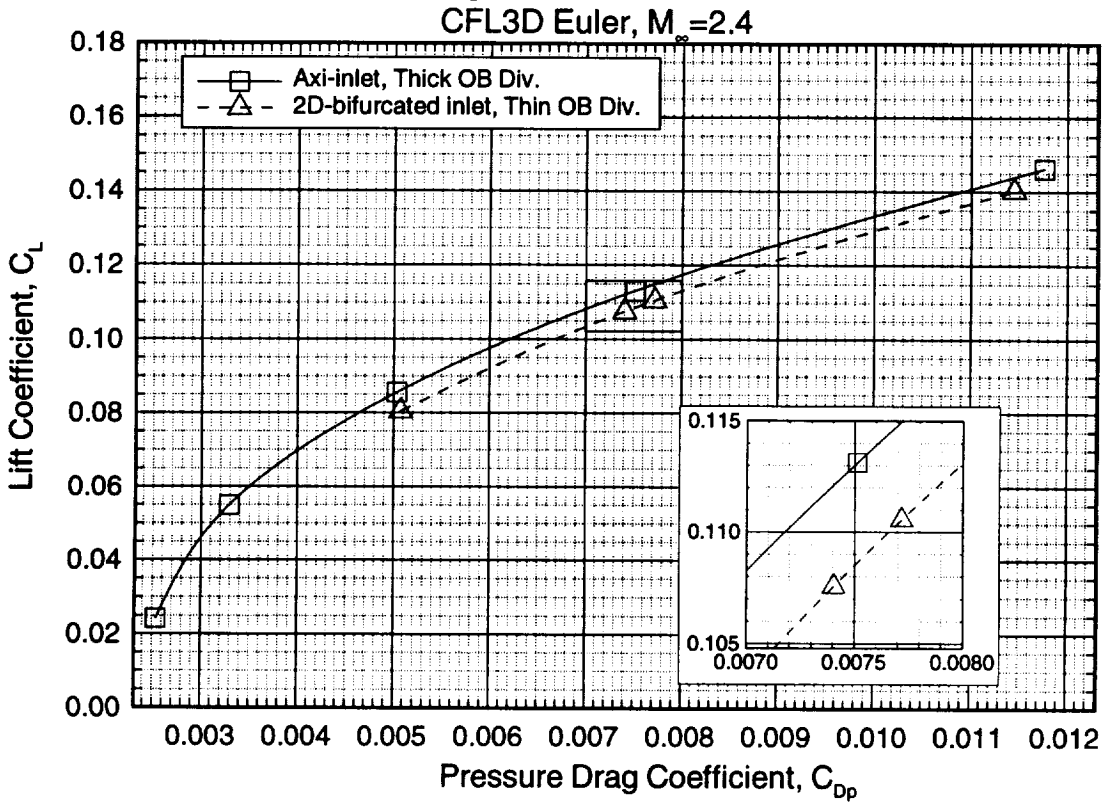
This figure compares the Opt5 wing/body/nacelle/diverter planform for axisymmetric and 2-D inlets. In both cases, nacelles are mounted in the aft location. It can be observed that the 2-D inlet is longer by about 8 feet and it extends forward.

Comparison of Lift Curves Opt5 W/B/N/D with Axisymmetric and 2-D Inlets CFL3D Euler, $M_\infty=2.4$



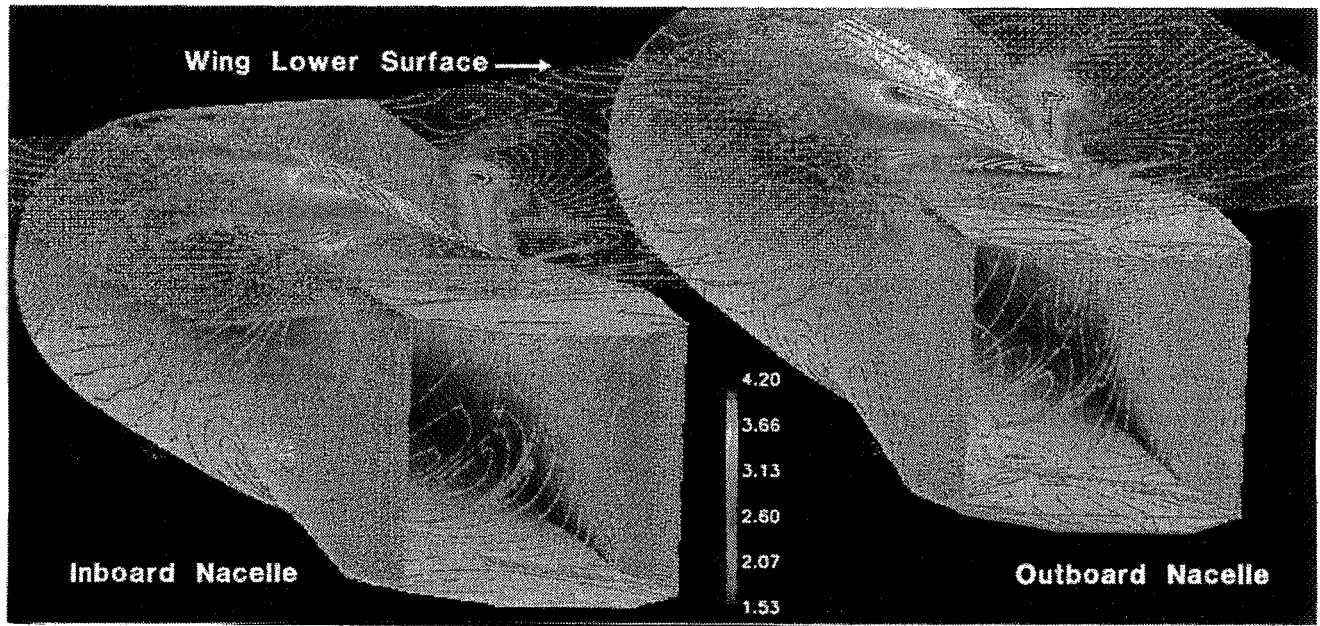
The lift curve slopes are essentially the same. The large expansion region underneath the wing shown in the Mach number contours of the 2-D inlets results in lower lift values compared to the axisymmetric inlets.

Comparison of Pressure Drag Polars Opt5 W/B/N/D with Axisymmetric and 2-D Inlets in Aft Position



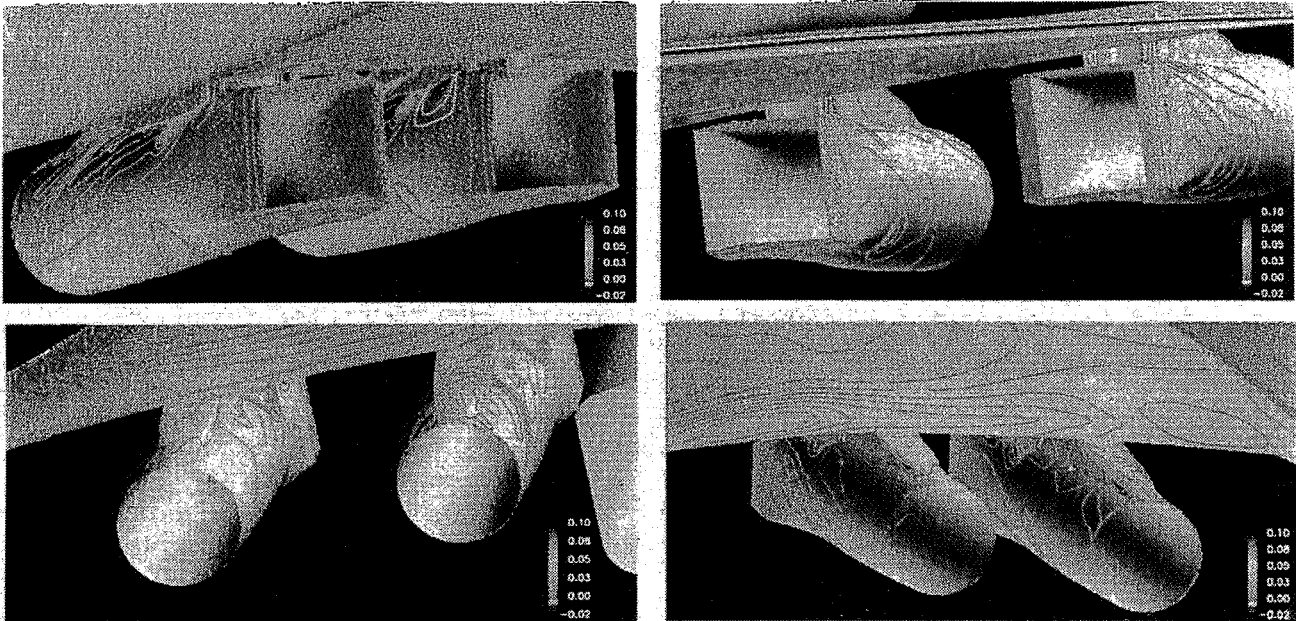
This figure compares the drag polars for Opt5 W/B/N/D configuration with axisymmetric and 2-D inlets. At the design cruise point, the drag of the 2-D inlet configuration is nearly 4.5 counts higher than that of the axisymmetric inlet. Looking at the surface pressure distributions as well as the drag contours of axisymmetric and 2-D inlet nacelles shown in the earlier charts, it can be seen that the 2-D inlet nacelle experiences more drag than the axisymmetric inlet nacelle. Note that these results correspond to the unoptimized wing/body geometry with the current nacelle position.

Mach Number Contours for the M2.4-7A Opt5 Wing/Body/Nacelle/Diverter Configuration
 Nacelles in Aft Position with 2-D Inlets , CFL3D Euler, $M_\infty = 2.4$, $\alpha = 2.0^\circ$



The Mach number contours shown above indicate the presence of a strong diverter leading-edge shock and strong expansion regions in the high curvature areas of the channel region. When comparing with the Mach number contour charts from the axisymmetric configuration, one would clearly see that the shock and expansion waves are stronger for the 2-D inlet case. It is important to note that, in spite of having the same diverter streamwise wedge angle for both axisymmetric and 2-D inlet nacelles, the diverter shock angle is stronger for the 2-D inlet case due to the reduced relieving in the channel region for the 2-D inlet nacelles compared to the axisymmetric inlet nacelles.

Pressure Drag Contours for the M2.4-7A Opt5 Wing/Body/Nacelle/Diverter Configuration, Nacelles in Aft Position with 2-D Inlets, CFL3D Euler, $M_\infty = 2.4$, $\alpha = 2.0^\circ$



The four views shown above are similar to those for the axisymmetric inlets described earlier. The pressure drag contours shown above indicate the presence of a strong diverter leading-edge shock. The upper left corner view indicates a region of strong suction in the inboard region of the outboard diverter which is due to the strong expansion observed in that region in the Mach number contours. Unlike the axisymmetric nacelles, it seems that outside the channel region, the outer portion of the nacelles experiences higher drag.

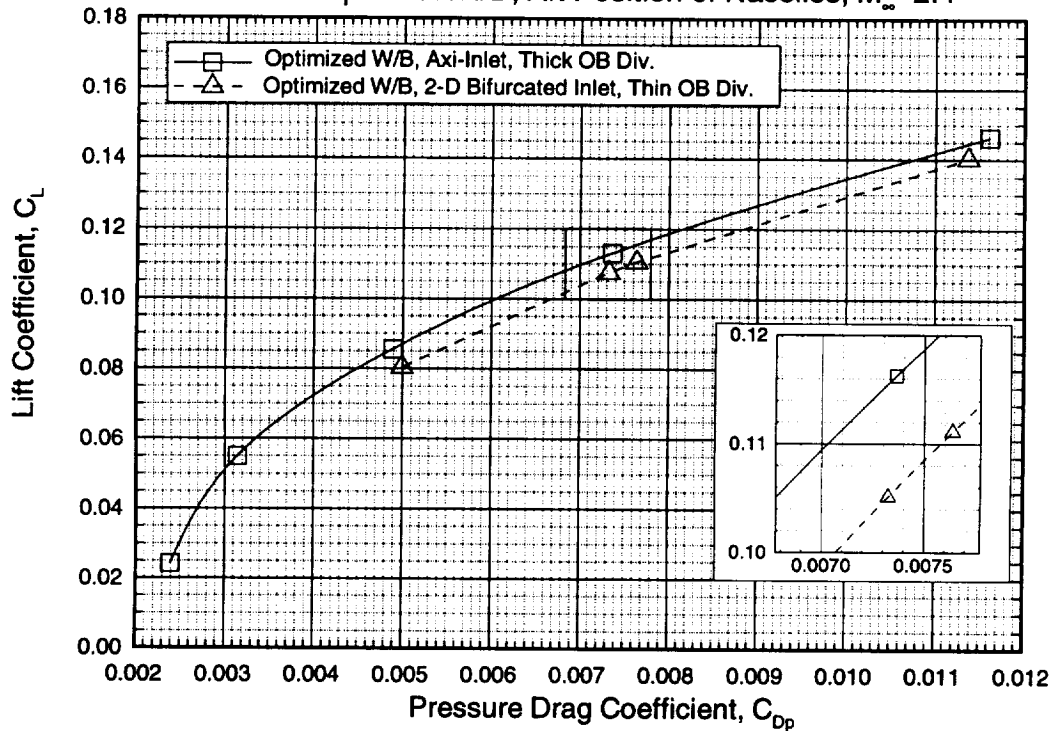
Geometry Optimization - Axisymmetric and 2-D Inlets

- FLO67/OPT67 nonlinear shape optimization code
 - Constrained optimization using ADS optimizer
- Nacelle pressure field applied to include nacelle effects
- 53 design variables including 8 wing twist, 35 wing camber, and 9 body camber variables
- 17 constraints including C_L , C_m , cargo, break, floor, door, cabin height, etc.

Since proper PAI has a paramount effect on the effectiveness of the inlet designs, the W/B geometry needed to be optimized for optimum performance in the presence of each inlet nacelle concept. For this purpose, the FLO67/QNMDIFF optimizer that has been used to design the Opt5 configuration was chosen. The wing/body camber as well as wing twist were optimized for maximum supersonic cruise performance of the installed configurations. The constrained optimization maximized the cruise L/D for the design C_L of 0.11. The nacelle effects were imposed as nacelle pressure field effects only.

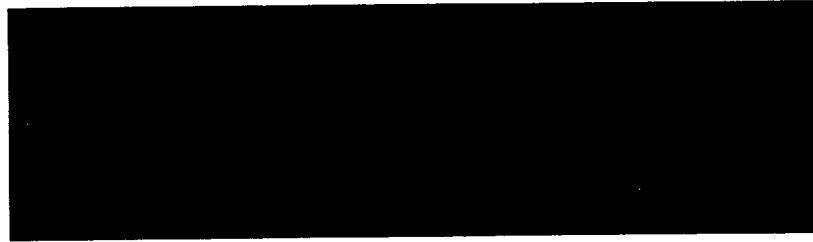
Estimated Pressure Drag Polar of Optimized Alternate Nacelle Config.

M2.4-7A Opt5 W/B/N/D, Aft Position of Nacelles, $M_\infty = 2.4$

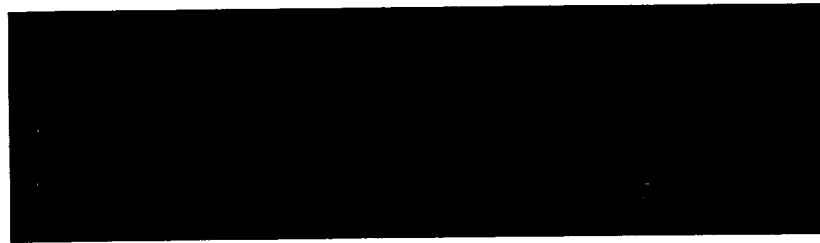


The optimization scheme described in the previous page was applied to optimize the W/B geometry for both the axisymmetric and 2-D inlet W/B/N/D configurations. The drag improvements obtained for each optimized geometry (1.5 counts for the W/B with axisymmetric inlets and 0.8 count for the W/B with 2-D inlets) was then individually subtracted from the baseline CFL3D Euler drag predictions for the two cases. This provides the estimate of the pressure drag values of the optimized W/B configurations with axisymmetric and 2-D inlet nacelles. From the figure shown above, it can be seen that the drag difference between the optimized configurations is nearly 5.2 counts. This large penalty for using the 2-D inlet instead of the axisymmetric inlet can probably be reduced by careful modification of the nacelle/diverter/wing channel geometry. Although a CFL3D analysis of the optimized geometry has not been made, the drag increment values noted here are considered reasonably accurate from our past experience.

Outboard Diverter Modification – M 2.4–7A Opt5 W/B/N/D

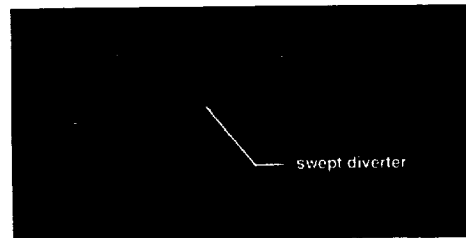
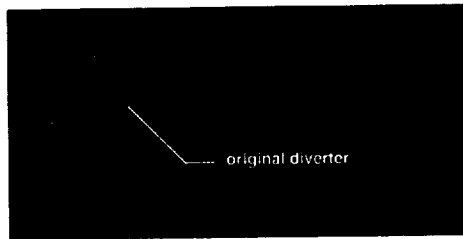


a) original diverter planform



b) modified diverter planform

Diverter Sweep Modification – M 2.4–7A Opt5 W/B/N/D

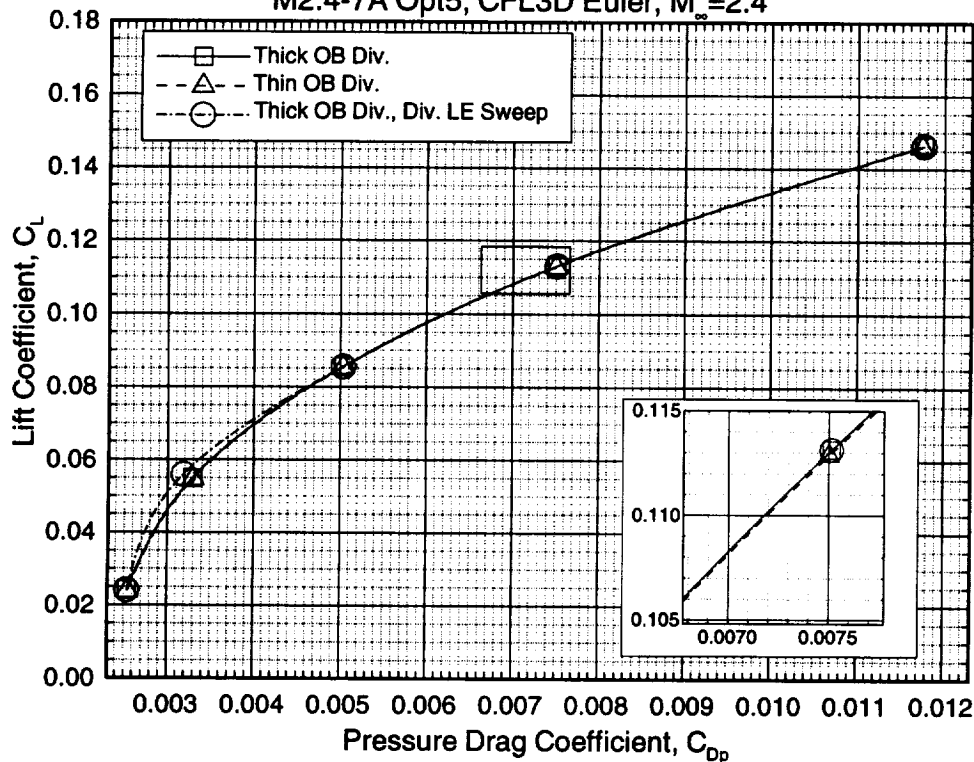


The outboard diverter for the Opt5 configuration was designed to be much thicker than the inboard diverter in order to provide a clean channel flow between the wing lower surface and the nacelles. The original outboard diverter and the 40% reduction in diverter width are shown in the planform view of the diverter in figure (a) and (b). It should be noted that the diverter wedge angle in the streamwise direction did not change significantly (~ 0.2 deg.) when compared to the original outboard diverter wedge angle. Although the channel criterion was met more easily in the aft nacelle location compared to the original nacelle position, the outboard nacelle still had to be translated down by 3.5" to avoid violation of the requirements for diverter minimum height to diverter leading–edge height ratio of 0.6.

Another nacelle/diverter modification study performed was that of changing the diverter leading–edge sweep angles of both diverters. The objective was to see if the diverter shock strength could be reduced by sweeping its leading edge. A sweep angle of approximately 45° was chosen and the grid modified in the nacelle blocks to accommodate this change. Surface grids for the original and swept diverters are shown in the figure above.

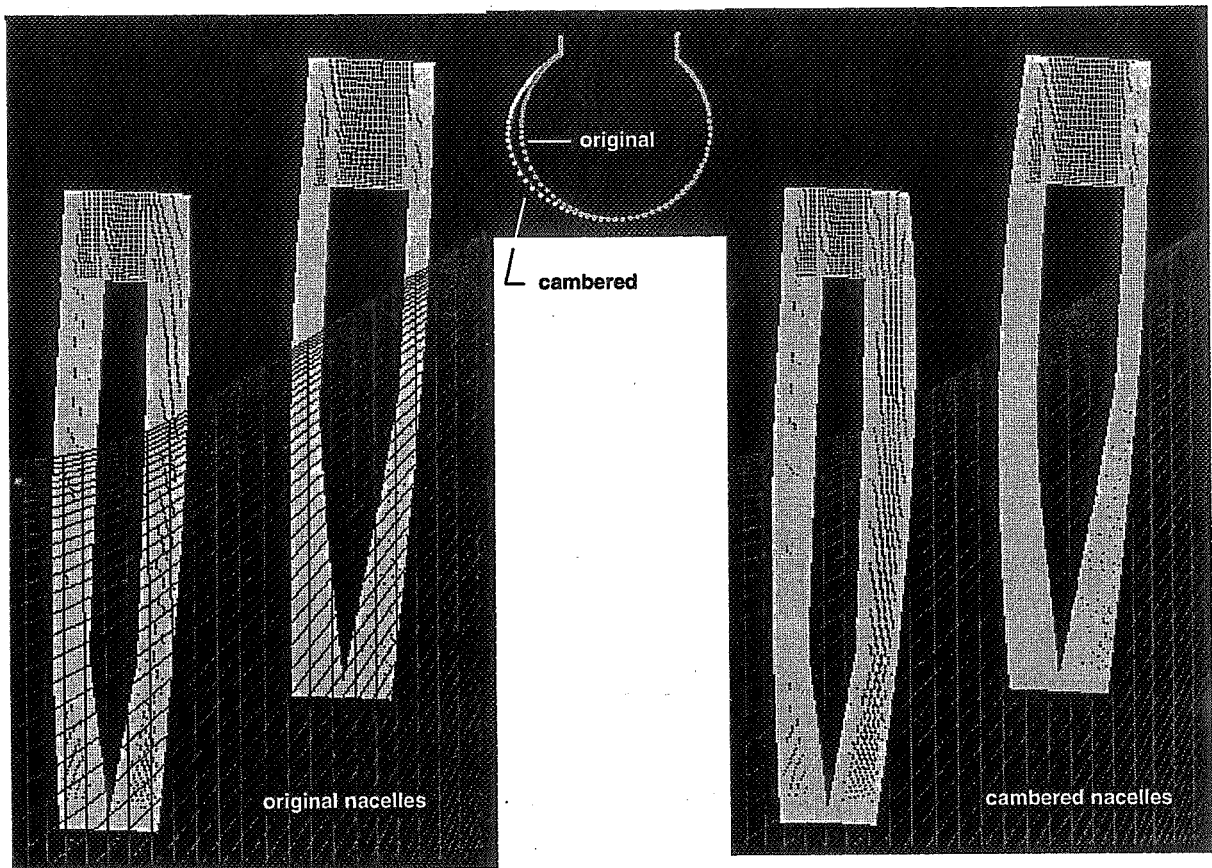
Pressure Drag Polars for Diverter Thickness and Sweep Effects Axi-Inlet, Axi-Nacelles, Aft Position

M2.4-7A Opt5, CFL3D Euler, $M_\infty=2.4$



This figure shows the effects of diverter thickness and diverter sweep on the drag polar. The drag and lift for the original and modified outboard diverters are essentially the same. Since the diverter wedge angle was kept the same in the streamwise direction, it is expected that there would not be a significant change in the diverter shock strength. The change in volume due to the thinner diverter is nearly compensated by the increase in its height. Comparing the original and swept diverters, no significant changes in drag or lift are seen near the cruise point ($C_L=0.11$).

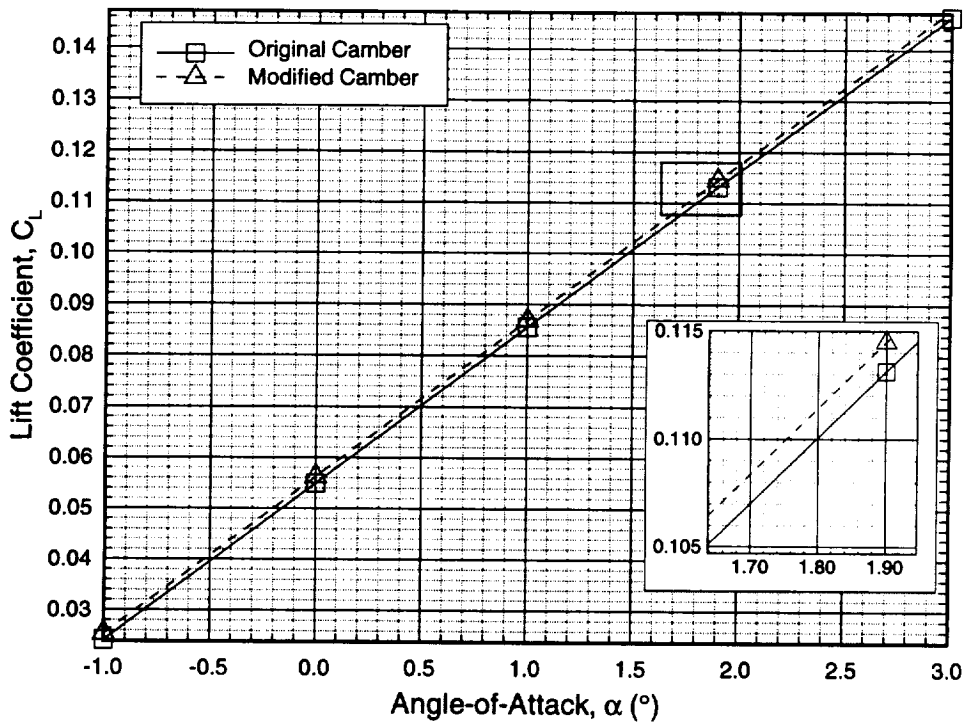
Nacelle Camber Modification – M2.4-7A Opt5 W/B/N/D



An important PAI parameter is the nacelle camber. The motivation for cambering the nacelles is to achieve a more favorable interference between the nacelle and the wing (cambering in side view) as well as between the two nacelles (cambering in planform). In the present nacelle camber investigation, only cambering of the nacelles in planform was studied. As a first attempt, an arbitrary manual cambering of the nacelles was applied on the outboard side of the inboard nacelle as well as the inboard side of the outboard nacelle to achieve favorable interference between the two nacelles. The figure above shows the details of the region and the extent of the nacelle camber studied. The camber study was performed on the Opt5 W/B/N/D with nacelles in the aft location.

Nacelle Camber Effects on Lift Curve

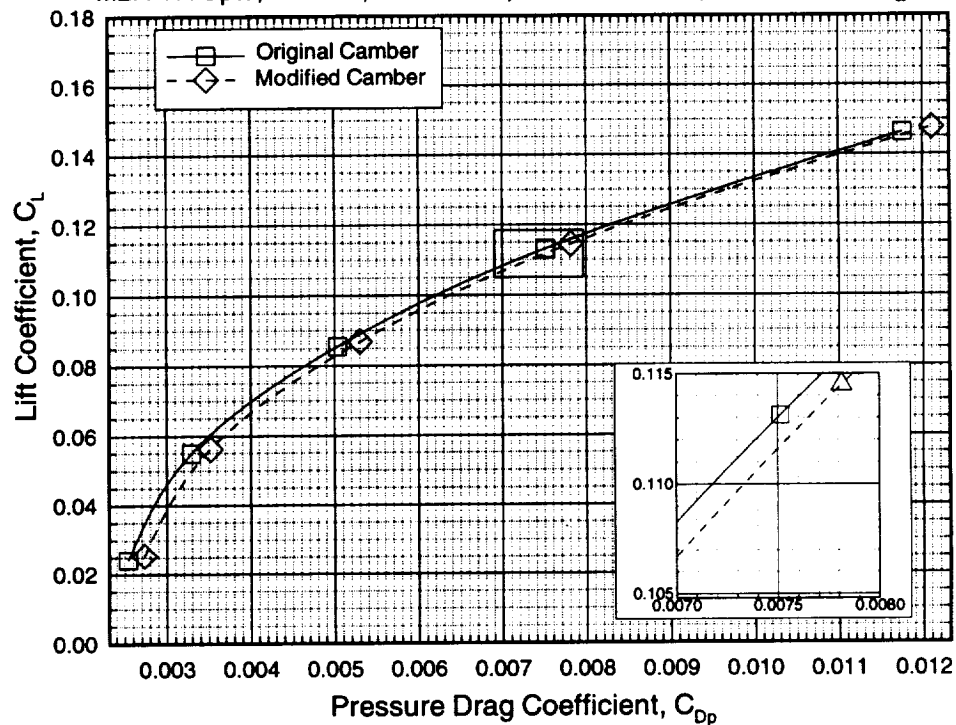
M2.4-7A Opt5, Axi-inlet, Aft Position, Thick OB Diverter, CFL3D Euler, $M_\infty=2.4$



This figure shows the lift curve for the original and cambered nacelles. There is a slight increase in lift due to the nacelle camber. This is due to the increased pressure on the cambered nacelles, as seen in the surface pressure distribution shown in the previous figure.

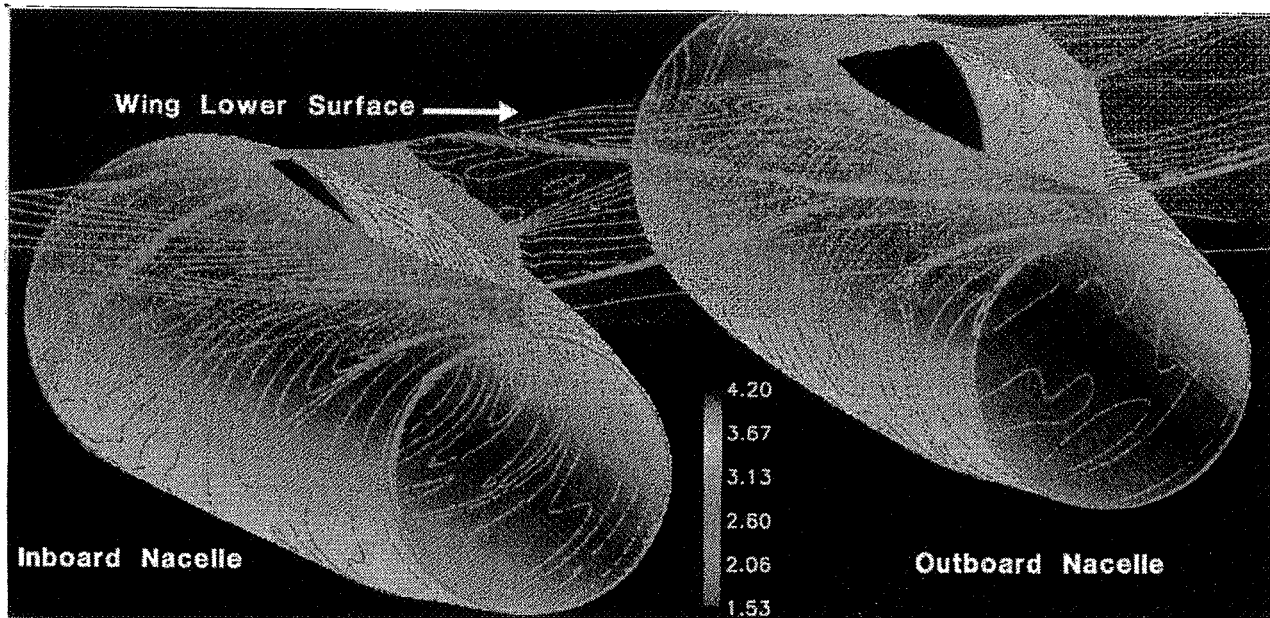
Nacelle Camber Effects on Pressure Drag Polar

M2.4-7A Opt5, Axi-inlet, Aft Position, Thick OB Divter, CFL3D Euler, $M_\infty=2.4$



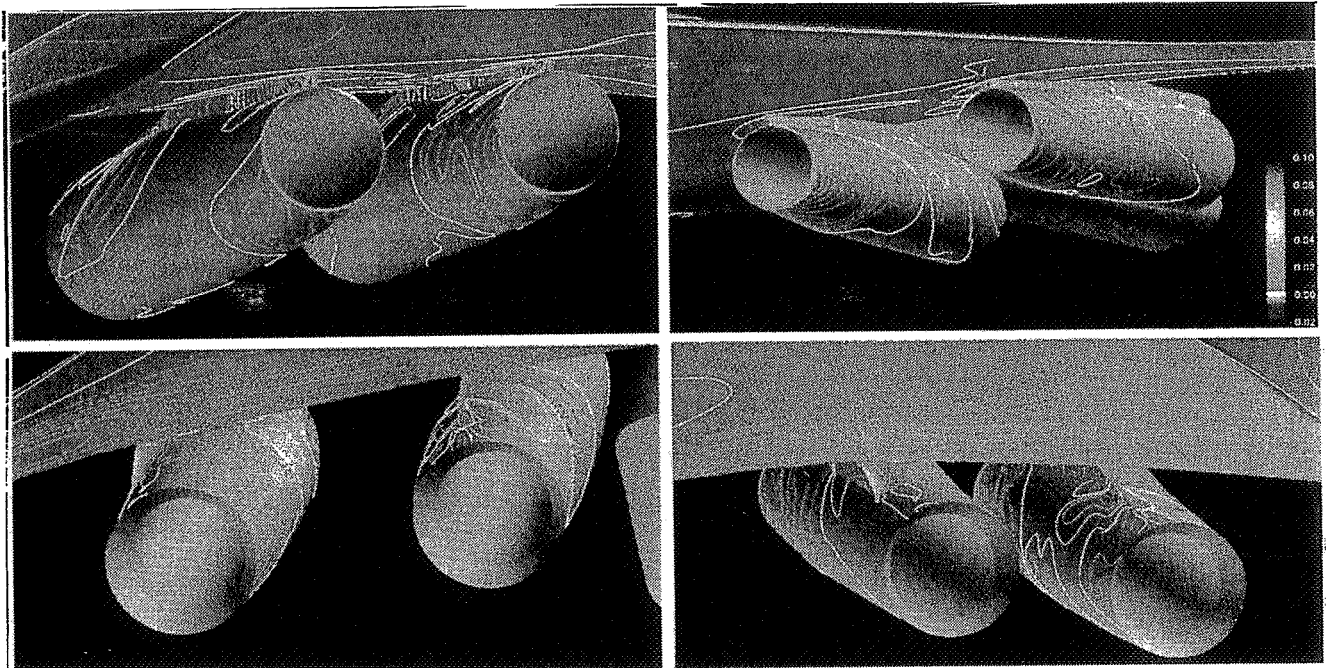
Drag polar for the case where both the inboard and outboard nacelles were cambered is compared with the polar for the original Opt5 nacelles. The increase in drag for the configuration with both inner and outer nacelles cambered is approximately 1.6 counts at the cruise $C_L = 0.11$. Examination of isolated drag changes for wing/fuselage and for each of the nacelles indicates that component drag was negligibly reduced for the wing/fuselage (~ 0.05 counts), and increased for both the inboard (~ 1.3 count), and outboard (~ 1.8 count) nacelles. The higher outboard nacelle drag is evident from the nacelle pressure distribution plots shown earlier. From a detailed analysis, it is determined that the diverter shock interference is much more drastic and results a significant increase in drag.

Mach Number Contours for the M2.4-7A Opt5 Wing/Body/Nacelle/Diverter Configuration, Nacelles in Aft Position with Both Nacelles Cambered, CFL3D Euler, $M_\infty = 2.4$, $\alpha = 1.9^\circ$



The same comments as for the axisymmetric nacelles at the aft position would apply here. However, a dark spot that is not present with the original nacelles in the aft position, is observed here on the front part of the outboard nacelle. This is one reason why the drag is increased with the modified camber.

Pressure Drag Contours for the M2.4-7A Opt5 Wing/Body/Nacelle/Diverter Configuration with Nacelles in Aft Position Both Nacelles Cambered
 CFL3D Euler, $M_\infty = 2.4$, $\alpha = 1.9^\circ$



The same description given earlier for visualizing the drag contours of the original nacelles applies here. Looking at the drag contours shown above and comparing it with the drag contours for the aft nacelle position without nacelle camber shown earlier, it can be seen that both the upper two views of this figure show smaller regions of thrusting effect as observed by the smaller regions of area contained in the white lines. As in the Mach contour plot, near the front portion of the nacelles, less suction is observed compared to the case with uncambered nacelles. For the cambered nacelles, the inboard side forward region of the outboard nacelle and the outboard side aft region of the inboard nacelle experience higher drag compared to the original nacelles.

Summary

- An aerodynamic assessment of axisymmetric and 2-D inlets was made using CFL3D Euler solutions
- 2-D inlets added nearly 4.5 counts more pressure drag than the axisymmetric inlets
- Wing/body optimization for the two inlet concepts resulted in 5.2 counts more pressure drag for 2-D inlets than the axisymmetric inlets
- Changes in nacelle location, diverter width, and diverter leading-edge sweep had only small effect on lift and drag for Opt5
- Nacelle cambering in planform increased lift; however, the drag penalty due to this cambering was large

The aerodynamic assessment of the optimized W/B with axisymmetric and 2-D inlet nacelles showed that the 2-D inlets produced about 5.2 counts more drag than the axisymmetric inlets for the M2.4-7A Opt5 wing/body/nacelle/diverter configuration. Part of this drag increment came as a result of the stronger shocks near the diverter leading edges. Also, the absence of three-dimensional relieving effect on the 2-D inlet nacelles resulted in a significant part of the drag penalty of 4.5 counts observed between the Opt5 W/B geometry with axisymmetric and 2-D inlet nacelles. For the 2-D inlet nacelles, it is shown that the channel region plays an important role on the the nacelle flow field. Care should be taken in properly designing this area.

The detailed study of the various nacelle/diverter shape and location changes showed that, except for the nacelle camber, these parameters did not significantly change the aerodynamic performance of the installation. As an important lesson of this study, it is understood that the integrated wing/body/nacelle/diverter optimizer should be capable of altering the nacelle camber in addition to the wing/body geometry. This will be pursued in our follow-on effort in this area.



High Speed Civil Transport (HSCT) Isolated Nacelle Transonic Boattail Drag Study and Results Using Computational Fluid Dynamics (CFD)

Anthony C. Midea
NASA Lewis Research Center
Cleveland, OH 44135

Thomas Austin
McDonnell Douglas Aerospace
Long Beach, CA 90807

S. Paul Pao
NASA Langley Research Center
Hampton, VA 23681

James R. DeBonis
NASA Lewis Research Center
Cleveland, OH 44135

Mori Mani
McDonnell Douglas Aerospace
St. Louis, MO 63166

Nozzle boattail drag is significant for the High Speed Civil Transport (HSCT) and can be as high as 25% of the overall propulsion system thrust at transonic conditions. Thus, nozzle boattail drag has the potential to create a thrust-drag pinch and can reduce HSCT aircraft aerodynamic efficiencies at transonic operating conditions. In order to accurately predict HSCT performance, it is imperative that nozzle boattail drag be accurately predicted.

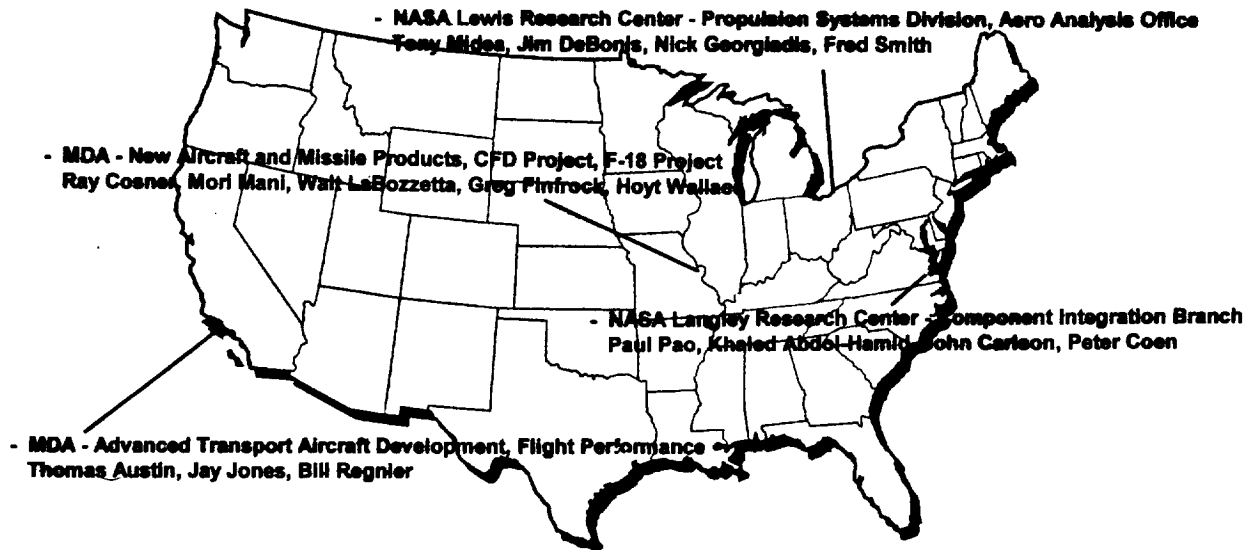
Previous methods to predict HSCT nozzle boattail drag were suspect in the transonic regime. In addition, previous prediction methods were unable to account for complex nozzle geometry and were not flexible enough for engine cycle trade studies. A computational fluid dynamics (CFD) effort was conducted by NASA and McDonnell Douglas to evaluate the magnitude and characteristics of HSCT nozzle boattail drag at transonic conditions. A team of engineers used various CFD codes and provided consistent, accurate boattail drag coefficient predictions for a family of HSCT nozzle configurations. The CFD results were incorporated into a nozzle drag database that encompassed the entire HSCT flight regime and provided the basis for an accurate and flexible prediction methodology.



Nozzle boattail drag is caused by the generation of shock wave systems and regions of boundary layer flow separation on the nozzle external boattail surfaces. The shock wave systems and flow separation are due to the effects of the local flow field over the nacelle afterbody geometric curvature, and these effects yield a peak in nozzle boattail drag coefficient at transonic conditions. For the High Speed Civil Transport (HSCT), nozzle boattail drag is significant in the transonic flight regime, and can be as high as 25% of the overall propulsion system thrust. Thus, nozzle boattail drag has the potential to create a thrust-drag pinch and can reduce HSCT aircraft aerodynamic efficiencies at transonic operating conditions (Mach 0.95 to Mach 1.1). HSCT vehicle sizing and mission performance can be significantly impacted by transonic nozzle boattail drag predictions. In order to accurately predict HSCT performance, it is imperative that nozzle boattail drag be accurately predicted.

Cooperating Teams

- o Investigation Coordinated by McDonnell Douglas (MDA)
- o Funded Internally by Four Participating Teams



- o Working Period: August 16, 1994 to March 2, 1995

Four teams of analysts were involved in the CFD study; NASA Lewis Research Center - LeRC (Propulsion Systems Division, Aerospace Analysis Office), NASA Langley Research Center - LaRC (Component Integration Branch), McDonnell Douglas Aerospace - Advanced Transport Aircraft Development (ATAD) and New Aircraft and Missile Products (NAMP). Each team participated in the study with unique flow solvers, which will be described later. In addition, all work was funded internally by each of the participating teams, respectively. The study began August 16, 1994 and was completed on March 2, 1995.

Outline

- o Background
 - o Goal/Approach
 - o AGARD Test Case
 - o Configuration Definition
 - o Grid Definition
 - o Groundrules
 - o Results
 - o Lessons Learned
 - o Summary/Conclusions
 - o Future Work
-

Background

- o **Equivalent Axisymmetric Area Method was Previous Method**
- o **Previous Boattail Drag Method Inadequate for Detailed HSR Design Studies**
- o **Based on Empirical Axisymmetric Nozzle Data**
- o **Axi Nozzle Data Updated for 2D Nozzles Using Linear Theory**
- o **Transonic Data Suspect at Large Boattail Angles Due to Boundary Layer Separation Effects**
- o **Nozzle Approximated Using Simple Geometry**
 - **3D Effects Ignored**
 - **Detailed Design Analysis Not Possible**
- o **Method Not Flexible Enough For Engine Cycle Trade Studies**
 - **Sidewalls and Radius of Curvature Not Accounted For**
- o **Dovetail Isolated CFD Study Results with Integrated Mean Slope (IMS) Database Update to Create Accurate Boattail Drag Prediction Method**

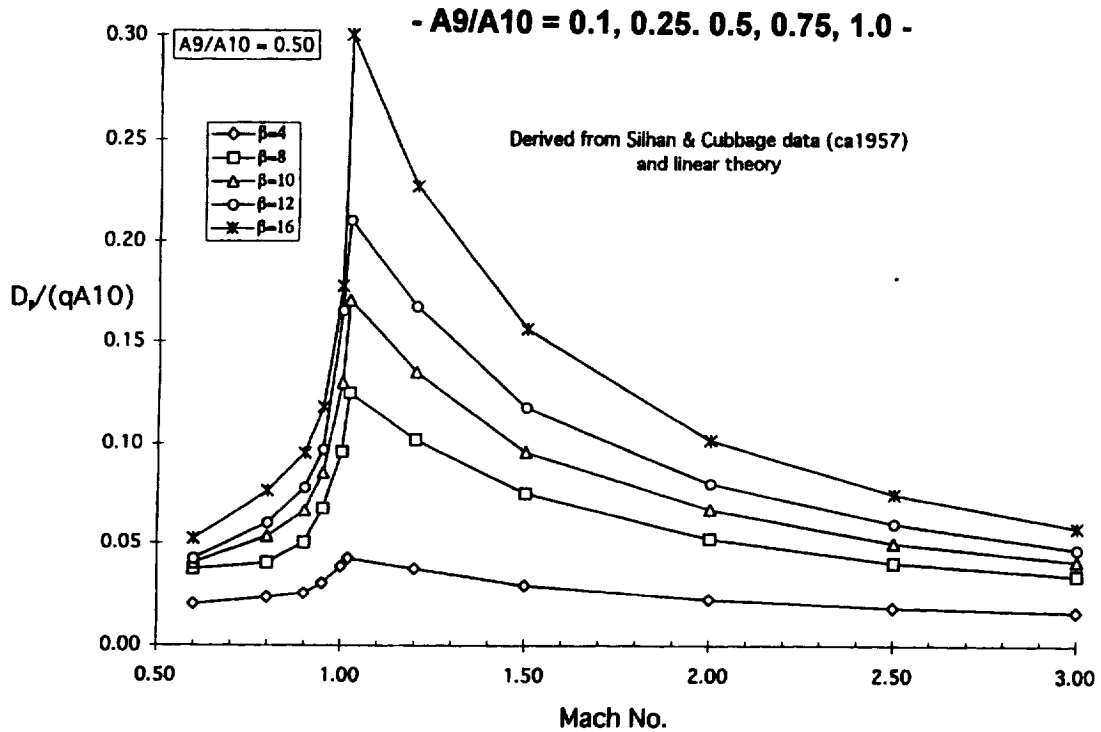
Prior to March 1995, HSCT nozzle boattail drag was predicted using an equivalent axisymmetric area method. This method was formulated by NASA and industry and assumed that nozzle geometry could be approximated with simple area ratio and length data. For axisymmetric nozzles, the method was based on an empirical axisymmetric nozzle database, (Silhan & Cabbage data).

For non-axisymmetric nozzles, the tables were updated, but the method of calculating boattail angle remained the same. In effect, the non-axisymmetric nozzle boattail angle was calculated assuming equivalent axisymmetric areas. The tables of empirical axisymmetric data were updated to represent non-axisymmetric nozzles using drag deltas between axi and non-axi nozzle types obtained from a parametric linear theory analysis. This approximation was adequate for the preliminary design phase of the HSCT project, but proved to be inadequate for detailed design studies.

Much of the HSCT propulsion system activity focused on non-axisymmetric nozzles. Detailed design studies of non-axisymmetric nozzles exposed various deficiencies with the previous boattail drag method. The original axisymmetric database yielded little transonic drag information, and the curves were approximate from Mach 0.9 to 1.1. Typically, boattail drag coefficient peaks in this Mach regime at all altitudes, thus, it was possible that the peak boattail drag coefficients and transonic drag rise characteristics were not being approximated correctly. In addition, the previous boattail drag method used a simple method to approximate nozzle geometry that ignored nozzle sidewalls, radius of curvature, 3-D effects and other detailed design characteristics.

In summary, the previous nozzle boattail drag prediction methodology for non-axisymmetric nozzles was not accurate in the transonic flight regime, and was not flexible enough to capture the effects on boattail drag due to detailed three-dimensional geometry changes. A new method was required to accurately predict boattail drag throughout the flight regime in a timely fashion. The approach taken was to employ an Integral Mean Slope (IMS) method using an upgraded nozzle boattail drag database. In addition, a concurrent activity was to be conducted employing advanced Navier-Stokes computational fluid dynamics (CFD) methods to update and substantiate the transonic portion of the updated nozzle drag database.

LeRC/PW Boattail Drag Tables Rectangular (2D) Nozzles

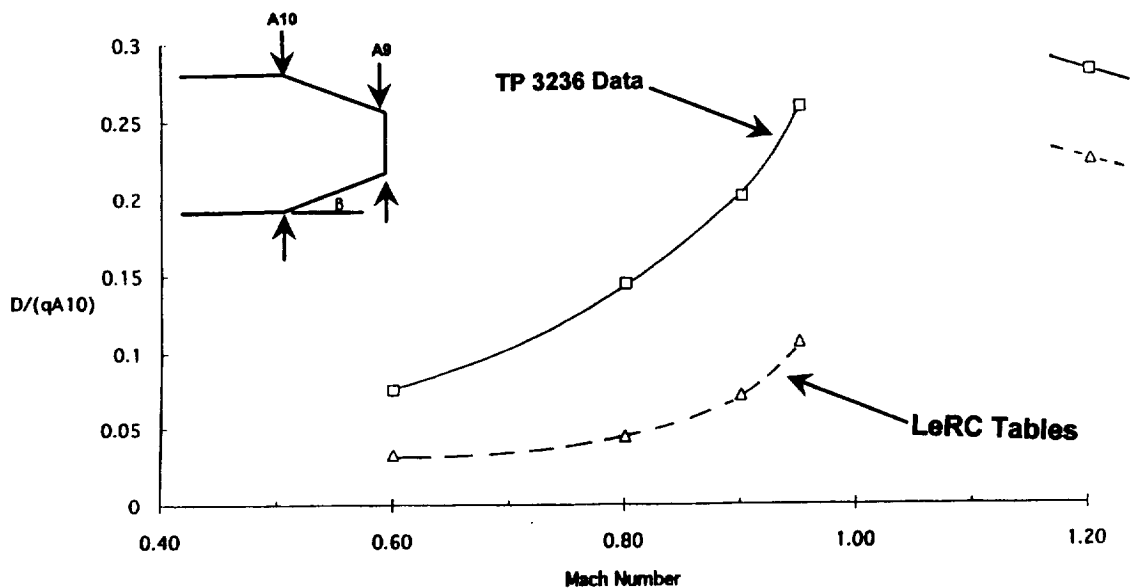


The previous method used a database based on empirical data. The empirical axisymmetric nozzle data were plotted and curve fitted to provide a continuous data set. Plots of nozzle boattail drag as a function of Mach number were made for constant area ratio with boattail flap angle as the independent variable. The boattail drag coefficient values in the database are a function of Mach number with boattail flap angle as the independent variable. The figure shows an example of one of these plots for the non-axisymmetric nozzle database with a constant nozzle area ratio (A_9/A_{10}) of 0.5. Similar plots exist for area ratios of 0.1, 0.25, 0.75 and 1.0. Nozzle height ratio was defined as the nozzle exit height (h_9) divided by the maximum nozzle external height (h_{10}), or h_9/h_{10} . Nozzle area ratio was defined as nozzle exit area (A_9) divided by maximum nozzle external area (A_{10}), or A_9/A_{10} . Boattail flap angle was calculated using A_9 , A_{10} and the divergent flap external length between A_9 and A_{10} . Nozzle boattail drag was then determined using the five empirical tables and the following inputs; (Mach number, A_9/A_{10} , and β).

Background

- Previous Method Comparison to Test Data - (Transonic 2D Nozzle Drag Characteristics)

NASA LaRC TP 3236, Configuration 9, No Plume
RC/DM = 0.40, $\beta = 17.9^\circ$, $A_9/A_{10} = 0.14$
Equivalent axis $\beta_{eq} = 12.65^\circ$

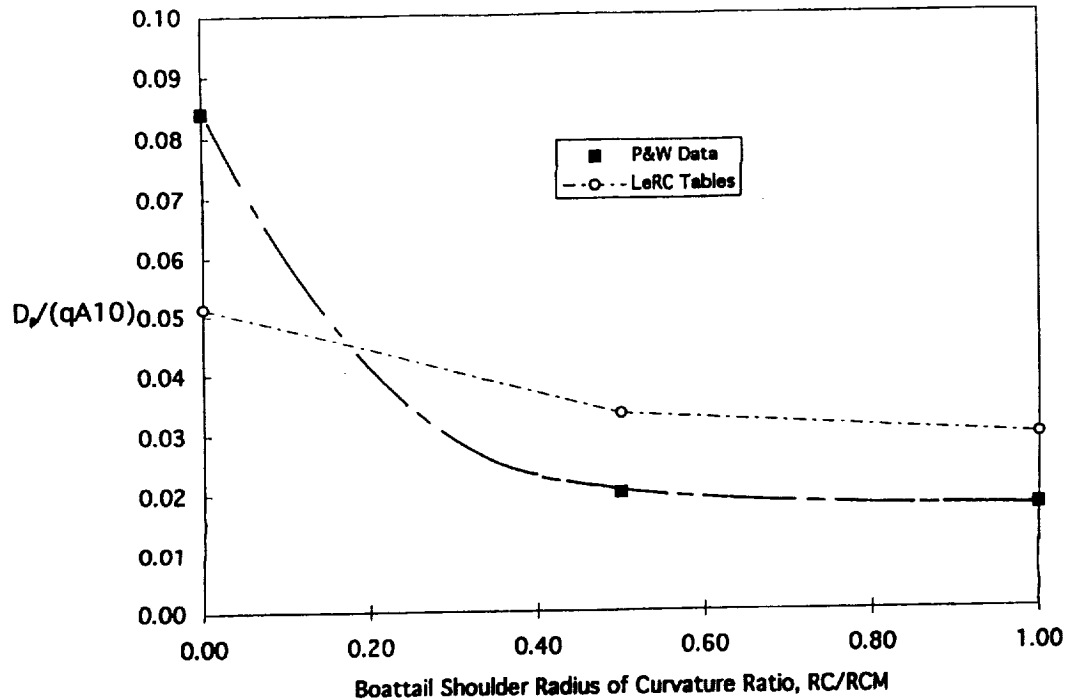


The figure shows a comparison of the previous non-axisymmetric method with experimental boattail drag data for a non-axisymmetric nozzle. The nozzle has a 17.9 degree boattail angle and an area ratio of 0.14. This comparison shows that the previous method significantly underpredicts transonic boattail drag coefficient for this specific nozzle configuration. Comparisons of various non-axisymmetric nozzles with experimental data were made using the previous method, and the results were consistent with the trends shown in this figure.

Comparison of Nozzle Drag Data w/Previous Method

- 2D Nozzle, $A_9/A_{10}=0.25$, $\beta = 16$ deg -

$M = 0.9$



This figure shows a comparison between the previous non-axisymmetric method with experimental boattail drag data for a non-axisymmetric nozzle. This comparison shows that the previous method cannot accurately approximate nozzle boattail drag trends due to detailed design geometry changes, such as changes in nozzle radius of curvature ratio (RC/RCM). Nozzle radius of curvature ratio is essentially a measure of the smoothness of the area distribution of the nozzle. A RC/RCM=0.0 indicates a nozzle with a sharp angle at the boattail flap hinge line. A RC/RCM=1.0 indicates a nozzle with no discontinuities in the area distribution from the nozzle maximum area to the nozzle exit. Because of its inability to characterize detailed nozzle geometry changes, the previous method was not flexible enough to conduct engine cycle and nozzle trade studies that are required to differentiate between detailed designs and perform component downselect activities.

Goal/Approach

- o **Goal: Develop Accurate Method to Provide Timely Boattail Drag Calculations for 2D M/E HSCT Nozzles by March 1995 (Nozzle Downselect Studies)**
- o **Impetus:**
 - **HSCT Nozzle Boattail Drag as High as 25% of Transonic Thrust**
 - **HSCT Nozzles Complex 3D Configuration**
 - **Limited Data Available for Non-axisymmetric Nozzles**
- o **Approach**
 - **Employ Advanced N-S CFD Methods to Update/Substantiate Database**
 - **Update MDA IMS Database Using CFD Results and Non-axi Nozzle Data**
 - **Analyze Interference Effects of Installed Nozzles/Nacelle (Phase II)**

Based on previous experience, transonic nozzle drag data would be difficult to obtain. The approach taken to achieve the above goal was to employ advanced Navier-Stokes computational fluid dynamics (CFD) methods to obtain accurate and reliable transonic nozzle drag coefficient data. In addition, a concurrent activity was initiated to implement an Integral Mean Slope (IMS) method using an updated nozzle boattail drag coefficient database to predict boattail drag. The IMS method is widely used and offers a detailed representation of the nozzle geometry in a timely fashion. The nozzle boattail drag database was to be updated using all known wind tunnel and flight test nozzle data for HSCT type nozzles. The transonic CFD boattail drag coefficient predictions were to be used to update and substantiate the IMS transonic nozzle boattail drag coefficient database. The new method was required in March 1995 for use in the nozzle downselect studies.

IMS Update Study Approach

- o Update IMS Database (MDA-NAMP w/MDA-ATAD IRAD)**
- o Base Update on Isolated Nozzles**
 - Applicable to Low Interference Nacelles**
 - Applicable for Sharp-Cornered to Full Radius Boattail Shoulders**
- o Updated IMS Results Presented to HSR Community on 1 March 1995**
- o CFD Results to Substantiate IMS Update**

The IMS database update activity was performance by MDA with internal funding. The update was based on isolated non-axisymmetric nozzles, and was applicable for low interference nacelles, and for a full range of radius of curvature ratios. The updated IMS results were presented to the HSR community in March 1995.

CFD Study Approach

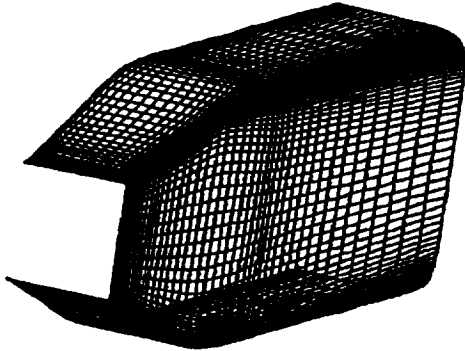
- o **Validate All Codes by Comparison with AGARD 17 Axi and 2D Nozzle Test Performance Data (NASTD & PAB3D Previously Validated, NPARC3D Validated as Part of This Study)**
 - **NASTD (McDonnell Douglas Aerospace)**
 - **PAB3D (NASA Langley Research Center)**
 - **NPARC3D (NASA Lewis Research Center)**

- o **Generate 3D Navier-Stokes CFD Solutions of HSCT MFTF 3765-100**
 - **Parametric Study of Nozzle Boattail Flap Angle and Area Ratio**
 - **Transonic Mach Numbers (0.95, 1.1 & 1.2)**
 - **Reference Cruise Geometry at Mach 2.4**
 - **A9/A10=0.5, Boattail Flap Angle=16 deg Test Case for All Participants For HSCT Explicit Code Validation**

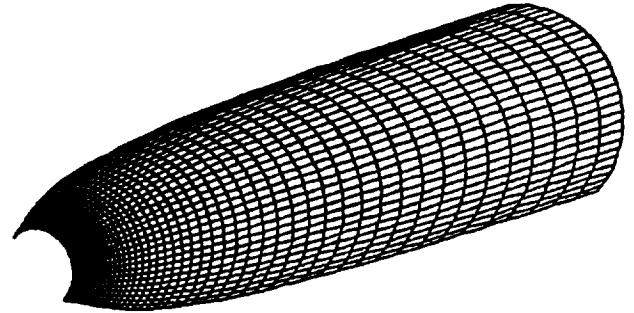
- o **Use CFD Results of Representative HSCT Nacelle Configurations to Provide Delta Cds at Transonic Conditions**

Three unique flow solvers were used in this study; NASTD (MDA), PAB3D (NASA LaRC) and NPARC (NASA LeRC). The first step in the approach was to validate these unique flow solvers for a representative configuration using well documented and tested nozzles from the Advisory Group for Aerospace Research and Development (AGARD) Working Group #17. After successful completion of this validation step, the three codes would be used to generate solutions for a series of HSCT specific nozzle configurations. A parametric study of nozzle boattail flap angles (12-20 degrees), area ratios (A9/A10=0.2-0.5), and Mach numbers (0.95-1.1) was to be conducted. The A9/A10=0.5, 16 degree boattail angle case was selected by team members to be a common case that all members would solve to provide a second validation. The final solutions to all of the configurations was then to be used to update and substantiate the IMS database.

AGARD 17 Test Case Nozzles



2D B.4 Nozzle



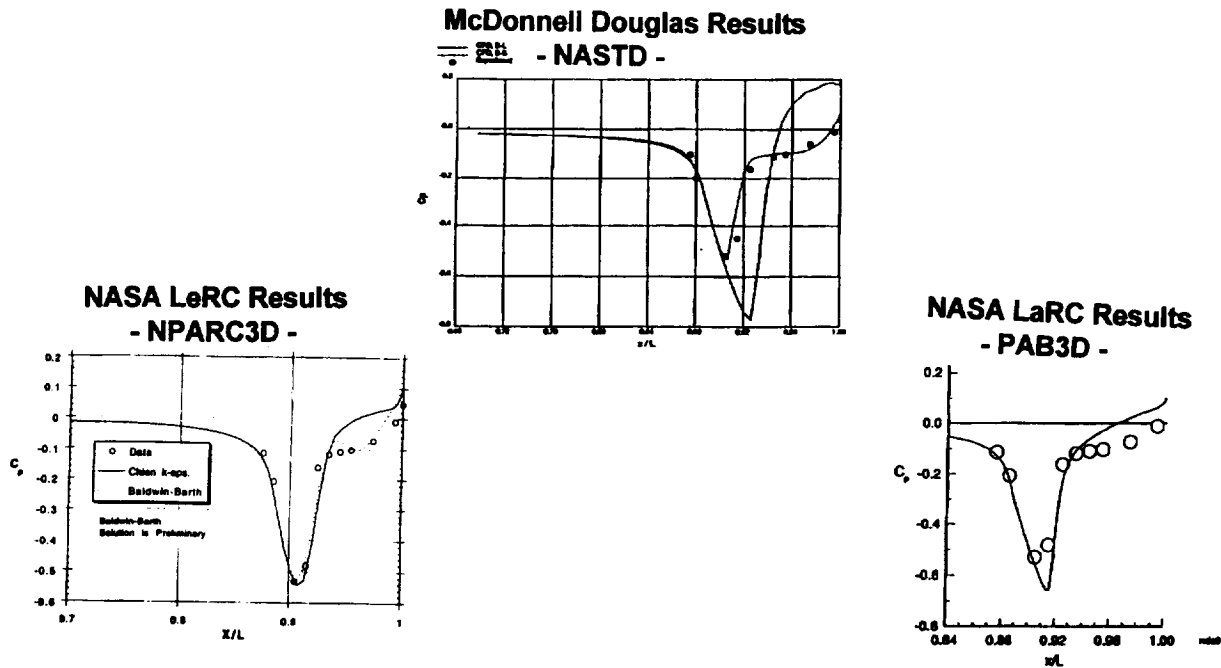
Axisymmetric B.1 Nozzle

Two of the nozzles from the AGARD Working Group #17 tests that were used for flow solver validation are shown in the figure. The B.4 nozzle is a two-dimensional nozzle without sidewalls. The B.1 nozzle is an axisymmetric nozzle. Three validation cases were executed at Mach 0.94 including; (a) axisymmetric nozzle (B.1), attached flow, (b) axisymmetric nozzle (B.1), separated flow, and (c) non-axisymmetric nozzle (B.4), separated flow. In general, the axisymmetric nozzle cases required significantly less computational resources than the non-axisymmetric case, and yielded consistent results for all of the CFD codes. While the axisymmetric cases were required for validation, the focus of this effort was placed upon the non-axisymmetric case, because this case closely resembled an HSCT type nozzle.

AGARD 17 Test Case Comparison Results

- B.4.2 2D C-D Nozzle -

Mach 0.94, NPR=4, Centerline Pressure Comparison

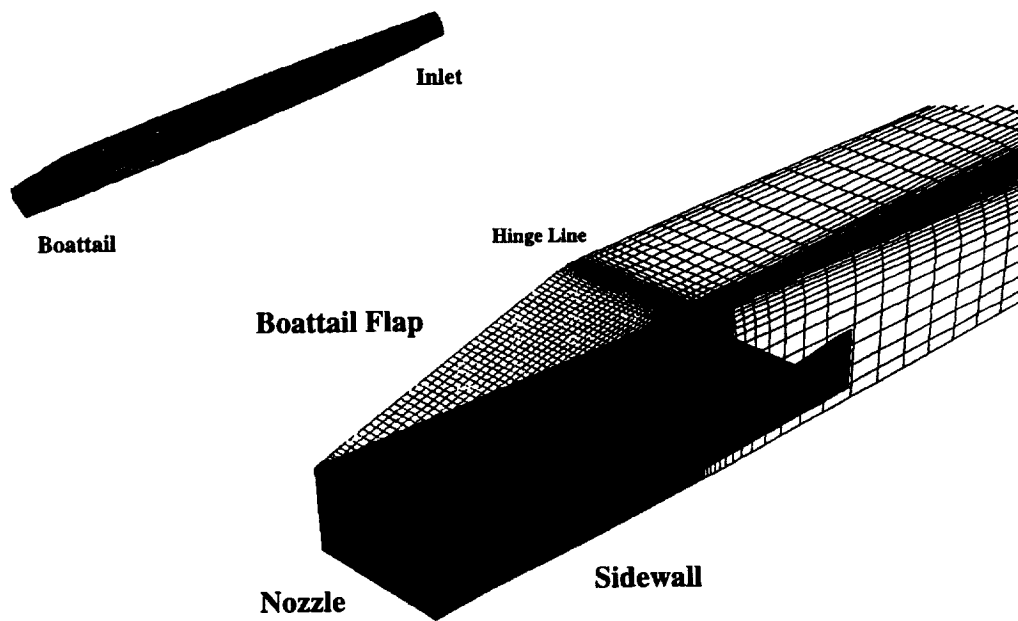


The B.4 nozzle closely approximated an HSCT type nozzle because it was a two-dimensional nozzle that experienced separated flow at transonic speeds. Although the B.4 did not have sidewalls, the nozzle still provided an opportunity to gain insight on how well the flow solvers could predict nozzle boattail pressure coefficient, and thus nozzle boattail drag.

The figure shows a comparison between nozzle B.4 centerline pressure coefficient test results and CFD predictions. Three plots are shown that graphically compare each of the three CFD codes involved in this study. The plots are set up to compare pressure coefficient as a function of non-dimensional distance (x/L) along the centerline, and the experimental results are identical for all three plots. From the NASTD plot, the conclusion can be drawn that NASTD with the Baldwin-Barth turbulence model accurately predicts the absolute values of experimental data as well as the trends with non-dimensional centerline distance. The NPARC plot using the Baldwin-Barth turbulence model also shows excellent agreement with the experimental data and closely resembles the NASTD prediction. In addition, the PAB3D plot exhibits excellent agreement with the experimental data. Note that PAB3D slightly overpredicts pressure coefficient near the trailing edge of the nozzle, and this could lead to a slight underprediction of drag coefficient for this specific case using a two equation, linear k- ϵ turbulence model.

The results of this figure, coupled with the excellent agreement between CFD and experimental results for the axisymmetric cases (not shown explicitly here), indicate that NASTD, NPARC and PAB3D are clearly capable of accurately predicting pressure coefficient distributions for HSCT type nozzles in the transonic flight regime. Thus, the CFD codes are validated with experimental pressure coefficient data. The next step was to ensure that the codes compared favorably with each other using the HSCT DSM nozzle.

Typical Isolated HSR Nacelle Configuration: Boattail Drag Study



The figure shows a typical isolated HSCT nacelle configuration used in the CFD study. The nacelle is full scale, and includes inlet, engine and nozzle components.

Configuration Definition: Inlet & Nozzle

Inlet

- o Generic Axi Inlet with Mass Flow Ratio Equal to 1.0
- o Upstream Inviscid Streamtube Modeled

Nozzle

- o Geometry Scaled to Full Scale MFTF 3765-100 Engine
- o Sidewalls Modeled
- o Corners Rounded with 8 In Radius Corner Per 3765-100 Design
- o Sharp Transition At External Flap Hinge Line (Radius of Curvature Ratio, $RC/RCM=0.0$)
- o Internal Nozzle Plenum Chamber, Throat, Diffuser and Exit Modeled
- o Internal Nozzle Angle Fixed at 1.5 deg to Maintain Constant Exit Flow Divergence Angle
- o Boattail Flap Angles (12, 16 and 20 deg) Chosen to Encompass Actual Transonic Boattail Angle = 13.68 deg
- o Nozzle Height Ratios (0.2 and 0.5) Chosen to Encompass Actual Transonic Area Ratios = 0.274 to 0.320

The inlet was modeled as a generic, axisymmetric inlet with a mass flow of 1.0 (no spillage). Also, the upstream inviscid streamtube was modeled. The nozzle geometry was based on the latest HSCT non-axisymmetric nozzle design (Downstream Mixer (DSM) mixer/ejector nozzle). The nozzle geometry was scaled to the full scale mixed flow turbofan (MFTF) size, which is described below. The nozzle sidewalls were modeled, and the corners of the nozzle were rounded with 8 inch radii to match the DSM design. The nozzle was designed with a sharp transition at the external flap hinge line, thus representing a radius of curvature ratio (RC/RCM) of zero. Internally, the nozzle plenum chamber, throat, diffuser and exit were modeled, and the nozzle was modeled with hot gas. The internal nozzle angle was fixed at 1.5 degrees to maintain constant exit flow divergence angle.

A family of nozzles was studied at three Mach numbers; $M=0.95$, 1.1 and 1.2. Various nozzle boattail angle and nozzle area ratio values were modeled to represent a wide array of nozzle configurations. Boattail angles of 12, 16 and 20 degrees were chosen to encompass the range of boattail angles expected at transonic conditions. Also, nozzle height ratios of 0.2 and 0.5 were chosen to encompass the range of area ratios expected at transonic conditions. The height ratios correspond to area ratios of 0.187 and 0.467, respectively, which were rounded to 0.2 and 0.5, respectively, for convenience. The matrix of nozzle configurations studied is described later.

Configuration Definition: Engine Cycle

- o **3765-100 Best Represented HSCT Cycle at Time of Study**
 - **Mixed Flow Turbofan Designed by PW/GE**
 - **Demonstrated Feasible HSCT Aircraft Performance**
 - **BPR = 0.622 (sea level static)**

- o **Datapak A8, PT8, and TT8 Used to Define Plenum Conditions For Internal Nozzle Flow Modelling**

At the time of this study, the 3765-100 MFTF was the leading engine cycle candidate. This cycle is a mixed flow turbofan, designed by Pratt & Whitney and General Electric, and has a fan pressure ratio of 3.7, and airflow lapse rate of 65% and requires 900 lb/s of corrected airflow at sea level static conditions. The airflow lapse rate is simply the percentage of cycle flow at cruise versus takeoff conditions. For this cycle, the cycle required airflow at cruise is 65% of the required takeoff airflow. This cycle has a bypass ratio of 0.622, and has demonstrated feasible HSCT aircraft performance. Area and pressure data were obtained from the engine company datapack to define the nozzle plenum conditions; (throat area, pressure and temperature). Therefore, the hot gas flow should closely approximate the actual 3765 MFTF cycle installed with a DSM type nozzle.

Configuration Definition: Nacelle

- o Full Scale Nacelle Based on PW/GE 3765-100 MFTF Design**
- o Isolated Nacelle Modeled**
- o Wing Installation Effects Not Modeled**
- o One-Quarter of Nacelle Modeled**
 - Assumed Horizontal and Vertical Streamwise Symmetry**
 - Reduced Computational Resources**
- o Forebody Nacelle Geometry Identical to Actual 3765-100 MFTF**

The inlet, engine cycle and nozzle components were integrated, and a nacelle shape was chosen. The nacelle shape is axisymmetric at the inlet cowl lip, and continuously transitions from axisymmetric to non-axisymmetric ending at a non-axisymmetric (2D) shape at the external flap hinge line. From the hinge line aft to the nozzle exit, the nozzle is entirely non-axisymmetric. The nacelle was modeled as full scale and was based on the 3765-100 airflow requirements. This study only examined the isolated nacelle, and did not explore the effects of integrating the nacelle with a wing. Therefore, wing effects were not modeled. One-quarter of the nacelle was actually modeled with CFD grid, and horizontal and vertical streamwise symmetry were assumed. This saves considerable computational resources with no loss in accuracy of results.

CONFIGURATION RUN MATRIX

Configuration	A_9/A_{10}	Boattail	M_∞	Team
N0010	1.0	0°	0.95, 1.10, 1.20	NASA Langley
N1202	0.2	12°	0.95, 1.10, 1.20	NASA Lewis
N2002	0.2	20°	0.95, 1.10, 1.20	NASA Langley
N1205	0.5	12°	0.95, 1.10, 1.20	MDA-ATAD
N1605	0.5	16°	0.95, 1.10, 1.20	MDA-ATAD MDA-NAMP NASA Langley NASA Lewis
N2005	0.5	20°	0.95, 1.10, 1.20	MDA-NAMP

The configuration run matrix is shown in the figure. The N1605 configuration was the baseline configuration that was studied by all four teams. The 16 in the configuration designation represents the boattail angle in degrees, and the 05 represents an area ratio of 0.5. Each team was responsible for the N1605 configuration and one other configuration. Because each configuration was to be run at three Mach numbers (0.95, 1.1 and 1.2), this represented a total of 6 CFD runs per team member. NASA LaRC was also responsible for the N0010 configuration, which contributed three additional CFD runs and were critical for the purposes of this study. The N0010 configuration represents a nozzle with zero boattail angle, and an area ratio of 1.0. In this study, only the drag due to the nozzle is of interest, thus, the drag of the N0010 nacelle must be subtracted from the drag of all the other CFD runs (at the respective Mach number) to obtain the nozzle specific drag at any given condition.

NACELLE CONFIGURATIONS

CASE	M_∞	A_8/A_9	A_9/A_{10}	Boattail Angle	Equivalent Boattail Angle	Boattail Flap Length
N0010	0.95	0.709	1.0	0°	0.00°	174.4 in.
	1.10	0.651				
	1.20	0.606				
N1202	0.95	0.709	0.2	12°	8.82°	174.4 in.
	1.10	0.651				
	1.20	0.606				
N2002	0.95	0.709	0.2	20°	14.46°	107.1 in.
	1.10	0.651				
	1.20	0.606				
N1205	0.95	0.709	0.5	12°	7.60°	107.0 in.
	1.10	0.651				
	1.20	0.606				
N1605	0.95	0.709	0.5	16°	9.94°	82.0 in.
	1.10	0.651				
	1.20	0.606				
N2005	0.95	0.709	0.5	20°	12.51°	65.3 in.
	1.10	0.651				
	1.20	0.606				

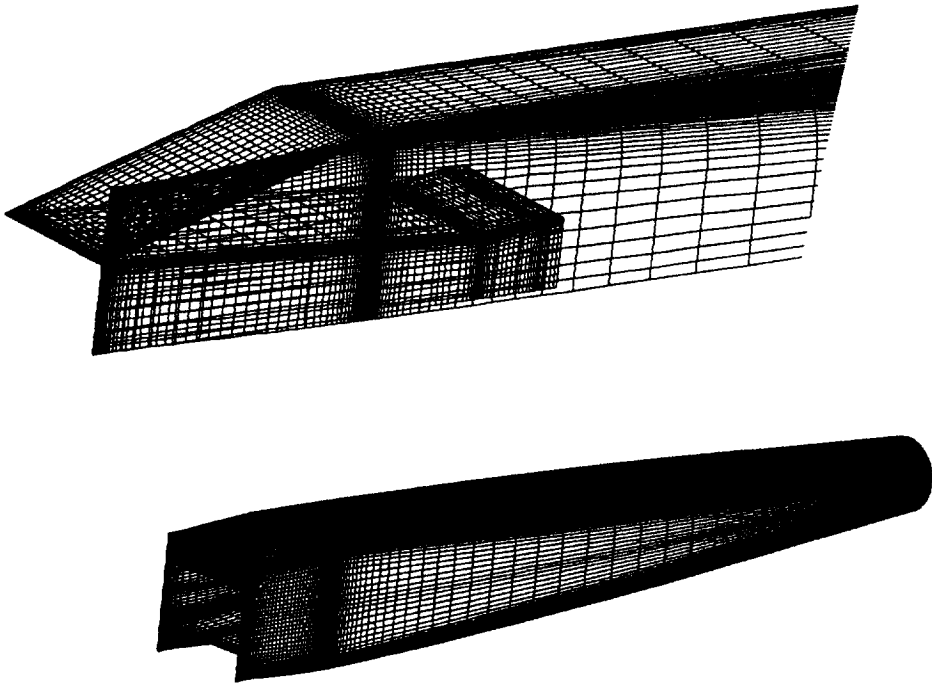
Additional detailed nacelle information is presented in the figure. The nozzle throat to exit area ratio (A_8/A_9), boattail angle, equivalent boattail angle, and flap length are given. The equivalent boattail angle is the equivalent axisymmetric nozzle boattail angle, and is defined by the nozzle area ratio and boattail flap length.

CFD Grid Definition

- o **MDA Defined Grid Topologies and Generated Initial Grids**
- o **NASA LaRC Optimized the Final Surface and Volume Grids**
- o **3D, Structured, Patched, Viscous, Multi-Block CFD Grids**
- o **External and Internal Surfaces Modeled as Viscous Surfaces**
- o **Viscous Grid Generated to Model Free Shear Layers in Nozzle Exhaust**
- o **Nozzle Sidewall Trailing Edge Modeled with Zero Thickness**
- o **All Zones Point-Matched Except for Upstream and Far-Field Zones**
- o **Nozzle Plenum Chamber Configuration Based on AGARD B.4 Config**
- o **Approx. 1.5 Million Grid Points Per Configuration**

All grid topologies and initial grids were defined by MDA for this study. NASA LaRC optimized the final surface and volume grids for use by all teams. The grids were 3D, structured, patched, viscous, multi-block grids. The external and internal surfaces were modeled as viscous surfaces, and a viscous grid was generated to model free shear layers in the nozzle exhaust. The nozzle sidewall trailing edge was modeled with zero thickness, and the sidewalls ended at the trailing edge of the external flaps. All zones were point matched except for upstream and far-field zones. The nozzle plenum chamber configuration was based on the AGARD non-axisymmetric nozzle configuration. A total of approximately 1.5 million grid points were used for each individual configuration. A non-dimensional viscous height of $y^+ = 2$ was employed to define the first grid cell spacing off the viscous surfaces.

Nacelle CFD Grid



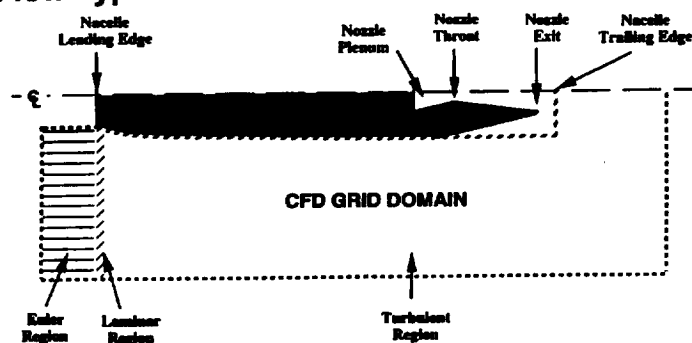
This figure shows a typical nacelle grid for a full nacelle and a side view of a representative quarter nacelle complete with the internal and external nozzle characteristics.

Groundrules

- o **CFD Convergence Criteria**
 - Converged Boattail Pressure Drag Force Levels
 - Converged Internal Nozzle Massflow Rate Levels
 - Reduction of L2 Residuals in Boattail Region by 3 Orders of Mag

- o **Boattail Drag Computations**
 - Pressure Drag on Boattail Defined as the Integration of $(P - P_{inf})$ Over Respective Nacelle Surfaces
 - Skin Friction Drag Not Computed
 - Delta Drag Coefficient Computed Using Nacelle Reference Config (Cruise Configuration)

- o **CFD Flow Type Definition**



The CFD convergence criteria were as follows. The boattail pressure drag force level must converge within 0.1% of the total drag force. In addition, the internal nozzle exit massflow rate level required convergence within 0.25% of the intake massflow rate, (e.g. conservation of mass). Finally, the L2 residuals must be reduced in the boattail flap region by three orders of magnitude. All three criteria must be met as a condition for a converged solution.

Nozzle boattail drag was computed using the predicted pressure distributions on the boattail surfaces. Integration of the pressure distributions over the respective nozzle boattail surfaces yielded the nozzle boattail drag results. The surfaces used in the integration included the nozzle flaps and nozzle sidewalls. Skin friction drag was not computed. Because the nozzle boattail drag for each of the configurations was influenced by the presence of the nacelle forward of the nacelle maximum area, the reference nacelle drag (configuration N0010) was subtracted from the actual boattail drag for each configuration. The reference nacelle had zero boattail angle.

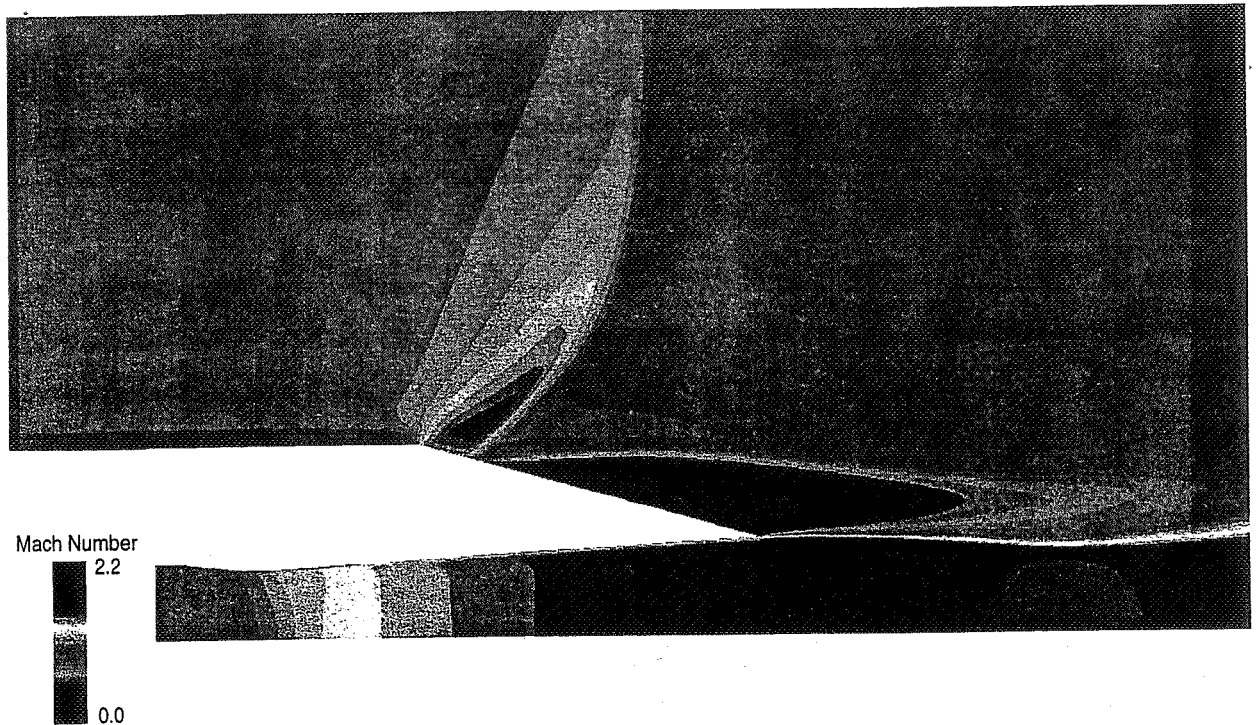
The CFD flow type definition groundrules are shown in the figure. An Euler region was defined just prior to the nacelle configuration to simulate the captured streamtube, and a small laminar region was defined at the nacelle leading edge to simulate transition. The problems were set up in this fashion to allow the flow solvers to begin the solution free of discontinuities. The remaining nacelle was modeled as a turbulent region.

COMPUTED NOZZLE BOATTAIL DRAG RESULTS

Configuration	Boattail	A_9/A_{10}	M_∞	$C_{d, \text{boattail}}$	$C_{d, \text{boattail}}$ [lb]	Team	CFD Code
N1202	12	0.2	0.95	0.1087	550.0	NASA LeRC	PARC3D
N1202	12	0.2	1.10	0.1827	1238.8	NASA LeRC	PARC3D
N1202	12	0.2	1.20	0.1840	1484.7	NASA LeRC	PARC3D
N1205	12	0.5	0.90	0.0422	191.7	MDA-ATAD	NASTD
N1205	12	0.5	0.95	0.0501	253.5	MDA-ATAD	NASTD
N1205	12	0.5	1.10	0.0809	548.3	MDA-ATAD	NASTD
N1205	12	0.5	1.20	0.0985	794.7	MDA-ATAD	NASTD
N1605	16	0.5	0.90	0.0504	228.7	MDA-ATAD	NASTD
N1605	16	0.5	0.95	0.0678	342.9	MDA-ATAD	NASTD
N1605	16	0.5	1.10	0.1847	1252.7	MDA-ATAD	NASTD
N1605	16	0.5	1.20	0.1645	1327.6	MDA-ATAD	NASTD
N1605	16	0.5	0.95	0.1426	721.1	MDA-NAMP	NASTD
N1605	16	0.5	1.10	0.1969	1335.5	MDA-NAMP	NASTD
N1605	16	0.5	1.20	0.1802	1454.6	MDA-NAMP	NASTD
N1605	16	0.5	0.95	0.0939	474.9	NASA LaRC	PAB3D
N1605	16	0.5	1.10	0.2094	1419.9	NASA LaRC	PAB3D
N1605	16	0.5	1.20	0.1962	1583.6	NASA LaRC	PAB3D
N1605	16	0.5	0.95	0.1343	679.1	NASA LeRC	PARC3D
N1605	16	0.5	0.95	0.1284	649.4	NASA LeRC	PARC3D
N1605	16	0.5	1.10	0.2084	1413.5	NASA LeRC	PARC3D
N1605	16	0.5	1.20	0.1960	1581.8	NASA LeRC	PARC3D
N2002	20	0.2	0.95	0.1728	873.9	NASA LaRC	PAB3D
N2002	20	0.2	1.10	0.3759	2548.9	NASA LaRC	PAB3D
N2002	20	0.2	1.20	0.3594	2900.6	NASA LaRC	PAB3D
N2005	12	0.5	0.95	0.1707	863.2	MDA-NAMP	NASTD
N2005	12	0.5	1.10	0.2414	1637.2	MDA-NAMP	NASTD
N2005	12	0.5	1.20	0.2209	1782.6	MDA-NAMP	NASTD

The nozzle boattail drag CFD solutions are tabulated and summarized in this figure.

Mach Number Contours Along Centerline - 1605 Configuration, Mach 0.95 -

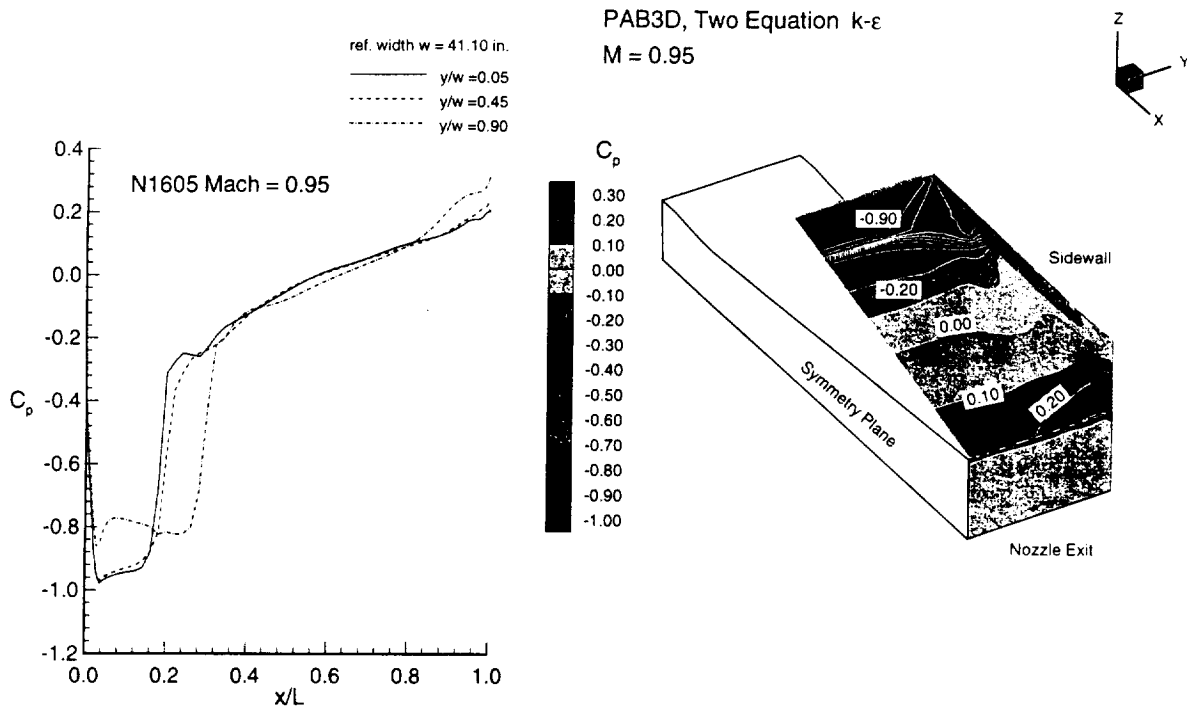


Prior to commencing the entire CFD study for all of the configurations, a baseline case was chosen to validate drag coefficient results between codes for an HSCT specific nozzle. The 16 degree boattail case with an 0.5 area ratio (1605) was chosen as the baseline case, primarily because this case effectively represented the median of the configuration with respect to boattail flap angle. This case was studied by all four teams, and is presented in detail on the following charts.

The figure shows the Mach number contours along the centerline of the top flap of the 1605 nozzle at Mach 0.95. The flow is uniform prior to the nozzle hinge line, and begins to expand at the nozzle flap hinge line. For this case, the external flow expands around the nozzle boattail flap hinge line and recompresses through a normal shock wave just downstream of the expansion wave. Significant separation from the afterbody surface occurs behind the normal shock wave, and the flow does not reattach on the surface.

Pressure Coefficient Contours

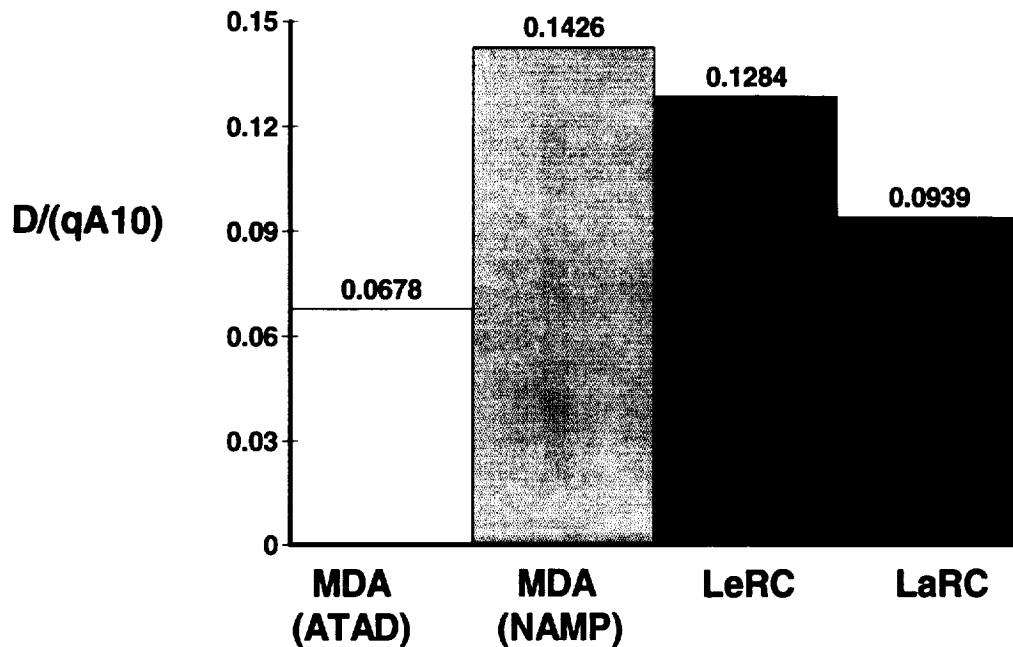
- 1605 Configuration, Mach 0.95 -



This figure shows the pressure contours and distribution as a function of non-dimensional flap length on the top nozzle flap surface for the 1605 configuration at Mach 0.95. Three different sections of the flap are presented on the pressure coefficient plot, with the $y/w=0.05$ representing the flap centerline. Examining the centerline curve shows that the pressure coefficient reflects the effect of the expansion wave at approximately $x/L=0.04$, and the significant separation above $x/L=0.16$. Pressure coefficient distributions for all CFD codes exhibited the same trends for the 1605 nozzle at Mach 0.95, with slight variations in shock/expansion wave location.

Comparison of 1605 CFD Data

- Mach 0.95 -

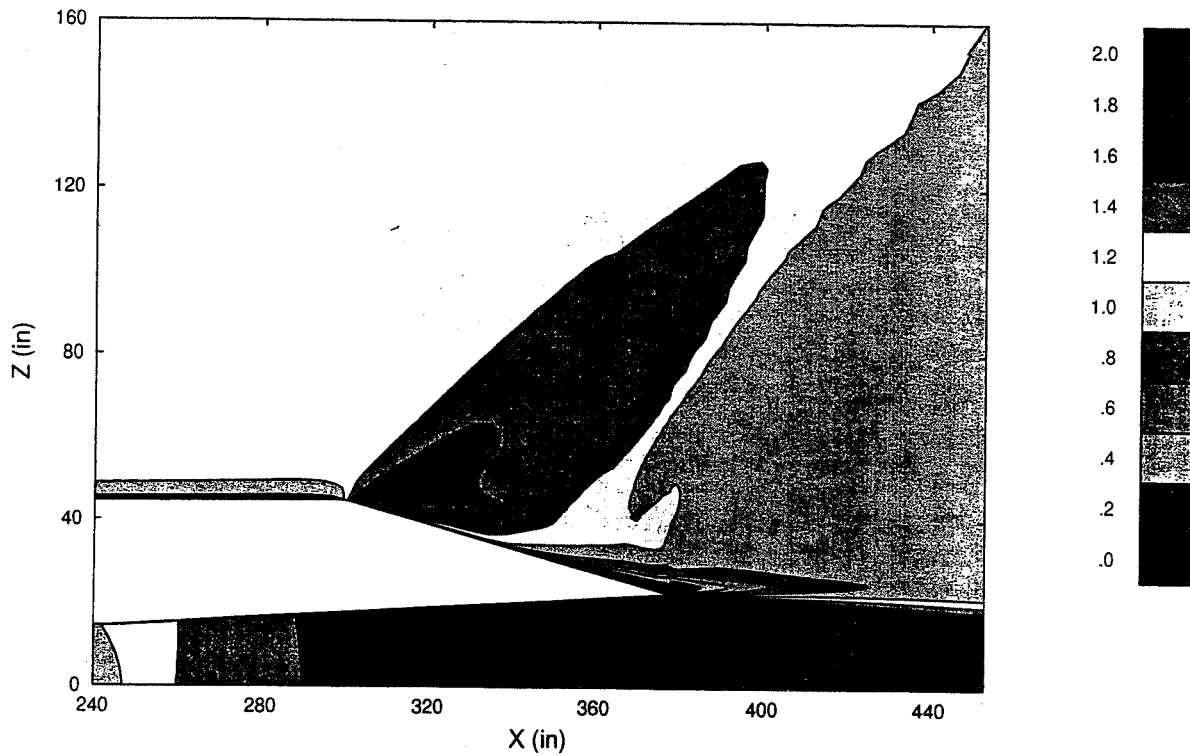


This figure shows the final drag coefficient results for the 1605 configuration at Mach 0.95. McDonnell Douglas results are represented by MDA-NAMP and MDA-ATAD, respectively. NASA Lewis and Langley results are represented by LeRC and LaRC, respectively. The Mach 0.95 case for the 1605 configuration yielded the largest discrepancies between team member results of all the test cases. Note that the MDA-NAMP and LeRC results are within 10%. This is good agreement considering the highly unstable nature of this separated flow problem. The problem is complicated by the fact that the problem is subsonic, sonic and supersonic along a streamline, and the fact that the codes must resolve exactly the location of the supersonic transition. Also, the agreement between MDA-NAMP and LeRC results is consistent with the AGARD validation results, which show nearly identical pressure coefficient distributions for the non-axisymmetric nozzle at the Mach 0.94 condition. For this Mach 0.95 case, the boattail drag coefficient likely lies in the ballpark of the MDA-NAMP and LeRC results.

The MDA-ATAD results for the 1605 configuration at Mach 0.95 should have been very close to the MDA-NAMP results due to the fact that the NASTD was the flow solver for both cases. However, MDA-ATAD computations at Mach 0.95 yield significantly lower pressure drag results than MDA-NAMP results. The MDA-ATAD solution of the 1605 configuration at Mach 0.95 encountered numerical convergence challenges that were attributable to the grid packing density in the vicinity of the nozzle boattail hinge line coupled with significant flow separation over the entire boattail surface. The consensus of the team is that the MDA-ATAD solutions significantly underpredict nozzle boattail drag at Mach 0.95, and should not be used.

The LaRC results for the 1605 configuration at Mach 0.95 are approximately 30% lower than the MDA-NAMP and LeRC results. This is consistent with the results from the AGARD validation study for the B.4 nozzle at Mach 0.94.

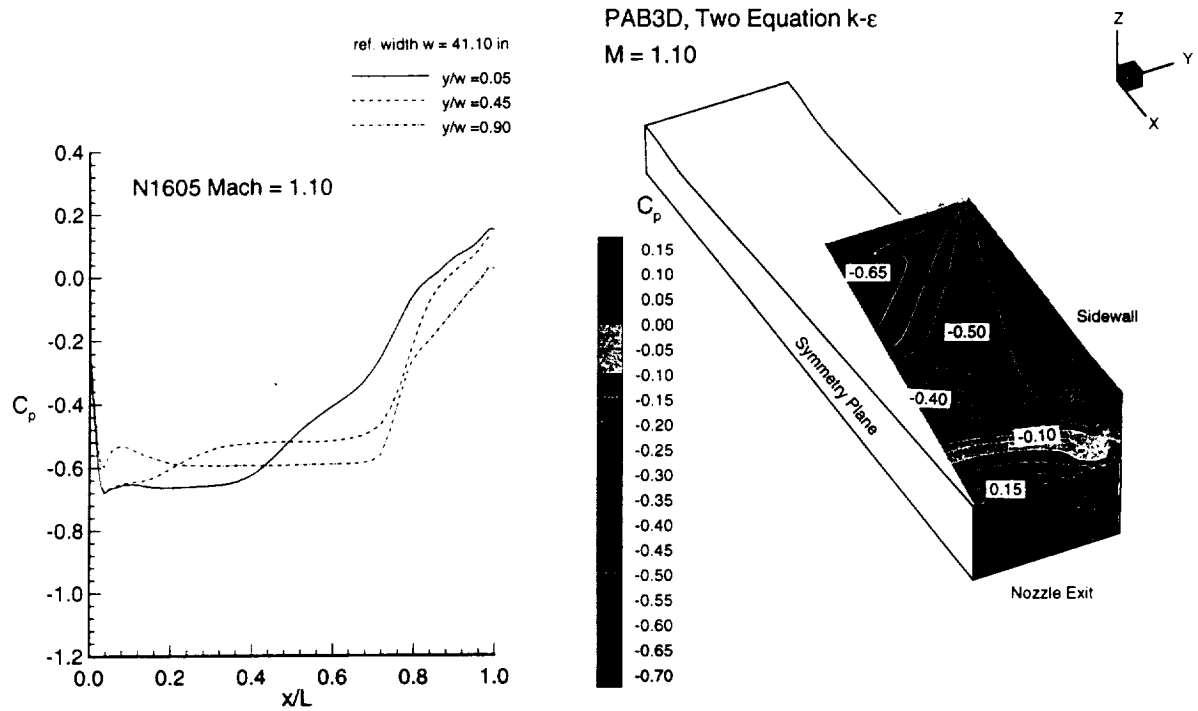
Mach Number Contours Along Centerline - 1605 Configuration, Mach 1.1 -



This figure shows the Mach number contours along the centerline of the top flap of the 1605 nozzle at Mach 1.1. The flow is uniform prior to the nozzle flap hinge line, and begins to expand at the nozzle flap hinge line. For this case, the external flow expands around the nozzle boattail flap hinge and recompresses through a normal shock wave located at approximately the halfway point of the nozzle flap length. Separation from the afterbody surface occurs behind the normal shock wave, and the flow does not reattach on the surface. The flow separation is not as severe as the Mach 0.95 case was, and the solution for the Mach 1.1 case is not as challenging as the previous Mach 0.95 solution.

Pressure Coefficient Contours

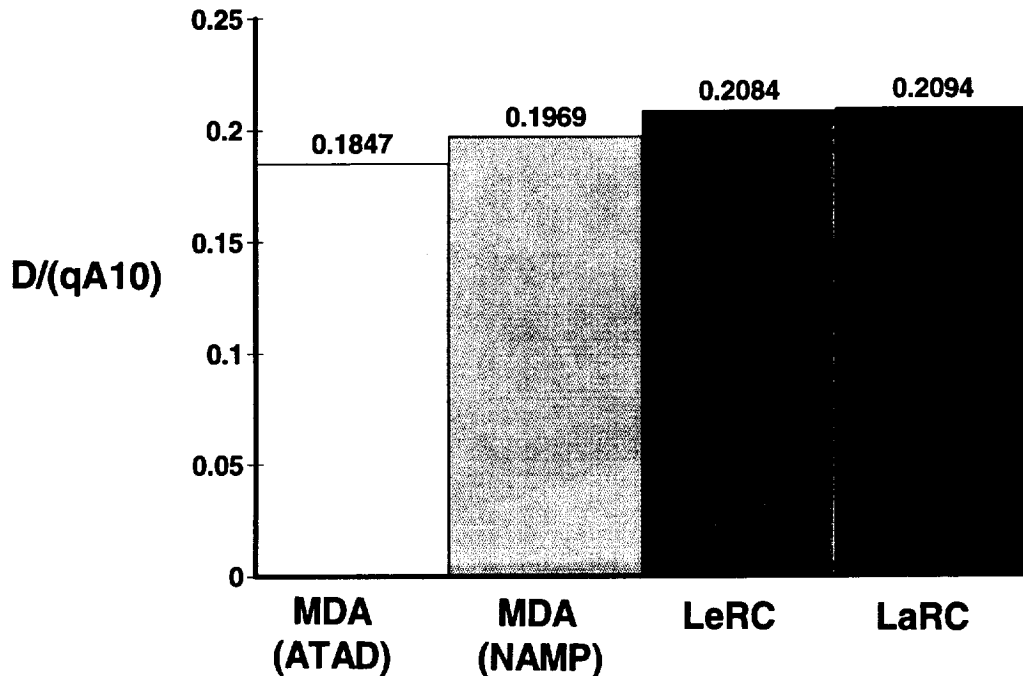
- 1605 Configuration, Mach 1.1 -



This figure shows the pressure contours and distribution as a function of non-dimensional flap length on the top nozzle flap surface for this configuration. Examining the centerline ($y/w=0.05$) curve on the pressure coefficient plot shows that the pressure coefficient reflects the effect of the expansion wave at approximately $x/L=0.04$, and the separation above $x/L=0.4$. Note that the pressure recovery is not as significant for this configuration, compared to the Mach 0.95 case, which indicates that the Mach 1.1 case has significantly less separation than the Mach 0.95 case. Pressure coefficient distributions for all CFD codes exhibited the same trends for the 1605 nozzle at Mach 1.1, with slight variations in shock/expansion wave location.

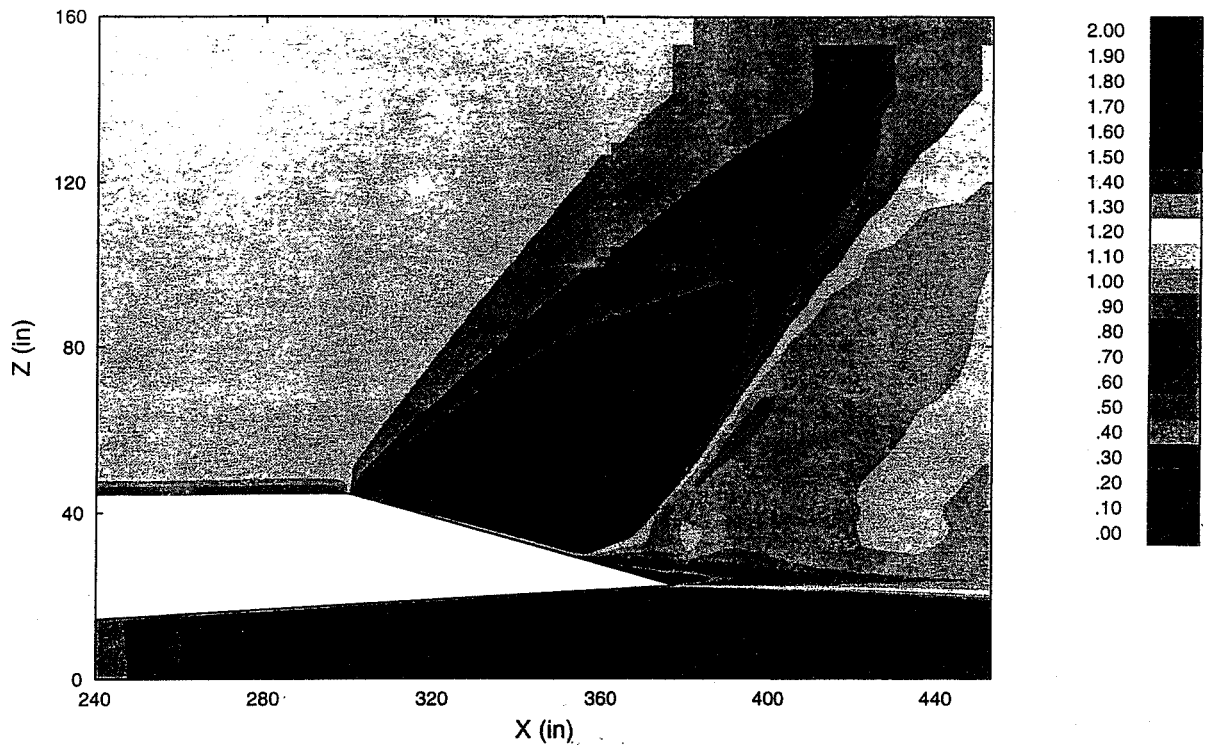
Comparison of 1605 CFD Data

- Mach 1.10 -



This figure shows the final drag coefficient results for the 1605 configuration at Mach 1.1. Because the separation for this case was less severe than the Mach 0.95 case, the CFD codes were better able to predict the flow characteristics, and the results were consistent. For example, the MDA-NAMP and NASA results agreed within 5%. Even more striking, the LeRC and LaRC results agreed within 0.5%. The MDA-ATAD results were approximately 10% lower than the MDA-NAMP results even though the grid was identical for both applications. The team chose to use the MDA-NAMP results due to the higher user experience level. For the Mach 1.1 case, the boattail drag coefficient could accurately be predicted as the average of the MDA-NAMP, LeRC and LaRC results.

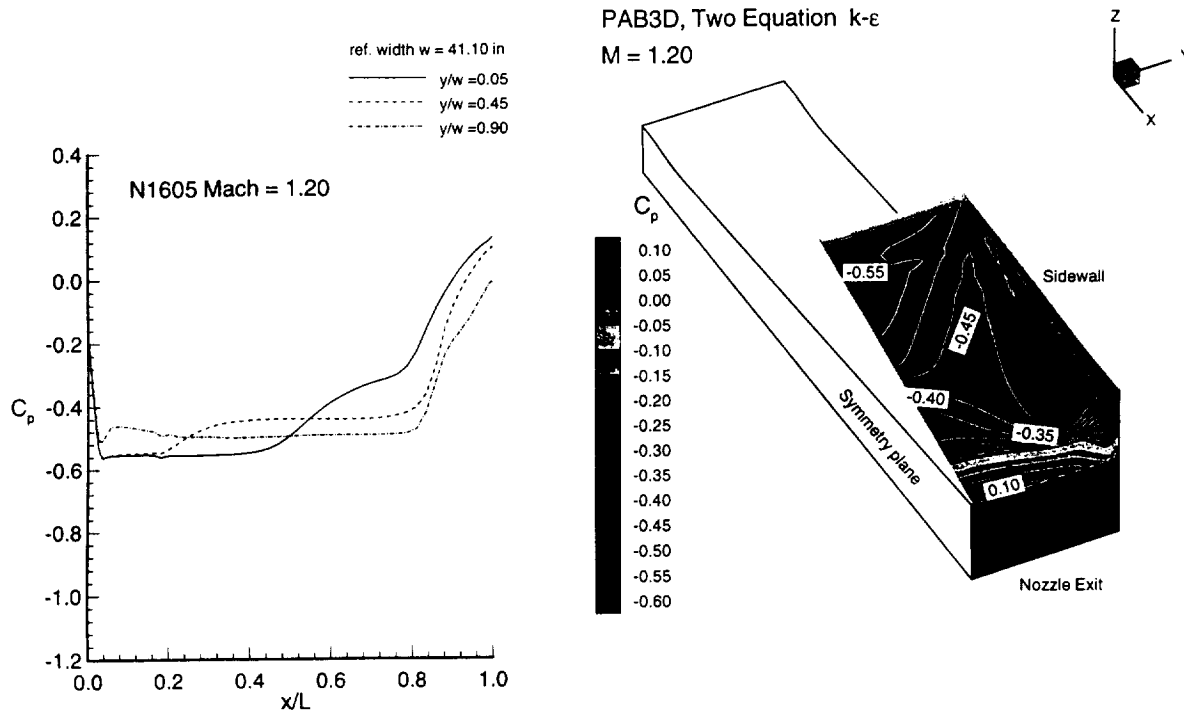
Mach Number Contours Along Centerline - 1605 Configuration, Mach 1.2 -



This figure shows the Mach number contours along the centerline of the top flap of the 1605 nozzle at Mach 1.2. The flow is uniform prior to the nozzle flap hinge line, and begins to expand at the nozzle flap hinge line. For this case, the external flow expands around the nozzle boattail flap hinge line and recompresses through a normal shock wave located approximately three-quarters of the way down the nozzle flap length. Separation from the afterbody surface occurs behind the normal shock wave, and the flow does not reattach on the surface. The flow separation is less severe than the Mach 1.1 case, and therefore, the Mach 1.2 case is the most straightforward solution of the three Mach numbers studied.

Pressure Coefficient Contours

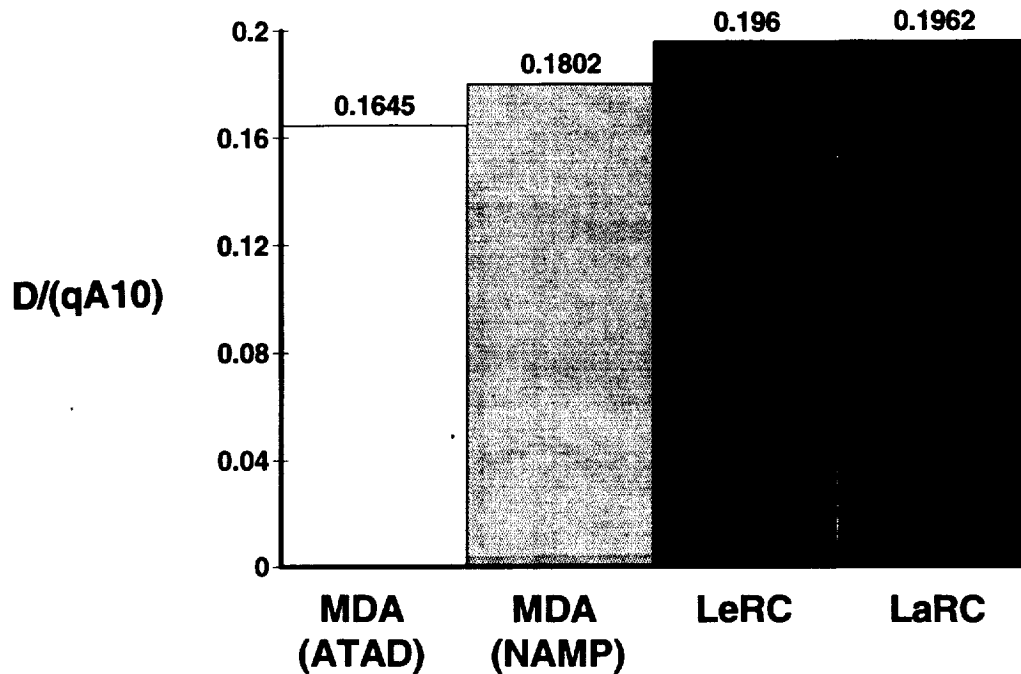
- 1605 Configuration, Mach 1.2 -



This figure shows the pressure contours and distribution as a function on non-dimensional flap length on the top nozzle flap surface for this configuration. Examining the centerline ($y/w=0.05$) curve on the pressure coefficient plot shows that the pressure coefficient reflects the effect of the expansion wave at approximately $x/L=0.04$, and the separation above $x/L=0.75$. Note that the pressure recovery is not as significant for this configuration, compared even to the Mach 1.1 case, which indicates that the Mach 1.2 case has significantly less separation than the Mach 1.1 case. Pressure coefficient distributions for all CFD codes exhibited the same trends for the 1605 nozzle at Mach 1.2, with slight variations in shock/expansion wave location.

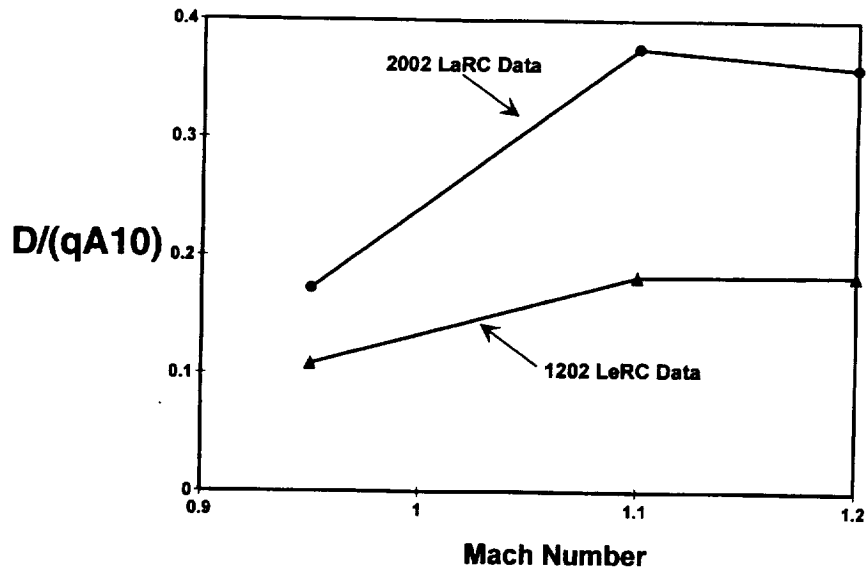
Comparison of 1605 CFD Data

- Mach 1.20 -



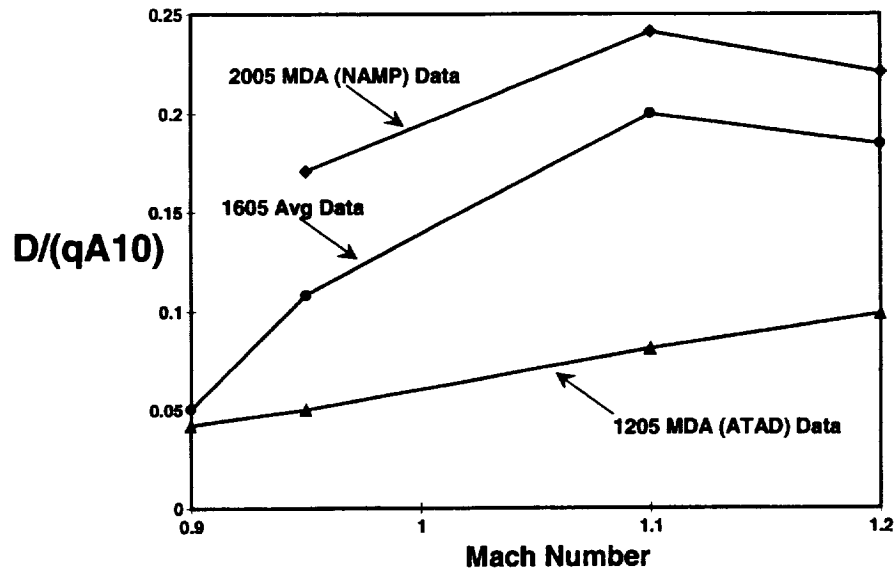
This figure shows the final drag coefficient results for the 1605 configuration at Mach 1.2. Because the separation for this case was less severe than the other cases, the CFD codes were able to predict consistent results. For example, MDA-NAMP and NASA results agreed within 8%. Once again, the LeRC and LaRC results were essentially identical. Again, the MDA-ATAD results were approximately 8% lower than the MDA-NAMP results even though the grid was identical for both applications. The team chose to use the MDA-NAMP results due to the higher user experience level. For the Mach 1.2 case, the boattail drag coefficient could accurately be predicted as the average of the MDA-NAMP, LeRC and LaRC results.

A9/A10 = 0.2 CFD Predictions



This figure shows nozzle boattail drag coefficient as a function of Mach number for the 0.2 area ratio solutions. LaRC was responsible for the 2002 solutions (top line) and LeRC was responsible for the 1202 solutions (bottom line). The 2002 solution at Mach 0.95 is probably underpredicted based on the AGARD validation study results presented earlier, and should be considered a ballpark estimate for this specific case. The 1202 solution at Mach 1.2 is suspicious because nozzle boattail drag coefficient should be lower at Mach 1.2 than at Mach 1.1. This same anomaly is evident for both 12 degree boattail angle configurations.

A9/A10 = 0.5 CFD Predictions



This figure shows the solutions for the 0.5 area ratio solutions. MDA-NAMP was responsible for the 2005 solutions (top line), while MDA-ATAD was responsible for the 1205 solutions (bottom line). Again, the 1205 solutions appear to be uniformly underpredicted, and should not be used as absolute values. The 1605 solutions (middle line) represent the average of MDA-E and LeRC solutions for Mach 0.95, and the average of MDA-NAMP, LeRC and LaRC solutions for Mach 1.1 and 1.2.

Comparison of CFD Results to 95 IMS Database

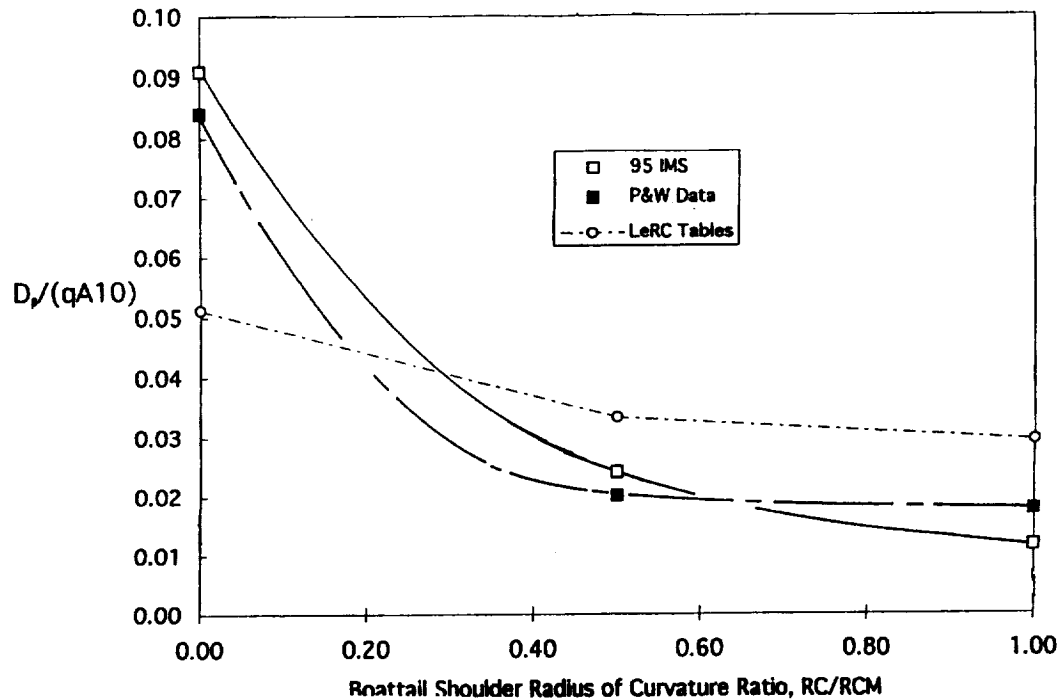
- o IMS Validation**
- o Mach 0.95, 1.1, and 1.2**

As described earlier, the CFD results were to be used to substantiate and enhance the concurrent IMS database update activity. Before comparisons between CFD and IMS are made, a brief comparison of IMS to experimental data will be discussed.

Comparison of Nozzle Drag Data w/Previous Method

- 2D Nozzle, $A_9/A_{10}=0.25$, $\beta = 16$ deg -

$M = 0.9$

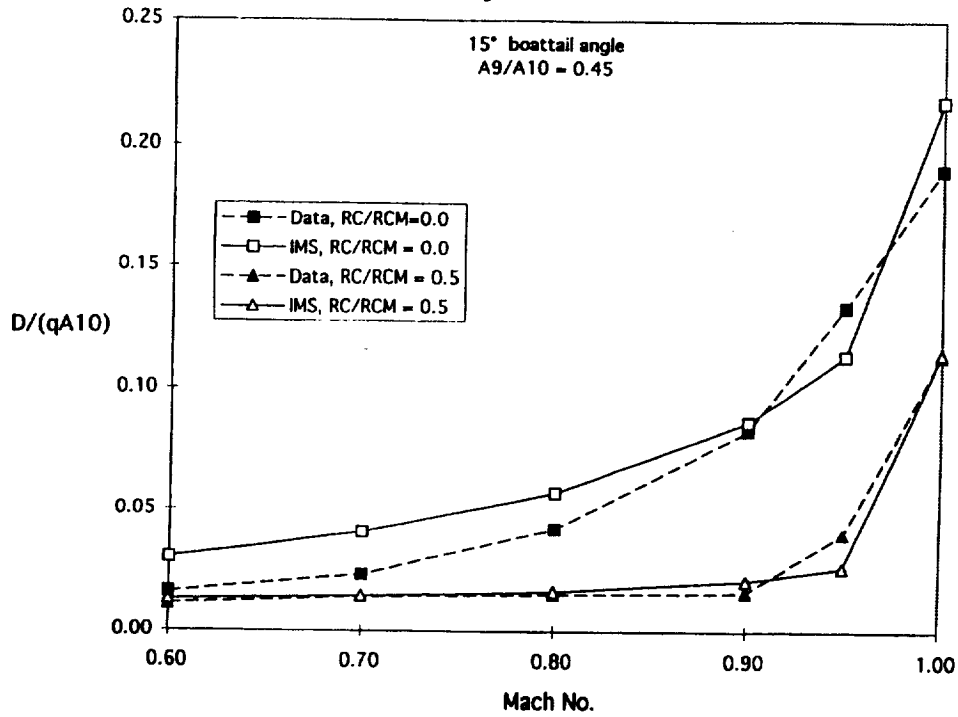


This figure shows a plot that was presented earlier comparing the previous boattail drag coefficient method with experimental data. It has been updated here by adding the new IMS database predictions. The IMS database values are shown as the line with the open symbols, and show excellent agreement with the non-axisymmetric experimental data for the entire range of radius of curvature ratio values.

Nozzle Drag Correlation, IMS vs Test

NASA TMX-1517

Axisymmetric Nozzles

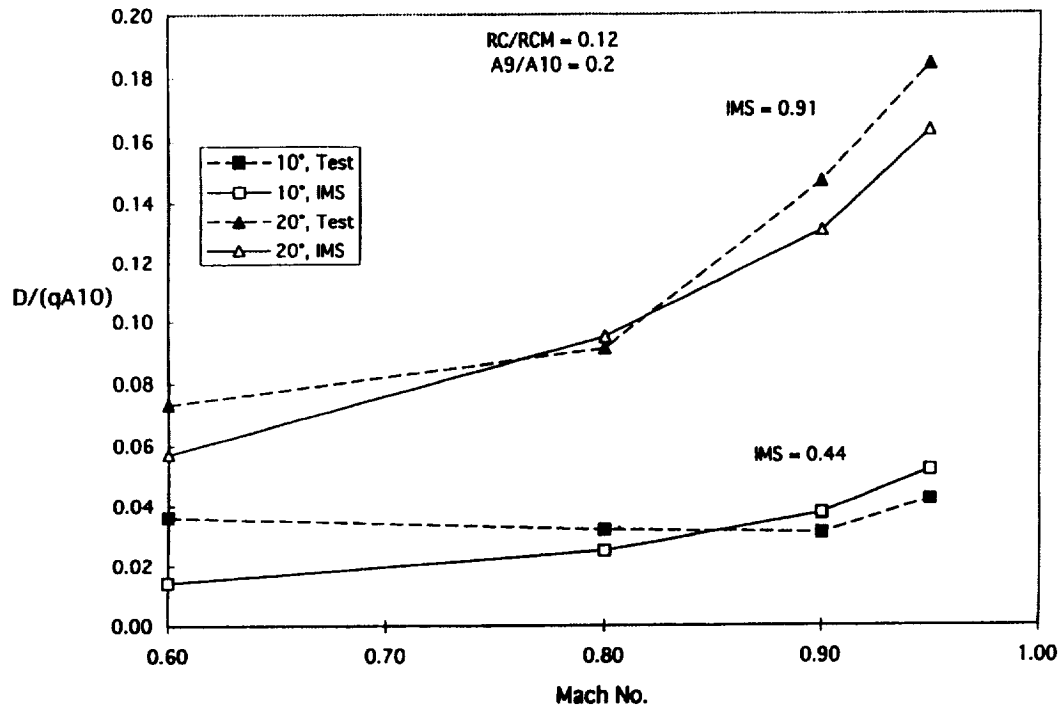


This figure shows a comparison of IMS predictions for an axisymmetric nozzle with a 15 degree boattail flap angle and an area ratio of 0.45. In this figure, the lines with darkened symbols represent the experimental data, while the lines with the open symbols represent the IMS predictions. The plot is nozzle boattail drag coefficient versus Mach number, and the IMS predictions agree without bias with the experimental data for two different radius of curvature ratios (0.0 and 0.5).

Nozzle Drag Correlation, IMS vs Test

NASA TP-3440

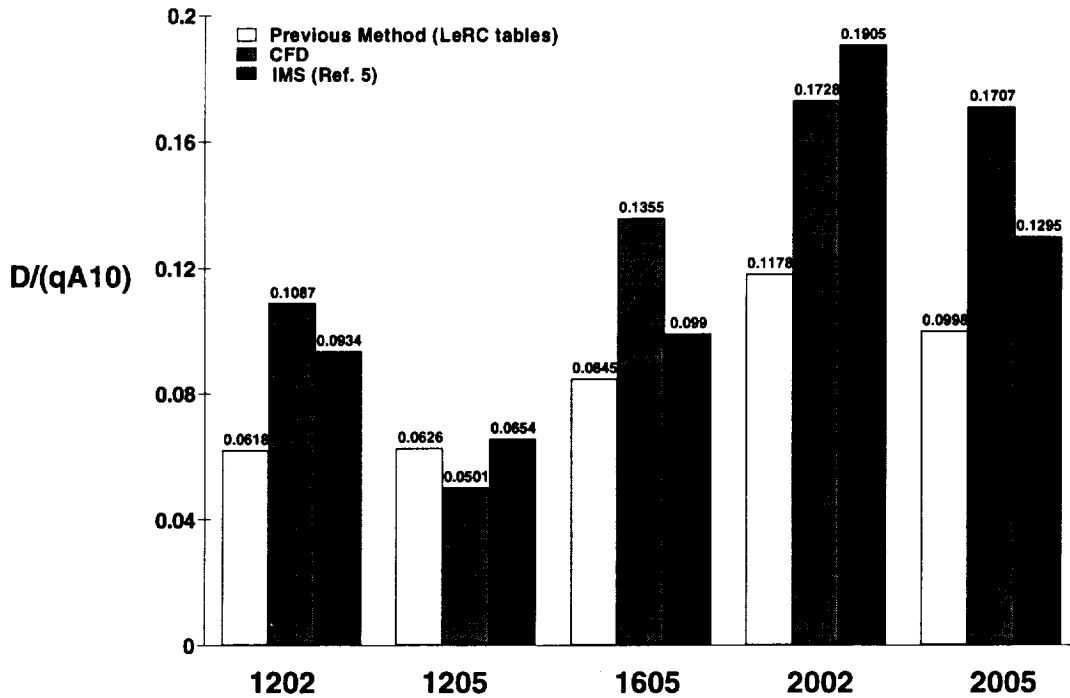
2D Nozzles



This figure shows a comparison of IMS predictions for a non-axisymmetric nozzle with a radius of curvature ratio of 0.12 and an area ratio of 0.2. Again, the experimental data is represented by the darkened symbols, while the IMS predictions are represented by the open symbols. The plot is nozzle boattail drag coefficient versus Mach number, and the IMS predictions agree without bias with the experimental data for two different boattail flap angles (10 and 20 degrees). Based on these comparisons and additional supporting information not shown explicitly here, it is clear that the IMS prediction method with the recently updated database accurately predicts axisymmetric and non-axisymmetric nozzle boattail drag coefficient for complex geometry nozzles. Comparison with CFD results on HSCT specific nozzles would fully substantiate this new methodology for the HSCT project.

Isolated Nozzle Boattail Drag Coefficient Prediction Comparison

- Referenced to A10
- Mach 0.95

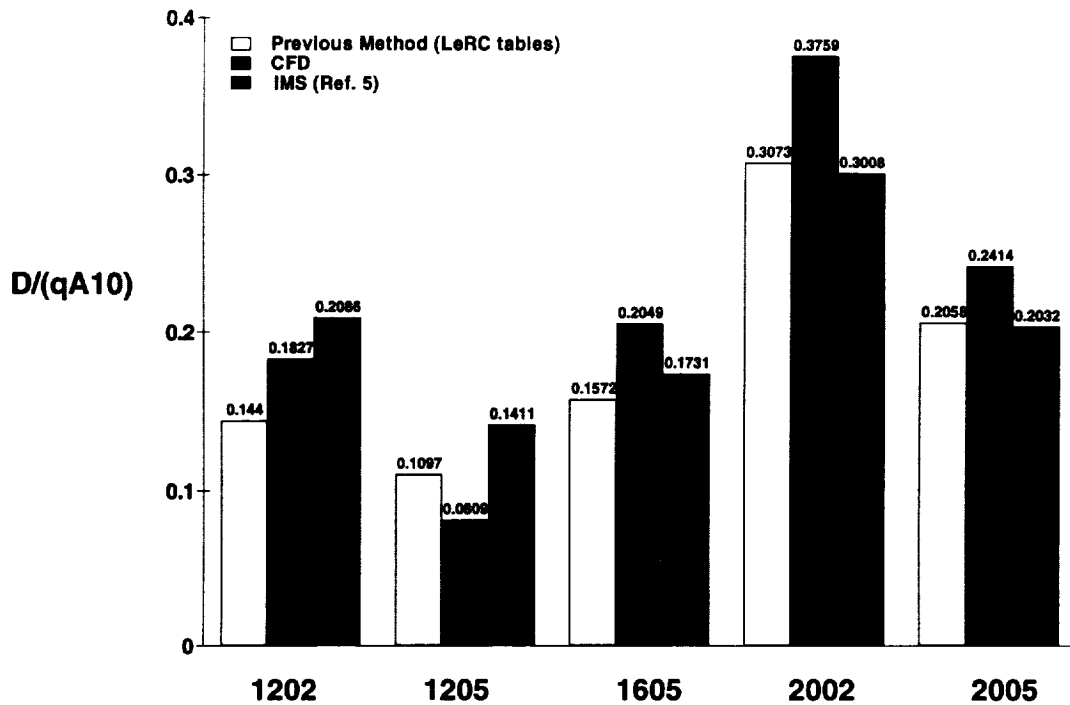


This figure shows a comparison of the IMS, CFD and previous method predictions at Mach 0.95. Each of the six geometry configurations are shown individually on the bar graph. In general, the IMS and CFD predictions generally agree within 10-15%, and there is no apparent bias or trend with boattail angle or area ratio. Due to the fact that the Mach 0.95 case was highly separated and difficult to obtain CFD solutions for, the CFD results in the figure should only be used to substantiate the IMS predictions. The previous method consistently underpredicts the IMS estimates by as much as 50%. No further conclusions can be drawn from this case.

Isolated Nozzle Boattail Drag Coefficient Prediction Comparison

- Referenced to A10

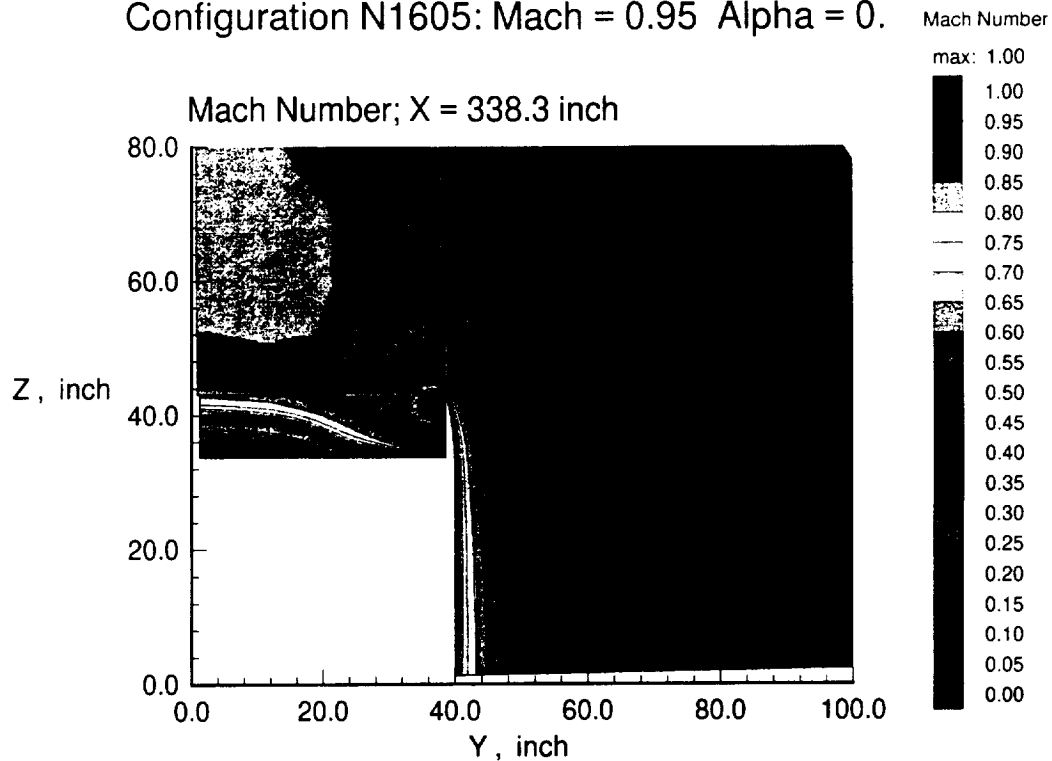
- Mach 1.10



This figure shows the same comparison at Mach 1.1. In general, the IMS and CFD predictions generally agree, but there is an apparent trend with boattail angle. At a 12 degree boattail angle, the IMS prediction is slightly higher than the CFD prediction for the area ratio of 0.2. At a 16 degree boattail angle, the predictions also agree very closely. At a 20 degree boattail angle, the CFD predictions are higher than the CFD predictions for both area ratios studied. It is likely that this trend is caused by sidewall effects, and is discussed in detail later. The previous method consistently underpredicts the IMS estimates for boattail angles less than 20 degrees. For the 20 degree boattail angle cases, the previous method and the IMS predictions agree within 1%, but both represent estimates for nozzles without sidewalls.

Isolated Nacelle Drag Study: Flow Cross Section

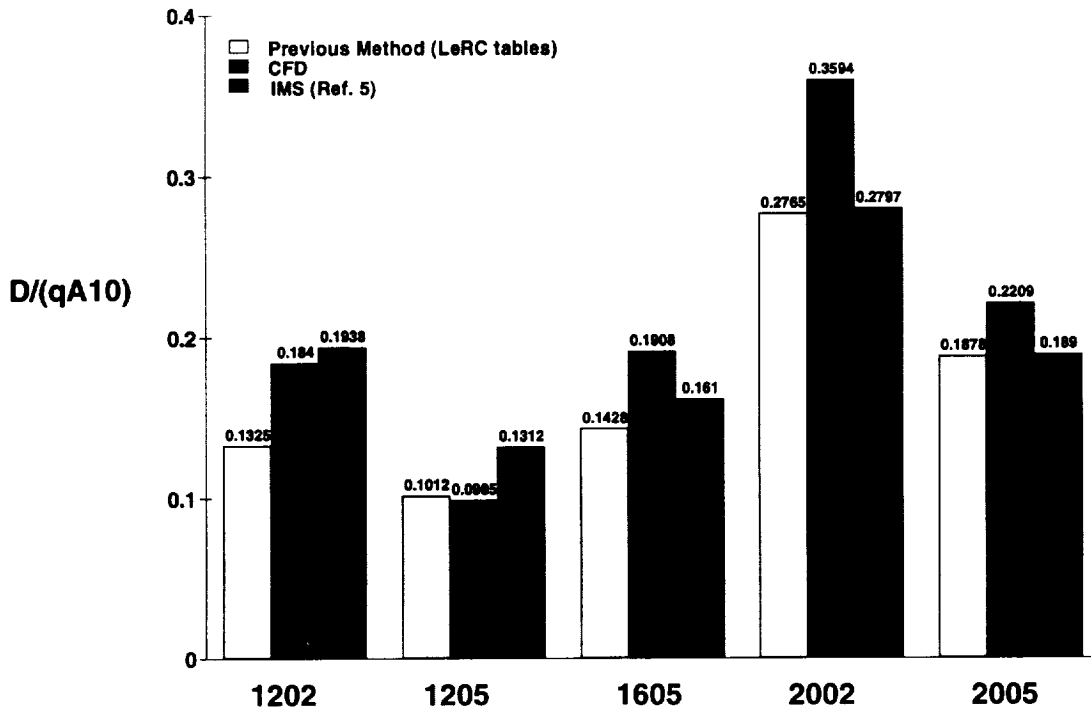
Configuration N1605: Mach = 0.95 Alpha = 0.



The IMS and previous method predictions are based on non-axisymmetric nozzles without sidewalls. The CFD predictions use the DSM nozzle, which does have sidewalls. Based on the results of the CFD studies, the sidewalls on a non-axisymmetric nozzle cause a decrease in the pressure relief from the top of the nozzle flap to the ambient flow due to end-plating and vortex trapping effects, and thus may cause an increase in drag coefficient. An example of this flow phenomena is shown in the figure, which depicts an aft facing forward view of the DSM nozzle. Higher pressure ambient flow is shown rolling over the top of the sidewall and pressurizing the top of the nozzle boattail flap. If the sidewall is removed, the pressurizing of the flap may increase, and the boattail drag coefficient may be reduced. One possible explanation of the trend shown in the previous figure is that as boattail angle increases, the effect of the sidewall on the boattail flap increases. At 12 degrees, the sidewall does not significantly impact the pressurization of the nozzle boattail flap. However, at 16 and 20 degrees boattail angle, the effect of the sidewall may significantly impact the prediction of nozzle boattail drag coefficient. A follow-on study is underway to update the IMS database for sidewall effects. Also, an on-going CFD study will evaluate the delta nozzle boattail drag coefficient due to removing the sidewalls using various configurations evaluated in this study.

Isolated Nozzle Boattail Drag Coefficient Prediction Comparison

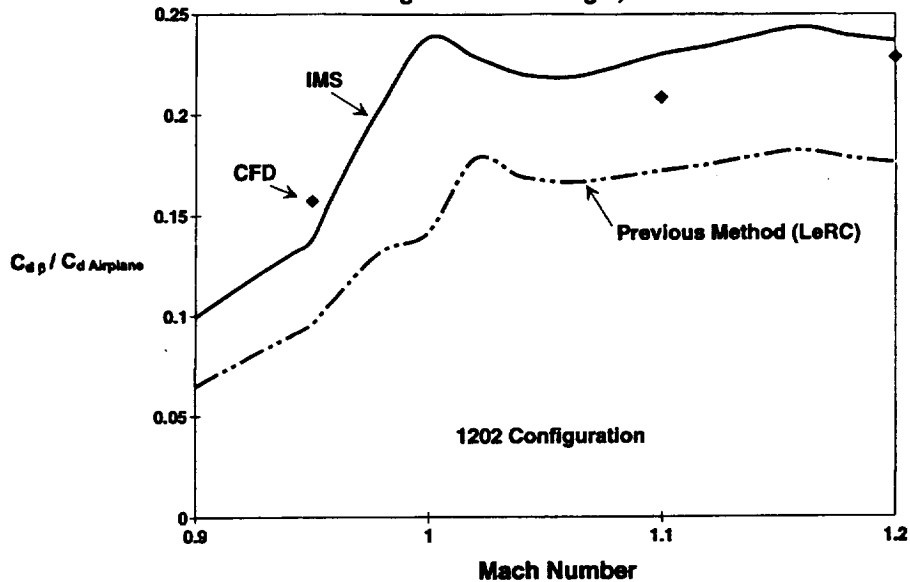
- Referenced to A10
- Mach 1.20



This figure shows the same comparison at Mach 1.2. In general, the IMS and CFD predictions generally agree. Again, there is an apparent trend with boattail angle, and the conclusion is the same as for the Mach 1.1 case. The sidewalls appear to affect the 16 and 20 degree boattail angle CFD predictions. In addition, the previous method underpredicts IMS estimates for boattail angles less than 20 degrees, which is consistent with the Mach 1.1 results. Like the Mach 1.1 results, the previous method and IMS estimates agree closely for the 20 degree boattail angle cases.

Comparison of CFD, IMS and Previous Method Drag Ratios

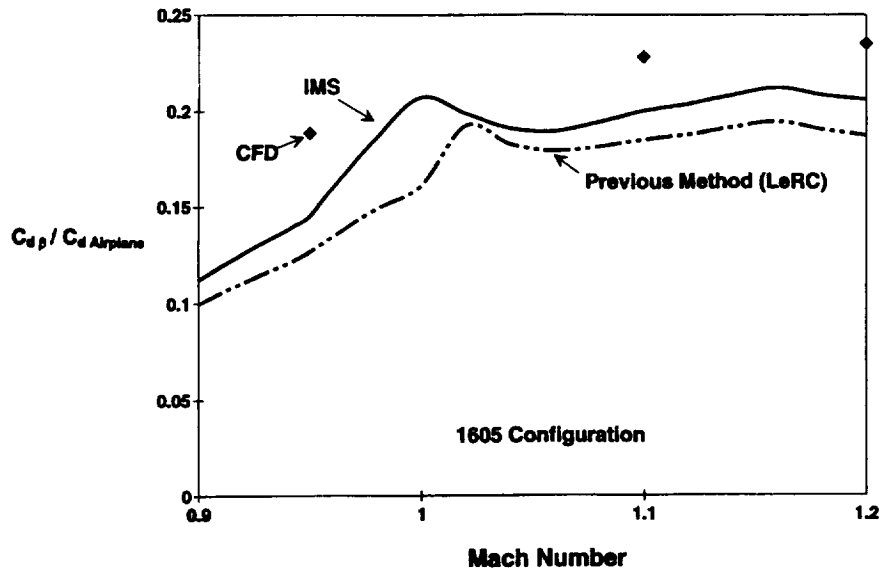
- Ratio of Boattail Drag Coefficient to Aircraft Total Drag Coefficient
- Referenced to Aircraft Wing Area
- 12 Degree Boattail Angle, $A_9/A_{10} = 0.187$



This figure shows a comparison of CFD, IMS and previous method nozzle drag coefficient predictions normalized with total HSCT airplane drag coefficient for the 1202 configuration. All drag coefficients are referenced to the airplane wing area for this comparison, and the total airplane drag coefficient includes the nozzle boattail drag element. For the 1202 configuration, the CFD and IMS predictions are of the same magnitude, and this substantiated that the previous method significantly underpredicts nozzle boattail drag coefficient. The previous method predicts that nozzle boattail drag accounts for approximately 15% of the total airplane drag above Mach 1.0, while the CFD and IMS predict that nozzle boattail drag accounts for 20-25% of the total airplane drag above Mach 1.0. Because the HSCT nozzle would likely operate at transonic boattail angles of approximately 12 degrees, the more accurate CFD and IMS predictions would significantly affect the aircraft transonic performance, and thus would impact the airplane sizing and mission performance.

Comparison of CFD, IMS and Previous Method Drag Ratios

- Ratio of Boattail Drag Coefficient to Aircraft Total Drag Coefficient
- Referenced to Aircraft Wing Area
- 16 Degree Boattail Angle, $A_9/A_{10} = 0.467$



This figure shows the same comparison for the 1605 configuration. The CFD predictions are consistently larger than the IMS predictions for this case primarily because of the sidewall effects discussed earlier. However, the previous method underpredicts nozzle boattail drag for this configuration, and the replacement of the previous method with the IMS prediction methodology yields a method that is more applicable to the HSCT nozzle trade studies because of the updated nozzle drag coefficient database and additional nozzle geometrical flexibility. On average, the IMS method predicts 15-20% higher boattail drag for this configuration than the previous method.

Lessons Learned

- o **CFD Grids Must Be:**
 - **Generated by One Organization**
 - **Thoroughly Checked Out Prior to Production Runs**

- o **Multiple CFD Flow Solvers Can Be Used to Compute a Matrix of Solutions**
 - **AGARD17 Validation Check**
 - **Common Configuration Test Case**
 - **Resources**

- o **Configurations With Freestream Mach Numbers Close to 1.0 (0.95) and Large Boattail Angles Pose Serious Challenges and Limitations**
 - **Current CFD Codes**
 - **Current Turbulence Models (Affects Shock Position and Pressure Recovery)**
 - **Solutions Grid Dependent**

- o **Required 1 Month (Calendar Time) Per Case for Final Results**

- o **BI-Weekly Telecons, and Goal-Oriented Schedule Resulted in Focused Program and Provided Timely Results**

The most significant lesson learned is that multiple CFD flow solvers can be used to compute results for a matrix of configurations. In this case, multiple flow solvers were used by multiple team members located throughout the country. The key to a successful program using this team approach involves setting up a stringent validation process. Prior to solving HSCT specific configurations, each flow solver was required to solve an established configuration (AGARD) with proven experimental data. Upon completion of this exercise, each team member was required to analyze the baseline configuration. The program did not begin in earnest until all team members agreed on the results from analyzing the baseline configuration. This strategy worked well for this team, and proved that multiple CFD flow solvers can be used. The major benefit of this strategy is that it spreads the computational resource requirements throughout the team, and reduces the overall time required for the entire program.

In order to minimize differences in the results between flow solvers, the inputs must be kept as standardized as possible. In general, that means using the same grids and the same type of turbulence model. The CFD grids should all be generated by the same organization, and should be thoroughly checked out using one of the flow solvers prior to distribution to the rest of the team. Small changes can be made to the grids by each team member to better suit their respective flow solver, but these changes should be kept to a minimum to reduce the possibility of grid dependent differences in the solutions. Also, similar turbulence models should be used to ensure that result differences do not stem from the difference in turbulence models. This effect could be significant for highly separated configurations.

Configurations with freestream Mach numbers close to 1.0, and large boattail angles pose serious challenges and limitations. Current CFD codes and turbulence models have difficulty solving equations when Mach number approaches unity, and this affects shock position and pressure recovery. Thus, solutions to these types of configurations tend to be grid dependent.

Summary

- o **Previous Boattail Drag Method Inadequate**
- o **IMS Method w/CFD Validation Preferred Method**
 - **Update Database Using Non-Axi Test Data**
 - **In Place by March 1995 for Use in Nozzle Downselect Studies**
- o **CFD Codes Validated with AGARD 17 Nozzle Test Data**
- o **Full Scale 3765-100 MFTF Nacelle Configuration Used**
- o **27 CFD Cases Run, (Approx. 1.5 Million Points Each)**
- o **Pressure Drag on Boattail Computed for All Cases**
- o **All CFD Cases Successfully Completed Prior to Commencement of Nozzle Downselect Studies**

Nozzle boattail drag is significant for the HSCT and can be as high as 25% of the overall propulsion system thrust at transonic conditions. Thus, nozzle boattail drag has the potential to create a thrust-drag pinch and can reduce HSCT aircraft aerodynamic efficiencies at transonic operating conditions. In order to accurately predict HSCT performance, it is imperative that nozzle boattail drag be accurately predicted.

Previous methods to predict HSCT nozzle boattail drag were suspect in the transonic regime. In addition, previous prediction methods were unable to account for complex nozzle geometry and were not flexible enough for engine cycle trade studies. A computational fluid dynamics (CFD) effort was conducted by NASA and McDonnell Douglas to evaluate the magnitude and characteristics of HSCT nozzle boattail drag at transonic conditions. A team of engineers used various CFD codes and provided consistent, accurate boattail drag coefficient predictions for a family of HSCT nozzle configurations. The CFD results were incorporated into a nozzle drag database that encompassed the entire HSCT flight regime and provided the basis for an accurate and flexible prediction methodology.

Four teams of analysts were involved in the CFD study: NASA-Lewis Research Center, NASA Langley Research Center, and McDonnell Douglas Aerospace. Three CFD flow solvers were used, and were validated using Advisory Group for Aerospace Research and Development (AGARD) data, and a baseline HSCT nozzle configuration. Once the CFD codes were validated, the matrix of nozzle configurations were defined and predictions of nozzle boattail drag were generated. Each configuration studied incorporated a 3765 mixed flow turbofan and an axisymmetric inlet. 27 total CFD cases were run, and each case was comprised of approximately 1.5 million data points. Pressure drag on the boattail surfaces was computed and nozzle boattail drag coefficient was generated via a post-processed pressure integration. All CFD cases were successfully completed in a timely fashion.

Conclusions

- o **CFD Solutions Grid Dependent for Mach 0.95, Large Boattail Angle Cases**
 - **Significant Separation**
 - **Large Variation in CFD Results Between Teams**

- o **CFD Solutions at Mach 1.1 & 1.2 Well Defined**
 - **Good Agreement Between Teams**

- o **CFD Substantiates IMS Transonic Predictions**
 - **Part of IMS vs CFD Cd Difference Due to Sidewall Effect**
 - o **IMS Underpredicts at Boattail Angles > 16 deg**
 - **IMS Overpredicts for 12 deg Boattail Angle Cases**
 - **Transonic Wind Tunnel Data Required to Quantify Sidewall Fence Effect**

- o **CFD Accurately Predicts Isolated Nozzle Boattail Pressure Profiles**
 - **Consistent Results Using 3 Different Codes**

The CFD solutions were grid dependent for the Mach 0.95, large boattail angle cases. These cases experienced significant separation, and resulted in a large variation (30%) between team results for the baseline configuration. The CFD results at Mach 1.1 and 1.2 were well defined, and there was excellent agreement between the team results. NASA LeRC and LaRC agreed within 1% for these cases. The CFD and IMS method results at Mach 0.95 generally agreed within 30%, but no clear bias was apparent in the comparison. Therefore, the Mach 0.95 CFD results were only used to substantiate the approximate magnitude of the IMS predictions at Mach 0.95. The Mach 1.1 and 1.2 CFD results were generally within 20% of the IMS predictions, but showed a bias that could have been caused by the DSM nozzle sidewalls. The CFD predictions included nozzle sidewalls, while the IMS database did not include sidewalls. Because of this difference, the CFD predicted slightly higher nozzle drag coefficients for higher boattail angle cases (16 and 20 degrees), and this was consistent with the expected sidewall flow effect. Future work with CFD will quantify the sidewall effect, and incorporate this effect into the IMS database. For the Mach 1.1 and 1.2 cases, the CFD results substantiated the magnitude of the IMS predictions, and were incorporated as part of the nozzle drag coefficient database for use in future HSCT propulsion system performance calculations.

For this study, the CFD flow solvers accurately predicted isolated nozzle boattail pressure profiles and boattail drag coefficients. Consistent results were obtained using three different flow solvers. The results corroborated with the IMS database and provided a more applicable method for accurate prediction of transonic HSCT nozzle boattail drag.

ACKNOWLEDGMENTS

The authors wish to thank the following team members for their dedicated effort. The success of this study is directly related to the excellent quality of the results generated by the following personnel; Nick Georgiadis, Fred Smith and Joe Holcomb of NASA Lewis Research Center; Khaled Abdol-Hamid, John Carlson, and Peter Coen of NASA Langley Research Center; Ray Cosner, Chris Culbertson, Greg Finrock, Jay Jones, Rob Jonietz, Walt LaBozzetta, Bill Regnier and Hoyt Wallace of McDonnell Douglas Aerospace.

REFERENCES

1. Silhan, F.V., and Cabbage, J.M., "Drag of Conical and Circular-Arc Boattail Afterbodies at Mach Numbers from 0.6 to 1.3", NACA Research Memorandum RM L56K22, January 1957.
2. Bangert, L.S., and Carson, G.T. Jr., "Effect of Afterbody Geometry on Aerodynamic Characteristics of Isolated Nonaxisymmetric Afterbodies at Transonic Mach Numbers", NASA Technical Paper TP 3236, September 1992.
3. Stevens, H.L., Thayer, E.B., and Fullerton, J.F., "Development of the Multi-Function 2-D/C-D Nozzle", AIAA Paper 81-1491, July 1981.
4. Wallace, H.W., Hiley, P.E., Reinsberg, J.G., and Booher, M.E., "Advanced Nozzle Concepts Program Final Report; Summary of Results and Nozzle Integration Design Criteria", AFWAL-TR-81-3165, Volume I, January 1982.
5. Wallace, H.W., "Nozzle Boattail Drag Topics", Presentation (unpublished) to the Propulsion System Evaluation Team of the NASA Lewis Research Center Critical Propulsion System Components Program, St. Louis, MO, March 1995.
6. Cooper, K., "NPARC 2.0 Features and Capabilities", AIAA 95-2609, Presented at the 31st Joint Propulsion Conference, July 10-12, 1995.
7. Abdol-Hamid, K.S., Carlson, J.R., and Lakshmanan, B., "Application of Navier-Stokes Code PAB3D to Attached and Separated Flows with a $k-\epsilon$ Turbulence Model", NASA Technical Paper TP 3840, 1994.
8. Bush, R. H., "A Three-Dimensional, Zonal, Navier-Stokes Code for Subsonic Through Hypersonic Propulsion Flow Fields", AIAA 88-2830, Presented at the 24th Joint Propulsion Conference, July 1988.
9. AGARD Fluid Dynamics Panel (Working Group #17): Aerodynamics of 3D Aircraft Afterbodies, AGARD Advisory Report AR-318, September, 1995.
10. Carlson, J.R., Pao, S.P., Abdol-Hamid, K.S., and Jones, W.T., "Aerodynamic Performance Predictions of Single and Twin-Jet Afterbodies", AIAA 95-2622, Presented at 31st Joint Propulsion Conference, July 1995.
11. Compton, W.B. III, Abdol-Hamid, K.S., and Abeyounis, W.K., "Comparison of Algebraic Turbulence Models for Afterbody Flow with Jet Exhaust", AIAA Journal, Volume 30, pp. 2716-2722, November 1992.
12. DeBonis, James R., Georgiadis, Nicholas J., Smith, Crawford F., "Validation of the NPARC Code for Nozzle Afterbody Flows at Transonic Speeds", NASA Technical Memorandum 106971, Presented at the 31st Joint Propulsion Conference, July 10-12, 1995.
13. Cosner, R.R., "CFD Validation Requirements for Technology Transition", AIAA 95-2227, Presented at 26th AIAA Fluid Dynamics Conference, June 19-22, 1995.
14. Shrewsbury, G.D., "Effect of Boattail Juncture Shape on Pressure Drag Coefficients of Isolated Afterbodies", NASA TM X-1517, March 1968.
15. Carlson, J.R., and Asbury, S.C., "Two-Dimensional Converging-Diverging Rippled Nozzles at Transonic Speeds", NASA Technical Paper TP 3440, July 1994.

Transonic Drag Study for the Installed Ref. H Axisymmetric Nozzle Boattail Configurations

Chih Fang Shieh, Jay Jones, Shreekant Agrawal
McDonnell Douglas Aerospace
Long Beach, CA 90807-5309

The transonic drag study for the installed Ref. H nozzle boattail was carried out by a NASA/Industry team. The primary objective of this study was to use CFD to estimate the installed nozzle boattail transonic drag for the Ref. H configuration. The nozzle boattail configurations included 2-D (Boeing/Northrop Grumman tasks) and axisymmetric (MDA tasks) configurations. The results of the axisymmetric nozzle boattail study, the MDA tasks, are reported here.

The CFL3D Navier-Stokes code with the Baldwin-Barth turbulence model was used for the axisymmetric nozzle boattail drag study. Two configurations were analyzed: the axi/transonic (boattail angle approximately 14°) and the axi/supersonic (boattail angle approximately 2°) configurations. In this study, the CFL3D code was first validated for a 2-D nozzle at transonic condition, the AGARD B.4.2 nozzle, where shock-induced flow separation occurs in the boattail region. Then, the code was further validated for the Ref. H wing/body at $M_\infty=0.9$ and 1.1 for $Re_C = 40$ million. In addition, the isolated nozzle boattail drag, and the installed wing/body/nacelle/diverter drag were computed. Based on the CFL3D solutions, the installation and interference drag due to the nacelle installation were calculated.

During the course of this study, numerical instability was experienced for all of the cases calculated. Although the numerical instability problem for the AGARD B.4.2 nozzle and the Ref. H wing/body was overcome, the problem for some of the installed nozzle boattail configurations still exists. With the limited converged solutions for the installed axi/transonic configuration, favorable interference between the wing and the nacelle installation was obtained.

Objective

- Apply CFD to estimate boattail drag for the installed Ref. H nozzle boattail configurations in the transonic regime.
 - 2-D configurations: Boeing/Northrop-Grumman
 - Axisymmetric configurations: MDA
 - 2-D and Axisymmetric: NASA LaRC

The objective of this study was to apply CFD to estimate boattail drag for the installed Ref. H nozzle boattail configurations in the transonic regime. To achieve this objective, the Boeing/Northrop-Grumman team was assigned to study 2-D nozzle configurations, MDA was assigned to study the axisymmetric configuration. Since different CFD methods were to be used by the different organizations, the NASA LaRC was to carry out calculations on the selected cases on the 2-D and the axisymmetric geometries to determine the degree of consistency between different methods.

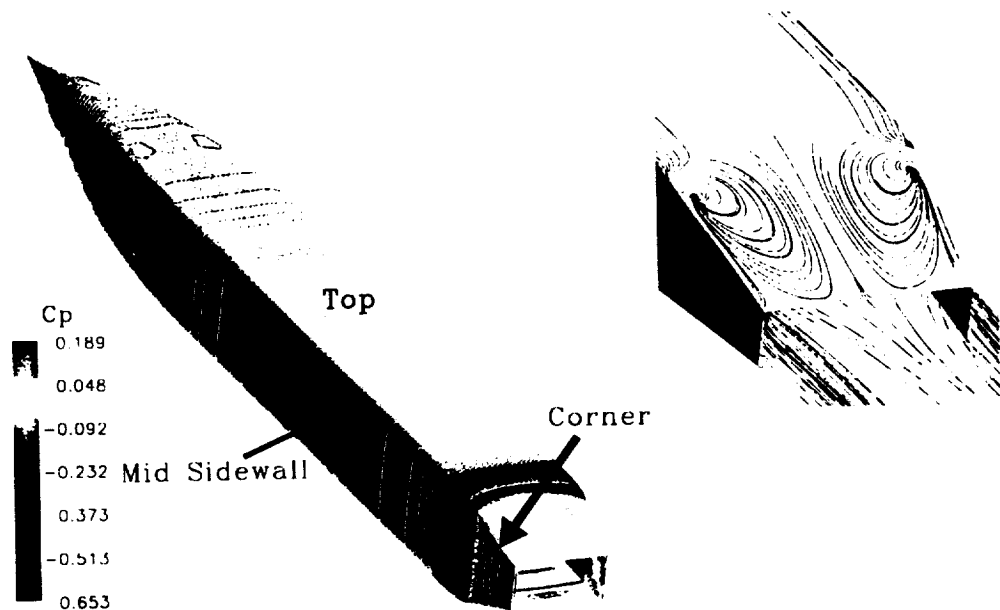
MDA Approach

- Installed Ref. H axisymmetric nozzle boattail drag study
 - CFL3D code validation for a 2-D nozzle boattail (Shock-induced flow separation in transonic flow)
 - Ref. H wing/body analysis ($Re_c = 40$ million).
 - Isolated axisymmetric nozzle boattail analysis
 - Installed axisymmetric nozzle boattail analysis

To complete the MDA tasks for the installed ref. H axisymmetric nozzle boattail drag study, the CFL3D code was first validated for an isolated 2-D nozzle, the AGARD B.4.2 nozzle. Special interest was focused on the shock-induced flow separation in the boattail region at transonic speed. The code was then validated for the Ref. H wing/body case at $Re_c = 40$ million. Then, the code was applied to analyze the isolated axisymmetric/transonic (axi/transonic), and the supersonic (axi/supersonic) configurations. Finally, the installed axisymmetric nozzle boattail configurations were analyzed, and the installation drag and interference drag were calculated.

CFL3D Code Validation for the AGARD B.4.2 Nozzle

(CFL3D, Baldwin-Barth Turbulence model, $M_\infty = 0.938$, $Re = 21$ million)



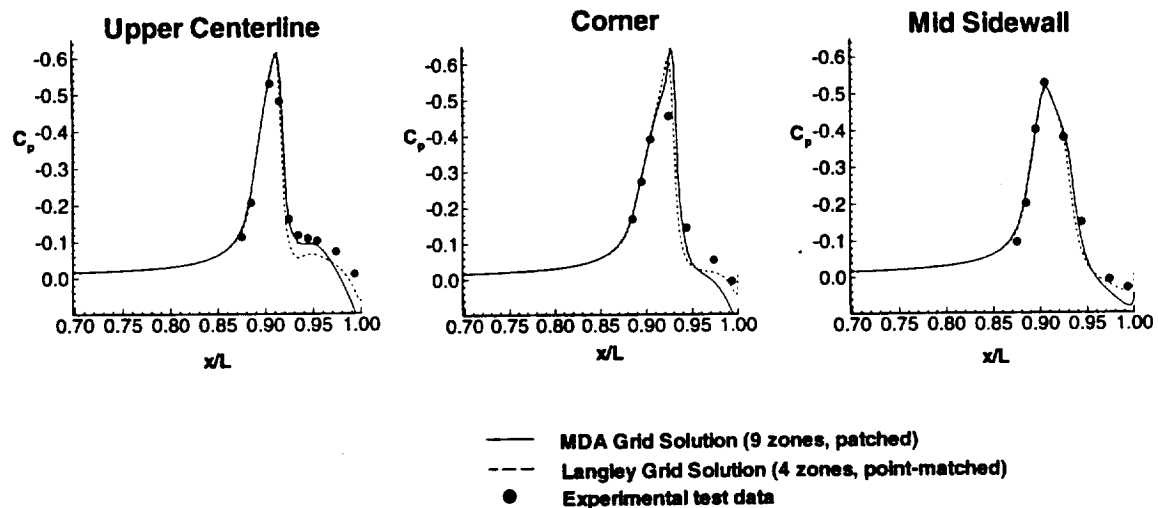
The surface pressure distributions and the computed surface oil flow pattern (CFL3D with the Baldwin-Barth turbulence) are shown for the AGARD B.4.2 nozzle ($M_\infty = 0.938$, $\alpha = 0^\circ$) for which experimental test data are available. Based on the reference body length ($L = 64.03$ inches), flow at $Re = 21$ million was analyzed. Shock-induced flow separation in the boattail region is clearly seen.

During the analysis, the grid distribution effect and the turbulence model effect on the solutions were carried out. Two computational grids were used: a 9-zone MDA patched grid (approximately 1 million grid points) and a 4-zone NASA LaRC point-matched grid (approximately 1.3 million grid points). Regardless of the differences in total number of grid points, computational domain extent, and the actual grid point distributions, these two grids had similar values of y^+ (less than 3). In general, the computed surface pressures in the boattail region agreed well with the available experimental data (see the next figure).

Turbulence models used in this study were: (a) Baldwin-Barth (B-B) and (b) Spalart-Allmaras (S-A). Solutions with the S-A turbulence model showed a greater numerical instability than the B-B model. For this reason, only the solutions with the B-B turbulence model were carried out to a fully converged state (approximately 6000 iterations were required). The slow convergence rate was due to the slow settlement of the flow separation location.

Pressure Distribution Comparisons for the AGARD B.4.2 Nozzle

(CFL3D, Baldwin-Barth turbulence model, $M_\infty=0.938$, $Re=21$ million)



The computed pressure distributions in the boattail region of the AGARD B.4.2 nozzle are shown. The computational results were obtained from the CFL3D code (Baldwin-Barth turbulence model) with two grids, i.e. the MDA 9-zone patched grid and the NASA LaRC 4-zone grid (see discussions on the previous page).

In general, the computed surface pressures in the boattail region agree well with the available experimental data. The shock location is accurately predicted. However, the solution from the 9-zone grid shows better agreement with the experimental data in shock strength on the top of the boattail. The solution from the 4-zone grid, on other hand, shows better agreement in pressure recovery at the boattail trailing edge. The differences in the solutions are due to the different point distributions employed in the two grids. For the 9-zone grid, the grid lines were stretched toward the expected shock location and the boattail trailing edge. For the 4-zone grid, on the other hand, the grid spacing was relatively uniform in the boattail region.

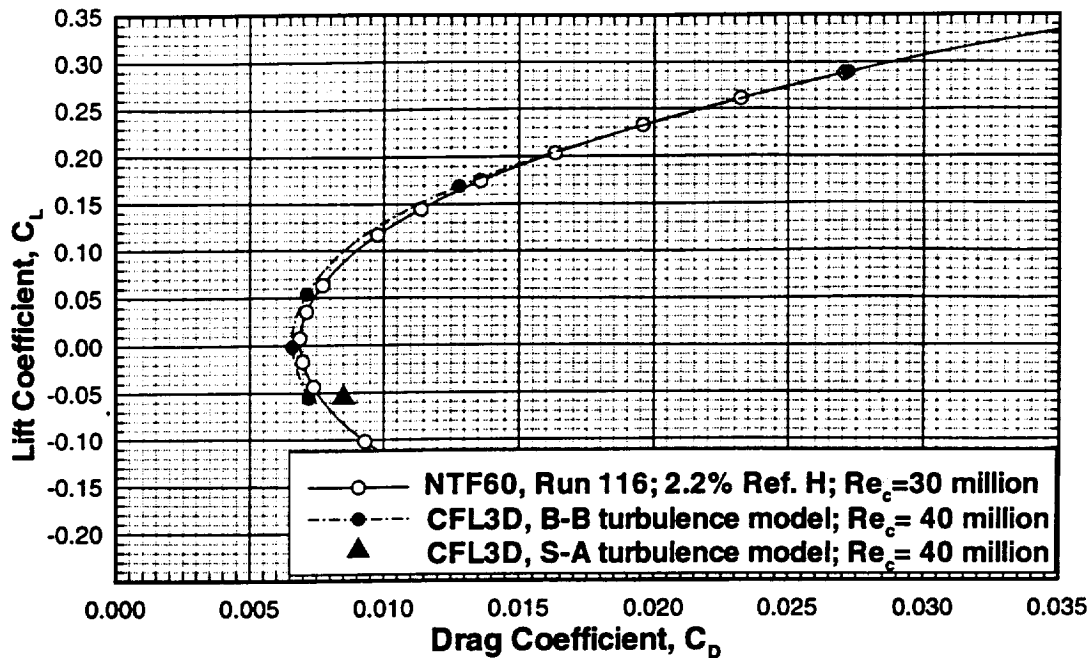
Ref. H Wing/Body Analysis

- Computational grid
 - C-O wing/body grid, 1.25 million grid points
 - y^+ less than 2 on the wing
- CFL3D solutions
 - Baldwin-Barth, Spalart-Allmaras, and Baldwin-Lomax (D-S) turbulence models
 - Baldwin-Barth turbulence model selected for W/B/N/D studies
 - Drag polars ($M_\infty=0.9, 1.1$; $Re_C = 40$ million); Baldwin-Barth turbulence model

A C-O grid topology was used for the Ref. H wing/body calculations. The total number of grid points used was approximately 1.25 million with y^+ less than 2 on the wing. Initially, flows for $M_\infty=0.9$ and 1.1 with $\alpha=0^\circ$ and 2° at $Re_C = 40$ million were computed. Solutions obtained from the CFL3D code with different turbulence models, i.e. the Baldwin-Barth (B-B), the Spalart-Allmaras (S-A), and the Baldwin-Lomax (Degani-Schiff option) turbulence models, were compared with the available wind-tunnel test data ($Re_C = 30$ million). It was concluded that the solutions with the B-B turbulence model agree better with the experimental test data (see next figure).

Based on the previous B.4.2 nozzle and the present Ref. H wing/body CFD experiences, the B-B model was selected for the installed Ref. H axisymmetric nozzle boattail drag study. Prior to the installed nozzle boattail study, the drag polars for the Ref. H wing/body configuration were obtained using the CFL3D code with the B-B turbulence model for $M_\infty=0.9$ and 1.1 ($Re_C = 40$ million) with $\alpha=0^\circ, 1^\circ, 2^\circ, 4^\circ$ and 6° . These W/B drag polars will be shown later with the computed W/B/N/D results.

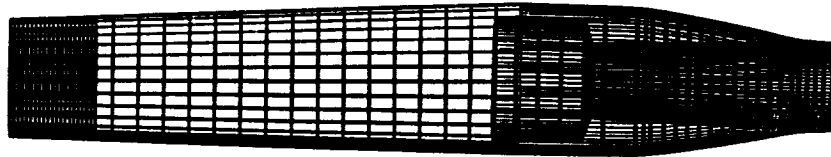
Ref. H Wing/Body Drag Polars; $M_\infty=0.9$



CFL3D results with the Baldwin-Barth (B-B) and the Spalart-Allmaras (S-A) turbulence models for $Re_c=40$ million are compared with the available wind-tunnel test data ($Re_c=30$ million). The comparison indicates that the B-B turbulence model results agree better with the experimental test data. Further study indicated that the overprediction in C_D by the S-A model was caused by the over-prediction in turbulence length scale implemented in the CFL3D code (version 4.0). The length scale calculations has recently been modified in a newer CFL3D version. However, the wing/body cases were not re-calculated for the S-A turbulence model in the present study.

Isolated Axisymmetric Nozzle Boattail Analysis

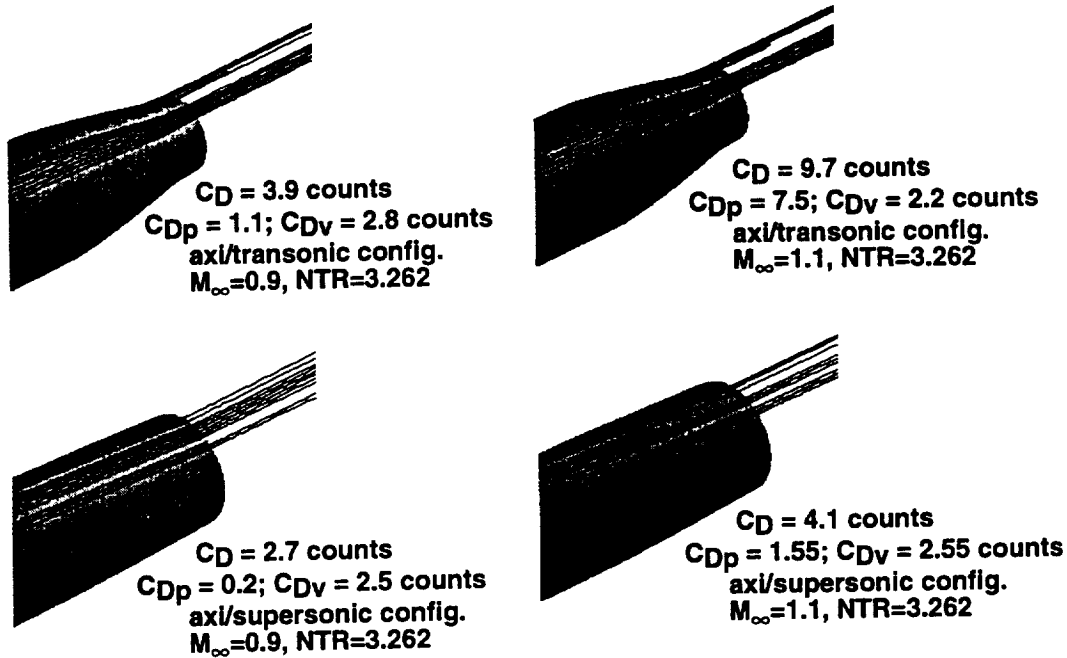
- Ref. H axi/transonic and axi/supersonic nozzle boattail configurations
 - $M_\infty = 0.9, 1.1$; Baldwin-Barth turbulence model
 - 3-zone; 2.0 million grid points
 - Flow normal to the nacelle inlet face, no spillage at nacelle inlet
 - $M_{\text{nozzle}}, T_t, P_t$, and flow angles specified in the nozzle plenum



Solutions for the isolated Ref. H axisymmetric transonic (axi/transonic) and supersonic (axi/supersonic) nozzle boattail configurations were obtained for the $M_\infty=0.9$ and 1.1 cases. The free stream flow direction was set normal to the nacelle inlet face, i.e. $\alpha=0^\circ$. Nacelle inlet pressure was specified such that no flow spillage occurred at the nacelle inlet. The nozzle total pressure, total temperature, and nozzle flow angles at the nozzle plenum were also specified. Solutions were obtained using CFL3D with the Baldwin-Barth turbulence model. A 3-zone grid with 2 million grid points was used.

Computed Oil Flow Particle Traces for the Isolated Ref. H Nozzle Boattail Configurations

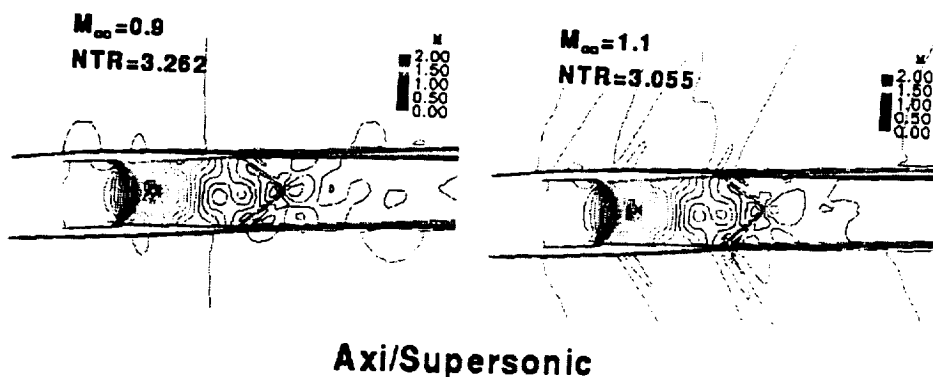
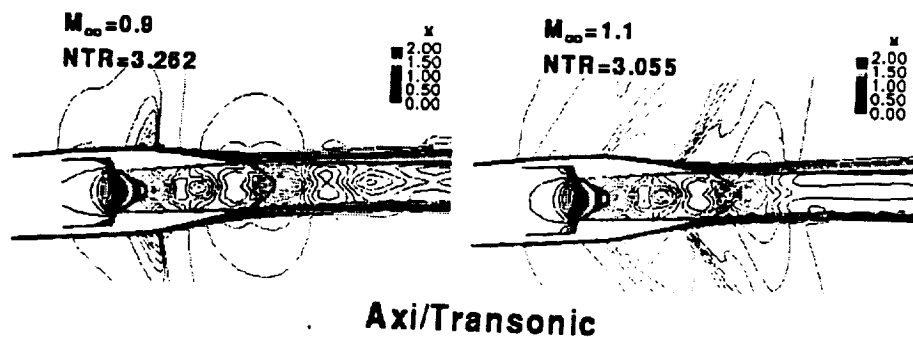
(CFL3D, B-B turbulence model, $Re_c=40$ million, NPR=5.0)



The computed oil flow particle traces for the isolated Ref. H axi/transonic and axi/supersonic nozzle boattail configurations are shown for the $M_\infty=0.9$ and 1.1 cases. For all of the cases studied, no evidence of flow separation is observed. Also shown in this figure are the total C_D based on the wing reference area for these isolated nozzle boattail configurations at different free stream conditions. The CFL3D solutions indicate that C_D increases with increasing M_∞ . The C_{Dp} and C_{Dv} shown in the figure represent the pressure drag and the viscous drag, respectively. It is clearly seen that the pressure drag is the primary source of the total drag for the $M_\infty=1.1$ transonic configuration case.

Mach Contours for the Isolated Ref. H Nozzle Boattail Configurations

($Re_c=40M$; $\alpha=0^\circ$; $NPR=5.0$; $T_\infty=390^\circ R$)



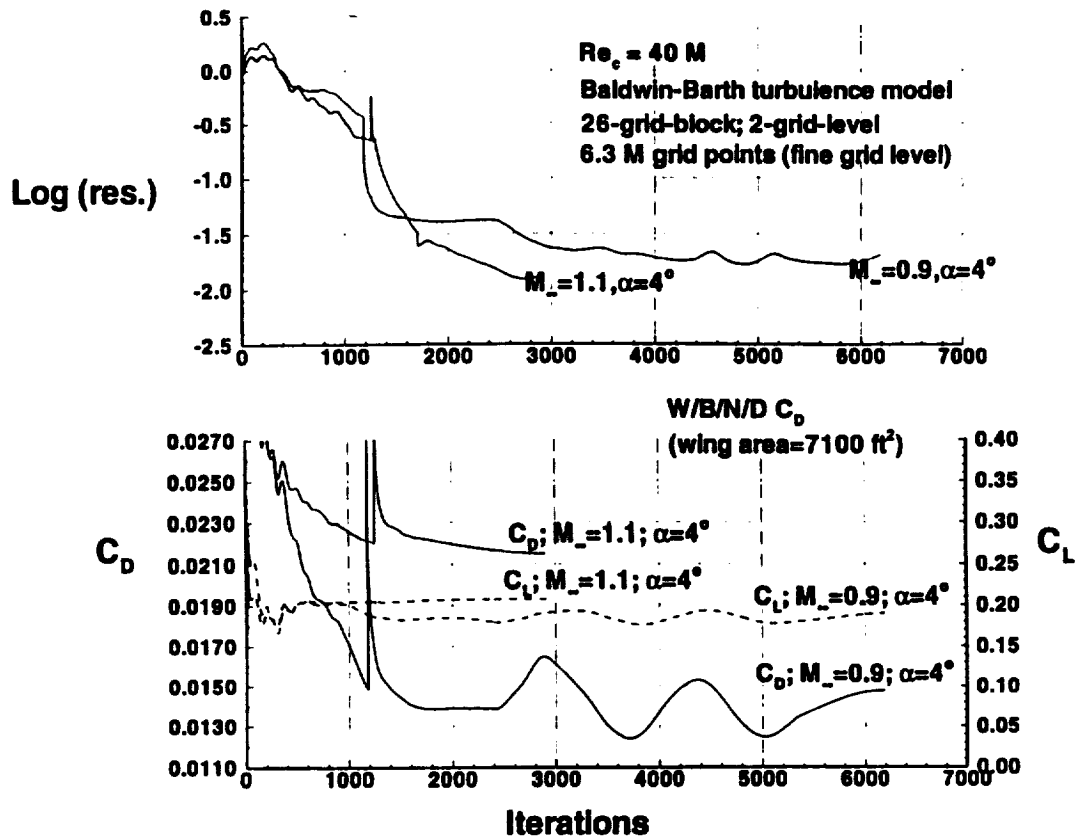
Mach contours for the isolated Ref. H axi/transonic boattail configuration are shown. For the $M_\infty=1.1$ case, the shock moves toward the boattail trailing edge (the nozzle exit face) and the pressure drag becomes significantly higher than for the $M_\infty=0.9$ case. Similar phenomena is observed for the axi/supersonic configuration. Details of the breakdown of the boattail drag for these configurations are shown on the previous chart.

Installed Ref. H Nozzle Boattail Analysis

- Installed Ref. H axi/transonic nozzle boattail configuration
 - $M_\infty = 0.9, 1.1$; $\alpha = 2^\circ, 4^\circ, 6^\circ$; $Re_C = 40$ million, Baldwin-Barth turbulence model
 - 26-zone, 6.3 million grid points

A 26-zone grid with 6.3 million grid points was used for analyzing the installed Ref. H axisymmetric nozzle boattail configuration. The cases included $M_\infty = 0.9$ and 1.1 with 2° , 4° , and 6° angles-of-attack at $Re_C = 40$ million. The CFL3D code with the Baldwin-Barth turbulence model was used. The flow analysis approach used for the isolated nozzle boattail cases was fully implemented for the installed cases. Similar to the isolated nozzle boattail cases, the nozzle flow conditions were specified in the nozzle plenum.

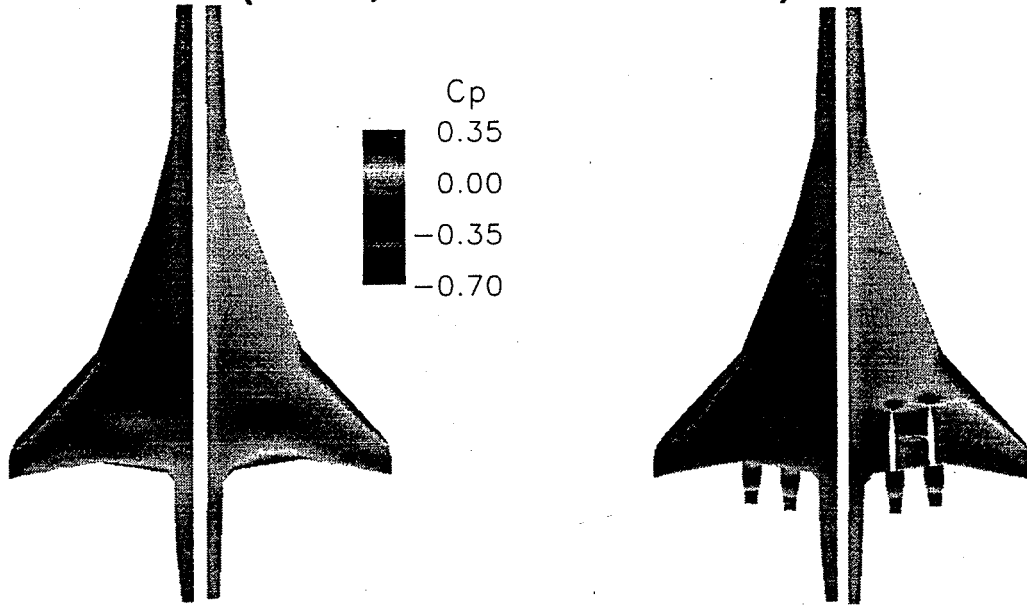
Installed Ref. H Axi/Transonic Nozzle Boattail CFL3D Convergence History



The CFL3D convergence histories for the $M_\infty=0.9$ and 1.1 ($\alpha=4^\circ$) are shown. This figure illustrates that many iterations are required to converge the $M_\infty=0.9$ case. The $M_\infty=1.1$ case, however, converges relatively quickly. Detailed flow field study for the $M_\infty=0.9$ case indicated that the shock location fluctuated near the upper wing trailing edge and caused the oscillation in C_D and C_L as seen in the convergence histories. The value of y^+ was less than 2 on the wing and was considered adequate for the present turbulent flow simulations. In addition to the $\alpha=4^\circ$ case, the $\alpha=2^\circ$ and $\alpha=6^\circ$ cases were also calculated. However, numerical instability developed for these cases. The cause for the instability problem was not fully understood during the course of this study.

Pressure Distributions for the Ref. H W/B and W/B/N/D Configurations

$M_\infty = 0.9$, $\alpha = 4^\circ$, $Re_c = 40$ million
(CFL3D, B-B turbulence model)



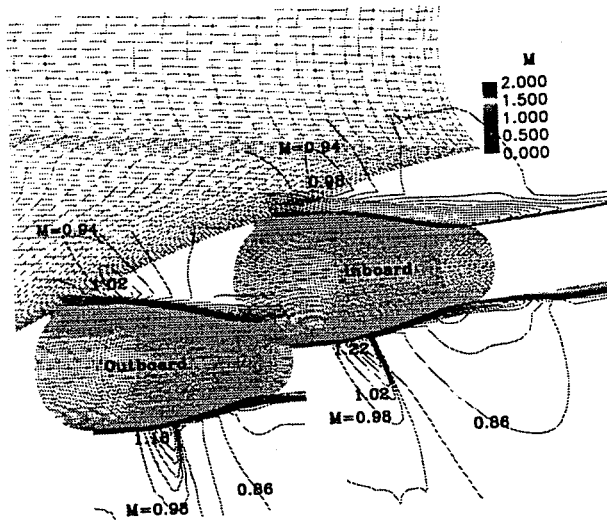
Upper surface Lower surface
 $C_L = 0.1692$, $C_D = 0.01280$

Upper surface Lower surface
 $C_L = 0.1880$, $C_D = 0.01466$

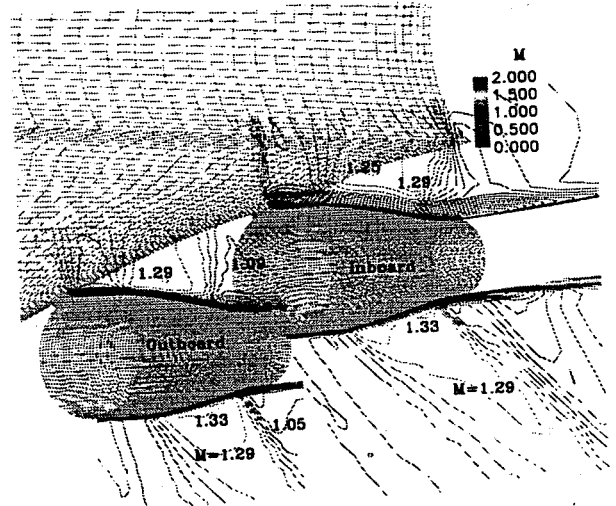
Wing pressure distributions for the $M_\infty = 0.9$, and 1,1; $\alpha = 4^\circ$ cases are shown. Comparing the upper wing surface pressure distributions of the wing/body case ($M_\infty = 0.9$, $\alpha = 4^\circ$) with the installed axi/transonic configuration, favorable interference is indicated. For the installed case, the nacelle installation reduces the flow re-compression at the trailing edge of the upper wing and reduces the flow expansion in the boattail region. Details of the interference effect in the boattail region will be shown later.

Comparing the lower wing surface pressure distributions, higher pressure is observed in the diverter leading-edge region for the installed case. However, the flow re-compression at the wing trailing edge is weaker comparing with the wing/body case. A shock is observed between the two diverters as seen in the figure.

Mach Contours for the Installed Ref. H Axi/Transonic Nozzle Boattail Configuration



$M_\infty=0.9, \alpha=4^\circ$

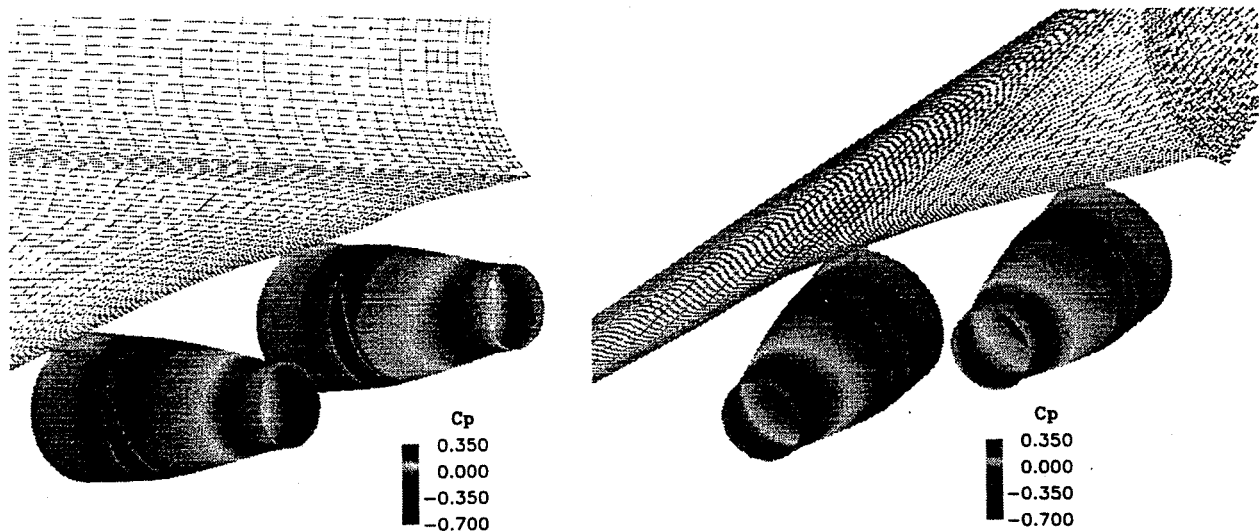


$M_\infty=1.1, \alpha=4^\circ$

(CFL3D, Baldwin-Barth turbulence model, $Re_c = 40$ million)

Shown above are Mach contours in the boattail region for the installed Ref. H axi/transonic nozzle boattail configuration for $M_\infty=0.9$. Similar to the isolated axi/transonic configuration, the boattail shock is clearly seen at the bottom of the boattail. However, on top of the boattail, favorable interference between the wing and the boattail is observed. As discussed earlier, the favorable wing and boattail interference (see the previous wing pressure distribution comparisons) reduces flow expansion in the boattail region. The boattail shock in that region completely disappears for both of the inboard and the outboard nozzle boattails as shown in above. Evidence of thick boundary layer in that region is also observed on the top of the boattail. Similar phenomenon is observed for the $M_\infty=1.1$ case.

Pressure Distributions at the Boattail Region for the Installed Axi/Transonic Nozzle Boattail Configuration

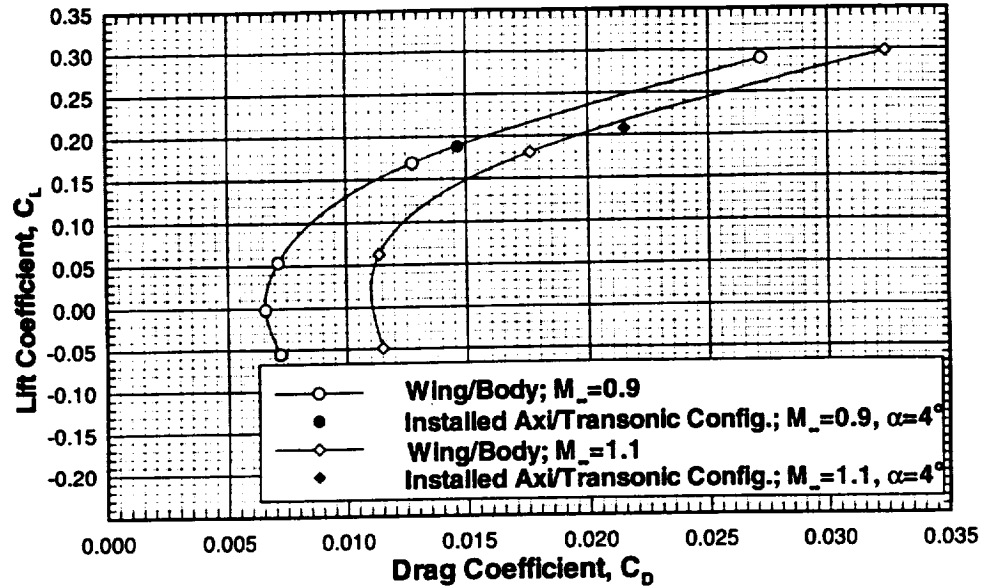


$$M_{\infty}=0.9, \alpha=4^{\circ}$$

(CFL3D, Baldwin-Barth turbulence model, $Re_c=40$ million)

The pressure distributions in the boattail region ($M_{\infty}=0.9, \alpha=4^{\circ}$) for the installed Ref. H axi/transonic configuration are shown. The extent of the favorable wing and boattail interference (no shock or weaker boattail shock) is limited to the upper half of the boattail surface. At the lower half of the boattail surface, the boattail shock indicates no favorable interference.

Drag Polars; CFL3D Navier-Stokes Analysis Baldwin-Barth Turbulence Model; $Re_C=40$ million



The C_L and C_D results for the full-scale installed Ref. H axi/transonic nozzle boattail configuration ($M_\infty=0.9, 1.1$) are shown. Also shown are the Ref. H wing/body drag polars. One concludes that the installation drag (the installed Ref. H nozzle boattail drag minus the Ref. H wing/body drag at a given C_L) for the $M_\infty=0.9; \alpha=4^\circ$ case is small. The installation drag for the $M_\infty=1.1$ case is approximately 10 counts at $C_L=0.205$. Calculations of the installation drag and the interference drag are shown on the next chart.

Installed Ref. H Axi/Transonic Configuration Installation and Interference Drag

Installation drag = $C_{D_{W/B/N/D}} - C_{D_{W/B}}$ (at constant C_L)

Interference drag = $C_{D_{W/B/N/D}} - C_{D_{W/B}} - 4C_{D_{Iso. Nacelle}}$

	C_D at $M_\infty=0.9; C_L=0.19$	C_D at $M_\infty=1.1; C_L=0.205$
Ref. H wing/body drag	146.0	205.0
Isolated Axi/Transonic (4)	15.6	38.8
Installed Axi/Transonic	146.0	215.0
Installation drag	0	10
Interference drag	-15.6	-28.8

Installation and interference drag values for the installed Ref. H axi/transonic nozzle boattail configuration are shown. The drag values are calculated at constant C_L 's for which CFL3D solutions are available, i.e. at $C_L=0.19$ and 0.205 for $M_\infty=0.9$ and 1.1 , respectively. For the cases calculated, favorable interference is obtained.

Summary and Conclusions

- CFL3D code (B-B turbulence model) validated for
 - AGARD B.4.2 nozzle and Ref. H W/B ($Re_c = 40$ million).
- Attached flow predicted for the isolated axi/transonic and axi/supersonic configurations.
 - Higher total drag for $M_\infty = 1.1$ is due to higher pressure drag at the boattail region.
- Favorable interference for the installed Ref. H axi/transonic configuration for $M_\infty = 0.9$ and 1.1 at $C_L \approx 0.2$.
- Numerical instability was overcome for the wing/body and the isolated nozzle boattail cases. For the installed case, the numerical instability requires further study. For the installed axi/supersonic case, solutions were not obtained due to grid quality problem in some of the grid zones.

Overall summary and conclusions from this study are described here.

Acknowledgments

HSR PAI Working Group

Eric Unger, Alan Arslan, Yoram Yadlin (MDA)

John Carlson (NASA LaRC)

Anthony Midea (NASA LeRC)

This study was conducted under the HSR Configuration Aerodynamics task. Numerous inputs were made by the PAI working group members. Special thanks are directed to Eric Unger for his help in completing the grid modifications for the installed wing/body/nacelle/diverter (W/B/N/D) cases, to Alan Arslan for his help in completing the CFL3D code validation, to Yoram Yadlin for his help in preliminary W/B/N/D grid generation, to John Carlson for technical discussions throughout the study, and to Anthony Midea for making computer time available for us to complete the B.4.2 isolated nozzle study.

Installed Transonic 2D Nozzle Nacelle Boattail Drag Study

Michael B. Malone and Charles C. Peavey
Northrop Grumman Military Aircraft Systems Division
Pico Rivera, California 90660

The Transonic Nozzle Boattail Drag Study was initiated in 1995 to develop an understanding of how external nozzle transonic aerodynamics effect airplane performance and how strongly those effects are dependent on nozzle configuration (2D vs. axisymmetric). MDC analyzed the axisymmetric nozzle. Boeing subcontracted Northrop-Grumman to analyze the 2D nozzle. All participants analyzed the AGARD nozzle as a check-out and validation case. Once the codes were checked out and the gridding resolution necessary for modeling the separated flow in this region determined, the analysis moved to the installed wing/body/nacelle/diverter cases.

The boat tail drag validation case was the AGARD B.4 rectangular nozzle. This test case offered both test data and previous CFD analyses for comparison. Results were obtained for test cases B.4.1 ($M=0.6$) and B.4.2 ($M=0.938$) and compared very well with the experimental data.

Once the validation was complete a CFD grid was constructed for the full Ref. H configuration (wing/body/nacelle/diverter) using a combination of patched and overlapped (Chimera) grids. This was done to ensure that the grid topologies and density would be adequate for the full model. The use of overlapped grids allowed the same grids from the full configuration model to be used for the wing/body alone cases, thus eliminating the risk of grid differences affecting the determination of the installation effects. Once the full configuration model was run and deemed to be suitable the nacelle/diverter grids were removed and the wing/body analysis performed. Reference H wing/body results were completed for $M=0.9$ ($\alpha=0.0, 2.0, 4.0, 6.0$ and 8.0), $M=1.1$ ($\alpha=4.0$ and 6.0) and $M=2.4$ ($\alpha=0.0, 2.0, 4.4, 6.0$ and 8.0). Comparisons of the $M=0.9$ and $M=2.4$ cases were made with available wind tunnel data and overall comparisons were good.

The axi-inlet/2D nozzle nacelle was analyzed isolated. The isolated nacelle data coupled with the wing/body result enabled the interference effects of the installed nacelles to be determined. Isolated nacelle runs were made at $M=0.9$ and $M=1.1$ for both the supersonic and transonic nozzle settings. All of the isolated nacelle cases were run at $\alpha=0$.

Full configuration runs were to be made at Mach numbers of 0.9, 1.1, and 2.4 (the same as the wing/body and isolated nacelles). Both the isolated nacelles and installed nacelles were run with inlet conditions designed to give zero spillage. This was to be done in order to isolate the boattail effects as much as possible. Full configuration runs with the supersonic nozzles were completed for $M=0.9$ and 1.1 at $\alpha=4.0$ and 6.0 (4 runs total) and with the transonic nozzles at $M=0.9$ and 1.1 at $\alpha=2.0, 4.0$ and 6.0 (6 runs total). Drag breakdowns were completed for the $M=0.9$ and $M=1.1$ showing favorable interference drag for both cases.

***First NASA/Industry High Speed Research Configuration
Aerodynamic Workshop***

Generalized Compressible Navier-Stokes Code

- NASA Ames ARC Thin-Layer Navier-Stokes Algorithm
- Implicit, Node-Based Finite-Volume Scheme
- Multi-Block Structured Grids for Complex Geometries
- Class 1, 2, 3, & 4 Patched Block Interface Mappings
- Chimera Overlapping Grid Block Option
- Grid Sequencing & Multigrid Convergence Acceleration
- Menter's SST 2-Equation, Spalart-Allmaras, & Baldwin-Barth Turbulence Models
- Extensive Boundary Condition Menu

NORTHROP GRUMMAN

The CFD code used was the GCNSfv developed by Northrop/Grumman. It is based on the ARC3D thin-layer Navier-Stokes algorithm created at NASA Ames. The convergence method is an implicit, node-based finite-volume scheme. Complex geometries are analyzed by using multi-block structured grids. The boundary conditions between blocks can be specified as patched class 1 through 4, where the class 1 is point-to-point matching, class 2 is incremental point-to-point matching, class 3 is arbitrary face matching, and class 4 is arbitrary sub-face matching. A Chimera overlapping grid block option is also available. To reduce processing time, grid sequencing and multigrid convergence schemes can be used. GCNS provides three turbulence models to the user: Menter's SST 2-equation model, the Spalart-Allmaras model, and the Baldwin-Barth model. GCNSfv offers a wide variety of boundary conditions including propulsion specific conditions such as characteristic inflow (mass flow ratio and corrected mass flow, inlet bleed) and outflow (nozzle pressure ratio, nozzle temperature ratio) conditions. The code runs at approximately 12 μ s/iteration/gridpoint on the Cray C-90 and parallelization allows the code utilize six of the available sixteen processors allowing effective use of the multi-task batch queue.

Transonic Boattail Drag Validation

- **Analyze AGARD 2D Nozzle Test Case B.4**
- **Validate GCNSfv Solution With Test Data**
- **Determine Grid Size and Spacing Requirements to Accurately Model the Flow**

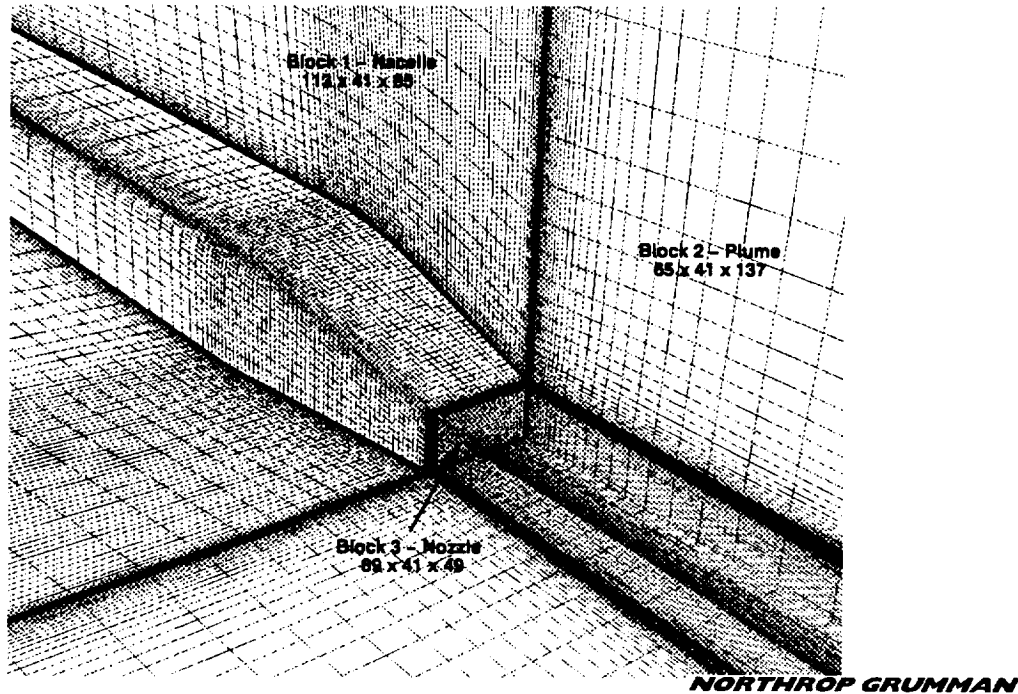
NORTHROP GRUMMAN

The purpose of modeling the AGARD B.4 test case was to validate the Northrop Grumman CFD method (GCNSfv) on a geometry similar to that of the Reference H 2D nozzle nacelles. AGARD test case B.4.2 ($M=0.938$) is a particularly difficult case with a shock induced separation. The test case was also used to determine the appropriate grid spacings required to accurately model the flow and give some insight on how to build the grids for Reference H configuration.

**First NASA/Industry High Speed Research Configuration
Aerodynamic Workshop**

AGARD Nozzle B.4 Validation Case

Computational Grid - Quarter Symmetry

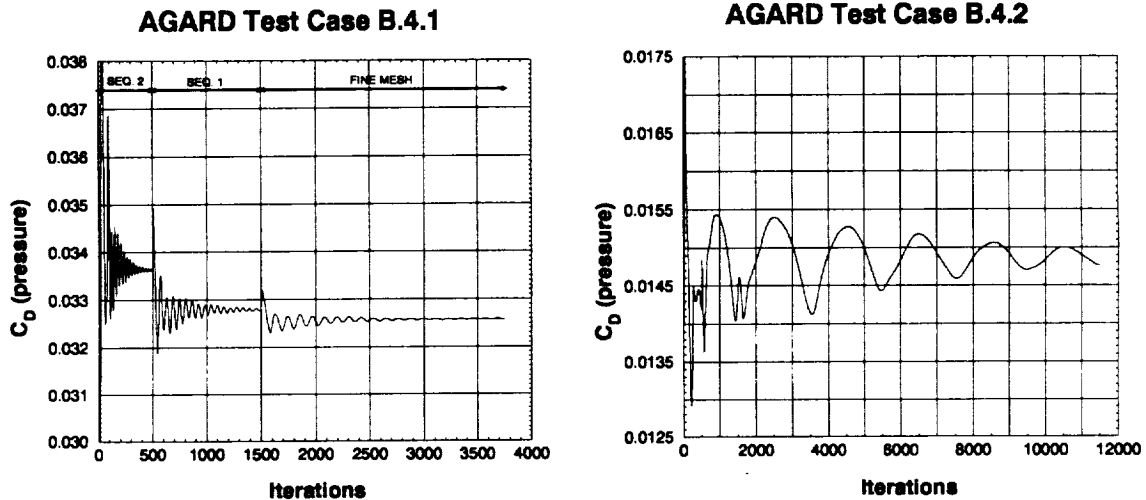


The CFD grid for the AGARD nozzle is shown. The outer surface grid of the nacelle was generated from the existing LaRC grid using the identical axial grid distribution while increasing the circumferential grid density. Additionally, the topology of the nozzle and plume blocks were changed and the extent of the grid to the far field was expanded. The test condition of $\alpha = -0.02$ was approximated as $\alpha = 0.0$ to enable a quarter symmetric model and reduce run time.

**First NASA/Industry High Speed Research Configuration
Aerodynamic Workshop**

Boattail Drag Validation Case

AGARD B.4 Test Case – Drag Convergence History



NORTHROP GRUMMAN

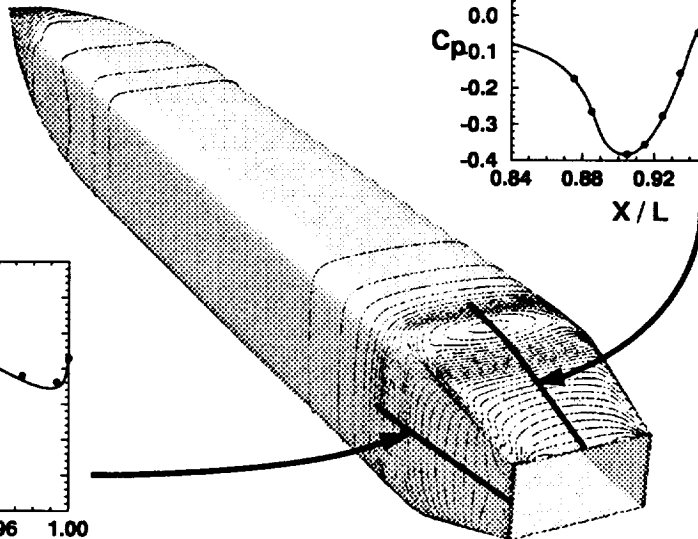
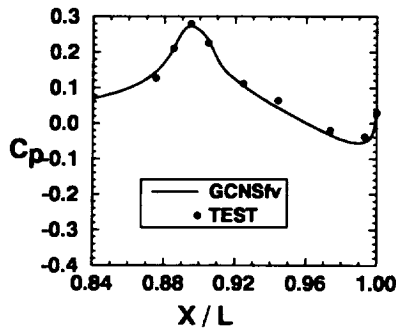
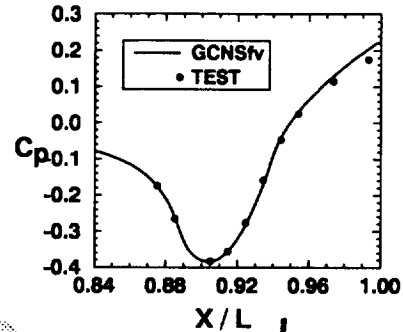
Drag convergence histories are plotted for the B.4.1 and B.4.2 test cases. The drag coefficient is only the pressure component, viscous drag calculations are not currently tracked by GCNSfv. The plots illustrate that a lot of iterations are required to converge the transonic (B.4.2, $M=0.938$) case. The subsonic case (B.4.1, $M=0.6$) converges very quickly at all sequence levels. Careful monitoring of the solution for the transonic case showed that the shock location and strength set up very quickly, but the separated flow on the nozzle upper surface continued to fluctuate. This is what causes the oscillatory nature seen in the convergence history. Values of y^+ were less than 3.0 everywhere on the surface which should be more than adequate for the turbulence model (Menter $k-\omega$ SST).

**First NASA/Industry High Speed Research Configuration
Aerodynamic Workshop**

Boattail Drag Validation – AGARD Test Case B.4.1

Contours of C_p on Surface
 C_p min, max, delta: -0.40, 0.30, 0.0225

M = 0.600
 $Re_L = 17.3 \times 10^6$
NPR = 4.00
NTR = 0.987
 $T_\infty = 548.32$ R

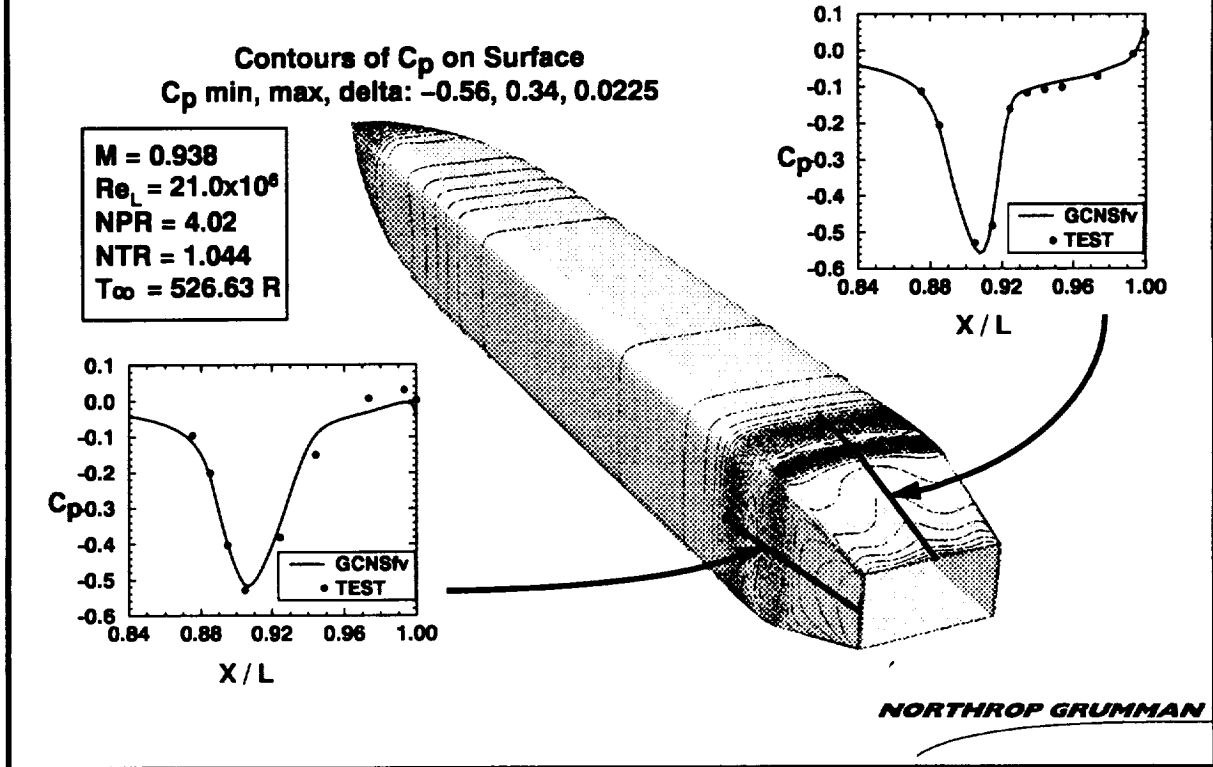


NORTHROP GRUMMAN

Contours of C_p on the surface are shown for case B.4.1. Flow conditions for test case B.4.1 are $M=0.6$, $Re_L=17.3 \times 10^6$, $NPR=4.0$, nozzle temperature ratio (NTR , T_{tot}/T)= 0.987 , and free stream static temperature was 548.32 R. Line plots comparing C_p to test data (rows 1 and 5) and their locations are also shown. The solution agrees well with the test data.

**First NASA/Industry High Speed Research Configuration
Aerodynamic Workshop**

Boattail Drag Validation – AGARD Test Case B.4.2

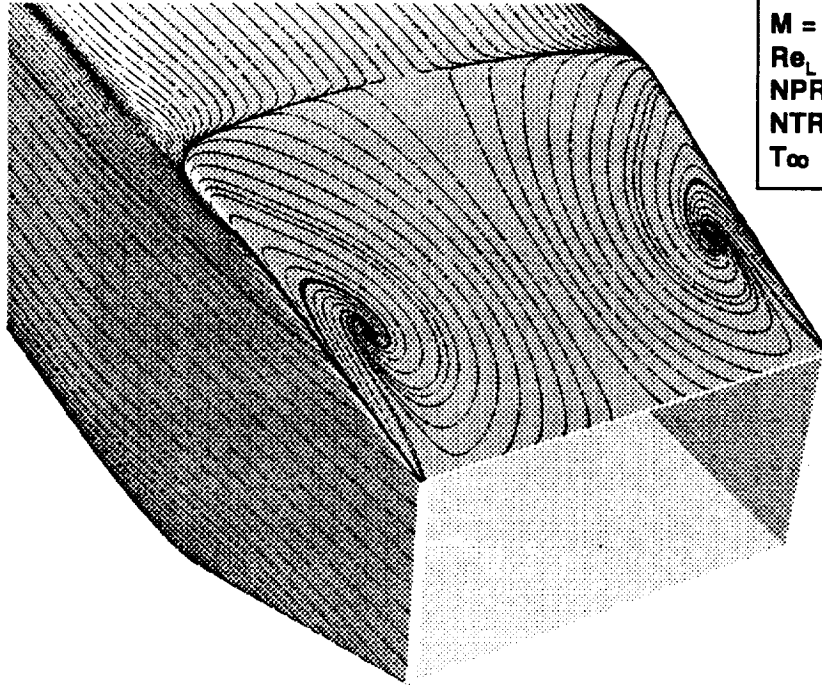


Contours of C_p on the surface are shown for case B.4.2. Flow conditions for test case B.4.2 are $M=0.938$, $Re_L=21.0 \times 10^6$, $NPR=4.002$, $NTR=1.044$, and free stream static temperature was 526.63 R. Line plots comparing C_p to test data (rows 1 and 5) and their locations are also shown. As shown the solution agrees well with the test data, predicting shock location and strength to give the correct pressure recovery on the upper surface..

**First NASA/Industry High Speed Research Configuration
Aerodynamic Workshop**

GCNSfv CFD Analysis – AGARD Test Case B.4.2

Simulated Surface Oil Flow



$M = 0.938$
 $Re_L = 21.0 \times 10^6$
 $NPR = 4.02$
 $NTR = 1.044$
 $T_\infty = 526.63 \text{ R}$

NORTHROP GRUMMAN

Surface oil flows (streamlines restricted near the surface) are shown for test case B.4.2. The streamlines clearly show the separation line and reverse flow on the rear upper surface.

***First NASA/Industry High Speed Research Configuration
Aerodynamic Workshop***

Wing/Body Validation

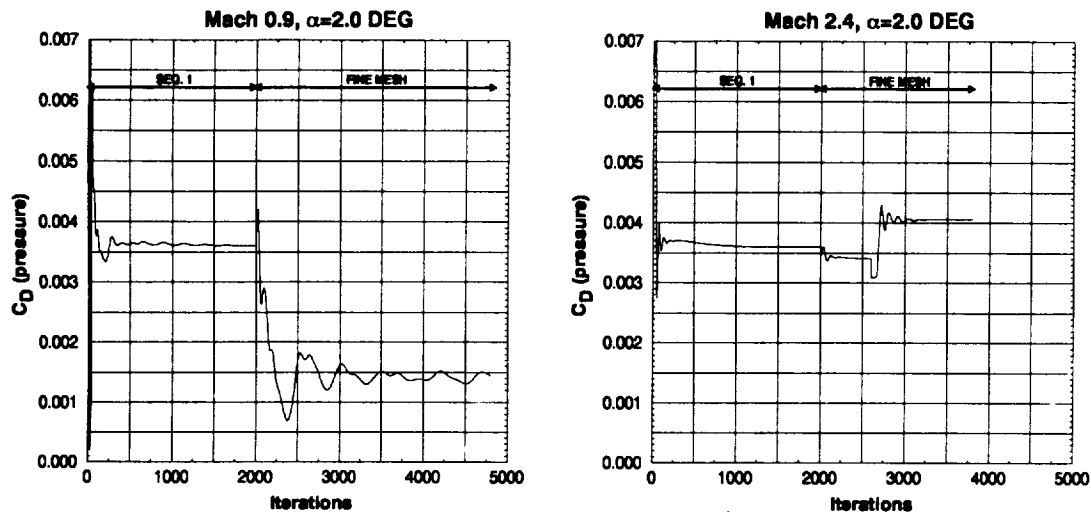
- **Model Ref. H Wing/Body (Without Tails) at Re=40 Million**
- **Compare M=0.9 and M=2.4 Runs to Test Data**
- **Use FOMOCO for Force and Moment Integrations**
- **Fuselage Integrated to F.S.=2764.3 to Account for Sting**
- **CFD Data Corrected to Test Reynolds Number Using Flat Plate Skin Friction Data**

NORTHROP GRUMMAN

The wing body runs were made using the grids from the full configuration model. Wind tunnel data was available for M=0.9 and 2.4, although runs were also made at M=1.1 for the interference drag analysis. All of the CFD analysis for this task was run at $Re=40 \times 10^6$. The M=0.9 results were compared to the NTF wind tunnel data at a $Re=30 \times 10^6$ and the M=2.4 results were compared to the ARC 9x7 data at $Re=7 \times 10^6$. The CFD data was corrected to the appropriate Reynolds number using flat plate skin friction corrections. In addition, the fuselage in the CFD analysis was integrated only up to the fuselage station 2764.3 to account for the presence of the sting in this test configuration. The wing/body CFD analysis was used for validation and in the drag buildup calculations. The NASA-Ames integration code, FOMOCO, was used to post-process the (overset grid) solutions and produce the total force and moment coefficients including pressure and viscous contributions.

First NASA/Industry High Speed Research Configuration Aerodynamic Workshop

Wing/Body - Drag Convergence History



NORTHROP GRUMMAN

The drag convergence histories for the Mach 0.9 and 2.4 cases at 2 degrees angle of attack are shown. In GCNS the pressure drag coefficient was calculated at each iteration, but as a means of reducing processing time, the viscous drag convergence history is not generated by GCNS. The overlapping region of the wing and body grids was counted twice in GCNS. This method is permissible because only the convergence trend is of interest. Each case was run 2000 iterations on the sequenced grid prior to iterations on the fine mesh.

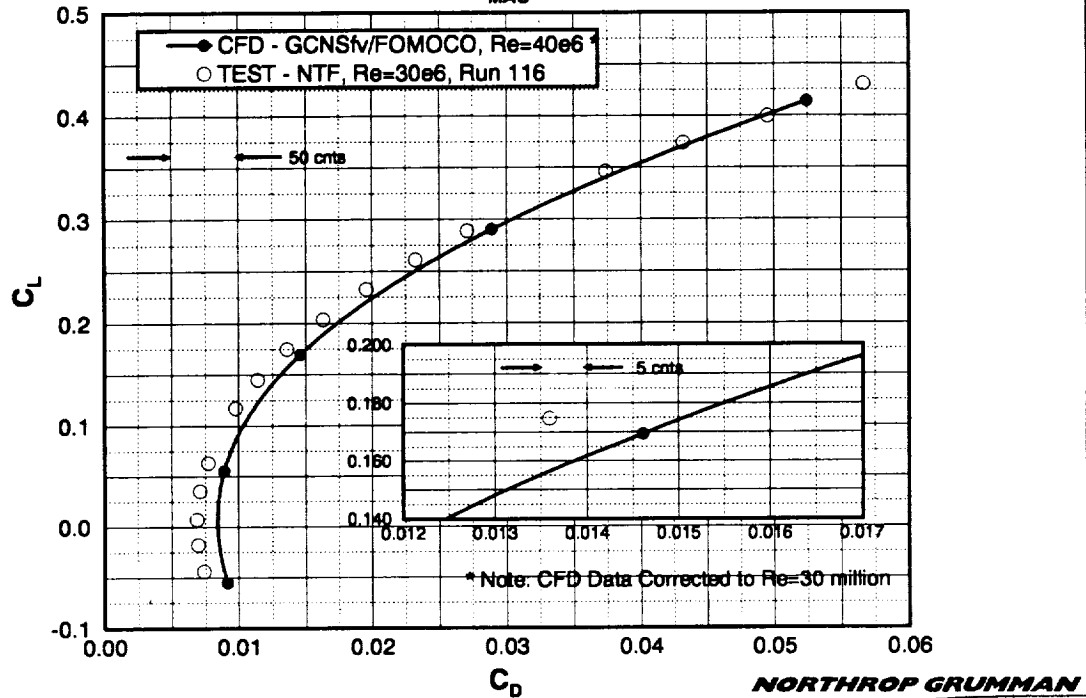
The pressure drag converged at approximately 36 counts (0.0036) for the Mach 0.9 sequenced grid. Fine mesh iterations began after 2,000 sequenced grid iterations. After 1,500 iterations on the fine mesh (cumulative iteration number 3,500), the pressure drag decreased to approximately 14 counts (0.0014) and oscillated in a 2 count bandwidth. An additional 1,200 fine mesh iterations failed to further damp out this trend. The oscillations in pressure drag are due to the transonic effects in the flowfield.

For the Mach 2.4 case, the sequenced grid converged quickly to 36 counts (0.0036). As in the Mach 0.9 case, the fine mesh iterations began after 2,000 sequenced grid iterations. After 1300 fine mesh iterations (cumulative iteration number 3,300), the pressure drag increased and converged at 41 counts (0.0041) with less than a tenth of a count (0.00001) of variation.

**First NASA/Industry High Speed Research Configuration
Aerodynamic Workshop**

Wing/Body Validation – Boeing Ref. H Configuration

**Ref. H Wing/Body Drag Polar
Mach 0.9, $Re_{MAC}=30$ million**

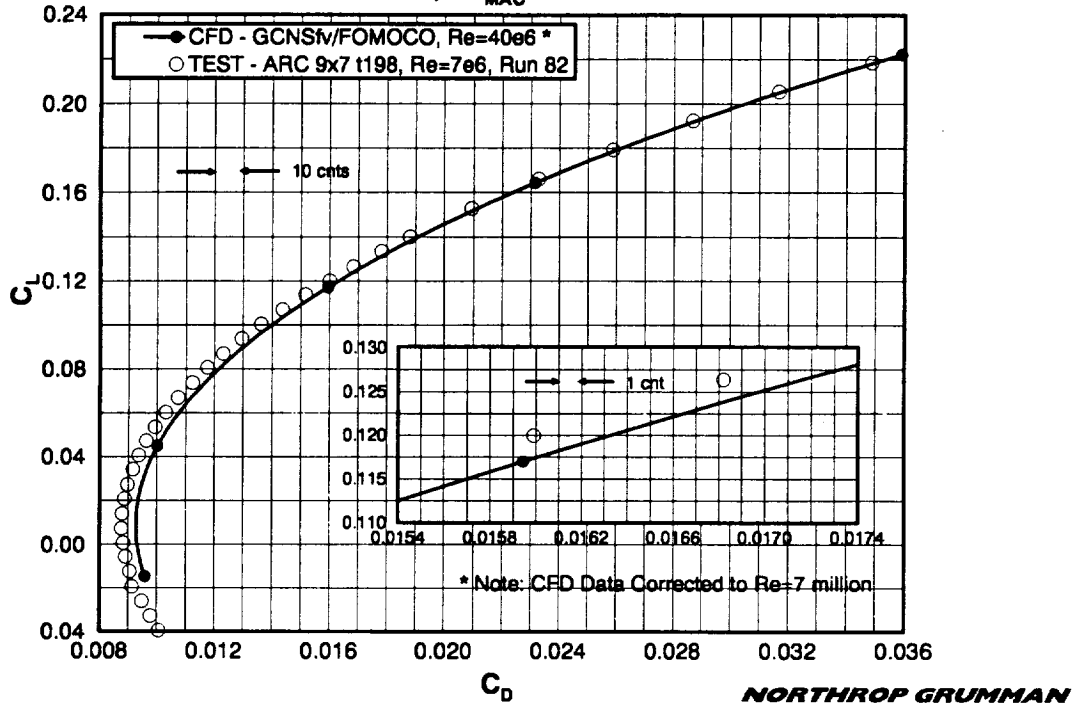


A drag polar for the Mach 0.9 case is shown comparing the CFD analysis to the NTF wind tunnel data. The inset highlights the area around $\alpha=4^\circ$ and shows the CFD data, after correcting to $Re=30 \times 10^6$, is about 15 counts high.

**First NASA/Industry High Speed Research Configuration
Aerodynamic Workshop**

Wing/Body Validation – Boeing Ref. h Configuration

Ref. H Wing/Body Drag Polar
Mach 2.4, $Re_{MAC}=7$ million



A drag polar for the Mach 2.4 case is shown comparing the CFD analysis to the ARC 9x7 wind tunnel data. The inset highlights the area around the cruise lift point and shows the CFD data, after correcting to $Re=7 \times 10^6$, is about 3 counts high. This data compared much better than the $M=0.9$ case.

***First NASA/Industry High Speed Research Configuration
Aerodynamic Workshop***

Isolated Nacelles

- **Model Isolated Nacelle with Transonic and Supersonic Nozzle Settings**
- **Nacelles Run at Zero Angle of Attack with Inlet Face Aligned to the Freestream Flow**
- **Orientation Allowed Half Model to be Generated**
- **Drag Integrations Included Only the External Surfaces**

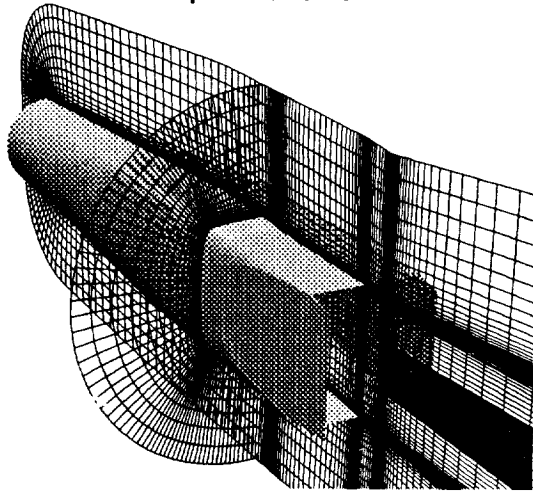
NORTHROP GRUMMAN

Isolated nacelles were run at $M=0.9$, 1.1, and 2.4 for the supersonic nozzle setting and at $M=0.9$ and 1.1 for the transonic nozzle setting. The nacelle geometry was oriented with the inlet face normal to the freestream flow and run at zero angle of attack. Half models of the nacelle were generated using similar grid spacings and topologies as the installed nacelles. The grids for the installed nacelles could not be used directly because they included the integrated diverter. Only the external surfaces were considered in the force integrations. Inlet and nozzle (including the parts of the side walls scrubbed by the nozzle flow) surfaces were not included.

**First NASA/Industry High Speed Research Configuration
Aerodynamic Workshop**

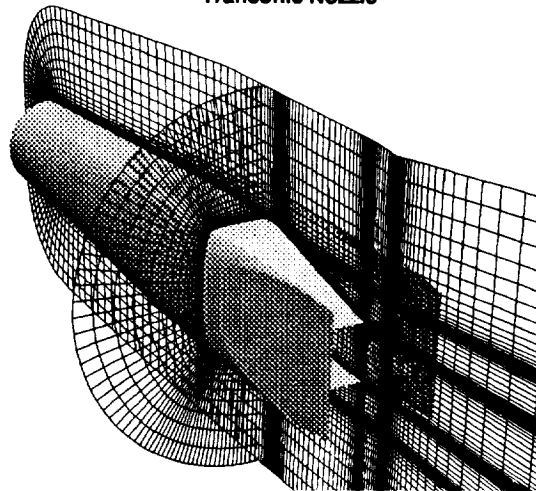
Isolated 2D Nozzle Nacelle – Computational Grid

Supersonic Nozzle



4 Blocks, 1.25 Million Grid points

Transonic Nozzle



6 Blocks, 1.5 Million Grid points

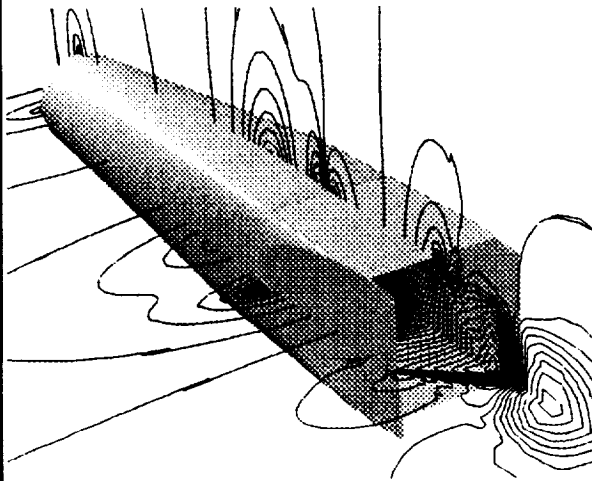
NORTHROP GRUMMAN

Grids for the isolated nacelles are shown. The supersonic nozzle case used four blocks and 1.25 million grid points and the transonic nozzle case used six blocks and 1.5 million grid points. Both geometries were run half symmetric. Again, to provide grid consistency between cases, the transonic nozzle case used the same nacelle grid as the supersonic nozzle with the addition of two "wedge" blocks to model the deflected nozzle flaps.

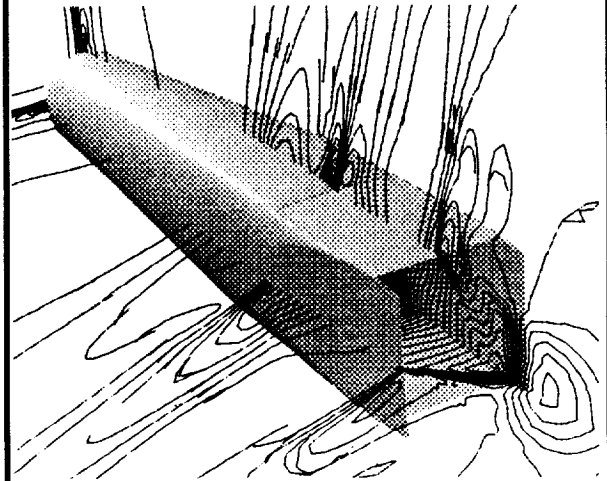
**First NASA/Industry High Speed Research Configuration
Aerodynamic Workshop**

Isolated 2D Nozzle Nacelle, Supersonic Configuration

Mach=0.9, NTR=3.264, NPR=5.0



Mach=1.1, NTR=3.056, NPR=5.0



Contours of C_p on the symmetry and half planes

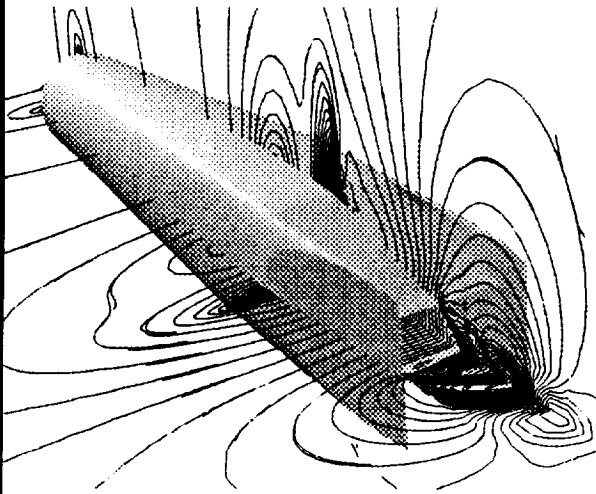
NORTHROP GRUMMAN

Pressure contours on the symmetry and horizontal mid-planes are shown for the isolated nacelle with the supersonic nozzle setting at Mach numbers of 0.9 and 1.1. Effects of the nozzle flap hinge line and the side wall tapering can be seen in the contours but the flow stays attached for both cases.

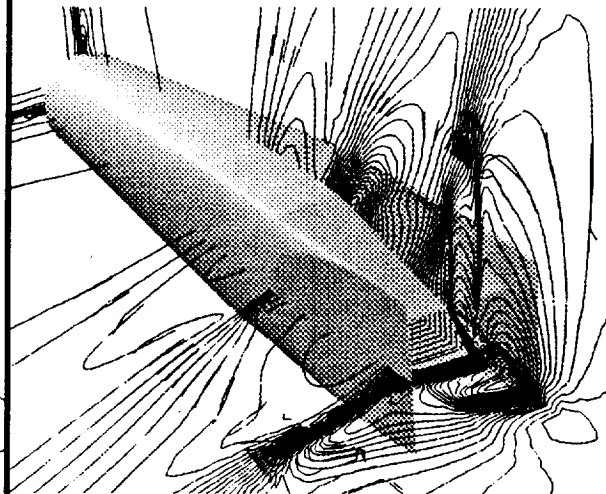
**First NASA/Industry High Speed Research Configuration
Aerodynamic Workshop**

Isolated 2D Nozzle Nacelle, Transonic Configuration

Mach=0.9, NTR=3.264, NPR=5.0



Mach=1.1, NTR=3.056, NPR=5.0



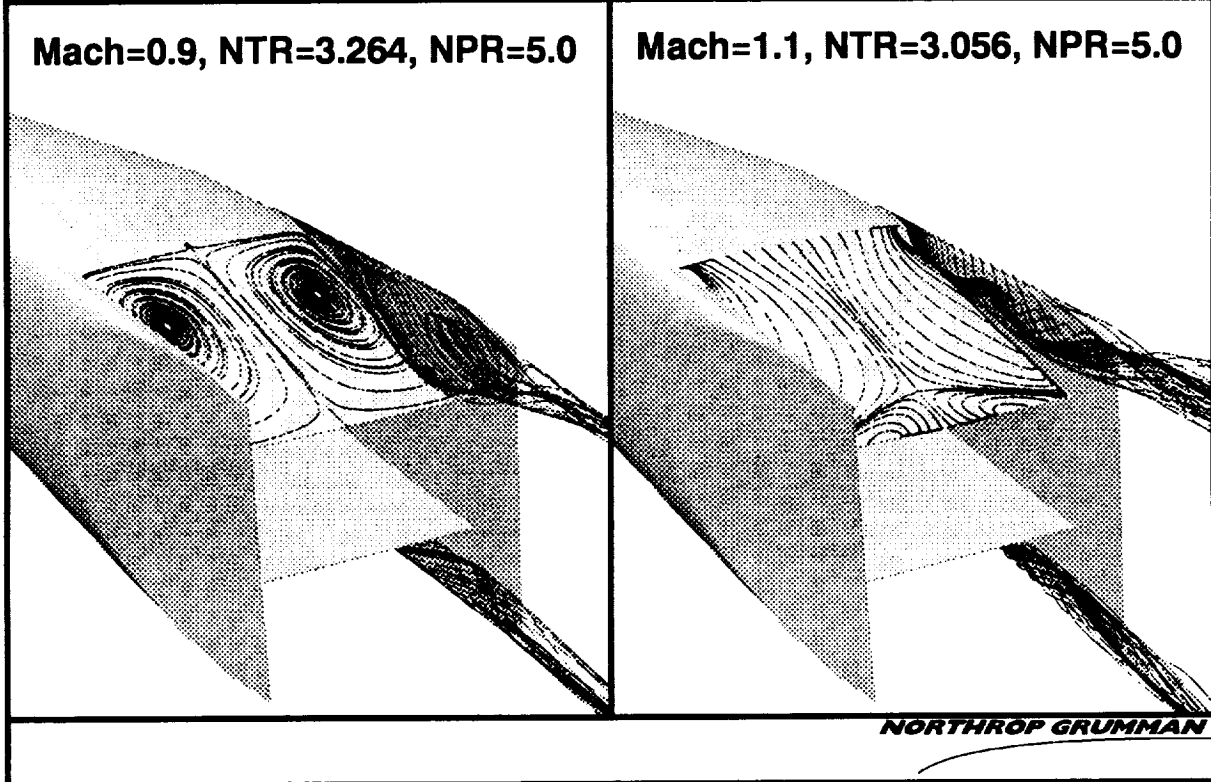
Contours of Cp on the symmetry and half planes

NORTHROP GRUMMAN

Pressure contours on the symmetry and side planes are shown for the isolated nacelle with the transonic nozzle setting at Mach numbers of 0.9 and 1.1. For the $M=0.9$ case a normal shock develops at the nozzle hinge line, separating the flow over the flap upper surface giving way to a pressure recovery. In the Mach 1.1 case the flow shocks weakly at the hinge line but, stays attached, smoothly recompressing until a normal shock forms at the trailing edge, where the flow is turned by the plume. By staying attached and accelerating over the surface the flow causes a lower pressure region in this case.

**First NASA/Industry High Speed Research Configuration
Aerodynamic Workshop**

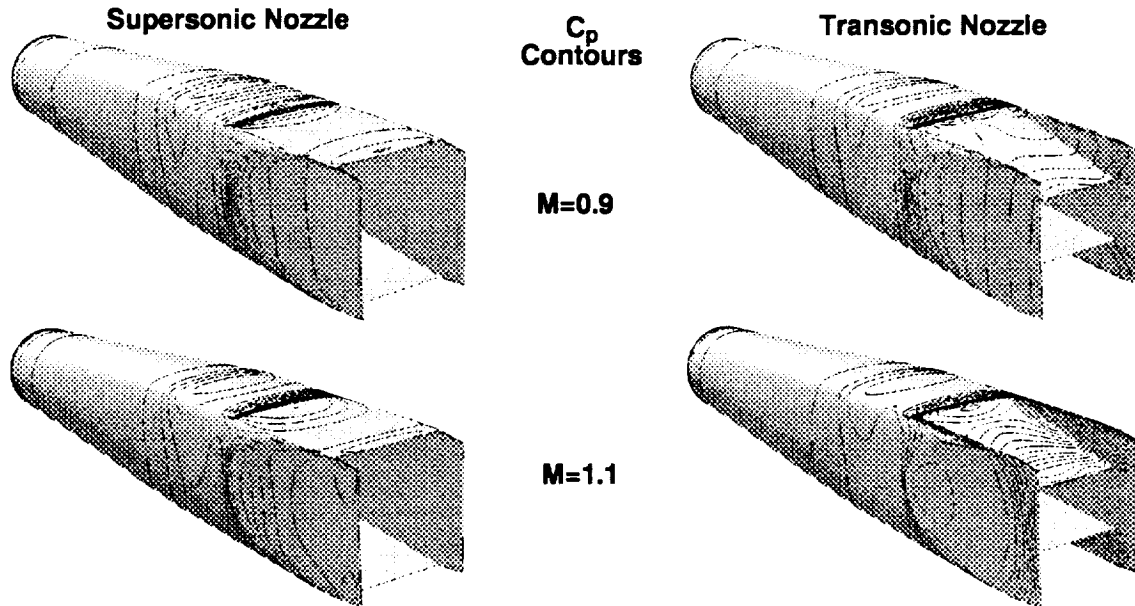
Isolated 2D Nozzle Nacelle, Transonic Configuration



Surface streamlines (simulated oil flow) and streamlines off of the side walls are shown for the isolated nacelle with the transonic nozzle setting for $M=0.9$ and 1.1 . As can be seen from the oil flows for the $M=0.9$ case the flow is separated over the entire flap upper surface. The surface oil flow for the $M=1.1$ case shows that the flow stays attached to nearly the nozzle exit.

**First NASA/Industry High Speed Research Configuration
Aerodynamic Workshop**

Isolated 2D Nozzle Nacelle



Mach	C_D SS Nozzle	C_D TS Nozzle	ΔC_D
0.9	0.000634	0.001102	0.000468
1.1	0.000878	0.002298	0.001420

NORTHROP GRUMMAN

For the thrust/drag bookkeeping, the difference in drag between the isolated nacelles with the supersonic and transonic nozzle settings is considered a thrust term. The geometries for the two configurations with C_p contours on the surface are shown for the Mach 0.9 and 1.1 cases. The table shows the drag values for each configuration and the delta between the supersonic and transonics nozzles which is the "boattail drag".

***First NASA/Industry High Speed Research Configuration
Aerodynamic Workshop***

Wing/Body/Nacelle/Diverter

- **Model Wing/Body/Nacelle/Diverter with Transonic and Supersonic Nozzle Settings**
- **Use the Force Integrations From the Full Configuration, the Wing/Body and the Isolated Nacelles to Determine the Interference Effects**

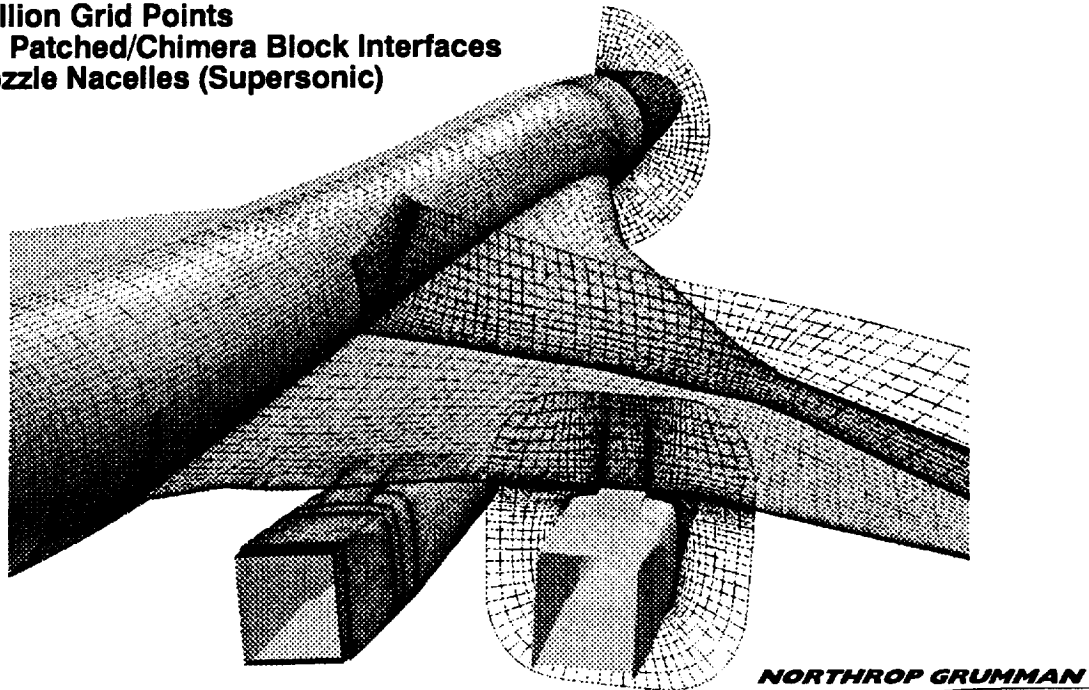
NORTHROP GRUMMAN

The full configuration (wing/body/nacelle/diverter) was modeled with the supersonic nozzle setting for Mach numbers of 0.9 and 1.1 and α of 4 and 6. The full configuration with the transonic nozzle setting was run at Mach numbers of 0.9 and 1.1 and α of 2, 4 and 6. The force integrations from the full configuration combined, with the wing/body and isolated nacelle forces yield the interference effects.

**First NASA/Industry High Speed Research Configuration
Aerodynamic Workshop**

CFD Model of the Boeing Reference H Configuration

**16 Blocks
4.8 Million Grid Points
Mixed Patched/Chimera Block Interfaces
2D Nozzle Nacelles (Supersonic)**

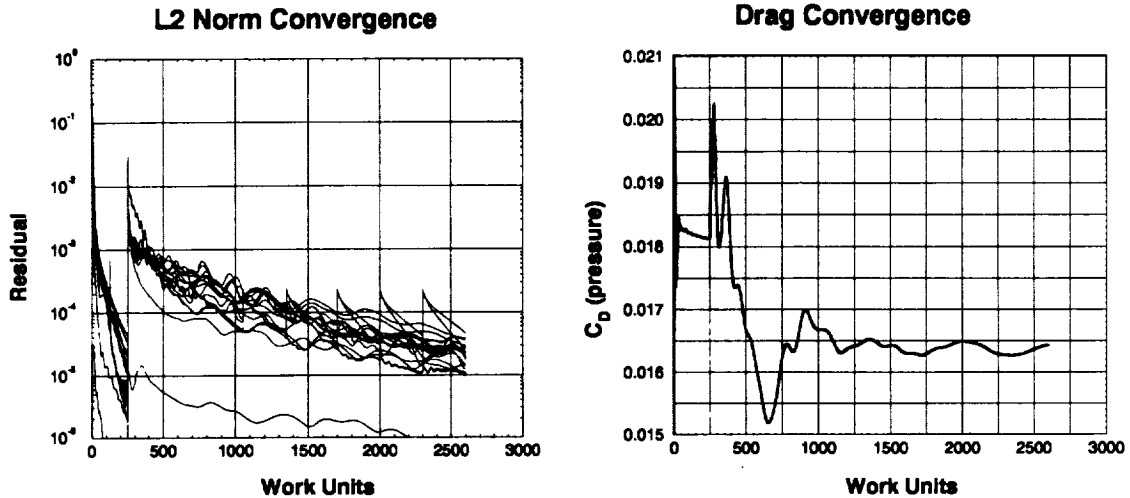


Surface grids and grid topologies for the full configuration (wing/body/nacelles/diverter) with the supersonic nozzle setting are shown. The model consisted of 16 blocks and 4.8 million grid points utilizing both patched and overlapped blocks. The large number of grid points was required to resolve the blunt trailing edges of the nacelle side walls and the nozzle flaps and hinge line. Overlapped (Chimera) blocks were used so that the blocks associated with the nacelle/diverter could easily be removed yielding the wing/body grid. This ensures that the gridding is consistent between the various configurations, eliminating grid changes as a possible influence on drag differences.

**First NASA/Industry High Speed Research Configuration
Aerodynamic Workshop**

CFD Model of the Boeing Reference H Configuration

Ref. H Wing/Body/Nacelle/Diverter Convergence History

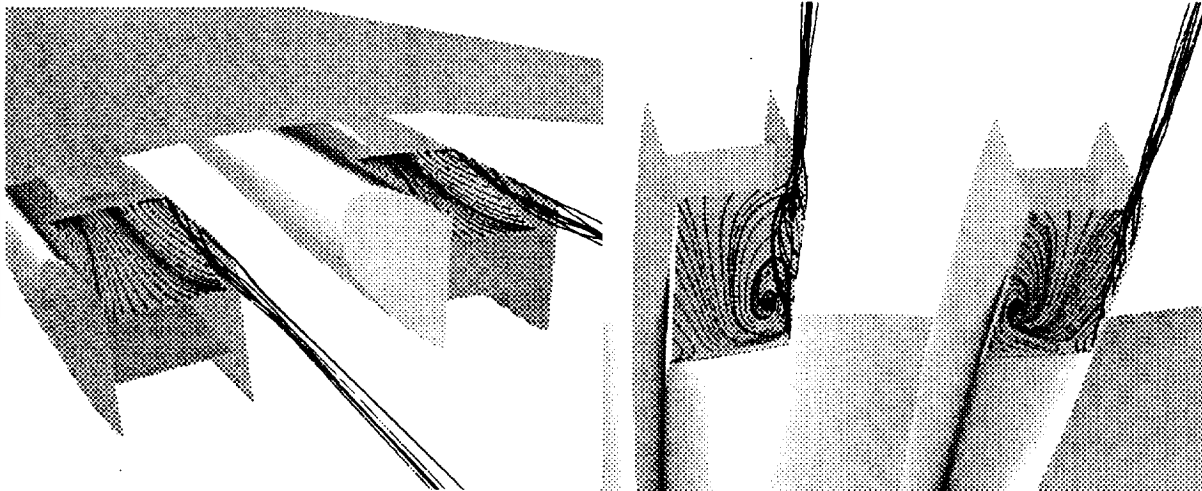


NORTHROP GRUMMAN

Convergence plots for the full configuration (wing/body/nacelle/diverter) with the supersonic nozzle setting are shown. This case was run at $M=0.9$, $\alpha=4^\circ$ with $NPR=5.0$ and $NTR=3.264$, and was used to test out the grid. The residual convergence plots shows the L2 norm of the Q vector as a function of work units (equivalent fine grid iterations) and shows roughly four orders of magnitude drop in residual. The lower sequence level (every other point in each direction) was run for 2000 iterations (250 work units) and the fine mesh for nearly 2500 iterations. The drag convergence plots shows a fluctuation of about 2 counts is still occurring after nearly 2500 iterations on the fine mesh. The range of y^+ was 1–3 over the entire vehicle which is adequate for the turbulence model. The Menter $k-\omega$ SST turbulence model was used for this and all the solutions presented. All of the full configuration solutions run to date were run 2000 iterations on the coarse mesh and 3000 iterations on the fine mesh. This took approximately 52 hours of Cray-C90 CPU time and a charged time of 35 hours for utilizing six processors.

**First NASA/Industry High Speed Research Configuration
Aerodynamic Workshop**

Ref. H Wing/Body/Nacelle/Diverter
Axisymmetric Inlet – 2D Nozzle, Mach 0.9, $\alpha=4.0^\circ$, $Re_{MAC}=40$ million



Top View

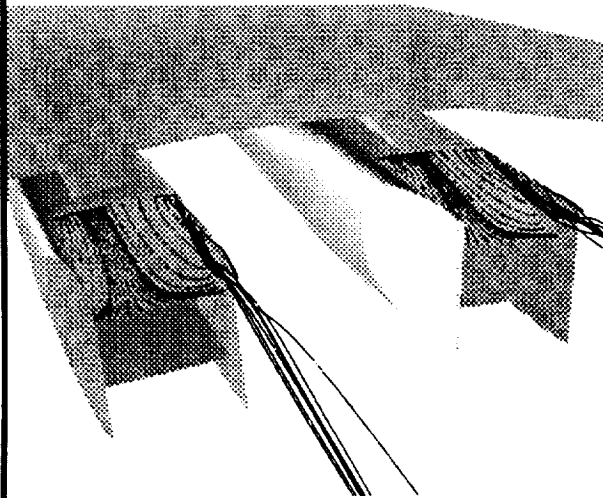
Bottom View

NORTHROP GRUMMAN

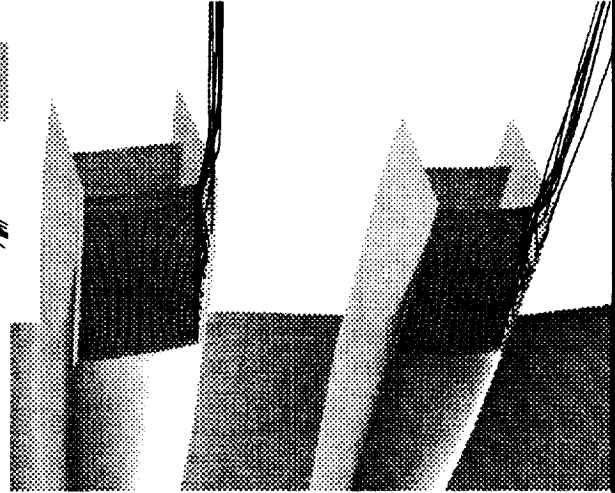
Surface streamlines (oil flows) and streamlines off the outboard side walls are shown for the installed nacelles with the transonic nozzle setting at Mach 0.9. Streamlines on the upper surface show that the flow remains attached over the upper surface due to the flow off of the wing upper surface. The streamlines on the lower surface, however, resemble the isolated nacelle with the nozzle flap fully separated. Nacelle alignment and mutual interference effects give an asymmetric separation on both nacelles.

**First NASA/Industry High Speed Research Configuration
Aerodynamic Workshop**

**Ref. H Wing/Body/Nacelle/Diverter
Axisymmetric Inlet - 2D Nozzle, Mach 1.1, $\alpha=4.0^\circ$, $Re_{MAC}=40$ million**



Top View



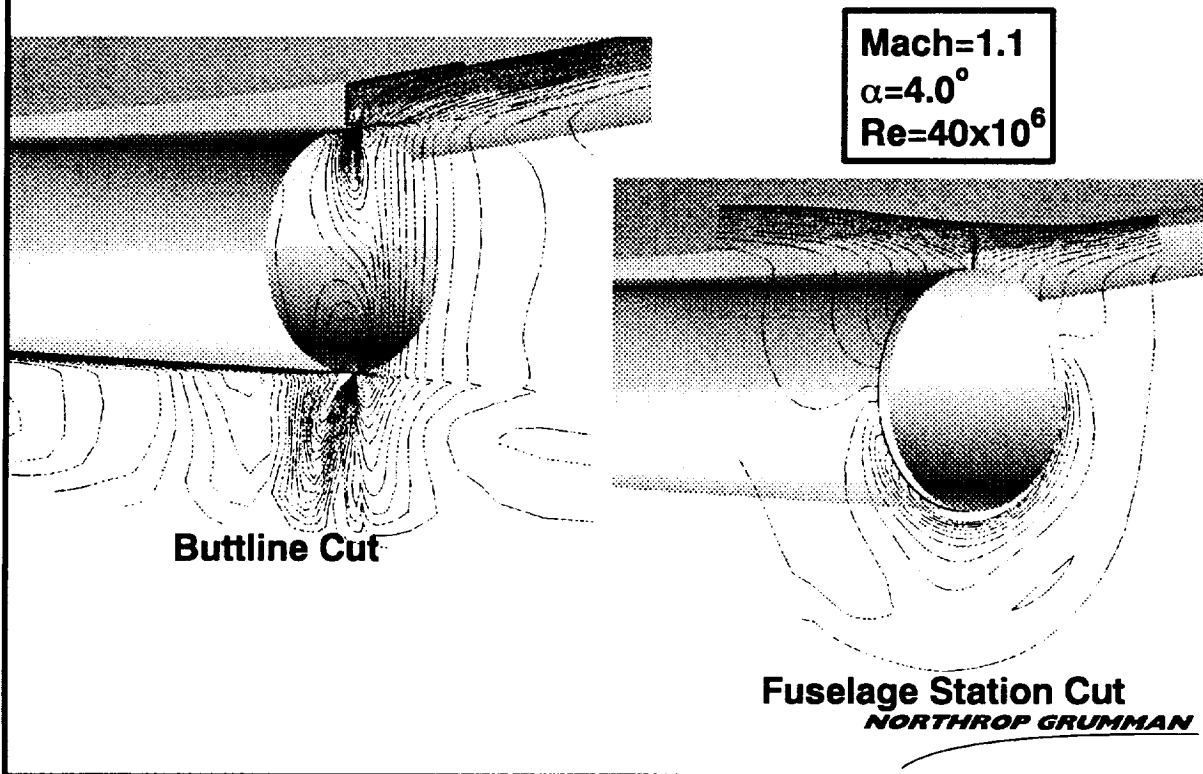
Bottom View

NORTHROP GRUMMAN

Surface streamlines (oil flows) and streamlines off the outboard side walls are shown for the installed nacelles with the transonic nozzle setting for Mach 1.1. As in the Mach 0.9 case, streamlines on the upper surface show that the flow remains attached over the upper surface due to the flow off of the wing upper surface. The streamlines on the lower surface again resemble the isolated nacelle at this Mach number with the nozzle flap attached until near the nozzle exit.

**First NASA/Industry High Speed Research Configuration
Aerodynamic Workshop**

**Full Configuration, 2D Nozzle Nacelles (SS)
Mach Contours Near Inboard Inlet**



Contours of Mach number near the inlet are shown for the full configuration at Mach 1.1 with the supersonic nozzle setting. While in the isolated nacelle analysis the inlet condition allowed the flow to be swallowed cleanly, the effects of the wing and diverter and the flow alignment of the nacelle itself cause some spillage to occur. Any drag increment due to this spillage is included in the interference drag.

**First NASA/Industry High Speed Research Configuration
Aerodynamic Workshop**

Drag Reduction: Interference Drag

CONSTANT ALPHA

$$CD' = CD_{WBDN} - CD_{isonac,tot,xyz}$$

$$CL' = CL_{WBDN} - CL_{isonac,tot,xyz}$$

WHERE:

$$CD_{isonac,tot,xyz} = [1,0] \bullet CF_{isonac,tot,xyz}$$

$$CL_{isonac,tot,xyz} = [0,1] \bullet CF_{isonac,tot,xyz}$$

$$CF_{isonac,tot,xyz} = [Y] [X1] CF'_{isonac_{\alpha=0},x'y'z'} + [Y][X2] CF'_{isonac_{\alpha=0},x'y'z'}$$

CF = [CD,CL] aircraft coordinate system

CF' = [CD',CL'] nacelle coordinate system

[X1] , [X2] : transformation matrices to rig inboard and outboard nacelles

$$[Y] = \begin{bmatrix} \sin(\alpha) & \cos(\alpha) \\ \cos(\alpha) & -\sin(\alpha) \end{bmatrix} = \text{transformation matrix to correct for angle of attack to get drag and lift}$$

Internal nacelle forces were not included in force analysis

NORTHROP GRUMMAN

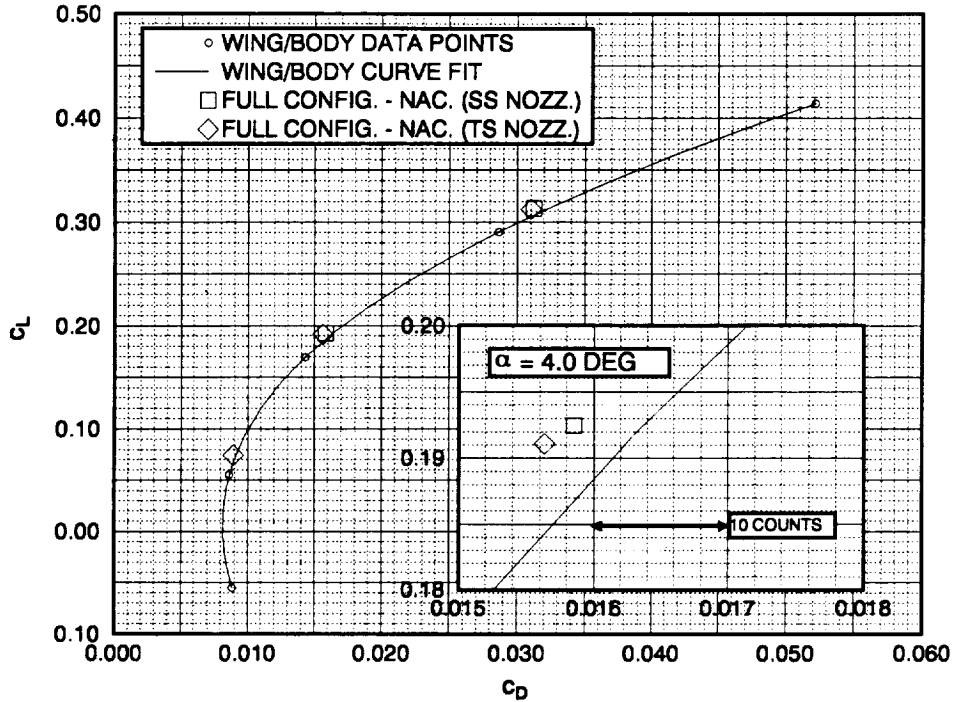
Drag polars (C_D' vs. C_L') were constructed by subtracting the drag and lift contributions of the isolated nacelles from the full configuration. The isolated nacelle forces, $CF'=[C_D',C_L']$ in x',y',z' , were transformed from the isolated nacelle coordinate system ($x'y'z'$) to the aircraft coordinate system (xyz). This rigging procedure was done for the inboard and outboard locations. Inboard and outboard transformations are expressed as [X1] and [X2] respectively. The vehicle angle of attack was needed to determine the lift and drag contributions of the isolated nacelles. The use of the [Y] matrix accomplished this transformation.

By subtracting the isolated nacelle forces from the full configuration, we are left with, by definition, wing/body + nacelle interference drag. The forces on the isolated nacelle and the nacelles of the full configuration include the external pressure and viscous forces only. Internal inlet and nozzle forces were not integrated.

**First NASA/Industry High Speed Research Configuration
Aerodynamic Workshop**

BOEING REF H CONFIGURATION

M=0.9, Re=40x10⁶, GCNS/FOMOCO



NORTHROP GRUMMAN

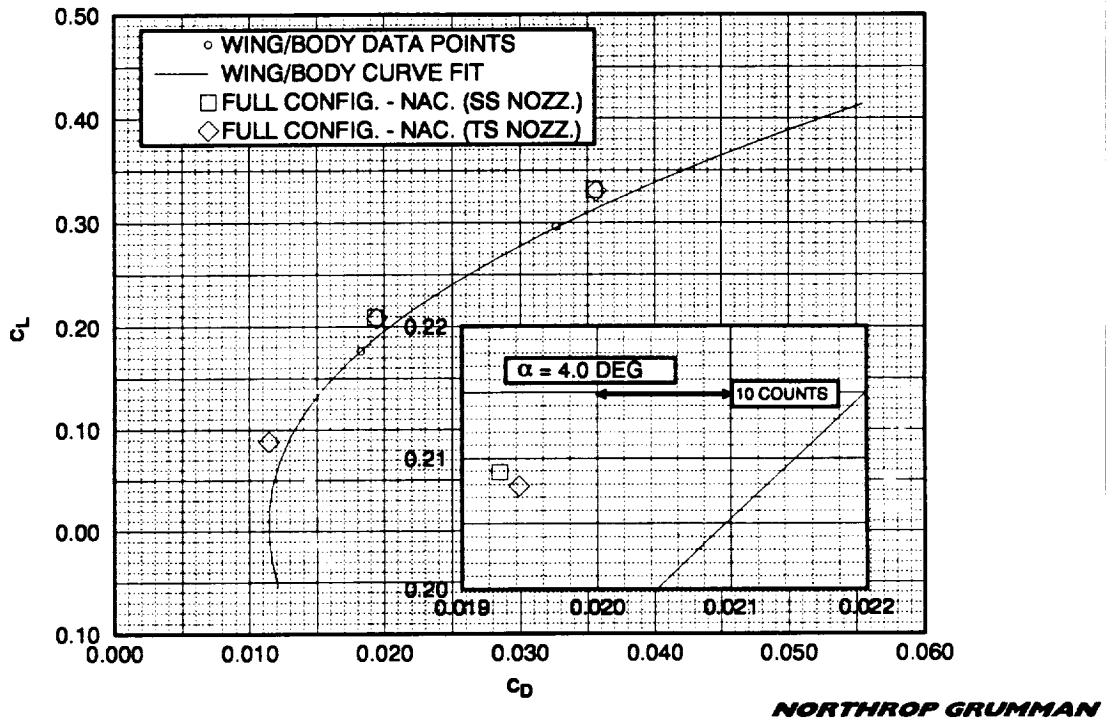
The constructed drag polar (full configuration – isolated nacelle) for M=0.9, Re = 40x10⁶ can be compared to the wing/body case. The difference between them is the nacelle interference drag. These drag polars are shown for the supersonic and transonic nozzle configuration.

For the runs performed, the interference drag is negative in all cases with a constant lift coefficient. The interference drag is determined by comparing the constructed drag polar to the wing/body configuration (see inset) at constant C_L . The drag increment from nacelle interference for the transonic nozzle is -0.00059 (-5.9 counts) at a $C_L=0.191$. For the supersonic nozzle at a $C_L=0.192$, the drag increment is -0.00049 (-4.9 counts). Both of these points correspond to a full configuration alpha of 4.0 degrees.

**First NASA/Industry High Speed Research Configuration
Aerodynamic Workshop**

BOEING REF H CONFIGURATION

M=1.1, Re=40x10⁶, GCNS/FOMOCO



NORTHROP GRUMMAN

The constructed drag polar (full configuration – isolated nacelle) for M=1.1, Re=40x10⁶ can be compared to the wing/body case. The drag polars shown are for the supersonic and transonic nozzle configurations. The wing/body polar was constructed by translating the five-point curve fit at M=0.9 so that it passed through the two data points run at M=1.1

For the runs performed, the interference drag is again negative in all cases with a constant lift coefficient. The drag increment from nacelle interference for the transonic nozzle is -0.00184 (-18.4 counts) at $C_L=0.208$. For the supersonic nozzle at $C_L=0.209$, the drag increment is -0.00209 (-20.9 counts). Both of these points correspond to a full configuration alpha of 4.0 degrees.

**First NASA/Industry High Speed Research Configuration
Aerodynamic Workshop**

Conclusions

- **Transonic Nozzle Boattail Drag is Significant for 2D Nozzle Nacelles**
- **Correlation of the Wing/Body Results with Wind Tunnel Data Was Adequate for Force Increments, But Could Be Improved**
- **All Conditions Analyzed Showed Positive Installed Interference Effects**
- **Installed Inlet Spill Effects Due to Local Wing Shape Get Included as Interference Effects**

NORTHROP GRUMMAN

The isolated nacelle analysis showed that the transonic nozzle boattail drag is significant for the 2D nozzle nacelles. Recall the boattail drag is defined as the difference in drag on the isolated nacelle between the supersonic and transonic nozzle settings at a given flow condition. For this study this difference was 4.68 drag counts at $M=0.9$ and 14.2 drag counts at $M=1.1$. Comparison of wing/body to full configuration (wing/body/nacelle/diverter) analyses showed positive interference effects for all cases, especially at $M=1.1$. Correlations between the GCNSfv solutions and the wind tunnel test data for the wing/body configuration leave room for improvement. Aggressive schedule and NAS resource limitations prevented any grid variations to improve correlation with the test data. While the isolated nacelles were run with inlet conditions to give $MFR=1.0$ and eliminate spill effects from the boattail region this could not be done for the installed nacelles where the flow is influenced by the local wing contouring and nacelle orientation to the flow. The effects of inlet spill get lumped into the interference terms.

***First NASA/Industry High Speed Research Configuration
Aerodynamic Workshop***

Recommendations for Future Work

- **Grid Resolution and Skin Friction Calculations Should be Resolved to Try and Improve the Wing/Body Correlations**
- **Nacelle Placement and Orientation Under the Wing Should Be Optimized for Drag and Inlet Performance**
- **Aft Diverter Height and Aft Diverter-to-Wing Integration Should Be Optimized for 2D Nozzle Nacelles**

NORTHROP GRUMMAN



Effects of grid spacing and resolution as well as the force intergrations should be investigated to try and improve the correlations. Flow near the inlets for the installed nacelles clearly show that the orientation and placement of the nacelles under the wing should be optimized to try and improve drag and inlet performance. Additional analysis should be done to determine the best aft diverter height and aft diverter-to-wing integration to minimize installed boattail drag.

AFTERBODY EXTERNAL AERODYNAMIC AND PERFORMANCE PREDICTION AT HIGH REYNOLDS NUMBERS

John R. Carlson
NASA-Langley, Hampton VA

1st. NASA/Industry HSR Configuration Aerodynamics Workshop
February 27-29, 1996

1st NASA/Industry HSR Configuration Aerodynamics Workshop
Afterbody External Aerodynamic and Performance Prediction
at High Reynolds Numbers

- Overview
- CFD Method
- Grid Convergence
- Reynolds Number Trends
- Concluding Remarks

slide 2

Historically there has been more experience with sub-scale testing and flow analysis. The last few decades have been addressing the issue of flight versus sub-scale flow more completely than before. In 1974, as part of the NTF run-up work, a set of simple test bodies were run in the 0.3-m Cryogenic Pilot Tunnel, obtaining a set of pressure data over a large Reynolds number range.

slide 0b

PAB3D is a Reynolds averaged Navier-Stokes method that has been extensively utilized for analysis of aerodynamic and propulsion-aerodynamic interactions involving shear flows, jet-plumes, and massively separated boundary layer flows. The last year of work has been used analyzing the capability of the anisotropic algebraic Reynolds stress turbulence models some results of which are to follow. The Girimaji ARSM is fairly recent work with PAB3D being the first RANS code to implement this work. Dr. Girimaji worked for both Shih and Lumley.

OVERVIEW

- Considerable model-scale experience and data base.
 - Wind tunnel data
 - Most CFD done on wind tunnel models
- Model-scale vs. Full-scale flow characteristics
 - Boundary layer growth modified
 - Subsequent changes in shocks and shock-b.l. interactions
 - Changes in drag and lift increments
- Cryogenic test performed on an axisymmetric afterbody (Reubush, 1974)
 - C_p , $C_{d,\beta}$ data obtained
 - Reynolds number range from 10 to 120 million

slide 2-//NASA/LaRC/RTG/AD/CIB/Carlson/20Feb96/

PAB3DV13R

- 3-D RANS Upwind Method
- Multiblock with general face patching and mesh sequencing
- Mixed Roe and van Leer solver schemes
- Third order solver accuracy with local time stepping
- Linear 2-equation k- ϵ turbulence model
- Algebraic Reynolds Stress turbulence models
 - Shih, Zhu, & Lumley
 - Girimaji
- Real gas and multi-species
- 23 words per grid point
- 38 μ sec per iteration per grid point (Cray YMP)

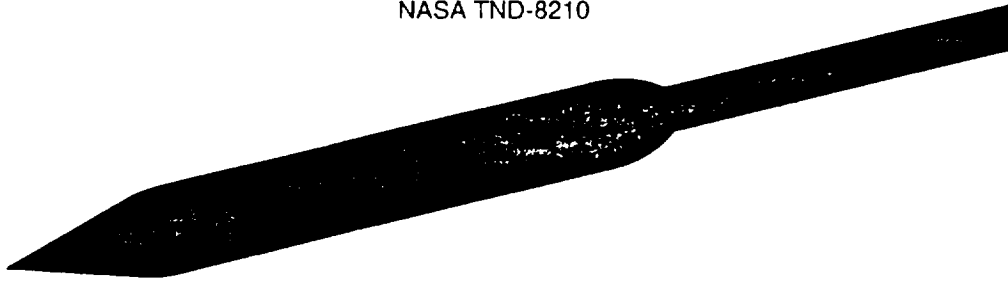
slide 4

NASA TND 8210 is a report by D.Reubush from 1974 when he performed a series of tests to determine Reynolds numbers effect for nozzle-boattail flows. Several models and nozzle configurations were tested in both the 0.3m Cyrogenic Pilot Tunnel and the 16-Foot Transonic Tunnel.

slide 5

Computations performed over a small Reynolds number range could tolerate using the same grid for each set of conditions. The range of these calculations though required a minimum of 3 grids to keep the nondimensional boundary layer parameter y^+ between 0.2 and 0.5. The assumption of a zero pressure flat plate flow using free stream conditions provide a fairly accurate first guess for boundary layer griding parameters.

AXISYMMETRIC AFTERBODY W/ SOLID STING
NASA TND-8210



Modeled after Configuration 1, NASA TND-7795

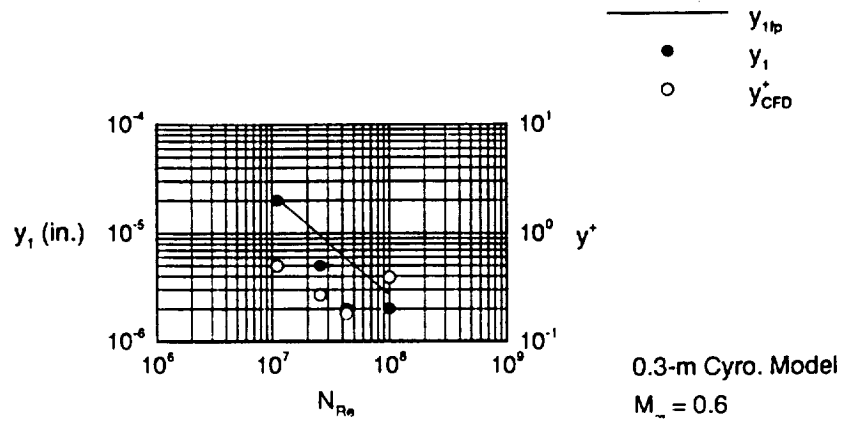
Two cryogenic model lengths for this nozzle

- L = 8 inches (1/6 th scale of Conf.1)

- L = 16 inches

slide 4 -//NASA/LaRC/RTG/AD/CIB/Carlson/27Feb96

AXISYMMETRIC AFTERBODY W/ SOLID STING
 y^+ Schedule



slide 5 -//NASA/LaRC/RTG/AD/CIB/Carlson/21Feb96

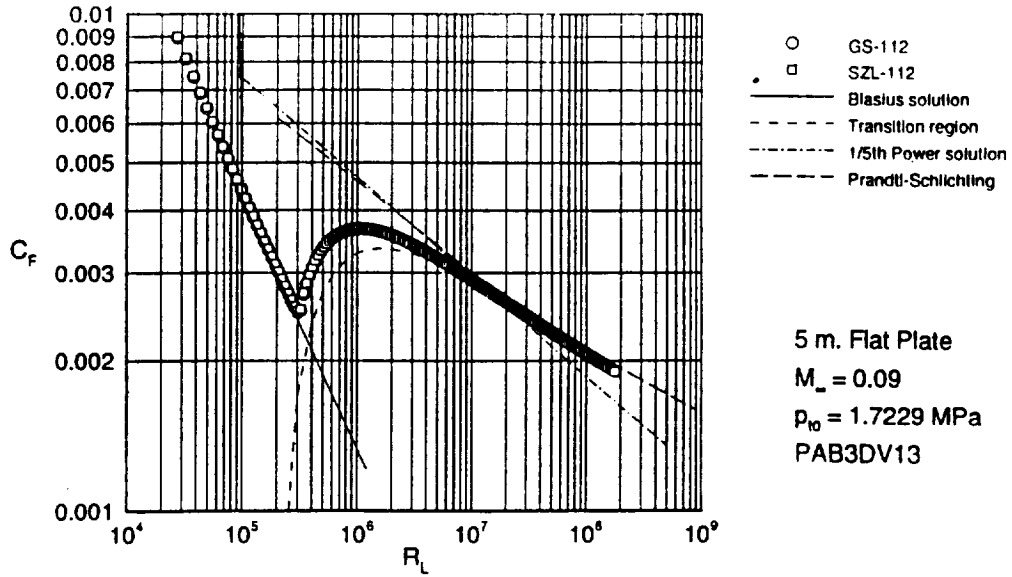
slide 6

Both algebraic Reynolds stress models Shih, Zhu and Lumley; and Gatski and Speziale had very consistent trends over the local Reynolds number range from less than 0.1 to 200. million following fairly closely the flat plate parameter of average skin friction. Prandtl-Schlichting is the predicted high Reynolds number trend of average skin friction.

slide 7

Fairly good grid convergence was achieved, shown by this representative plot at 43 million Reynolds number. The boundary layer at $M=0.6$ does separate downstream of 0.65, but this separation is due to purely the adverse pressure gradient of the boattail flow. The boundary layer separation that occurs at $M=0.9$ is a shock induced separation. Duplicate experimental data points are shown for an indication of data scatter.

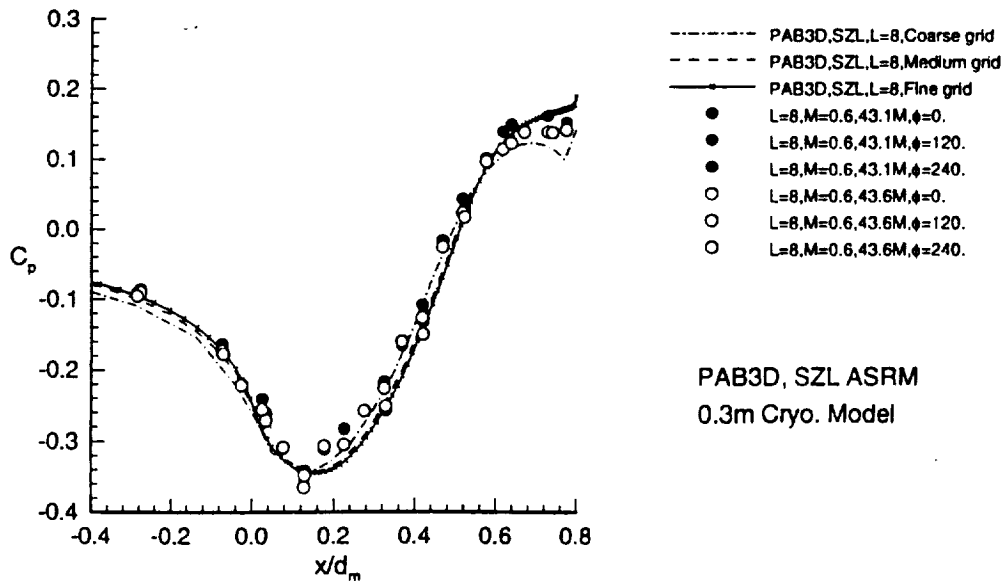
AVERAGE SKIN FRICTION - SUBSONIC FLAT PLATE



slide 6 -//NASA/LaRC/RTG/AD/CIB/Carlson/27Feb96

AXISYMMETRIC AFTERBODY W/ SOLID STING

Grid Convergence



slide 7 -//NASA/LaRC/RTG/AD/CIB/Carlson/27Feb96

slide 8

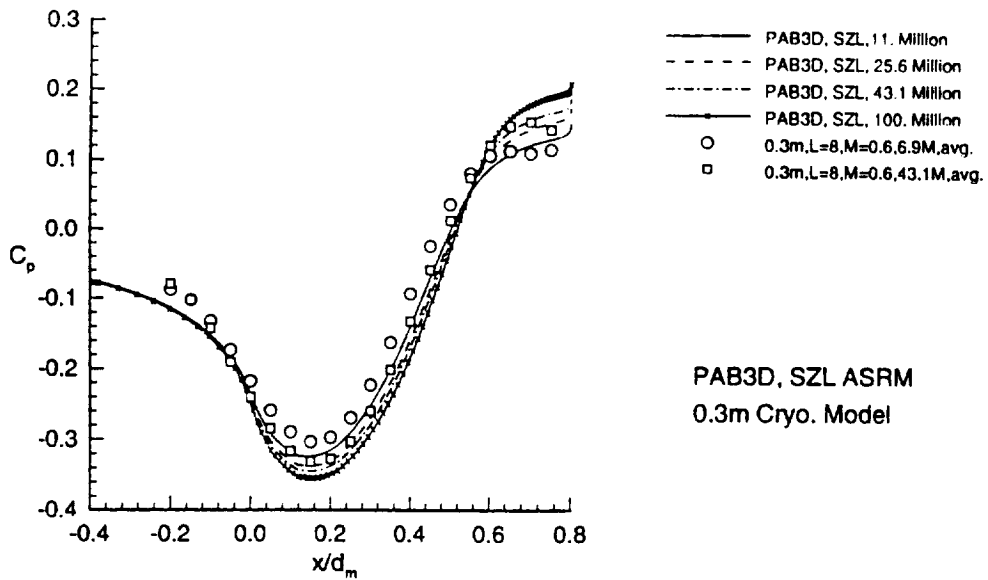
The CFD pressure distributions on the boattail show a very consistent Reynolds number trend with the shock strength generally increasing with Reynolds number and the pressure recovery increasing as well. The experimental data plotted was a cubic spline fit through several repeat points in an attempt to show a single "clean" distribution at the two Reynolds number settings. The spline was fairly poorly fitted upstream of $x/d_m = 0$. The change in the experimental pressure distributions with Reynolds number was slightly less than that predicted by CFD. The changes observed in the pressure distributions tended to cancel each other out when the integrated drag was obtained.

slide 9

Integrated pressure drag for several experimental models and for the CFD are shown. A conclusion drawn in NASA TND 7795 was the extreme sensitivity of pressure drag to very small changes in pressure distributions. The pressure distributions between the same model tested in both the 0.3m tunnel and 16-foot and the CFD are visually very similar, but as seen comparing the open diamond, triangle, and closed square with the open square around 10 million Reynolds number there appears to be about a factor of 2 difference in drag. The X around 12 million is the 48 inch model that the cryogenic models were designed after and whose drag was fairly closely matched by the CFD. Overall, there appears to be only a very mild variation in drag with Reynolds number at this Mach number.

Afterbody External Aerodynamic and Performance Prediction
at High Reynolds Numbers

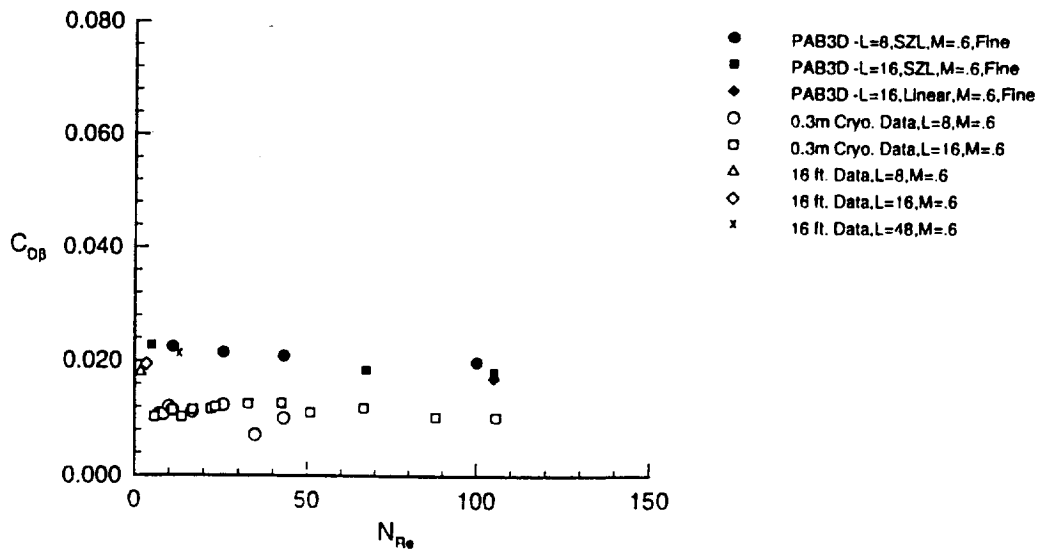
AXISYMMETRIC AFTERBODY W/ SOLID STING
Reynolds Number Variation of Boattail C_p



slide 8 -//NASA/LaRC/RTG/AD/CIB/Carlson/27Feb96

Afterbody External Aerodynamic and Performance Prediction
at High Reynolds Numbers

Reynolds Number Trend of Integrated Boattail Pressure Drag



slide 9 -//NASA/LaRC/RTG/AD/CIB/Carlson/27Feb96

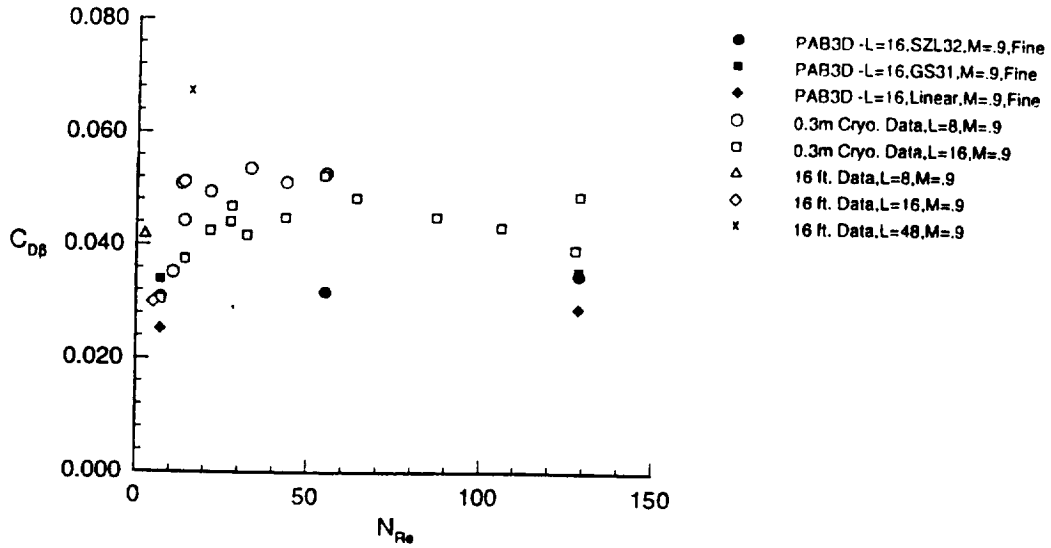
slide 10

A larger scatter in the integrated drag data occurs at $M=0.9$ resulting in no quantitative conclusion in the variation pressure drag with Reynolds number for the particular geometry, except that potentially it is fairly small.

slide 11

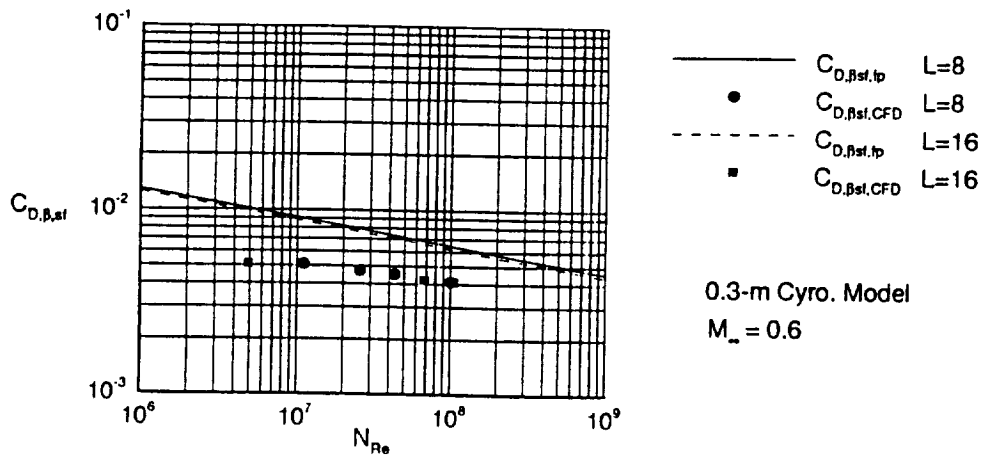
The wetted area equivalent flat plate skin friction numbers are compared to the skin friction calculated by the code. In general the change in skin friction is slightly lower using the CFD. The CFD was 5 counts below the 1-D theory at 10 million Reynolds number and about 2 counts below at around 100 million Reynolds number. These are drag coefficients based on the maximum body cross-sectional area.

Reynolds Number Trend of Integrated Boattail Pressure Drag



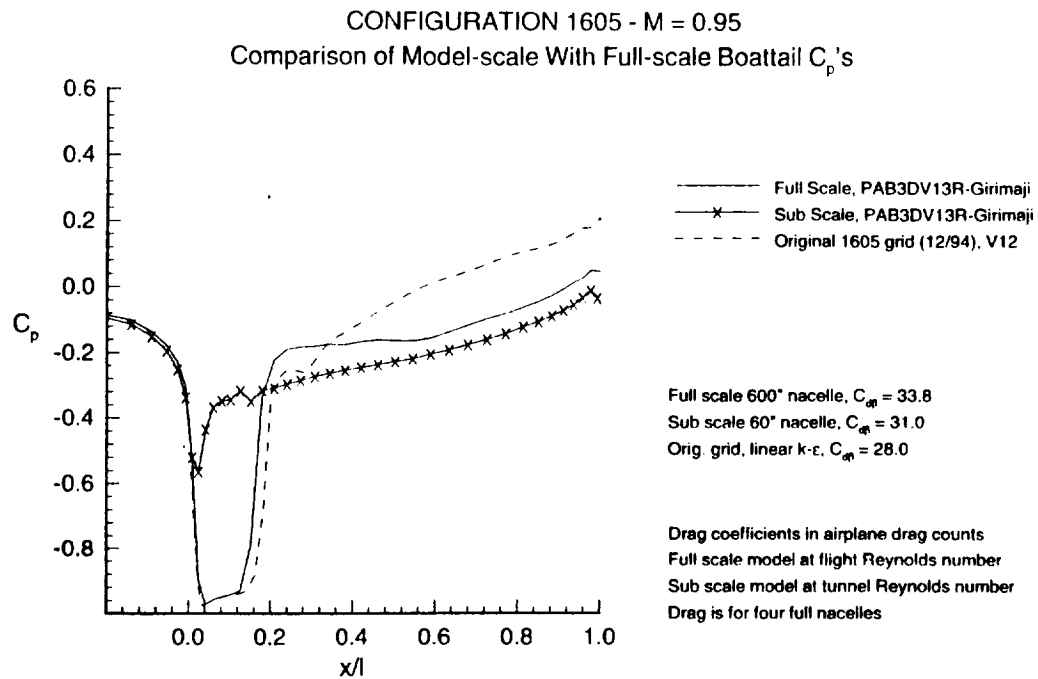
slide 10 -/NASA/LaRC/RTG/AD/CIB/Carlson/27Feb96

AXISYMMETRIC AFTERBODY W/ SOLID STING
Nozzle Boattail Skin Friction With Reynolds Number



slide 12

This CFD experiment concludes that the potential difference between the flow between a flight Reynolds number test and a sub-scale wind tunnel test are substantial for this particular nozzle boattail geometry. The early study was performed using a linear k-epsilon turbulence model. The present study was performed using the Girimaji formulation of an algebraic Reynolds stress turbulent simulation. The dashed line is the pressure distribution from the original isolated transonic boattail study leading up to the previous presentation by Midea, Pao, Austin and Mani; performed by Pao, Abdol-Hamid and Carlson. The solid line is the same flight scale geometry with some regridding performed for better grid convergence. The solid line with x is the same geometry scaled down to the size of a typical jet effects model that could be tested in the Langley 16-Foot Transonic Tunnel at a lower Reynolds number. In general, the shock is considerably weaker with a more extensive flow separation at the lower Reynolds number. It is likely due to the different boundary layer growth characteristics at the two Reynolds numbers.



slide 12 -/NASA/LaRC/RTG/AD/CIB/Pao, Abdol-Hamid, Carlson/27Feb96

- Skin friction characteristics with Reynolds number consistent
- Grid converged solutions obtained over Reynolds number range.
- Fairly accurate prediction of shock and separated flow pressure recovery.
- Reynolds number trend of surface static pressure coefficients qualitatively achieved.
- CFD slightly over-predicted change in pressure coefficients with Reynolds number.
- Integrated pressure drag on nozzle boattail generally off potentially due to tunnel effects.
- Conducted CFD experiment on configuration 1605. (PAB3DV13R, Girimaji ASM)
 - Full-scale model solution had a large separation and low recovery pressure.
 - Sub-scale model solution had a weaker shock and yet larger separation predicted.

REPORT DOCUMENTATION PAGE			Form Approved OMB No. 0704-0188	
Public reporting burden for this collection of information is estimated to average 1 hour per response, including the time for reviewing instructions, searching existing data sources, gathering and maintaining the data needed, and completing and reviewing the collection of information. Send comments regarding this burden estimate or any other aspect of this collection of information, including suggestions for reducing this burden, to Washington Headquarters Services, Directorate for Information Operations and Reports, 1215 Jefferson Davis Highway, Suite 1204, Arlington, VA 22202-4302, and to the Office of Management and Budget, Paperwork Reduction Project (0704-0188), Washington, DC 20503				
1. AGENCY USE ONLY (Leave blank)	2. REPORT DATE December 1999	3. REPORT TYPE AND DATES COVERED Conference Publication		
4. TITLE AND SUBTITLE First NASA/Industry High-Speed Research Configuration Aerodynamics Workshop			5. FUNDING NUMBERS WU 537-07-20-20	
6. AUTHOR(S) Richard M. Wood, Editor				
7. PERFORMING ORGANIZATION NAME(S) AND ADDRESS(ES) NASA Langley Research Center Hampton, VA 23681-2199			8. PERFORMING ORGANIZATION REPORT NUMBER L-17574A	
9. SPONSORING/MONITORING AGENCY NAME(S) AND ADDRESS(ES) National Aeronautics and Space Administration Washington, DC 20546-0001			10. SPONSORING/MONITORING AGENCY REPORT NUMBER NASA/CP-1999-209690/PT1	
11. SUPPLEMENTARY NOTES				
12a. DISTRIBUTION/AVAILABILITY STATEMENT Unclassified-Unlimited Subject Category 02 Availability: NASA CASI (301) 621-0390			12b. DISTRIBUTION CODE Distribution: Nonstandard	
13. ABSTRACT (Maximum 200 words) This publication is a compilation of documents presented at the First NASA/Industry High Speed Research Configuration Aerodynamics Workshop held on February 27-29, 1996 at NASA Langley Research Center. The purpose of the workshop was to bring together the broad spectrum of aerodynamicists, engineers, and scientists working within the Configuration Aerodynamics element of the HSR Program to collectively evaluate the technology status and to define the needs within Computational Fluid Dynamics (CFD) Analysis Methodology, Aerodynamic Shape Design, Propulsion/Airframe Integration (PAI), Aerodynamic Performance, and Stability and Control (S&C) to support the development of an economically viable High Speed Civil Transport (HSCT) aircraft. To meet these objectives, papers were presented by representative from NASA Langley, Ames, and Lewis Research Centers; Boeing, McDonnell Douglas, Northrop-Grumman, Lockheed-Martin, Vigyan, Analytical Services, Dynacs, and RIACS.				
14. SUBJECT TERMS High speed research; Aerodynamic design; Computational fluid dynamics; Aerodynamics; Stability and control; Performance; Propulsion airframe integration			15. NUMBER OF PAGES 349	16. PRICE CODE A15
17. SECURITY CLASSIFICATION OF REPORT Unclassified	18. SECURITY CLASSIFICATION OF THIS PAGE Unclassified	19. SECURITY CLASSIFICATION OF ABSTRACT Unclassified	20. LIMITATION OF ABSTRACT UL	

